13

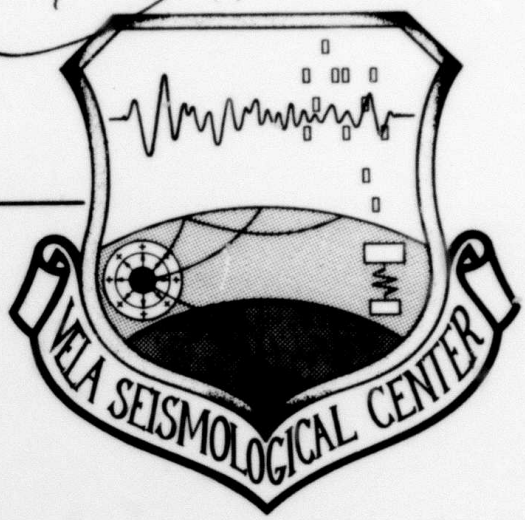

VSC-TR-81-15

REGIONAL AMPLITUDE-DISTANCE RELATIONS, DISCRIMINATION AND DETECTION

R. Blandford, R. Hartenberger, R. Naylor

Seismic Data Analysis Center
Teledyne Geotech
314 Montgomery Street
Alexandria Virginia 22314

13 JULY 81

APPROVED FOR PUBLIC RELEASE; DISTRIBUTION UNLIMITED.

Monitored By:
VELA Seismological Center
312 Montgomery Street
Alexandria, VA 22314

Sponsored by

The Defense Advanced Research Projects Agency (DARPA)

DARPA Order No. 2551

Unclassified

SECURITY CLASSIFICATION OF THIS PAGE (When Data Entered)

REPORT DOCUMENTATION PAGE

READ INSTRUCTIONS BEFORE COMPLETING FORM

1. REPORT NUMBER: VSC-TR-81-15	2. GOVT ACCESSION NO.: AD-A105722
3. RECIPIENT'S CATALOG NUMBER:	
4. TITLE (and Subtitle): REGIONAL AMPLITUDE-DISTANCE RELATIONS, DISCRIMINATION AND DETECTION	5. TYPE OF REPORT & PERIOD COVERED: Technical rept.
6. PERFORMING ORG. REPORT NUMBER: SDAC-TR-80-6	
7. AUTHOR(s): R. Blandford, R. Hartenberger, R. Naylor (Robert)	8. CONTRACT OR GRANT NUMBER(s): F08606-78-C0007, ARPA Order-2551
9. PERFORMING ORGANIZATION NAME AND ADDRESS: Teledyne Geotech, 314 Montgomery Street, Alexandria, Virginia 22314	10. PROGRAM ELEMENT, PROJECT, TASK AREA & WORK UNIT NUMBERS: VT/0709
11. CONTROLLING OFFICE NAME AND ADDRESS: Defense Advanced Research Projects Agency, 1400 Wilson Boulevard, Arlington, Virginia 22209	12. REPORT DATE: 03 Feb 81 13. NUMBER OF PAGES: 146
14. MONITORING AGENCY NAME & ADDRESS (if different from Controlling Office): VELA Seismological Center, 312 Montgomery Street, Alexandria, Virginia 22314	15. SECURITY CLASS. (of this report): Unclassified 15a. DECLASSIFICATION/DOWNGRADING SCHEDULE

16. DISTRIBUTION STATEMENT (of this Report)

APPROVED FOR PUBLIC RELEASE; DISTRIBUTION UNLIMITED.

17. DISTRIBUTION STATEMENT (of the abstract entered in Block 20, if different from Report)

18. SUPPLEMENTARY NOTES

Author's report date 15 November 1978

19. KEY WORDS (Continue on reverse side if necessary and identify by block number)

Regional Discrimination
Seismic Discrimination
Amplitude-Distance Relations
P_g, L_g
CTBT
NSS
RSTN

20. ABSTRACT (Continue on reverse side if necessary and identify by block number)

Amplitude-distance curves are different in the EUS and WUS; P_{max} decays as $r^{-2.5}$ and $r^{-3.0}$ in EUS and WUS, while for the maximum after 3.6 km/sec on the vertical component (termed L_g) the decay rates are r^{-2} and r^{-3}. The EUS results are in general agreement with the literature and with the data presented by Nersesov and Rautian (1964) for events on the northern margin of tectonic regions in the Soviet Union suggesting that discrimination results in the EUS are relevant to NSS stations within the Soviet Union.

Using these distance amplitude relations, network mean amplitudes at 1000 km

DD FORM 1 JAN 73 1473 EDITION OF 1 NOV 65 IS OBSOLETE

Unclassified

SECURITY CLASSIFICATION OF THIS PAGE (When Data Entered)

408 258

were computed for L_g and P_{max} for earthquakes and explosions in the EUS and WUS and a separation of 0.6 magnitude units was observed thus forming a regional discriminant. The L_g is larger for earthquakes than for explosions. This conclusion is somewhat uncertain in the WUS because of the large scatter in the explosion population. However, a reasonable explanation for this large scatter is that the small events at NTS are at such shallow depths in dry alluvium that the medium is weak, resulting in a low corner frequency. This decreases the ratio P_g/L_g since P_g contains comparatively more high frequency than L_g. The scatter probably would not be a problem in a true test ban situation since shots will be well buried to avoid surface collapse.

The WUS earthquake P_{max} versus L_g is displaced about 0.2 magnitude units from the EUS curve, reflecting the large P_g phase relative to L_g in the WUS.

The GNOME explosion and the Hebgen Lake earthquake, which are on the border between the EUS and WUS defined by Der, Massé and Gurski (1975), show differences in amplitude distance relations for the same event in different provinces. The greater WUS attenuation results in amplitudes at 10° of about 0.4 magnitude units below that in EUS.

Analysis of the SALMON and 18 February 1964 Alabama earthquake shows that there is no earthquake/explosion discrimination capability using maximum transverse to maximum radial amplitude ratios. We also find that the source spectra of the two events are identical between 1 and 10 Hz, that the L_g spectrum is different from the P spectrum and is therefore not the source spectrum, and that the L_g spectrum is contaminated by scattered coda from earlier phases so that high-frequencies observed in the L_g phase may not be predictable by any deterministic theory of L_g. Identical conclusions with respect to the P and L_g spectra were obtained by analysis of spectra of Soviet explosions as observed at NORSAR.

In the EUS, 10 Hz energy is observed out to 10°, and for Soviet shots observed at NORSAR, out to 33°. The peak in the S/N varies from 5 Hz at 11° to 2 Hz at 33°; however, for small events which have not yet been studied, the peak may well be at higher frequencies because of higher corner frequencies and because much of the noise on LRSM and NORSAR systems at 10 Hz may be system or quantization noise which can be reduced by more carefully designed systems.

Detection thresholds for a single element at the C3 subarray of NORSAR were determined to be m_b 0.9, 2.4, 3.3, and 3.9 at 5°, 10°, 15° and 20°, respectively. It should be noted that the lower frequency noise levels are high at NORSAR, which is near the sea, and thus that stations on continents might have lower thresholds at large distances where the lower frequencies are the most useful for detection.

REGIONAL AMPLITUDE-DISTANCE RELATIONS, DISCRIMINATION AND DETECTION

SEISMIC DATA ANALYSIS CENTER REPORT NO.: SDAC-TR-80-6

AFTAC Project Authorization No.: VELA VT/0709

Project Title: Seismic Data Analysis Center

ARPA Order No.: 2551

Name of Contractor: TELEDYNE GEOTECH

Contract No.: F08606-78-C-0007

Date of Contract: 01 October 1978

Amount of Contract: $377,990

Contract Expiration Date: 30 September 1979

Project Manager: Robert R. Blandford
(703) 836-3882

P. O. Box 334, Alexandria, Virginia 22313

APPROVED FOR PUBLIC RELEASE; DISTRIBUTION UNLIMITED.

ABSTRACT

Amplitude-distance curves are different in the EUS and WUS; P_{max} decays as $r^{-2.5}$ and $r^{-3.0}$ in EUS and WUS, while for the maximum after 3.6 km/sec on the vertical component (termed L_g) the decay rates are r^{-2} and r^{-3}. The EUS results are in general agreement with the literature and with the data presented by Nersesov and Rautian (1964) for events on the northern margin of tectonic regions in the Soviet Union suggesting that discrimination results in the EUS are relevant to NSS stations within the Soviet Union.

Using these distance amplitude relations, network mean amplitudes at 1000 km were computed for L_g and P_{max} for earthquakes and explosions in the EUS and WUS and a separation of 0.6 magnitude units was observed thus forming a regional discriminant. The L_g is larger for earthquakes than for explosions. This conclusion is somewhat uncertain in the WUS because of the large scatter in the explosion population. However, a reasonable explanation for this large scatter is that the small events at NTS are at such shallow depths in dry alluvium that the medium is weak, resulting in a low corner frequency. This decreases the ratio P_g/L_g since P_g contains comparatively more high frequency than L_g. The scatter probably would not be a problem in a true test ban situation since shots will be well buried to avoid surface collapse.

The WUS earthquake P_{max} versus L_g is displaced about 0.2 magnitude units from the EUS curve, reflecting the large P_g phase relative to L_g in the WUS.

The GNOME explosion and the Hebgen Lake earthquake, which are on the border between the EUS and WUS defined by Der, Massé and Gurski (1975), show differences in amplitude distance relations for the same event in different provinces. The greater WUS attenuation results in amplitudes at 10° of about 0.4 magnitude units below that in EUS.

Analysis of the SALMON and 18 February 1964 Alabama earthquake shows that there is no earthquake/explosion discrimination capability using maximum transverse to maximum radial amplitude ratios. We also find that the source spectra of the two events are identical between 1 and 10 Hz, that the L_g spectrum is different from the P spectrum and is therefore not the source spectrum, and that the L_g spectrum is contaminated by scattered coda from earlier phases so that high-frequencies observed in the L_g phase may not be

predictable by any deterministic theory of L_g. Identical conclusions with respect to the P and L_g spectra were obtained by analysis of spectra of Soviet explosions as observed at NORSAR.

In the EUS, 10 Hz energy is observed out to 10°, and for Soviet shots observed at NORSAR, out to 33°. The peak in the S/N varies from 5 Hz at 11° to 2 Hz at 33°; however, for small events which have not yet been studied, the peak may well be at higher frequencies because of higher corner frequencies and because much of the noise on LRSM and NORSAR systems at 10 Hz may be system or quantization noise which can be reduced by more carefully designed systems.

Detection thresholds for a single element at the C3 subarray of NORSAR were determined to be m_b 0.9, 2.4, 3.3, and 3.9 at 5°, 10°, 15° and 20°, respectively. It should be noted that the lower frequency noise levels are high at NORSAR, which is near the sea, and thus that stations on continents might have lower thresholds at large distances where the lower frequencies are the most useful for detection.

TABLE OF CONTENTS

LIST OF FIGURES

LIST OF FIGURES (Continued)

LIST OF FIGURES (Continued)

LIST OF FIGURES (Continued)

LIST OF FIGURES (Continued)

LIST OF TABLES

This Page
Intentionally
Left Blank.

INTRODUCTION

In 1958 the Geneva Conference of Experts suggested that a worldwide network of 180 seismic stations might constitute a feasible seismic monitoring system to enforce a comprehensive nuclear test ban (CTB). Such a large number of stations naturally included several inside the United States and the USSR, and there was, therefore, considerable research carried out in succeeding years on distance-amplitude relations and discrimination capabilities at "regional" distances of less than say, 20°.

In time it became less clear that internal stations within the USSR would be allowed, national means of verification were emphasized, and furthermore, seismologists realized that teleseismic signals were not so dominated by effects of complicated crustal structures as were the regional signals. Since the teleseismic signals were easier to understand, they could perhaps be relied upon more for discrimination. Thus, around 1963, emphasis shifted from studies at regional distances to those at teleseismic distances.

In 1977 it began again to seem possible that the USSR would allow stations within its borders, and so interest has been revived in regional discrimination. In retrospect, it seems clear that research was on the verge of major discoveries on the subject of regional discrimination in 1963, when emphasis was shifted to the teleseismic distances. In the interim, due to work related to earthquake risk, plate tectonics, and to some degree the ARPA discrimination program, substantial improvement in our understanding of the propagation of crustal phases has nonetheless occurred.

This paper begins with a review of the literature. Such a review is useful for all workers in the field as it aids in avoiding repetition of work, and shows the rather advanced state of existing knowledge. This advanced state was not recognized by the author, and most other workers in the field, when the subject of regional propagation and discrimination again opened up in 1977.

The review begins with work on propagation of P_n, P_g, S_n, L_g, and R_g and continues with the history of discrimination at regional distances up to 1978. New work performed especially for this report is discussed next; distance amplitude relations for P_n, P_g, L_g and for the maximum amplitude observed before and after S_n are presented for earthquakes and explosions in both the Eastern United States (EUS) and the Western United States (WUS). Considerable

care was taken in these analyses to avoid bias due to clipping, to discarding of clipped readings, or to missing the maximum excursion during examination of a film record. Use was made of the low gain analog tape data as necessary. Bias effects are maximized at close distances for large events and lead to estimates of the rate of decay of amplitude with distances which are too small. Care was also taken to plot noise levels on distance amplitude plots even if a signal could not be detected. This helps avoid the additional bias toward a small rate of decay which can occur when small amplitudes at large distances are not plotted because they are not detected, whereas the unusually large amplitudes are detected and are plotted.

By means of references to the work reviewed in the literature review, these results are then placed in context, and decay rates are attached to the amplitude-distance curves so that they may be used in magnitude estimation. Then these distance-amplitude relations are used to define event magnitudes (log amplitude at 1000 km) for each phase and the discrimination capability of a compressional and shear magnitude is investigated in a fashion analogous to the conventional M_s:m_b.

Finally, several topics are discussed with the aid of spectra of explosions and earthquakes. Among these are detection threshold, optimum filter for detection of regional events, and difference in source spectra for earthquakes and explosions.

REVIEW OF LITERATURE

Amplitude-Distance and Travel-Time

Press and Ewing (1952) apparently were the first to discuss the phases L_g and R_g. They discovered them on newly installed seismographs at Palisades, New Jersey, and associated them with earthquakes in California. The instrument response was nearly flat in the period range 1 to 18 seconds, and they reported dominant periods ranging from 1/2 to 6 seconds for the L_g phase which exhibited primarily transverse motion. The signal also exhibited reverse dispersion with the shorter periods arriving first. The arrival of these short periods was quite sharp, with a group velocity 3.51 ± .07 km/sec.

The R_g phase arrived at 3.05 ± .07 km/sec with periods between 8 and 12 seconds at maximum amplitude. It exhibited predominantly radial and vertical motion.

Another experimental investigation was reported by Båth (1955). He used a Wiechert instrument which he stated was not very sensitive to periods of less than 3.0 seconds. He determined that there were two statistically distinct L_g phases, arrivals at Uppsala from Eurasia; he referred to them as L_g^1 and L_g^2. The mean period for waves was L_g^1:5.8 sec, L_g^2:6.8 sec, R_g:9.2 sec; therefore, these observations cannot be of direct interest in the discrimination problem, lying as close as they do to the peak in the microseism band. The velocity ranges defined by Båth for the various phases are: L_g^1: $v > 3.46$ km/sec; L_g^2 $3.25 < v < 3.46$; R_g: $v < 3.25$. Båth further divided his population of L_g^2 arrival velocities into two groups, $L_g^{2'}$ and $L_g^{2''}$, using the velocity 3.36 km/sec. From reading his paper it is not clear to the present authors whether these distinct L_g arrivals are due to multipathing, to different Airy phases due to group velocity extrema or, in some cases possibly due to different structures along different paths to Uppsala. A considerable amount of plotted velocity scatter, as contrasted to multiple arrivals observed on single records is certainly due to inaccurate epicenters.

Båth's median L_g velocity was 3.45 km/sec as compared to 3.51 given by Press and Ewing. Since Båth suggests that errors of 0.15 km/sec would not be unexpected due to epicentral errors, the two results seem to be within experimental error of each other. Båth's median R_g velocity is 3.07, in good agreement with the 3.05 value of Press and Ewing.

Press and Gutenberg (1956) searched records from the Kern County earthquake of July 21, 1952 for the channel P wave phase analogous to the channel S waves which they hypothesized to make up L_g. They were successful, finding a phase with a mean velocity of 6.09 km/sec out to a distance of 37.5°. They suggested the name πg. In general they characterized it as having small amplitudes. Only two of their observations were at distances of less than 12°.

I. Lehman (1957) studied the properties of L_g as read on North American records. Hers appears to be the first discussion of the signal character as seen on Benioff short-period instruments. She observed that signals recorded at Palisades from an Oklahoma event had periods of 1/2 to 1 second. Observations in Pasadena of the same event had longer periods and apparently smaller amplitudes, although calibrations were not completely reliable. She speculated that this might be related to the larger felt areas of earthquakes in the East.

Oliver and Ewing (1957, 1958a,b) discussed the foregoing observations of L_g, and some of their own, in terms of fundamental Love wave dispersion and of fundamental and higher mode Rayleigh dispersion. They identified the L_g^1 and L_g^2 of Båth with successive extrema at 5 and 6 seconds period of the first higher Rayleigh mode; and pointed out that it would be only a coincidence of the structure that the velocities at these extrema were near the crustal shear velocity to which this higher Rayleigh mode tends in the high-frequency limit and which is the L_g velocity for high frequencies. R_g for periods greater than 2 seconds they identified with a broad plateau in the fundamental dispersion diagram; they showed how sediments could greatly reduce the fundamental Rayleigh mode velocities at high frequencies, resulting in a long, dispersed coda.

Romney (1959) made use of VELA Uniform data to report some of the first reliable amplitude distance data at regional distances. The data were taken along a profile extending from the Nevada Test Site (NTS) Southeast into Texas and thence Northeast to Maine. In Figure 1 we see the data (for the phase P_n) and note that out to 800 km a line drawn as the inverse cube of the distance provides a good fit.

Romney also discussed the L_g waves, noting that they propagated with a velocity of about 3.5 km/sec. In Figure 1 we see the amplitudes of these waves on all three components. Again, an amplitude decay as the inverse cube is suggested by Romney as appropriate out to the limit of observation (-2.5 fits better); and all three amplitude components seem equal to one another.

Characteristics of explosions[a]

Name	Date	Time Time GCT	North latitude	West longitude	Depth	Approx yield kt
Tamalpais	8 Oct 58	22:00:00.1	37°11'43"	116°12'01"	330'	0.072
Evans	29 Oct 58	00:00:00.1	37°11'42"	116°12'17"	810'	0.055
Neptune	14 Oct 58	18:00:00 ± 1	37°11'58"	116°11'59"	0'	0.090
Rainier	19 Sep 57	16:59:59.4	37°11'45"	116°12'11"	790'	1.7
Logan	16 Oct 58	06:00:00.1	37°11'03"	116°12'04"	835'	5.0
Blanca	30 Oct 58	15:00:00.1	37°11'09"	116°12'07"	840'	19.0

Amplitude of P waves versus distance

Logan		Blanca	
Distance km	Amplitude[a] mμ	Distance km	Amplitude[a] mμ
96.2	1,860 (P)	203.5	3,330
	14,500 (Pn?)	300.6	1,160
203.5	1,500	395.1	400
300.6	526	599.7	148
498.9	107	908.9	7.7
714.5	41	1036.0	5.2
1036.0	3.1	1215.1	49
1111.5	...[b]	1398.3	67
1313.1	17.4	1610.1	16
1610.1	5.1	1707.0	37
1803.7	6.3	1842.0	60
1902.1	13.9	2011.2	14
2111.3	11.4	2111.3	34
2305.0	64	2208.8	53
2506.0	19.5	2665.3	60
3017.4	<10[c]	3017.4	32
3502.0	<10[c]	3308.9	<10[c]
3717.5	~21[d]	3717.5	~44[d]
4020.6	17.2	4020.6	30.5

[a] P-wave amplitudes measured as half the maximum peak-to-trough displacement in the first few cycles of motion.

[b] Beginning P waves lost in noise from passing train.

[c] Signal not detected; noise estimated at 5 to 10 millimicrons.

[d] Estimated from College records.

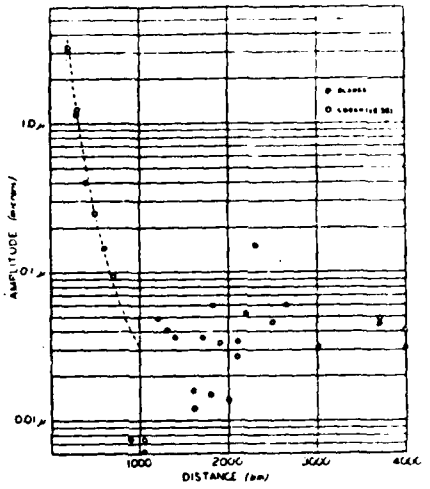

—Amplitude of P waves from a 19-kt underground explosion as a function of distance. The dashed curve is drawn proportional to the inverse cube of the distance.

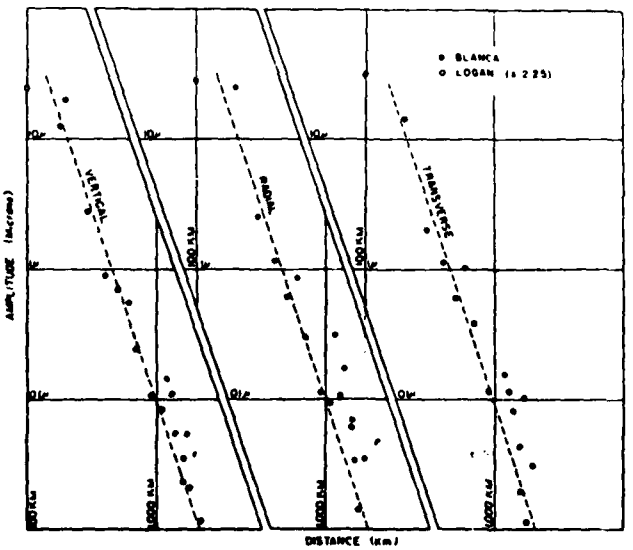

Amplitudes of 3.5-km/sec shear waves from a 19-kt underground explosion. Curves are drawn proportional to the inverse cube of the distance.

Figure 1. Distance-amplitude relations from Romney (1959) for P and L_g waves.

Shurbet (1960) analyzed the πg (Shurbet preferred to call it $\overline{P}$) phases of Press and Gutenberg (1956) further and concluded that the reason they did not propagate strongly to the east was the thinning of the crust. He relied on work by Ewing and Press (1959) stating that the M discontinuity is at 47 km beneath the Rockies and shallows to 35 km beneath the interior plains. If the attenuation of a phase is strongly controlled by structure, it clearly becomes important to be very careful about distance-amplitude relations.

Romney et al (1962) published substantial travel-time and amplitude data for the event GNOME. In Figures 2a-e their data shows how the P travel times could be contoured at regional distances, and how the trend of the $P_g(\overline{P})$ travel-times paralleled the P times and seemed to have only slightly greater variance about a smooth line drawn through the data than does P_n. With L_g, as pointed out by Romney et al, the situation is different. There seems to be much greater scatter and no apparent correlation with P_n and $\overline{P}$ travel times. Also in Figures 2d and e we reproduce the amplitude-distance data presented by Romney et al.

Brune and Dorman (1963) used signals from earthquakes in Northern Canada as recorded in Southeast Canada and at Palisades to extend the work of Oliver and Ewing discussed above, and also to investigate the properties of P_n and S_n. Figure 3 gives some of the relevant data.

Ryall and Stuart (1963) measured arrival times and amplitudes from eight NTS explosions along a profile to Ordway, Colorado. A short spread of instruments was set out at 28 locations along the profile so that phase velocity could be measured. Ryall and Stuart's distance-amplitude data for P_n and $\overline{P}$ are reproduced in Figure 4. While Romney et al (1962) apparently favored r^{-3} and r^{-4} for these two phases, best fits to Ryall and Stuart's data (on a different profile, of course) yield r -3.28 and r -3.52.

Press (1964) analyzed LRSM recordings of P_g and L_g as detailed in Figure 5. In deriving his Q values he assumed for both P_g and L_g that the amplitude decayed in the time domain as $r^{-1}\exp(-\pi r/UQT)$ with U = 3.5. (This is clearly incorrect for P_g for which U should be about 6.0.)

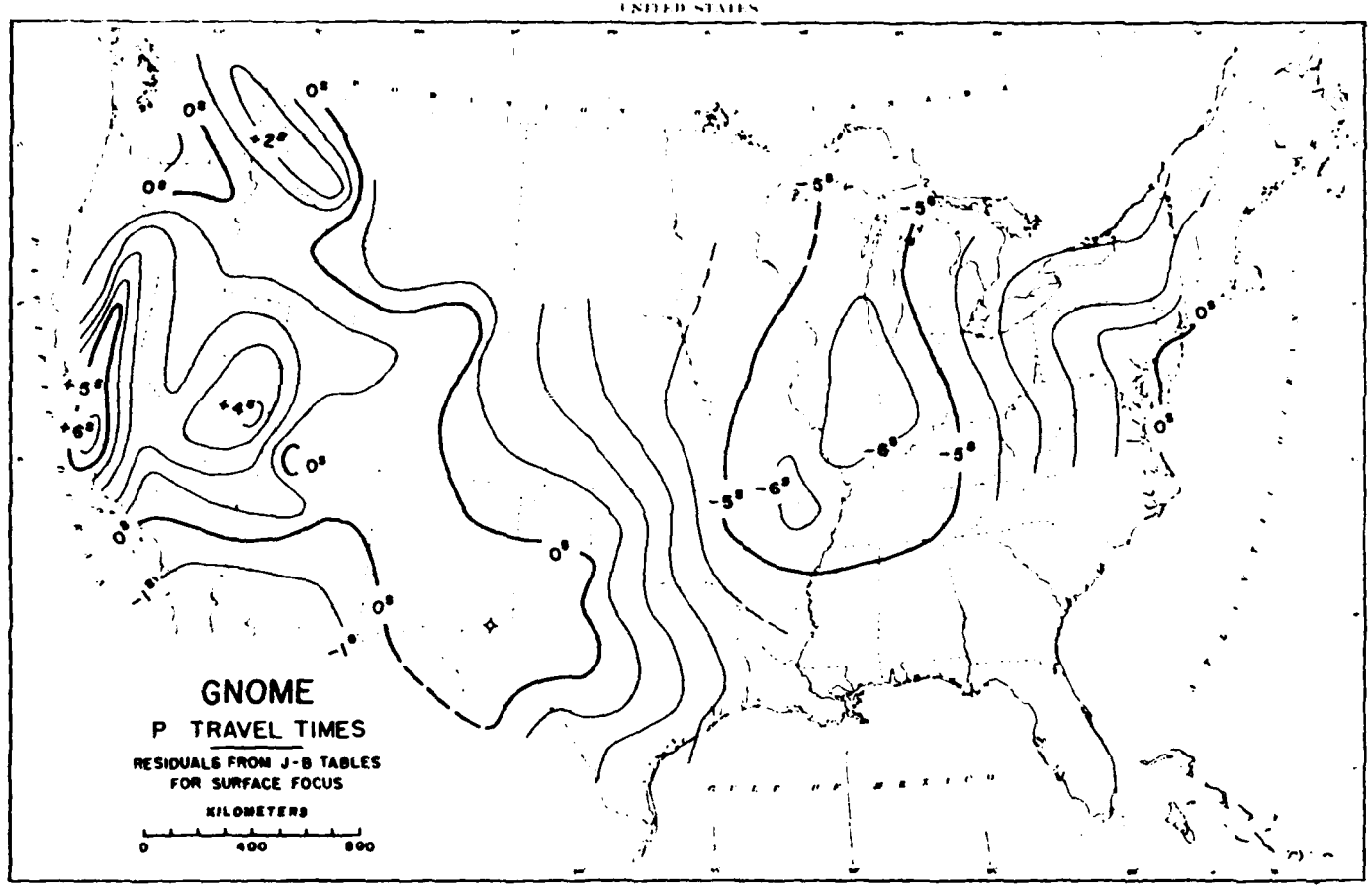

Contour map of P travel time residuals relative to J-B table

Figure 2a. Travel-time and distance amplitude relations for the event GNOME from Romney et al (1962).

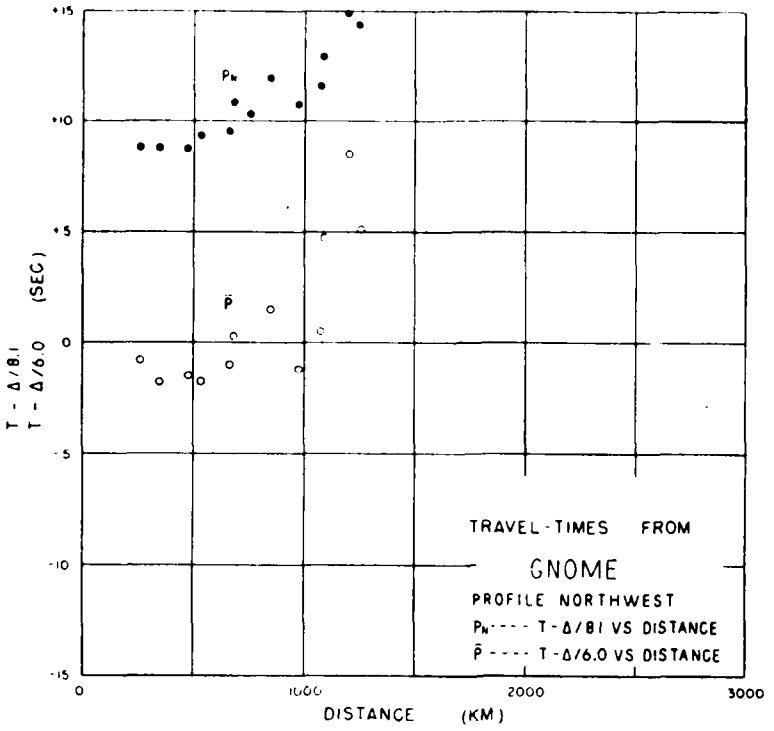

Comparison of P_n and $\bar{P}$ travel time residuals relative to constant velocities for northwest profile.

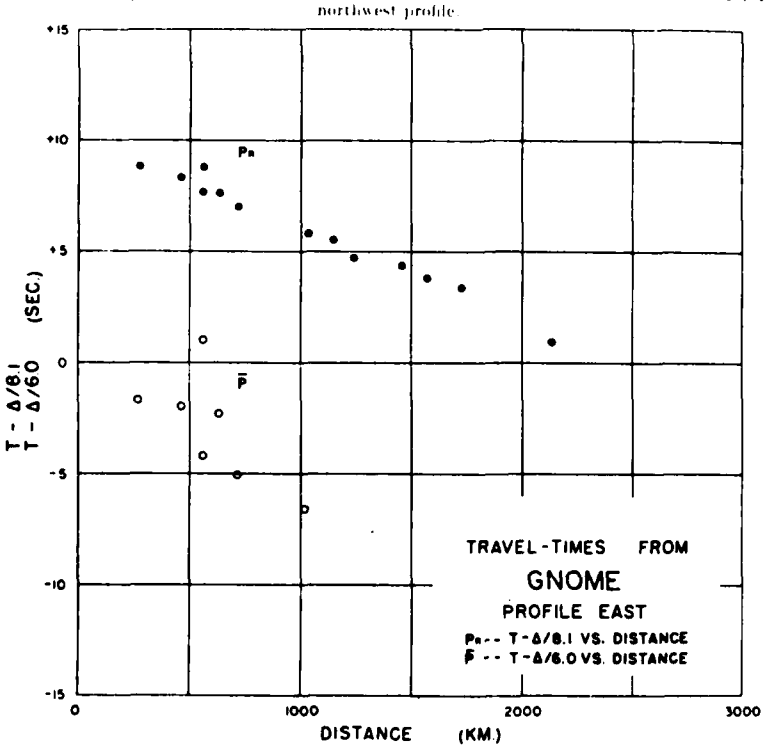

Comparison of P_n and $\bar{P}$ travel time residuals relative to constant velocities for profile east.

Figure 2b. Travel-time and distance amplitude relations for the event GNOME from Romney et al (1962).

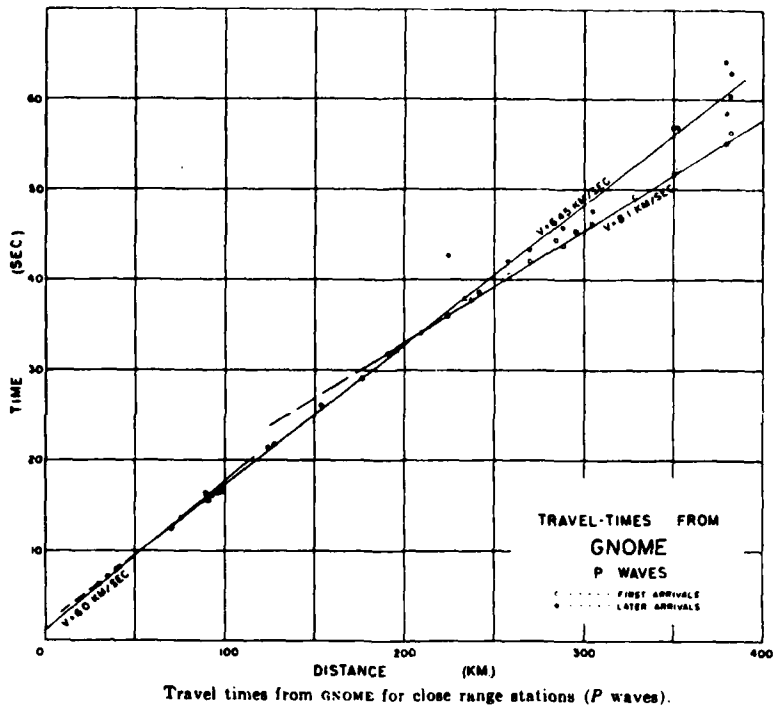

Travel times from GNOME for close range stations (*P* waves).

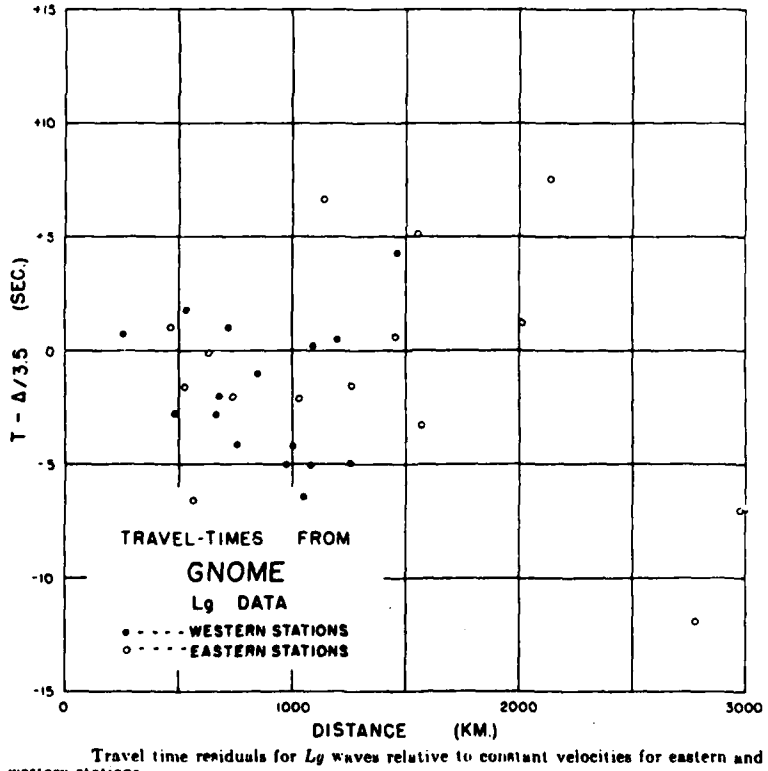

Travel time residuals for *Lg* waves relative to constant velocities for eastern and western stations.

Figure 2c. Travel-time and distance amplitude relations for the event GNOME from Romney et al (1962).

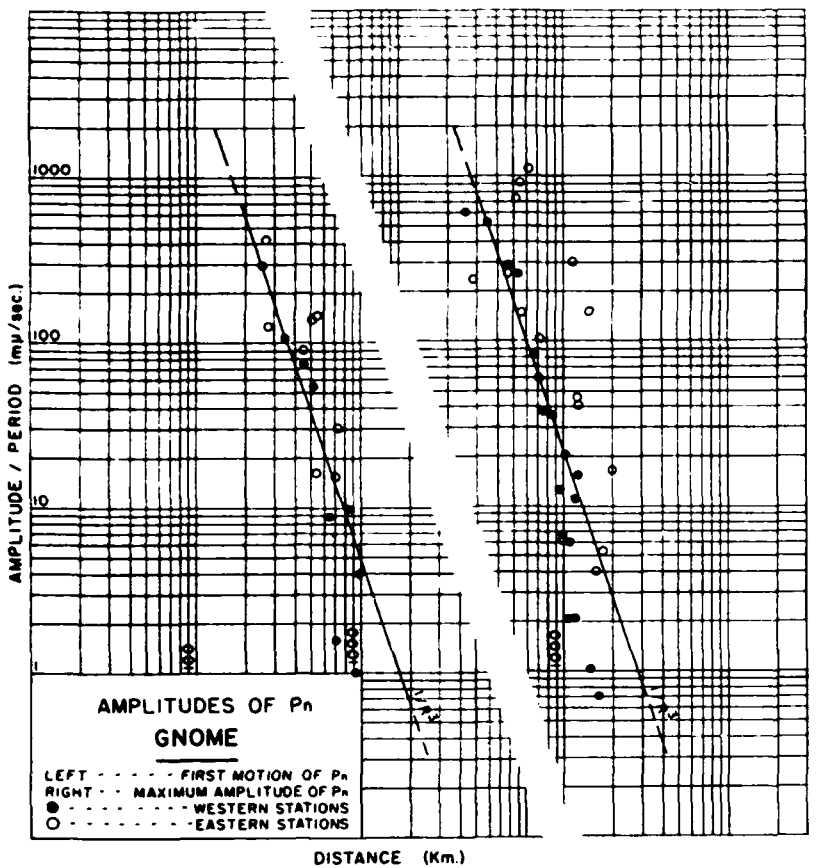

Amplitude graphs of first motion of *Pn* and maximum motion of *Pn* vs distance fo eastern and western stations.

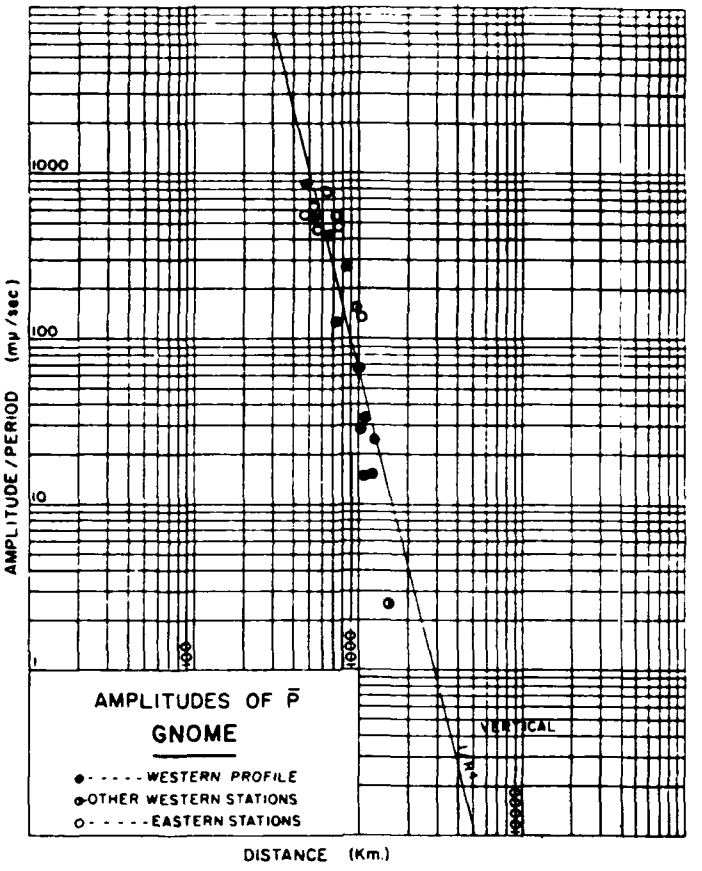

Amplitude graph of $\bar{P}$ vs distance for eastern and western stations.

Figure 2d. Travel-time and distance amplitude relations for the event GNOME from Romney et al (1962).

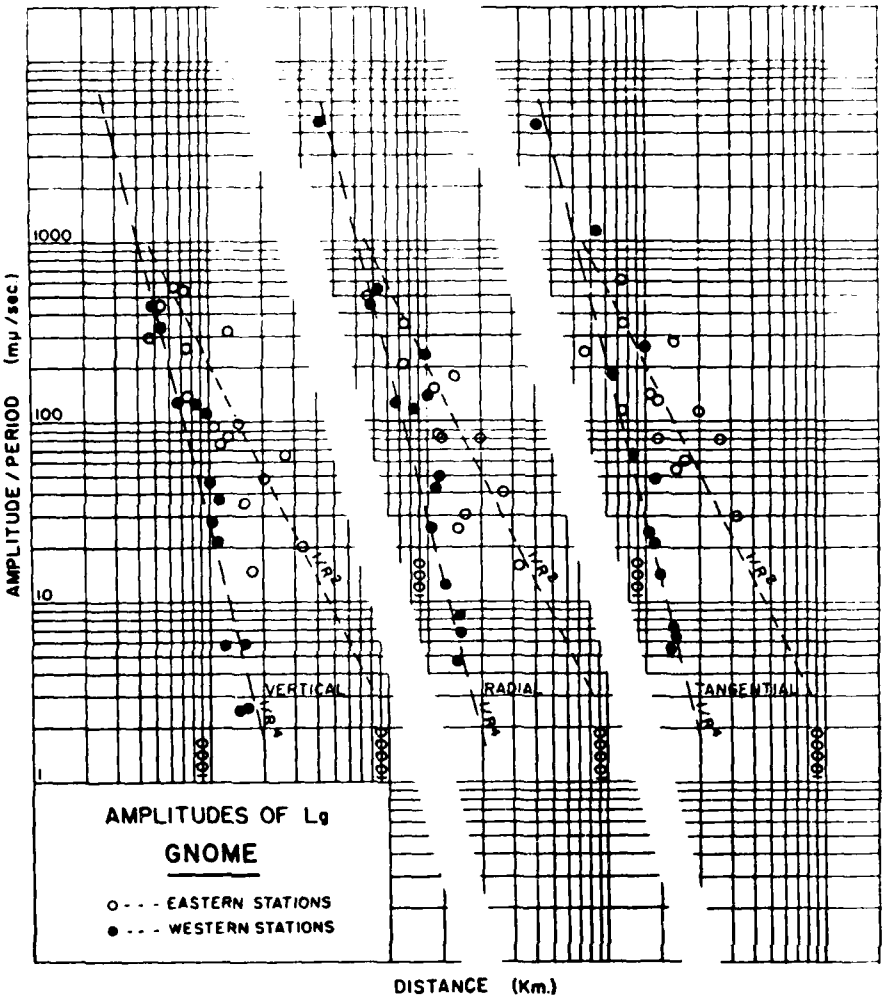

Amplitude graphs for three components of *Lg* vs distance for eastern and western stations.

Figure 2e. Travel-time and distance amplitude relations for the event GNOME from Romney et al (1962).

REFRACTION RESULTS FOR THE CANADIAN SHIELD

	Hodgson (1953a) Rockbursts	Hodgson (1953b) Timed Blasts	Hall and Brisbin (1961) Timed Blasts
P_1 (km/sec)	6.25	6.2	6.15
S_1 (km/sec)	3.54	3.54	3.65
h_1 (km)	—	—	16.5
P_2 (km/sec)	—	(7.1)	7.10
S_2 (km/sec)	—	(3.92)	4.10
h_2 (km)	—	—	18.7
P_n (km/sec)	8.18	—	8.17
S_n (km/sec)	4.85	—	4.60
H (km)	35–36 km (P waves)	—	35.2

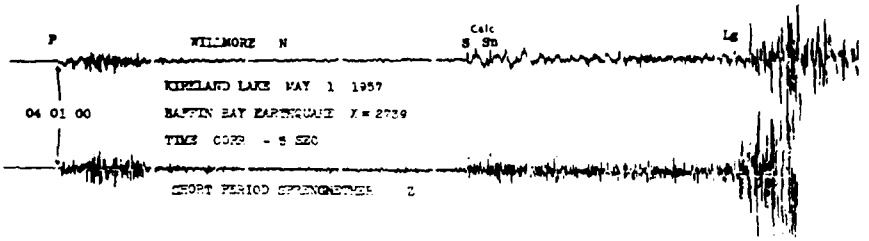

Kirkland Lake seismograms of the Baffin Bay earthquake of May 2, 1957. The epicenter is nearly due north of Kirkland Lake.

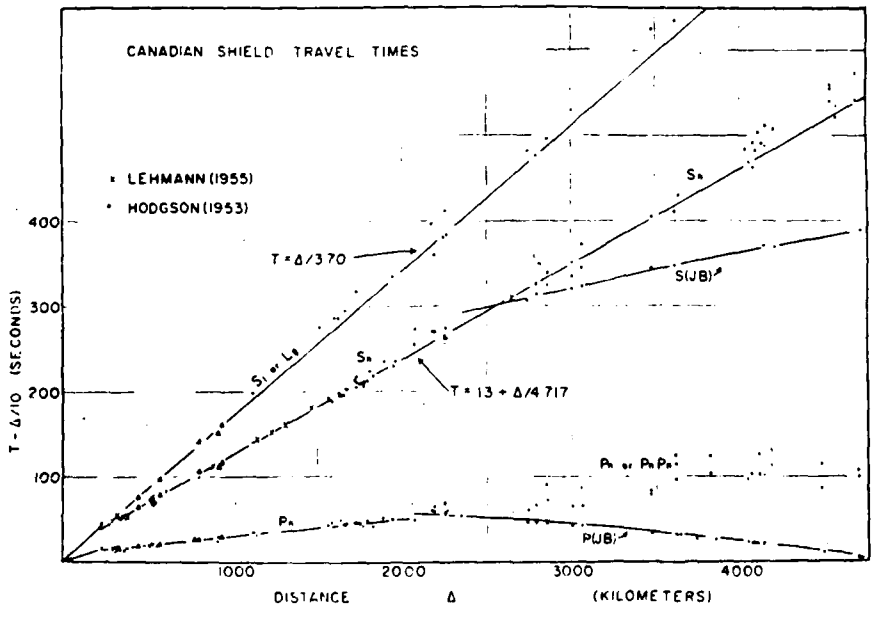

Travel-time data for the Canadian shield.

Figure 3. Signal characteristics and travel times for P_n and S_n from Brune and Dorman (1963).

The results of a study of seismic waves generated by eight nuclear explosions and recorded at 31 locations between the Nevada test site (NTS) and Ordway, Colorado, are discussed. The line of recording stations crosses the eastern part of the Basin and Range province, the Colorado plateaus, and the southern Rocky Mountains, and it extends into the Great Plains. In the eastern Basin and Range province and the western part of the Colorado plateaus ($0 \leq \Delta \leq 385$ km), the time-distance curves for P_g and P_n can be expressed, respectively, as $T_1 = 0.8 + \Delta/6.0$ and $T_2 = 5.8 + \Delta/7.6$. A third phase, tentatively identified as P^*, is represented by the equation $T_3 = 3.8 + \Delta/6.5$. Using the crustal structure and P_n velocity (7.9 km/sec) found for the NTS region by other authors, we find that the above relations indicate that the thickness of the crust increases from about 25 km at NTS to about 42 km in the western part of the Colorado plateaus. East of this boundary the velocity of P in the upper mantle increases to 8.0 km/sec; depth to the M discontinuity in the Colorado plateaus is approximately constant over the range $435 \leq \Delta \leq 645$ km. Beyond 850 km, first arrivals in the southern Rocky Mountains and Great Plains provinces indicate an apparent velocity of about 8.4 km/sec. Amplitudes of P_n attenuate according to the equation $A = A_0 \Delta^{-1/2} (\Delta - d)^{-0.7} e^{-0.0023\Delta}$ over the distance range $150 \leq \Delta \leq 850$ km ($d = 60$ km). This relation yields a value of Q, for P_n, of about 520. The amplitudes of P_g attenuate extremely rapidly, and beyond about 130 km this phase cannot be identified with certainty. An extension of the P_g travel-time branch at long distances could be associated with waves reflected beyond the critical angle, from the base of the crust. This phase, called P after Mohorovičić, appears to attenuate as $A = A_0 e^{-0.0028\Delta} \Delta^{-1.7}$. The value of Q indicated by this equation is about 200.

Nuclear Test Data

Shot	Name	Date (1962)	Location Latitude N	Location Longitude W	Origin Time, UT h	m	s	Yield, kt	Medium
I	Hardhat	Feb. 15	37°13.6′	116°03.6′	18	00	00.100	4.5	Granite
II	Chinchilla	Feb. 19	37°03.0′	116°01.8′	16	30	00.132	1.8	Alluvium
III	Cimarron	Feb. 23	37°07.7′	116°02.9′	18	00	00.160	11	Alluvium
IV	Brazos	March 8	37°07.33′	116°02.93′	18	00	00.120	7.8	Alluvium
VI	Hoosic	March 28	37°07.46′	116°02.03′	18	00	00.163	3	Tuff

Estimated Frequencies (f, cps) and Measured Amplitudes (A, mμ)

Amplitudes for shots I to V were scaled to the Hardhat explosion using shot factors; amplitudes for shot VI were shifted by an arbitrary amount to approximately scale to Hardhat.

Location Number	Shot	P_g f	P_g A	P_n f	P_n A	P^* f	P^* A
1	VI	4.0	8,100				
2	V					4.3	20,900
3	VI	4.5	434			2.2	60,700
4	VI	4.0	160				
5	VI	4.0	57.8				
6	V			2.2	1,140	2.4	3,210
8	V			2.5	147	3.0	6,440
9	III			4.0	241		
	IV			3.0	300	.5	2,530
	V			2.5	414	3.0	3,520
10	IV			3.0	222	3.0	3,890
11	VI					2.2	1,274
12	IV			3.8	153	3.0	637
13	VI					2.2	1,075
14	IV			3.6	194	3.3	765
17	IV			2.2	25.1	3.0	538
20	II			2.0	30.8		
21	I			4.0	19.5	3.0	81.0
	II			2.0	19.5	2.0	79.7
22	I			3.0	17.7	3.0	96.2
23	I			3.0	10.1	3.0	84.4
24	I			3.0	9.20	3.0	20.4
25	I			3.6	4.49	3.0	24.9
26	I					3.0	9.56
27	I					3.0	12.0
28	I					3.0	4.08

Figure 4a. Signal characteristics and amplitude distance relations from Ryall and Stuart (1963).

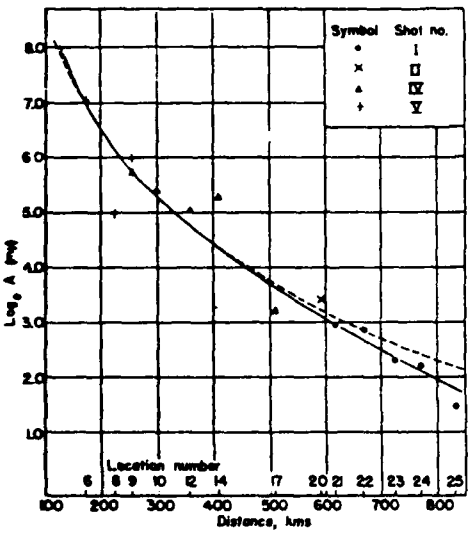

Measured amplitudes of $P_n(P_g)$ in millimicrons. Dashed line: $A = A_0\Delta^{-n}$; solid line: $A = A_0\Delta^{-1/2}(\Delta - d)^{-3/2}e^{-b\Delta}$.

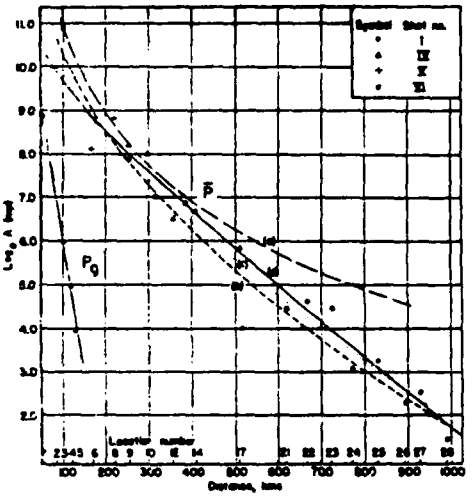

Measured amplitudes of P_g and $\bar{P}$, in millimicrons. Equations of curves: (*a*) $A = A_0\Delta^{-n}$; (*b*) $A = A_0\Delta^{-3}e^{-0.0004\Delta}$; (*c*) $A = A_0\Delta^{-1}e^{-0.0008\Delta}$; (*d*) $A = A_0\Delta^{-1/2}e^{0.0010\Delta}$.

Figure 4b. Signal characteristics and amplitude distance relations from Ryall and Stuart (1963).

Q Values for Continental Crust

Event	Phase	Region, relative to NTS	Mean Period	*Q*
Clearwater	*Lg*	ESE	1.4	430
Shoal	*Lg*	ESE	0 64	440
Aardvark	*Lg*	SE	1.1	510
Aardvark	*Lg*	NE	0.82	610
Cimarron	*Lg*	SE	0.84	380
Stillwater	*Lg*	SE	0.80	370
Ardmore	*Lg*	SE	0.8	415
				$\bar{Q}$ = 450 ± 30
Clearwater	*Pg*	ESE	0.81	180
Shoal	*Pg*	ESE	0.52	260
Aardvark	*Pg*	SE	0.82	134
Aardvark	*Pg*	NE	0.83	410
Cimarron	*Pg*	SE	0.68	205
Stillwater	*Pg*	SE	0.76	340
Ardmore	*Pg*	SE	0.76	276
				$\bar{Q}$ = 260 ± 40
Stillwater	Total Record	SE	0.66	300
	Total Record	SE	0.33	560
	Total Record	SE	0.22	780
Amarillo	Total Record	SE	0.66	320
	Total Record	SE	0.33	570
	Total Record	SE	0.22	600
				$\bar{Q}$ = 520 ± 75

Figure 5. Q and the implied amplitude distance relationships for P_g and L_g for various profiles from Press (1964).

Press' SE profile has four events, and Q varies from 370 to 510 for L_g and from 134 to 340 for P_g. Apparently there is a fair amount of scatter inherent in determinations of decay rates. The lowest Q of 134 corresponds to a period of 0.82 yielding a QT product of 109. This may be converted into a decay rate $r^{-4.6}$ which would fit fairly well the observations for $\overline{P}$ obtained from GNOME by Romney et al as seen in our Figure 2.

Nersesov and Rautian (1964) presented comprehensive results from a string of stations along the southern border of the USSR substantially within the seismically active region of the nation. The profile extended from the Pamirs on the Southwest to Lake Baikal on the Northeast.

An event on January 31, 1962 (at 00:05:57, 38.5°N, 70.3°E at 60 km depth, no reported magnitude according to NEIS) served as a reference event for this study. In Figures 6a-d we see amplitudes of $S(L_g)$, $P(P_g)$, P_n and P for this and other events as a function of distance. Analysis of the L_g data gives a decay rate of $r^{-2.1}$ out to 3000 km, and $r^{-2.3}$ out to 3500 km. This is in good agreement with average results derived from Press (1964), but is a smaller rate of decay than the r^{-3} suggested by Romney (1959).

In comparison wit[h] [R]omney et al (1962) the decay rate is much less than that of r^{-4} found on the western profile out of GNOME, but is in agreement with the Eastern profile.

Calculations based on Nersesov's composite amplitude graphs give as decay rates: L_g, 2.28 to 3000 km; P_g, 2.43 to 1500 km. Distance amplitude averages for P_n and P seem to be too erratic for meaningful averaging.

Nersesov noted that the maximum compressional amplitude on the record seemed to be a more stable measure of magnitude than any particular phase, amplitude is plotted in Figure 6d as two lines, one for earthquakes from Baikal region and one from elsewhere. He also has plotted a maximum shear wave amplitude. To a distance of 2000 km the slope for the shear wave is 2.24, and the slope for the compressional wave maximum is 2.3; with the compressional wave having perhaps 0.6 logarithmic units less amplitude than the shear maximum. (We shall see that for explosions the shear amplitude would presumably be more comparable to the compressional amplitude.)

Haskell (1964) attempted to explain theoretically the $P_g(\overline{P})$ amplitude decay rates found by Press (1964). He used elementary ray-theoretical methods to build up a picture of P_g as a superposition of leaking compressional modes.

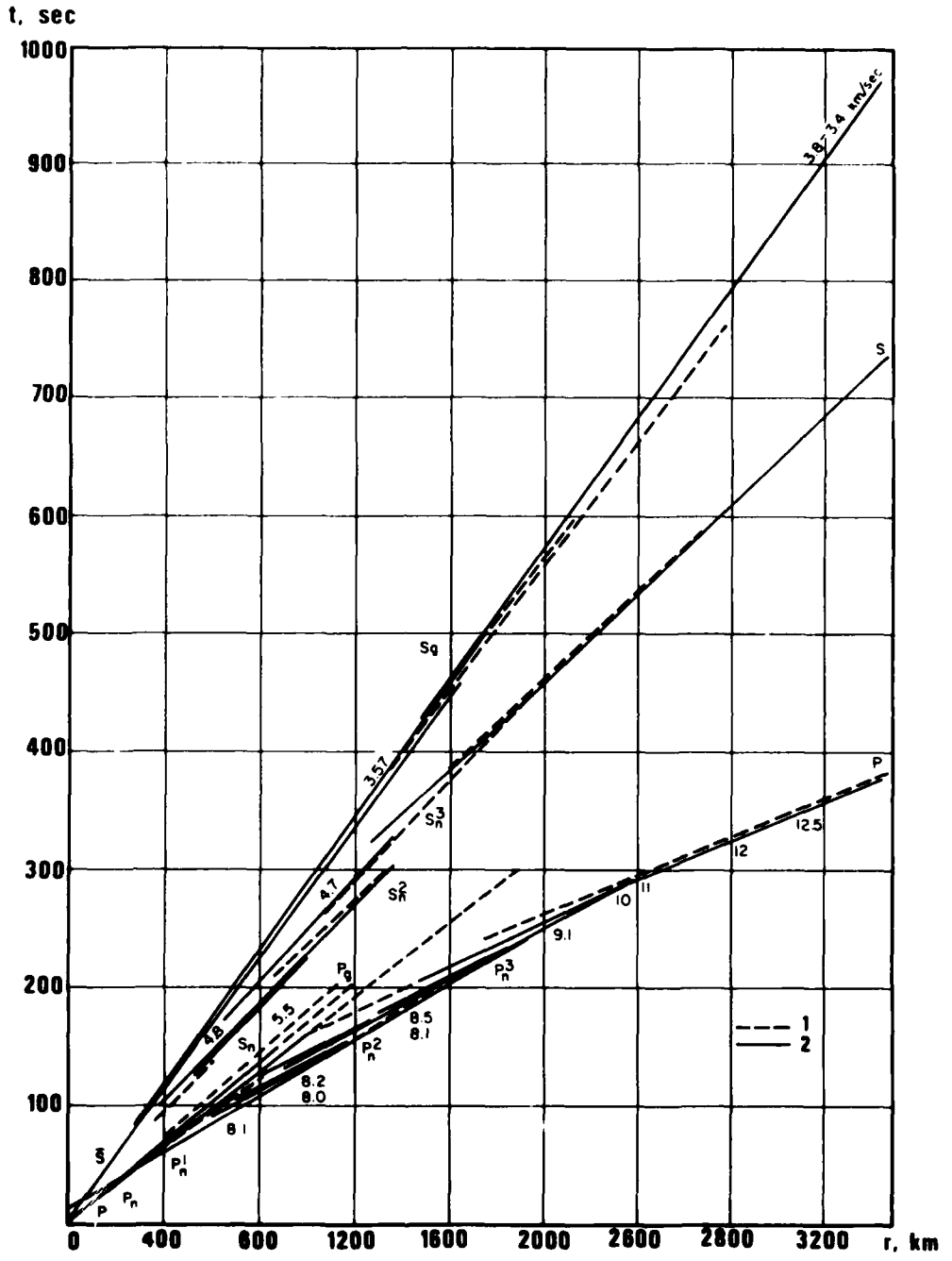

Figure 6a. Travel-time and amplitude-distance figures from Nersesov and Rautian (1964).

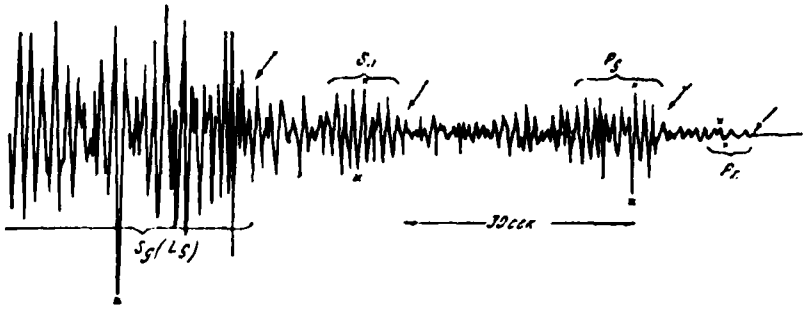

Measurement of Maximum Amplitudes

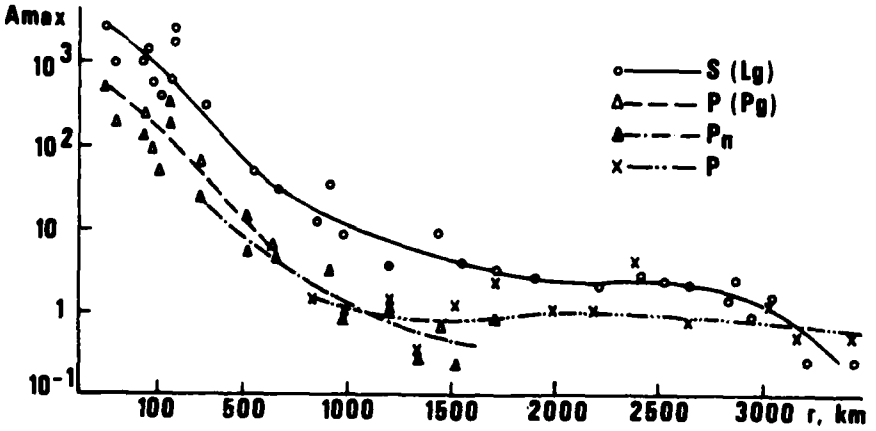

Amplitude for 31 January 1962 event

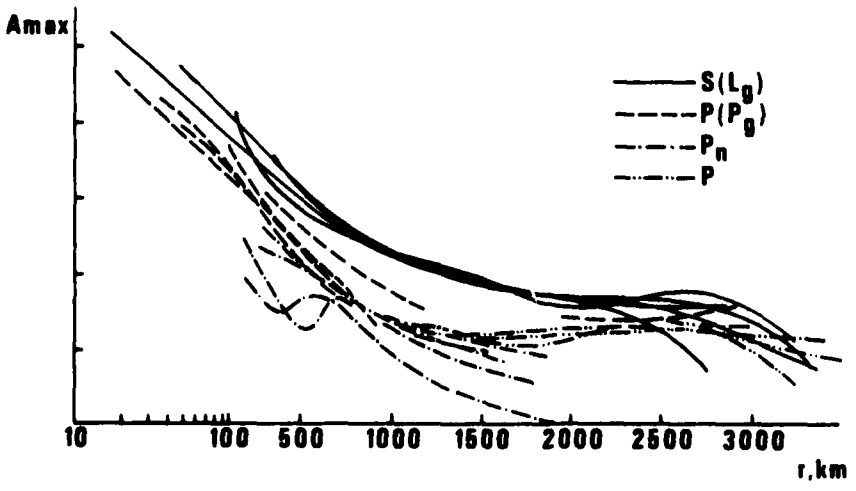

Composite Amplitudes for Central Asia

Figure 6b. Travel-time and amplitude-distance figures from Nersesov and Rautian (1964).

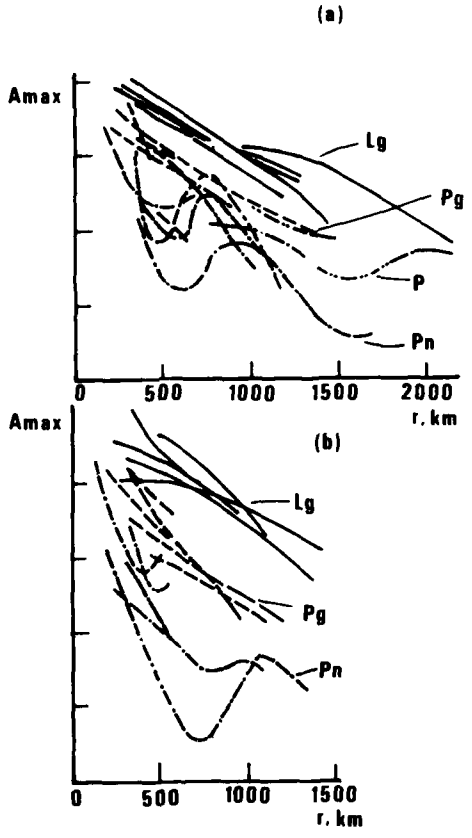

Composite amplitude curves for earthquakes of the Altai Sayan recorded to the southwest (a), and to the northeast (b).

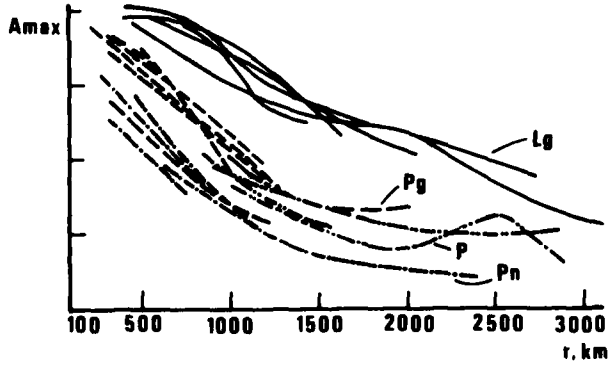

Composite amplitude curves for earthquakes of Pribaikal.

Figure 6c. Travel-time and amplitude-distance figures from Nersesov and Rautian (1964).

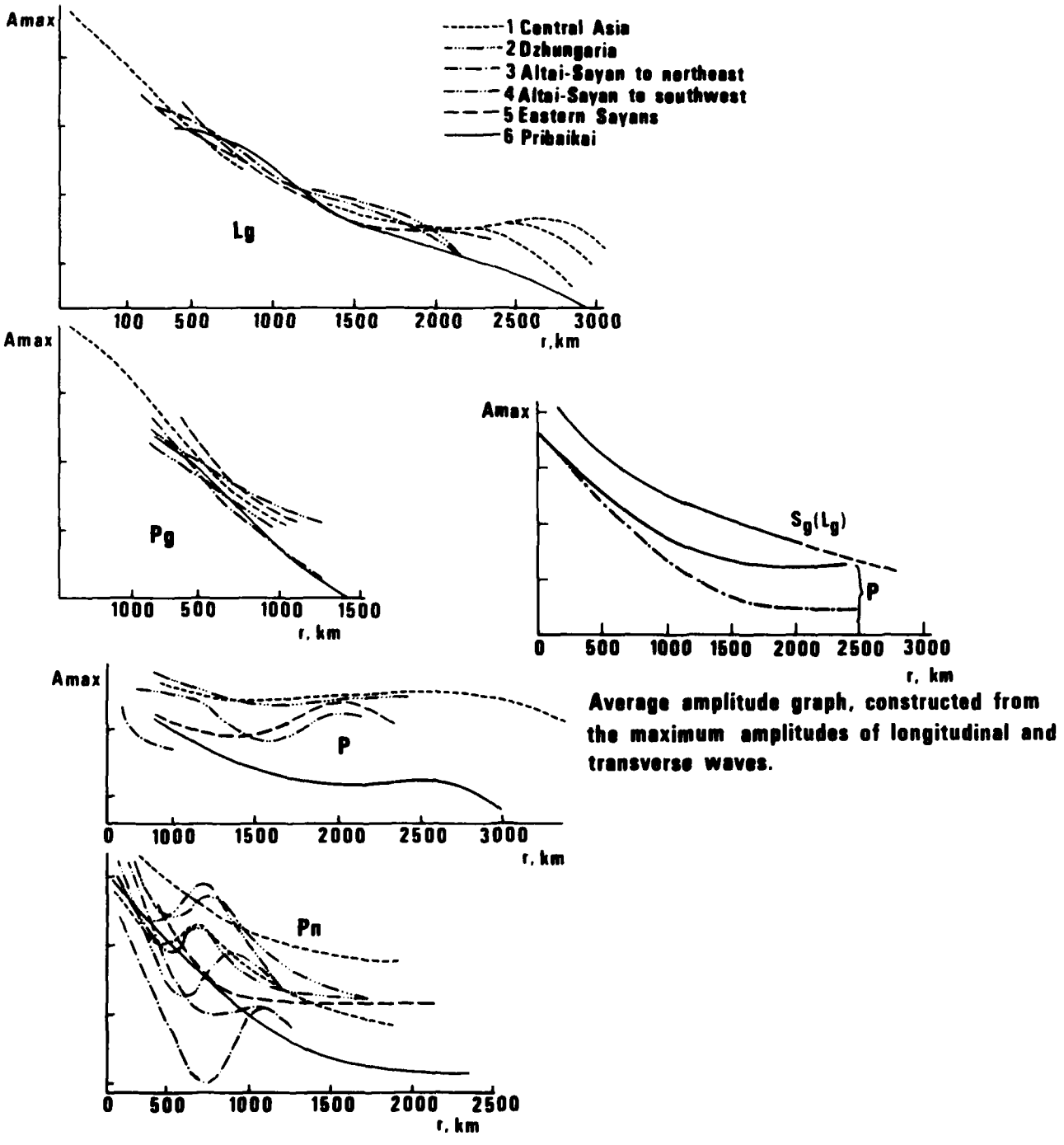

Composite amplitude graphs

Average amplitude graph, constructed from the maximum amplitudes of longitudinal and transverse waves.

Figure 6d. Travel-time and amplitude-distance figures from Nersesov and Rautian (1964).

He found that the existence of P_g could be associated with the occurrence of a common maximum in the group velocity curves for high-order multiple-P-reflection modes. It is notable that Haskell attempted to explain the Q quoted by Press of Q = 260; but since Press used too low a group velocity for P_g, the correct value for Q requiring explanation should be Q = 260 x (3.5/6.0) = 152. Haskell's theory was ray-theoretic; his calculated absorption depended exponentially upon the number of free-surface reflections encountered by each ray. Thus, the absorption was independent of frequency, and therefore, the estimated Q increased linearly with frequency. Haskell estimated a Q of 71 at 1 Hz; however, the observed dominant frequency in Press' data was 1.4 Hz, and values of 2 Hz are typically seen to be dominant in spectra. Thus one might as well have asserted that the theoretical Q was 140, in agreement with the Q (as corrected in this study) measured by Press. Thus, Haskell was not necessarily correct in asserting that a low-velocity surface layer is necessary to bring P_g theory and observation into agreement.

The situation is complicated even further by the extreme dependence of absorption on group velocity. At a distance of 1000 km the group velocity for which Haskell calculated his Q value arrives 2.8 seconds after the limiting velocity of 6 km/sec, while an arrival with twice the Q (due to fewer reflections) arrives after 1.4 seconds. Overall it does not seem possible to compare theory and observation using Haskell's theory except in the sense that it predicts a sharp arrival near the limiting velocity of P in the upper crustal layer. One must then attribute the long P_g coda often observed to multipathing, or to phases associated with multiple shallower layers or to other modes such as multiple P with one or two S legs.

Evernden (1967) published travel-time and distance-amplitude results for explosions in the WUS and EUS. In the EUS, he plotted P_n log(A/T) versus log distance and obtained the slopes shown in Figures 7a-d. The average slope was $r^{-2.0}$, and his magnitude relation was, therefore, as given in Figure 7a for m_{eus}.

Evernden asserts that investigation of P_g distance amplitude plots in many LRSM shot reports indicates that P_g decays in the WUS as r^{-3}. Plotting the interpolated P_g amplitude at 500 km versus m_b determined from regional observations using regional distance-amplitude formulas he produces Figure 7c. Regression on m_b yields a slope of 1.14; however, considering that both axes

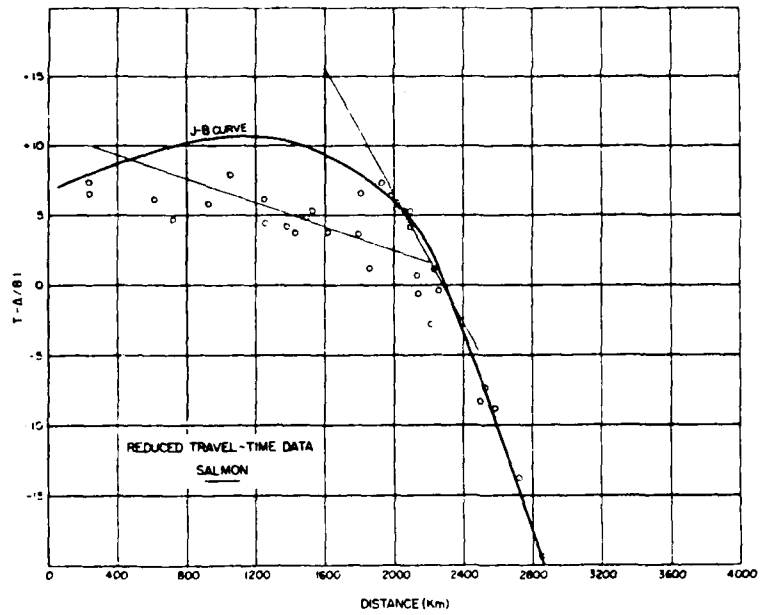

Reduced Travel-Time Data—SALMON Explosion.

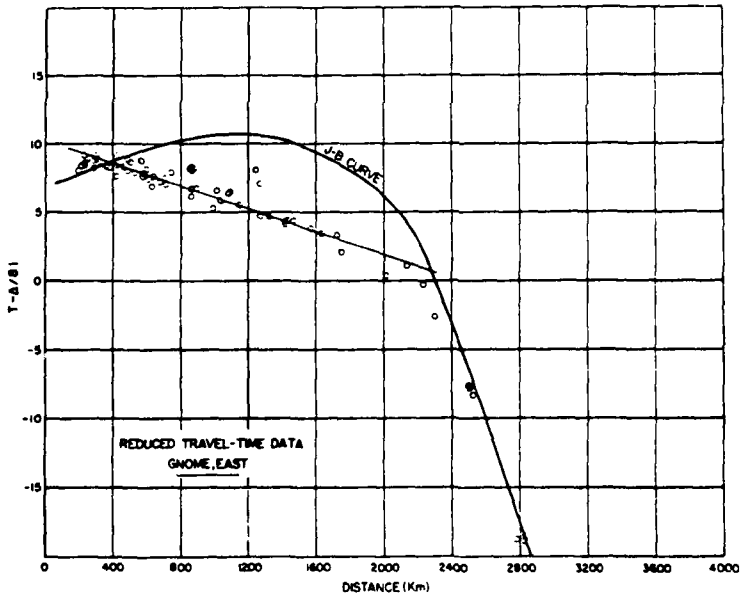

Reduced Travel-Time Data on Eastern Profile—GNOME Explosion.

	n
West Virginia Earthquake (25 Nov 1964)	−1.84 ± 0.23
Texas-Louisiana Earthquake (24 Apr 1964)	−2.26 ± 0.33
GNOME—Eastern Profile	−2.07 ± 0.39
SALMON	−2.37 ± 0.34
SS Village	−1.56 ± 0.36
Popular Bluff Earthquake (3 Mar 1963)	−1.88 ± 0.54
Average	−2.0

$$m_{rw} = m_{s.s} = -3.27 + \log A/T + 2 \log \Delta.$$

Figure 7a. Travel-time and amplitude-distance figures from Evernden (1967).

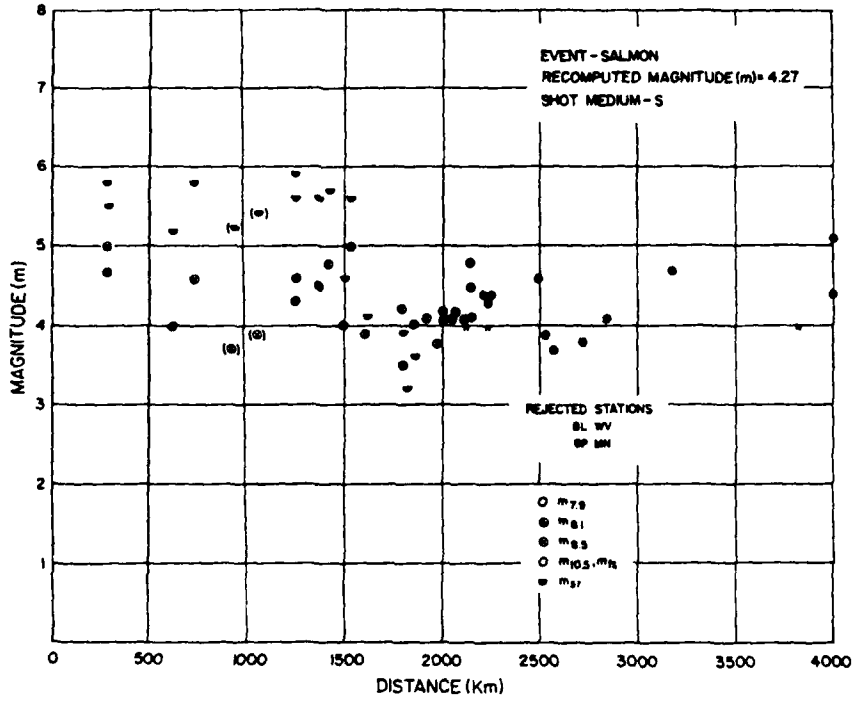

Magnitude versus Distance—SALMON Explosion.

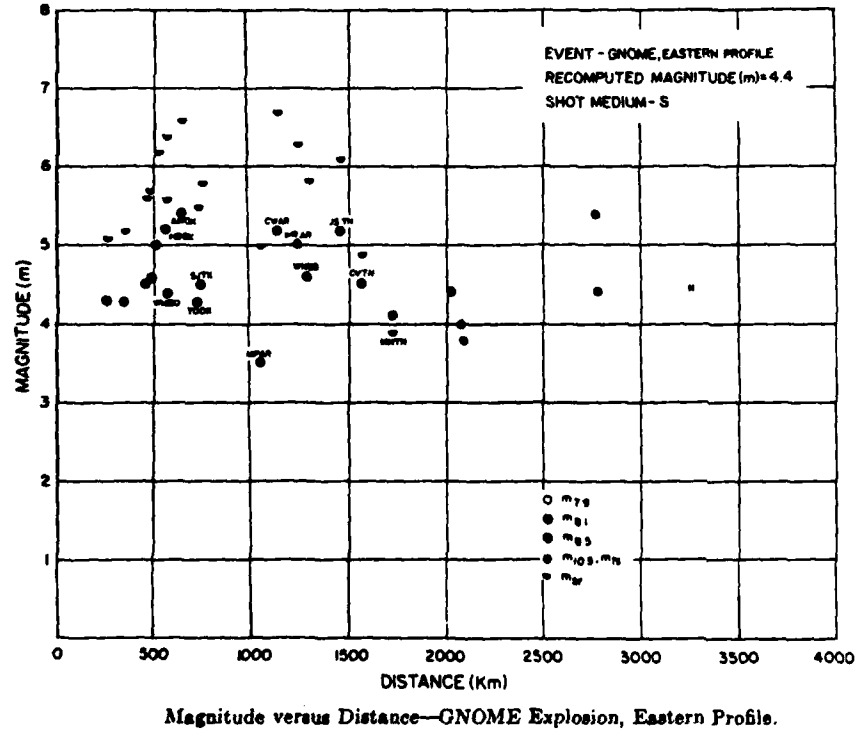

Magnitude versus Distance—GNOME Explosion, Eastern Profile.

Figure 7b. Travel-time and amplitude-distance figures from Evernden (1967).

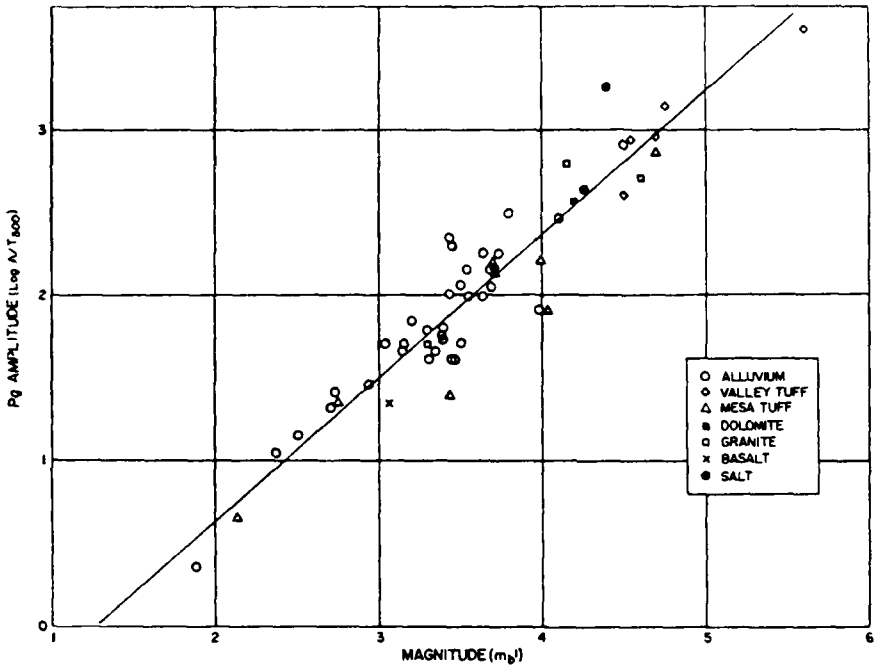

P_g Amplitudes versus $m_{b'}$.

$$m_{6.0} = 1.28 + 1.14 \log (A/T)_{500} \quad (9)$$

$$m_{6.0} = -8.00 + 1.14 \log A/T + 3.42 \log \Delta \quad (10)$$

$$m_{6.0} = 1.6 + \log (A/T) + 3 \log (\Delta/500) \quad \text{(Interpretation of this paper)}$$

Earthquakes	$(A/T)_{500}$	$m_{b'}$	$m_{6.0}$
Colona (5 Feb 1962)	40	3.1	3.11
Hebgen (25 Feb 1962)	50	3.2	3.22
Cache Creek (30 Aug 1962)	2500*	4.3	5.16
Cache Creek A/S (5 Sep 1962)	500*	4.1	4.36
Bridgeport (5 Apr 1962)	42	3.03	3.29
Fallon (20 Jul 1962)	240	4.4	4.16

* Based on WUS data.

Figure 7c. Travel-time and amplitude-distance figures from Evernden (1967).

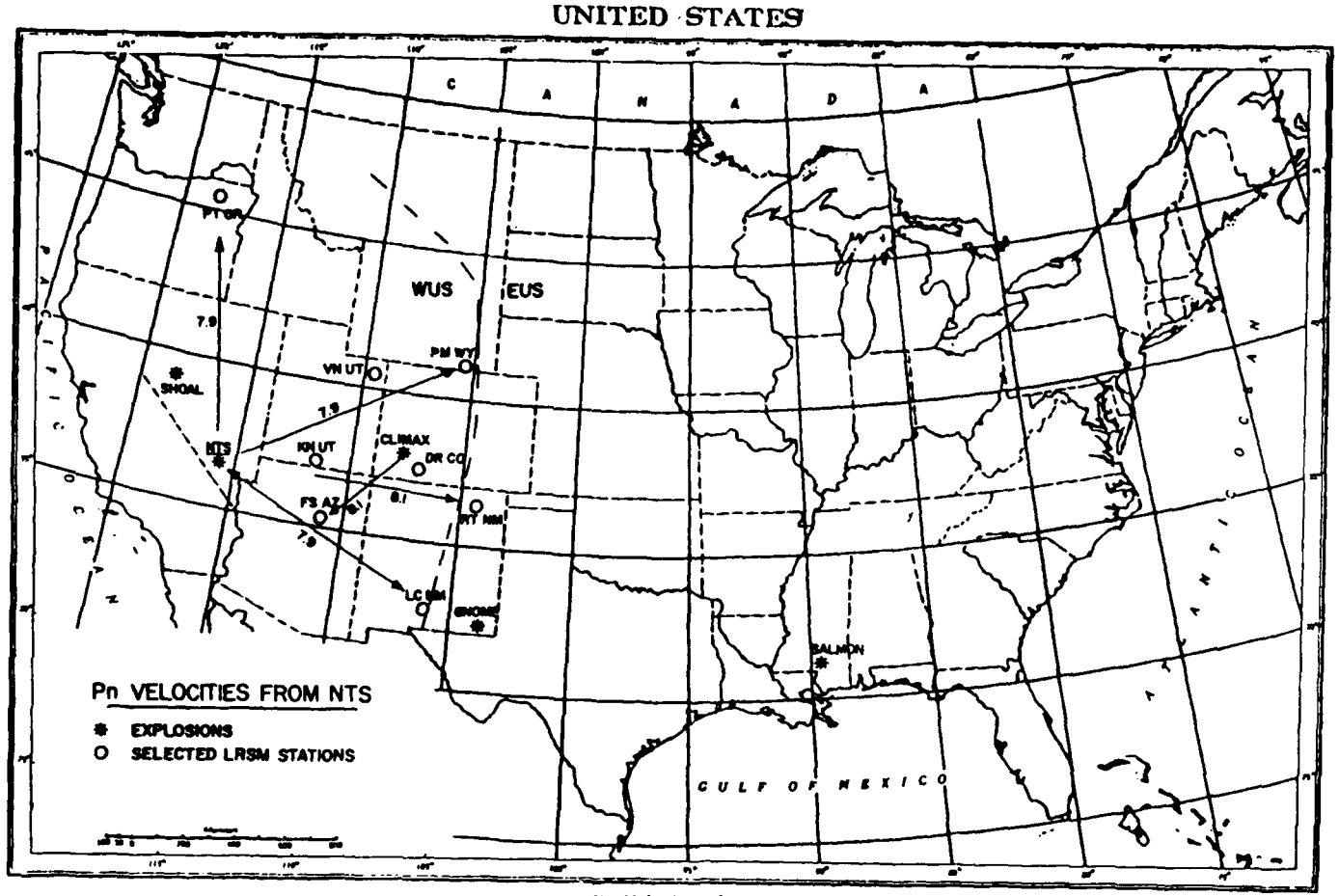

Figure 7d. Travel-time and amplitude-distance figures from Evernden (1967).

have error we cannot reject a slope of unity. Thus in place of Evernden's formula (10) as seen in Figure 7c we would write the expression immediately below it.

In the WUS Evernden concluded that the P_n phase was erratic, giving different amplitude-distance curves on different profiles, as Figure 7d attests. Evernden also asserted that the partition of amplitudes between refractors varied according to source parameters.

In 1969 Molnar and Oliver (1969) outlined the regions of favorable propagation for the phase S_n. In Figure 8 from Molnar and Oliver propagation across the Basin and Range Province in the WUS is seen to be non-existent. There is an indication that propagation is good further North along the West Coast of North America, and then becomes poor again along the concave side of the Aleutian Arc and into the Fairbanks region of Alaska. Obviously, however, more data is needed to fill out this picture.

Propagation across the Baltic Shield seems excellent, but through the mountain ranges of Southern Europe and Asia it is poor and, in particular, Molnar and Oliver state, "Moreover, paths crossing mountainous regions of Iran, Pakistan, and Turkey do not transmit S_n efficiently. There are some examples of S_n at MSH for short paths from the Hindu Kush, but in general, predominant frequencies at MSH are lower than at NDI (on the Indian Shield) for these earthquakes."

This quote would suggest that the SRO station MAIO presently co-located near MSH would be somewhat useful although not ideal for studies of earthquakes within the USSR.

In general, Molnar and Oliver discovered that S_n is not well propagated through regions which, on other grounds, are suspected of high attenuation due to melting.

Figure 9 shows results from Bollinger (1970) giving travel times for P_n, P_g, and L_g out to 1000 km in the EUS. In general, the P_g amplitude data are too sparse to permit determination of an amplitude-distance relation.

In Figure 10 we see Gumper and Pomeroy's (1970) travel-time curve for Africa.

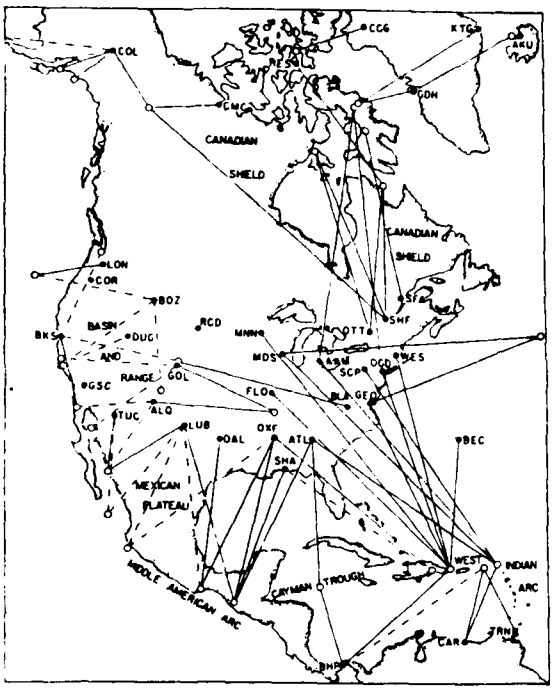

North America. Efficient transmission is indicated by solid lines; inefficient transmission, by dashed lines.

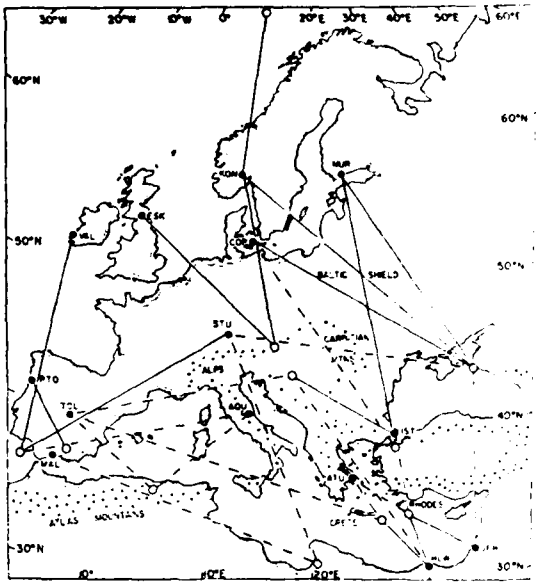

Europe.

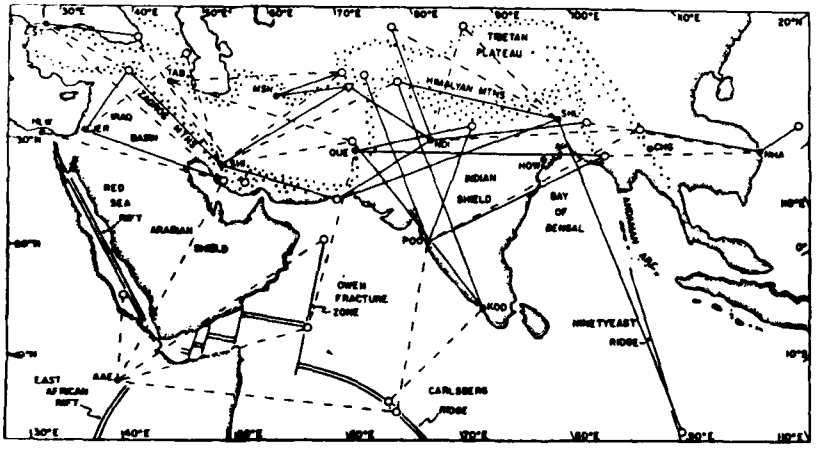

Asia and the Indian Ocean.

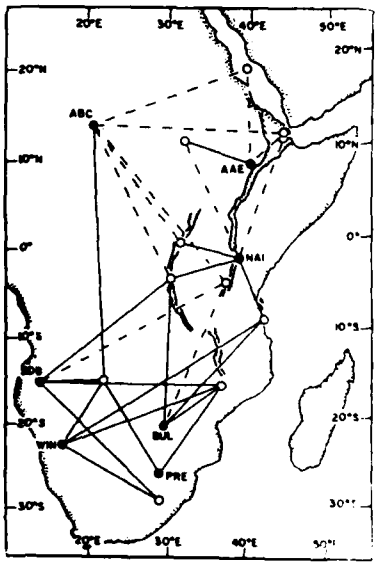

Africa.

Figure 8. Regions for good and poor propagation of S_n. (From Molnar and Oliver, 1969).

PARAMETERS FOR THE EARTHQUAKES STUDIED

No	State	Date	Latitude, Longitude (Degrees)	Origin Time (GMT)	No Sta	Std Dev TT Residuals	Magnitude Type and Source
1	Maryland	Sept 7, 1962	39 7-78 2	14-00-44.3	5	0.3	—
2	N Carolina	Oct 28, 1963	36 2-81 4	22-38-11 6	3	0.0	—
3	W Virginia	Nov 25, 1964	37 4-81 7	02-50-06 7	9	0.5	3 6, M_{LH}, Evernden (1967)
4	W Virginia	Apr 26, 1965	37 3-81 6	15-26-19 8	7	0 2	—
5	Virginia	May 31, 1966	37 6-78 0	06-19-00.5	11	1 6	3.7, M_{LH}, This Study
6	Virginia	Mar 8, 1968	37.3-80.8	05-38-15.2	7	0 4	4 1, M_{LH}, This Study

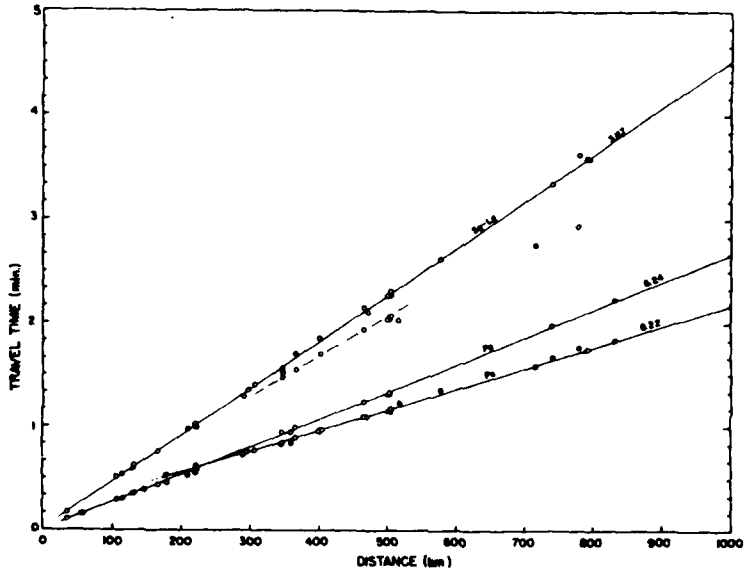

Travel time curves for six central Appalachian earthquakes, 1962-1968. (Data with center dot not used in analysis.)

MAGNITUDE DETERMINATION FOR TWO VIRGINIA EARTHQUAKES

Station	Δ(km)	Ampl. (m_μ)	T (sec)	M_{LH}
Earthquake of May 31, 1966				
BLA	221	340	0.8	4.04
SCP	358	19	0.6	3.34
ATL	739	33	1.4	3.84
WES	778	28	0.9	4.00
*WMO	1068	1.4	0.9	3.46
*RK-	1924	0.8	0.4	3.59
				Ave. 3.71
Earthquake of March 8, 1968				
*CPO	478	4.2	0.3	4.24
*WMO	1646	3.9	0.7	3.92
				Ave. 4.08

* Readings obtained from USCGS.

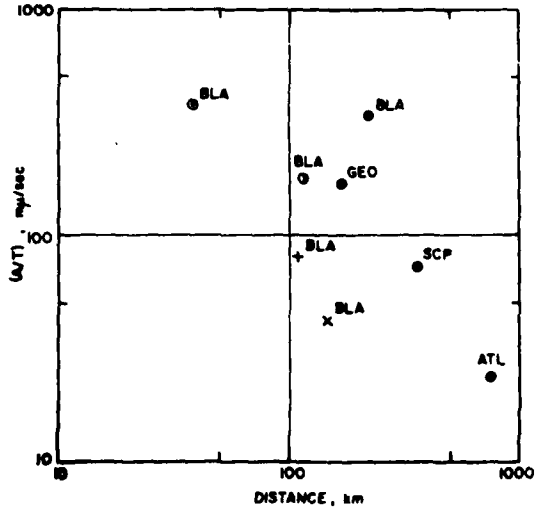

Amplitude/period versus epicentral distance for the *Pg* phase of central Appalachian earthquakes. Solid circles—May 31, 1966; Half-solid circle—Nov. 24, 1964; Circle-dot—March 8, 1968; Cross—April 26, 1965; ×—October 28, 1963.

Figure 9. Travel-time and amplitude-distance relations from Bollinger (1970).

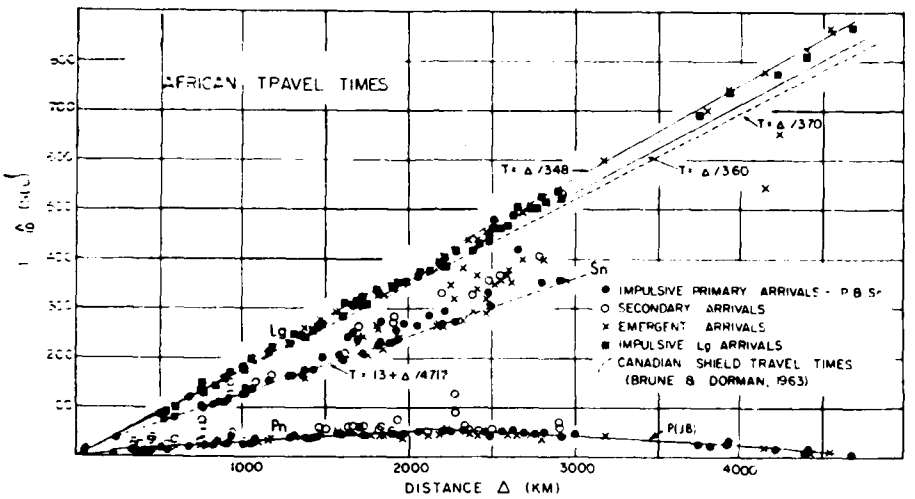

Travel-time data for the African continent. The travel-time curves $T = \Delta/3.70$ and $T = 13 + \Delta/4.717$ for the Canadian shield are shown for comparison.

Figure 10. Travel-time data for Africa from Gumper and Pomeroy (1970).

Baker (1970) (see Figure 11a-c) has published the most comprehensive data set for L_g; his data were taken from the LRSM shot reports of Nevada Test Site nuclear explosions. He concluded that the magnitudes determined from L_g showed substantially less scatter than did magnitudes determined from P_n. Baker fitted distance-amplitude relations to his event-normalized data over several distance ranges as seen in Figure 11a. Perhaps, the most trouble-free distance range is that of 200 to 2000 km. At smaller distances the number of stations is small; and possibly, some of the data could be clipped or amplitude measurements might be low because the maximum excursion was too faint on the film. At larger distances amplitudes are often enhanced by noise, only larger amplitudes are sometimes observed, and we move from the WUS to the EUS where there are different amplitude-distance relations. In the 200 to 2000 km distance range the fitted slope is -2.3, in good agreement with results derived from Press (1964) and Nersesov and Rautian (1964). Baker also presents magnitudes based on L_g, Figure 11b. He also calculated L_g station corrections (Figure 11c) and concluded that there is no apparent geographical pattern to them.

After Baker's study there are few publications in this field until Nuttli's (1973) study of earthquakes with epicenters near St. Louis. Nuttli chose to analyze the L_g phase as an Airy phase, and therefore, fit the data with an equation of the form $\Delta^{-1/3}(\sin \Delta)^{-1/2} \exp(-\gamma\Delta)$, where Δ is distance in degrees. He concluded that the data could not be fit adequately by a straight line in a log(amplitude):log(distance) plot. However, since such expressions are common in the literature, he did fit an expression of this form as seen in Figure 12. Nuttli was the first author to attach an absolute magnitude to his distance-amplitude scale. He accomplished this by connecting the L_g magnitude to that of P_n derived using the EUS formulas of Evernden (1967).

Nuttli's slope of -1.66 for L_g was not derived, but was, presumably, selected by analogy with the teleseismic formula for LR. Examination of Nuttli's Figure 12, shows that while one could not reject the slope of -1.66, the data do admit an interpretation of at least -2.0 for the distance range 3° to 30°. Even at closer distances, the only deviation from a slope of -2.0 plotted is that for the October 21, 1965 event at distances near 1.5°. One would be tempted to suspect that possibly at such close distances, the maximum excursion might be missed, or that data from clipped stations existed that could not be included in the plots.

SLOPE VALUES OF LOG A/T VERSUS LOG r FOR SEVERAL DISTANCE RANGES OF r

Approximate Range of r(km)	Slope of Best Fit Line for All Data Used*	Root Mean Square Error
50–250	−1.548	0.26788
250–500	−3.459	0.23249
200–1100	−2.710	0.26978
200–2000	−2.300	0.29621
200–4000	−2.162	0.30601
500–1500	−2.444	0.23944
1100–2500	−1.537	0.27357
1500–2500	−2.628	0.23501
2000–4000	−1.551	0.31006
2500–4000	−1.707	0.30473

* One slope and several intercepts—one for each event—were obtained for each distance range.

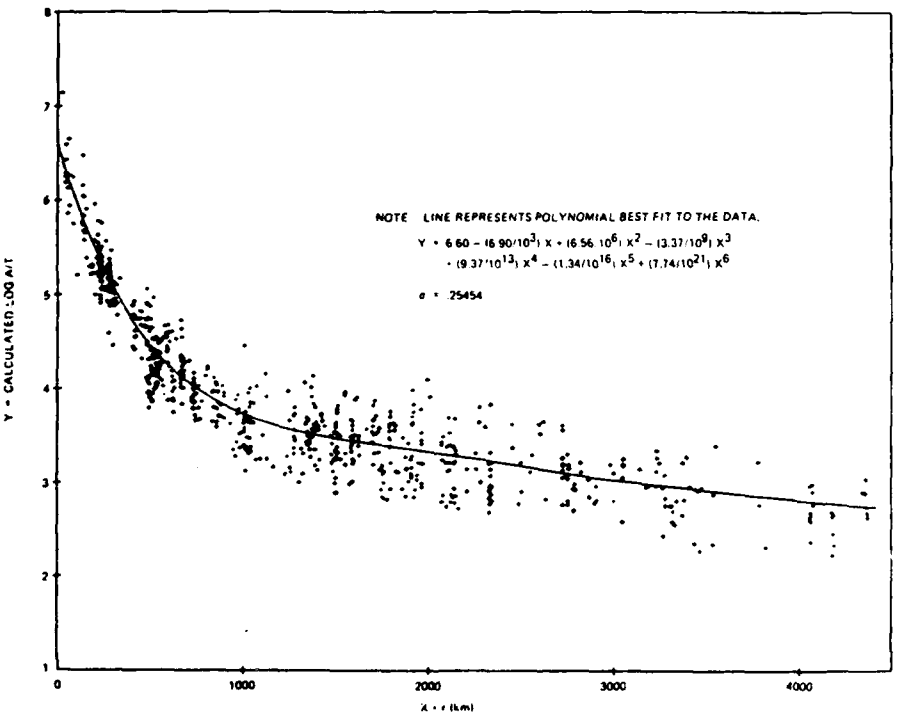

Plot of reported log A/T values versus epicentral distance.

$$Q = -0.14 + (6.90/10^3)r - (6.56/10^6)r^2 + (3.37/10^9)r^3 - (9.38/10^{13})r^4 + (1.34/10^{16})r^5 - (7.74/10^{21})r^6.$$

$$M = \log (A/T) + Q + s$$

Figure 11a. Amplitude-distance data, event magnitudes and station corrections for L_g from NTS from Baker (1970).

COMPARATIVE MAGNITUDE VALUES

Event	Calculated			Average of LRSM Station Reports		
	M	σ	Data points	m	σ	Data points
Greeley	6.39	0.259	20	6.16	0.401	22
Half Beak	5.96	0.169	17	6.02	0.597	20
Corduroy	5.84	0.217	22	5.62	0.455	28
Dumont	5.76	0.302	18	5.48	0.565	22
Bilby	5.71	0.277	21	5.74	0.351	40
Tan	5.59	0.230	17	5.56	0.486	22
Mississippi	5.40	0.295	47	5.01	0.447	51
Fore	5.39	0.277	29	5.18	0.372	39
Pile Driver	5.32	0.239	14	5.53	0.446	20
Bronze	5.31	0.169	18	5.22	0.312	31
Cup	5.27	0.217	26	5.25	0.336	31
Chartreuse	5.24	0.300	14	5.22	0.627	20
Clearwater	5.23	0.347	29	5.25	0.528	28
Chase III	5.20	0.296	18	4.63	0.532	29
Duryea	5.19	0.151	14	5.17	0.500	19
Wagtail	5.18	0.175	18	5.33	0.393	32
Buff	5.14	0.190	18	5.13	0.498	25
Klickitat	5.09	0.249	27	4.96	0.399	31
Turf	5.03	0.220	27	4.96	0.381	34
Charcoal	4.93	0.208	11	5.16	0.366	19
Haymaker	4.91	0.243	32	4.85	0.467	34
Rex	4.89	0.192	13	4.80	0.550	20
Aardvark	4.88	0.248	21	4.73	0.524	29
Salmon	4.88	0.227	17	4.58	0.739	37
Chase IV	4.87	0.309	13	4.74	0.386	16
Auk	4.83	0.247	23	4.90	0.346	30
Sedan	4.77	0.299	19	4.42	0.479	18
Par	4.75	0.180	23	4.78	0.286	30
Stones	4.74	0.305	22	4.85	0.454	27
Handcar	4.72	0.237	20	4.74	0.336	27
Pinstripe	4.65	0.180	8	4.51	0.566	15
Diluted Waters	4.63	0.286	10	4.47	0.367	23
Wishbone	4.60	0.183	17	4.84	0.358	22
Haymaker Collapse	4.57	0.266	26	—	—	—
Hardhat	4.56	0.324	31	4.91	0.698	34
Bilby Collapse	4.56	0.181	16	—	—	—
Mississippi Collapse	4.52	0.236	28	—	—	—
Shoal	4.49	0.208	14	4.91	0.347	39
Passaic	4.41	0.255	31	4.35	0.558	17
Merrimac	4.41	0.298	14	4.21	0.511	15
Dormouse Prime	4.40	0.271	18	—	—	—
York	4.32	0.263	23	4.41	0.513	22
Fisher	4.30	0.265	23	4.31	0.416	26
Marshmallow	4.29	0.114	16	4.22	0.450	22
Palanquin	4.25	0.232	15	4.33	0.364	18
Aeusiii	4.25	0.213	18	4.36	0.214	14
Hyrax	4.25	0.179	20	4.38	0.356	14
Dormouse	4.24	0.433	24	4.50	0.270	23
Peba	4.24	0.196	17	4.33	0.436	20
Madison	4.21	0.191	11	4.52	0.457	16
Casselman	4.16	0.233	18	4.58	0.333	17
Antler	4.06	0.209	6	4.69	0.728	8
Pack Rat	4.05	0.257	13	4.23	0.451	16
Agouti	4.03	0.185	18	4.49	0.247	17
Sacramento	4.02	0.183	10	4.08	0.293	8
Yuba	3.98	0.344	23	4.36	0.484	23
Des Moines	3.97	0.227	14	4.52	0.331	9
Merrimac Collapse	3.95	0.284	11	—	—	—
Platte	3.94	0.260	22	—	—	—
Codaw	3.93	0.233	18	4.32	0.343	17
Santee	3.91	0.318	16	4.10	0.211	18
Wichita	3.91	0.236	14	4.27	0.432	14
Ringtail	3.90	0.267	17	4.06	0.355	12
York Collapse	3.89	0.218	14	—	—	—
Stout	3.87	0.251	15	4.21	0.326	16
Chinchilla	3.84	0.308	20	—	—	—
Allegheny	3.84	0.352	14	4.03	0.352	11
Bobac	3.83	0.207	14	4.19	0.455	13
Kawash	3.82	0.285	18	4.11	0.262	15
Danny Boy	3.80	0.311	16	—	—	—
Red Hot	3.63	0.211	9	4.11	0.297	11
Chinchilla II	3.55	0.290	19	3.83	0.274	9
Roanoke	3.54	0.249	11	3.94	0.296	9
Mad	3.28	0.260	13	3.42	0.194	6
Small Boy	3.23	0.279	5	3.70	0.456	3
Bobac Collapse	3.17	0.230	10	—	—	—
Mink	3.14	0.416	6	3.75	0.112	6
Feather	2.66	0.280	7	3.22	0.194	6

Figure 11b. Amplitude-distance data, event magnitudes and station corrections for L_g from NTS from Baker (1970).

AVERAGE MAGNITUDES (NORMALIZED M = 5.0) AND RESIDUALS FOR STATIONS RECORDING FIVE OR MORE NTS EVENTS

	Station	Average M	Number of M's averaged	σ	Residual
AT NV	Austin, Nevada	5.26	13	0.190	0.26
AX2AL	Alexander City, La.	4.92	5	0.145	−0.09
BF CL	Bakersfield, Calif.	4.57	14	0.228	−0.43
BL WV	Beckley, W. Va.	5.16	6	0.114	0.16
BMO	Blue Mts. Obs., Oregon	5.00	25	0.172	0.00
BR PA	Berlin, Penna.	5.20	5	0.161	0.20
BX UT	Blanding, Utah	5.22	6	0.130	0.22
CP CL	Campo, Calif.	4.76	52	0.160	−0.24
CPO	Cumb. Plateau Obs., Tenn.	5.12	12	0.141	0.12
CR NB	Crete, Nebraska	5.13	8	0.135	0.13
CT OK	Clayton, Okla.	5.01	5	0.133	0.01
CU NV	Current, Nev.	4.77	6	0.214	−0.23
DR CO	Durango, Colo.	5.06	51	0.218	0.06
DV CL	Death Valley, Calif.	5.04	10	0.338	0.04
EB MT	East Braintree, Manitoba	4.78	5	0.315	−0.22
EP TX	El Paso, Texas	4.69	7	0.093	−0.31
FO TX	Ft. Stockton, Texas	4.96	6	0.204	−0.04
FM UT	Fillmore, Utah	5.03	45	0.186	0.03
FR MA	Forsyth, Mont.	5.02	5	0.195	0.02
FS AZ	Flagstaff, Arizona	4.98	45	0.156	−0.02
GE AZ	Globe, Ariz.	4.85	11	0.168	−0.15
GV TX	Grapevine, Texas	5.13	13	0.216	0.13
HB OK	Hobart, Okla.	5.21	12	0.231	0.21
HK WY	Hawk Springs, Wyo.	5.33	7	0.094	0.33
HL ID	Hailey, Idaho	4.96	52	0.147	−0.06
HL2ID	Hailey, Idaho (2)	4.91	8	0.124	−0.09
HN ME	Houlton, Maine	4.98	9	0.166	−0.02
HR AZ	Heber, Arizona	5.01	8	0.125	0.01
JP AT	Jasper, Alberta	4.86	6	0.164	−0.14
JR AZ	Jarome, Arizona	5.18	8	0.179	0.18
KC MO	Kansas City, Mo.	4.82	10	0.167	−0.18
KM CL	Kramer, Calif.	4.78	5	0.283	−0.22
KN UT	Kanab, Utah	5.11	68	0.156	0.11
LC NM	Las Cruces, N. M.	4.89	54	0.266	−0.11
LG AZ	Long Valley, Ariz.	5.11	10	0.150	0.11
ML NM	Mogollon, N. M.	4.80	6	0.105	−0.20
MN NV	Mina, Nevada	4.97	70	0.178	−0.03
MV CL	Marysville, Calif.	4.85	52	0.187	−0.15
NL2AZ	Naslini, Arizona	5.30	5	0.104	0.30
NP NT	Mould Bay, NWT, Canada	5.18	8	0.171	0.18
N2NV	Nevada Test Site	4.99	11	0.195	−0.01
PG BC	Prince George, B.C.	4.70	9	0.127	−0.30
PT OR	Pendleton, Oregon	4.79	29	0.196	−0.21
PM WY	Pole Mt., Wyoming	4.85	22	0.186	−0.15
RG SD	Redig, South Dakota	5.25	10	0.218	0.25
RK ON	Red Lake, Ontario	4.79	19	0.168	−0.21
RT NM	Raton, New Mexico	4.93	17	0.183	−0.07
RY ND	Ryder, North Dakota	5.12	6	0.133	0.12
SE MN	Sleepy Eye, Minn.	5.01	13	0.148	0.01
SF AZ	Snowflake, Arizona	5.09	15	0.100	0.09
SG AZ	Seligman, Arizona	5.01	6	0.095	0.01
SJ TX	San Jose, Texas	5.08	7	0.214	0.08
SK TX	Shamrock, Texas	5.15	5	0.048	0.15
SN AZ	Sunflower, Arizona	5.04	10	0.194	0.04
SS TX	Sanderson, Texas	4.86	33	0.343	−0.14
SV AZ	Springerville, Arizona	5.26	15	0.156	0.26
SW MA	Sweetgrass, Montana	4.98	10	0.116	−0.02
TC NM	T or C, New Mexico	5.26	13	0.117	0.26
TF CL	Taft, California	4.85	28	0.124	−0.15
TFO	Tonto Forest Obs., Ariz.	4.89	21	0.152	−0.11
TN CL	29 Palms, California	5.19	9	0.186	0.19
UBO	Uinta Basin, Obs., Utah	5.20	26	0.229	0.20
VN UT	Vernal, Utah	4.93	12	0.172	−0.06
WI NV	Winnemucca, Nevada	5.42	29	0.215	0.42
WM AZ	Williams, Arizona	5.08	13	0.176	0.08
WMO	Wichita Mts. Obs. Okla.	5.06	25	0.181	0.06
WN SD	Winner, South Dakota	5.10	16	0.151	0.10
WO AZ	Winslow, Arizona	5.06	8	0.157	0.06
MP AR	Mountain River, Ark.	5.00	13	0.183	0.00

Figure 11c. Amplitude-distance data, event magnitudes and station corrections for L_g from NTS from Baker (1970).

Epicentral Data for Earthquakes Used in This Study

Date	Origin Time, UT	Location
Nov. 9, 1968*	17h 01m 42.0s	37.95°N, 88.48°W
Oct. 21, 1965*	02h 04m 39.3s	37.51°N, 91.05°W
Aug. 14, 1965*	13h 13m 56.6s	37.23°N, 89.28°W
Mar. 3, 1963*	17h 30m 13.0s	36.7°N, 90.1°W

*From Stauder and Nuttli [1970]
†From Stauder and Nuttli [1965].
‡From Nuttli [1965]
§From Stauder and Bollinger [1963].

$$m_b = 3.75 + 0.90(\log \Delta) + \log A/T \qquad 0.5° \leq \Delta \leq 4°$$

$$m_b = 3.30 + 1.66(\log \Delta) + \log A/T \qquad 4° \leq \Delta \leq 30°$$

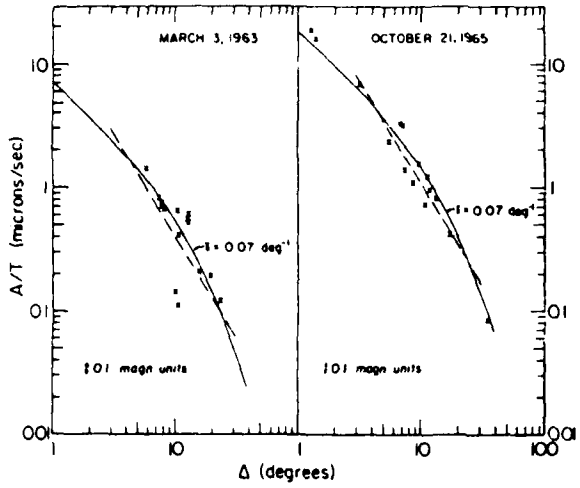

Observed A/T values of the Z component of 1-sec-period L_g waves for the earthquakes of March 3, 1963, and October 21, 1965, at stations in eastern North America. The solid line is a theoretical attenuation curve for an Airy phase with $\gamma = 0.07$ deg^{-1}. The dashed line is a straight line approximation to the theoretical curve over the distance interval $3° \leq \Delta \leq 30°$; over these distances it does not differ from the theoretical curve by more than about 0.1 magnitude unit. The arrows indicate 0.1 magnitude unit.

Body Wave and Surface Wave Magnitudes of Earthquakes

Date	M_S		m_b	
	20-Sec Teleseismic Surface Waves	3- to 12-Sec Rayleigh Waves	Teleseismic *P* Waves*	1-Sec L_g Waves
Nov. 9, 1968	5.26 ± 0.28 (2)	5.19 ± 0.19 (12)	5.50 ± 0.40 (30)	5.38 ± 0.23 (8)
Oct. 21, 1965	4.13 ± 0.32 (9)	4.09 ± 0.20 (31)	4.85 ± 0.23 (18)	5.04 ± 0.12 (14)
Aug. 14, 1965		2.54 (3)	3.81 ± 0.29 (9)	3.83 ± 0.39 (12)
Mar. 3, 1963		4.08 ± 0.20 (13)	4.76 ± 0.33 (6)	4.67 ± 0.10 (10)

Numbers in parentheses refer to number of observations.
*Also includes m_b values obtained from P_n data in the eastern United States by using Evernden's [1967] formula.

Comparison of Body Wave Magnitudes Obtained from L_g, P_n, and Teleseismic *P* Waves for Earthquakes in the Central United States

Date	Origin Time, UT	Location	m_b		
			L_g	P_n	Teleseismic *P*
Sep. 15, 1972	05h 22m 15.5s	41.6°N, 89.3°W	4.59 (7)	4.39 (7)	
June 4, 1967	16h 14m 12.8s	35.5°N, 90.9°W	4.41 (8)	4.49 (7)	4.28 (5)
Jan. 1, 1969	23h 35m 36.2s	34.8°N, 92.6°W	4.50 (9)	4.30 (9)	
July 21, 1967	09h 14m 48s	37.5°N, 90.6°W	4.37 (10)	4.21 (12)	4.55 (2)
Oct. 1, 1971	18h 49m 38.7s	35.8°N, 90.4°W	4.11 (6)	4.14 (4)	
Feb. 12, 1971	12h 44m 27.2s	38.5°N, 87.9°W	3.33 (4)	3.24 (5)	
June 9, 1972	19h 15m 19.1s	37.7°N, 90.4°W	3.27 (5)	2.96 (1)	
June 19, 1972	05h 46m 14.7s	37.0°N, 89.1°W	3.27 (5)	2.96 (1)	

Numbers in parentheses refer to the number of observations.

Figure 12. Amplitude-distance and event data for L_g from Nuttli (1963).

Bollinger (1973) published data points for L_g versus distance for three earthquakes and concluded that he could not reject Nuttli's slope of -1.66. However, we see that in Figure 13 the right-hand graph is really two earthquakes plotted as one. If the 1969 earthquake points are dropped by 0.4 magnitude units as is appropriate according to Bollinger's Table VI m_b values of 3.93 and 3.59 then the least squares slope becomes -2.03 instead of -1.63. In addition, one could not reject a slope of -2.0 through the 1969 W. Virginia earthquake.

Street (1976) determined slopes greater than 1.66 for four earthquakes in the St. Lawrence area. While some of the lowest amplitude points are from WUS stations, even in the East the slope is greater than 1.66 - perhaps approaching 2.5.

In 1977 Jones, Long and McKee published a study of attenuation in the Southeastern United States. In Figure 14 we reproduce their list of Southeastern United States earthquakes, together with reproductions of the absolute distance-amplitude curves of Richter and Nuttli. It seems to the author that one could not reject a slope of -2.0 between 4° and 9°. However, at 4° there is a striking discontinuity in the data which the authors do not discuss in detail; between 4 and 5 degrees the amplitude appears to increase by 0.5 magnitude units. This seems to be unusual behavior for a guided or surface wave. The data consists of 201 observations from 72 events; less than 3 observations per event. It seems to the present authors that this few observations per event could well lead to several biases of a statistical nature. Those of clipping, signal enhancement by noise, and missing small observations at large distances have already been discussed. The nature of errors, if any, which might result when only two observations are available (one of which must be "used up" in computation of the event magnitude) are unknown to the present authors, but the procedure seems intuitively somewhat unstable.

Ruzaikin et al (1977) have published a valuable survey of the propagation characteristics of L_g in Asia, using a technique very similar to that used by Molnar and Oliver (1969) for S_n. As we shall see later in this report, the amplitude ratio of the maximum motion after S_n to the maximum amplitude before S_n is a powerful regional discriminant, presumably because it is a measure of the ratio of shear to compressional energy at the source. Ruzaikin et al show, however, that the L_g phase, together with the R_g phase, can be drastically attenuated by structures associated with the Tibetan Plateau. The result is

Earthquakes Used for Magnitude Study

Earthquake	m_b (NOAA)	m_b (This Study)	Difference
*South Carolina May 19, 1971	3.45 n = 2	3.59 ± 0.19 n = 6	-0.14
*West Virginia Nov. 20, 1969	4.5 ± 0.4 n = 11	4.60 ± 0.30 n = 13	-0.10
Tennessee July 13, 1969	3.5 n = 4	3.96 ± 0.17 n = 6	-0.46
**Virginia May 31, 1966	3.57 ± 0.36 n = 8	3.51 ± 0.17 n = 6	+0.06
**West Virginia Nov. 24, 1964	3.62 ± 0.18 n = 9	3.42 ± 0.18 n = 4	+0.20
**Alabama Feb. 18, 1964	4.3 ± 0.7 n = 10	3.65 ± 0.78 n = 6	+0.65

* m_{sus} included in m_b (NOAA).

** Used in determination of B only; others used for both B and C determinations.

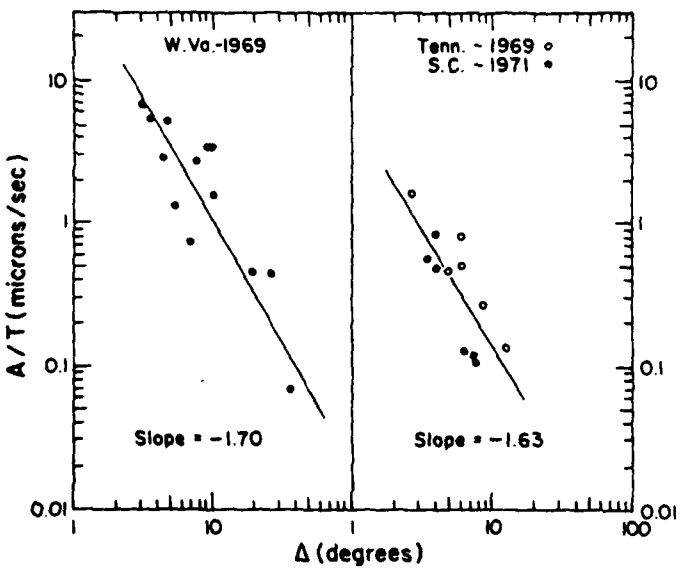

A/T versus Δ *plots for* three southeastern United States earthquakes. *A* is the maximum amplitude (microns) of the L_g phase on the short-period vertical seismogram and *T* is the corresponding period in seconds. Δ is the epicentral distance in degrees.

Figure 13. Event magnitude and amplitude-distance data from Bollinger (1973).

EVENTS WHICH OCCURRED IN THE SOUTHEASTERN UNITED STATES BETWEEN 1963 AND 1975

Event	Date	Latitude °N	Longitude °W	Origin Time UTC h	m	No. of Stations	Calculated Magnitude	Reported Magnitude
1	4 May 1963	32.2	79.7	21	01	2	3.3 ± 0.02	
2	6 Oct. 1963	33.92	82.51*	06	01	3	3.2 ± 0.25	
3	28 Oct. 1963	36.7	81.0	22	38	2	2.9 ± 0.08	
4	17 Feb. 1964	34.7	85.4*	22	47	2	3.3 ± 0.21	
5	18 Feb. 1964	34.8	85.5	09	31	4	4.2 ± 0.10	4.4 m_b
6	7 Mar. 1964	33.82	82.5*	12	03	3	3.3 + 0.15	
7	13 Mar. 1964	32.9	83.4	01	20	3	3.9 ± 0.15	4.4 m_b
8	20 Apr. 1964	34.0	81.1	19	05	2	3.5 ± 0.04	
9	12 Jun. 1965	34.5	83.8*	10	30	2	1.9 ± 0.05	
10	20 Jun. 1965	34.3	87.1*	12	30	3	2.6 ± 0.21	
11	9 Sep. 1965	33.5	80.8	14	42	3	3.9 ± 0.07	
12	10 Sep. 1965	33.5	80.8	02	32	3	3.0 ± 0.23	
13	12 Sep. 1965	34.8	81.3	18	25	4	2.9 ± 0.27	
14	8 Nov. 1965	34.2	82.8*	12	57	3	3.0 ± 0.05	
15	31 May 1966	37.6	78.0	06	19	2	4.1 + 0.12	3.1 m_b
16	29 Jun. 1967	33.6	90.9	13	57	2	3.6 ± 0.07	3.4 m_b
17	23 Oct. 1967	33.41	80.71	09	04	4	3 9 ± 0.21	3.8 m_b
18	10 Feb. 1968	36.54	89.90	01	34	4	4.3 ± 0.08	3.8 m_b
19	8 Mar. 1968	37.0	80.5	05	38	2	4.1 ± 0.18	3.9 m_b
20	22 Sep. 1968	34.0	81.5	21	41	2	3.5 ± 0.07	3.7 m_b
21	9 May 1969	33.92	82.5*	12	13	2	3.1 ± 0.14	
22	13 Jul. 1969	36.4	83.7	21	51	4	4.2 ± 0.10	3.5 m_b
23	20 Nov. 1969	37.4	81.0	01	00	2	4.7 ± 0.19	4.8 M_L, CGS
24	11 Dec. 1969	37.8	77.4	23	44	2	3.4 ± 0.06	4.3 m_b
25	13 Dec. 1969	35.08	83.04	10	19	4	3.7 ± 0.15	
26	30 Jul. 1970	37.01	82.25	18	48	5	3.3 ± 0.17	3.8 m_b
27	30 Jul. 1970	37.01	82.25	15	15	5	3.7 ± 0.11	4.0 m_b
28	31 Jul. 1970	37.7	83.4*	00	31	2	3.5 ± 0.14	
29	10 Sep. 1970	36.1	81.4	01	41	4	3.2 ± 0.13	
30	17 Nov. 1970	35.9	89.9	02	13	3	4.5 ± 0.06	3.6 m_b
31	14 Mar. 1971	33.1	87.9	17	27	2	3.6 ± 0.29	3.9 M_L, NOS
32	16 Mar. 1971	33.1	87.9	02	37	3	3.3 ± 0.19	
33	19 May 1971	33.3	80.56	12	54	2	3.9 ± 0 10	3.4 m_b
34	29 May 1971	36.0	82.0*	21	21	2	2.9 ± 0.08	
35	10 Jun. 1971	34.7	82.9*	04	19	3	2.8 ± 0.19	
36	13 Jun. 1971	33.7	86.6*	01	17	2	2.9 ± 0.03	
37	13 Jun. 1971	36.0	83.9	02	02	2	3.0 ± 0.04	
38	13 Jul. 1971	34.7	82.95	09	39	2	2.8 ± 0.13	
39	13 Jul. 1971	34.7	82.95	10	54	2	2.9 ± 0.12	
40	13 Jul. 1971	34.7	82.95	11	07	2	2.7 ± 0.02	
41	13 Jul. 1971	34.7	82.95	11	42	3	4.4 ± 0.10	
42	13 Jul. 1971	34.7	82.95	11	49	3	2.9 ± 0.06	
43	13 Jul. 1971	34.7	82.95	15	06	2	3.0 ± 0.17	
44	31 Jul. 1971	33.7	80.66	20	16	4	4.0 ± 0.16	
45	12 Sep. 1971	38.1	77.4	00	06	2	3.4 ± 0.08	
46	1 Oct. 1971	35.8	90.4	18	49	2	3.9 ± 0.08	4.11 M_{bLg}
47	9 Oct. 1971	35.9	83.5	16	43	2	4.0 ± 0.07	3.4 m_b
48	22 Oct. 1971	36.0	83.0	21	55	3	3.3 ± 0.11	
49	1 Feb. 1972	36.25	90.9	05	42	3	4.0 + 0.06	4.1 m_b 3.9 M_L, SLM
50	3 Feb. 1972	33.5	80.4	23	11	4	4.3 ± 0.16	4.5 m_b
51	7 Feb. 1972	33.46	80.58*	02	46	4	3.2 ± 0.02	

Figure 14. Event list and amplitude-distance data from Jones and Long (1977).

Event	Date	Latitude °N	Longitude °W	Origin Time UTC h	m	No. of Stations	Calculated Magnitude	Reported Magnitude
52	7 Feb. 1972	33.46	80.58°	02	53	4	3.2 ± 0.08	
53	29 Mar. 1972	36.2	89.6	20	38	2	4.1 + 0.05	3.7 m_b
54	5 Sep. 1972	37.6	77.7	16	00	2	3.6 ± 0.04	3.3 M_{bLg}, BLA
55	25 May 1973	33.9	90.8	14	40	2	2.7 ± 0.04	
56	27 Oct. 1973	28.7	81.0	06	21	2	3.5 ± 0.17	
57	30 Oct. 1973	35.7	84.0	22	58	4	3.5 ± 0.13	3.4 M_{bLg}, SLM
58	30 Nov. 1973	35.8	84.0	07	48	5	4.5 ± 0.16	4.6 M_{bLg}, BLA
59	14 Dec. 1973	35.7	83.8°	20	58	4	3.1 ± 0.08	
60	19 Dec. 1973	33.0	80.3	10	16	2	3.0 ± 0.12	
61	8 Jan. 1974	36.2	89.39	01	12	3	4.4 ± 0.04	4.3 M_{bLg}, SLM
62	12 Mar. 1974	35.66	89.79	12	30	2	3.3 + 0.09	4.1 m_b 3.2 M_{bLg}, SLM
63	13 May 1974	36.71	89.39	06	52	2	4.1 ± 0.01	4.1 M_{bLg}, SLM 3.8 $m_{b\ sus}$
64	30 May 1974	37.38	80.42	21	28	2	3.7 ± 0.22	3.6 M_{bLg}, BLA
65	2 Aug. 1974	33.87	82.49	08	52	4	4.3 ± 0.12	4.9 M_{bLg}, GS 4.3 m_b 4.8 M_{bLg}, SLM
66	22 Nov. 1974	32.9	80.15	05	25	3	4.4 ± 0.08	4.7 m_b
67	10 Dec. 1974	31.3	87.5	06	01	4	3.5 ± 0.02	3.0 M_{bLg}, SLM
68	25 Dec. 1974	35.78	90.01	13	21	2	3.0 ± 0.03	3.0 ML
69	1 Mar. 1975	33.55	87.99	11	50	2	4.1 ± 0.26	3.2 M_{bLg}, SLM
70	1 Apr. 1975	33.2	83.2°	21	09	2	3.9 ± 0.43	
71	24 Jun. 1975	33.72	87.84	11	11	2	3.7 ± 0.03	4.5 m_b
72	29 Aug. 1975	33.82	86.6	04	22	4	4.4 ± 0.27	4.4 M_{bLg}, SLM 3.5 m_b

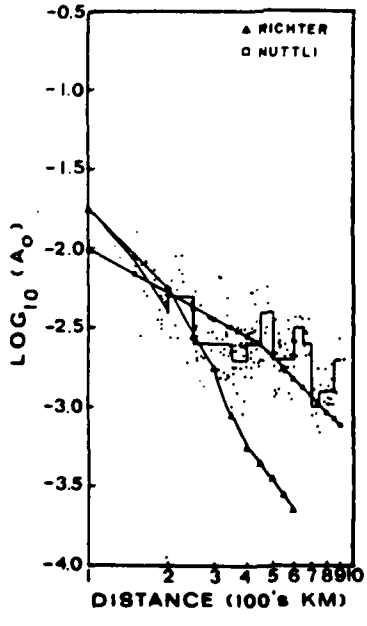

Figure 14(Cont.). Event list and amplitude-distance data from Jones and Long (1977).

that earthquake signals which pass through such structures are recorded looking like explosions. For example, comparison of Figures 15a-d from Ruzaikin et al shows this effect. Signals 1-11 are recordings similar to those seen in the EUS from WUS earthquakes. Signals 13 through 15 are similar to typical explosion records, and Signals 16 through 19, although they are from earthquakes, are more explosion-like than those from any explosion we have observed in the United States.

Figures from Ruzaikin et al show the character of received L_g signals at stations TLG, NSB, and BDN. Figure 15d from Ruzaikin et al shows some of the obstacles to efficient L_g propagation. Figures similar to these will be required for accurate application of the L_g phase as a discriminant.

Bollinger (1977) has measured L_g amplitudes and periods for the list of events shown in Figure 16. He used Nuttli's (1970) formula to compute station magnitudes and then plotted the normalized amplitudes as a function of distance. For 4° to 30° we have fitted a least-squares slope of -2.1 as indicated in the figure. At shorter distances, the slope seems less, but again, one must worry about clipping and missed maximum cycles at such distances for events of magnitude above 4.0 and there are 6 such events in Bollinger's data set.

Tables I, II, and III give a summary of the amplitude-distance exponents implied by the papers reviewed thus far, together with the exponents which we have determined in this paper from Western United States and Eastern United States data. In general the results found in this study are compatible with those found by earlier workers.

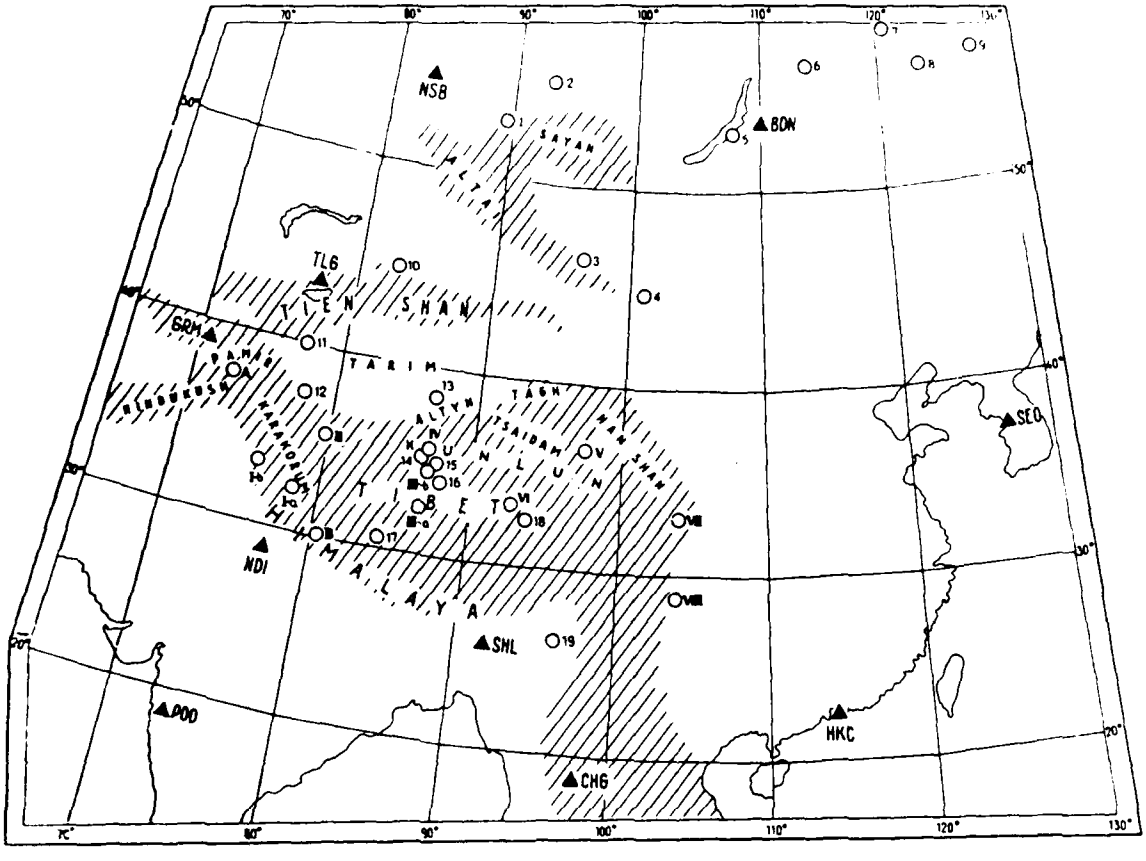

Map of Asia showing stations used; epicenters of earthquakes for which seismograms are shown in Figures 2 (Arabic numerals), 3 (Roman numerals), and 4 (A and B); and areas of high mountains (hatched regions).

Figure 15a. L_g propagation characteristics in Asia according to Ruzaikin et al (1977).

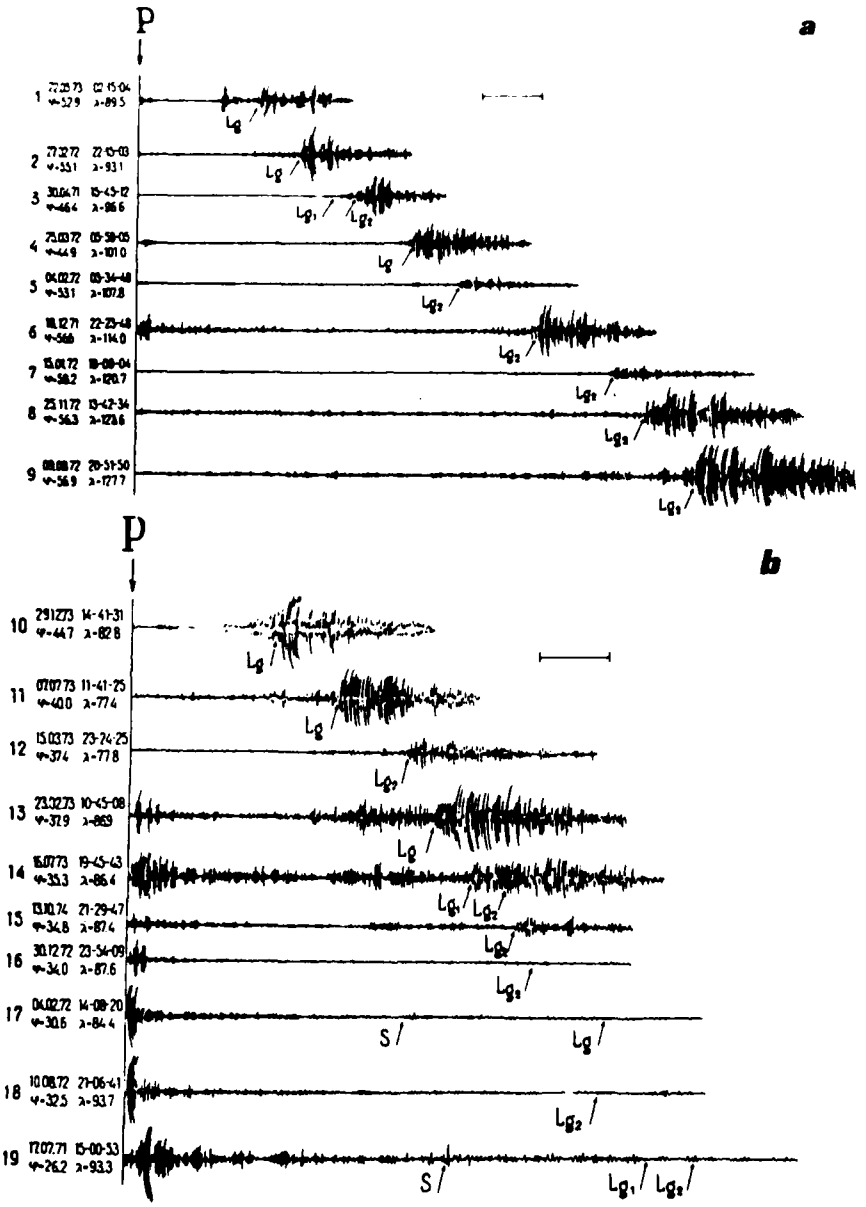

Seismogram of selected events (Arabic numerals in Figure 1) recorded at a temporary station between Talgar (TLG) and Novosibirsk (NSB). Events 1-9 are a profile extending east to Baikal, and events 10-19 a profile to the south. Recordings are from a narrow band system between 1.4 and 2.3. Scale at upper right shows 1 min.

Figure 15b. L_g propagation characteristics in Asia according to Ruzaikin et al (1977).

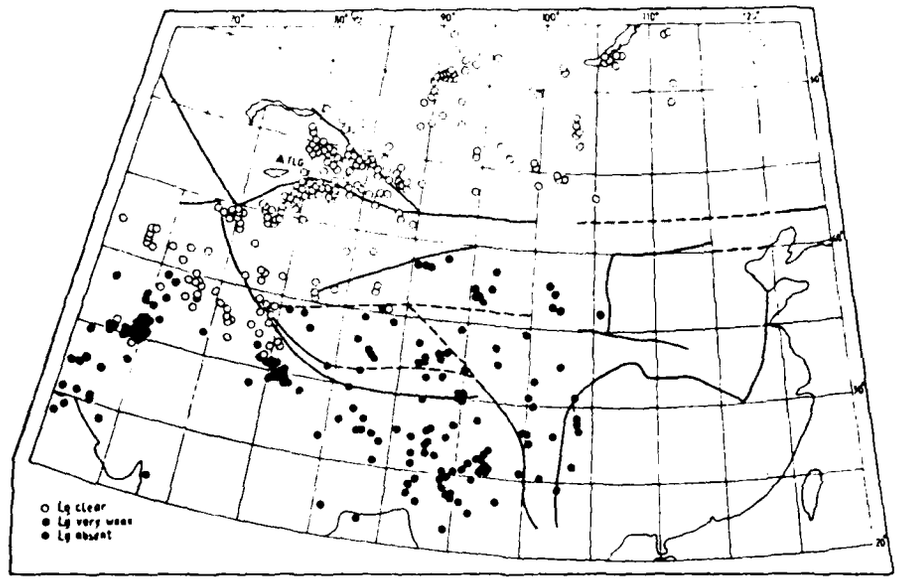

Map of earthquakes for which Lg is clear, weak, or absent on seismograms recorded at Talgar (TLG). Heavy lines indicate faults shown on the Soviet tectonic map of Asia.

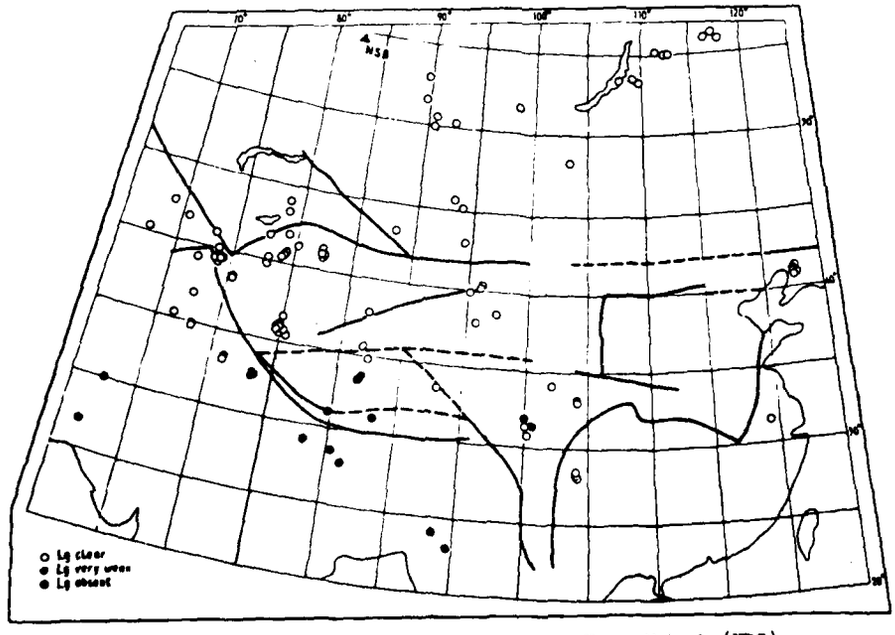

Same as Figure 5a but for Novosibirsk (NBS).

Figure 15c. L_g propagation characteristics in Asia according to Ruzaikin et al (1977).

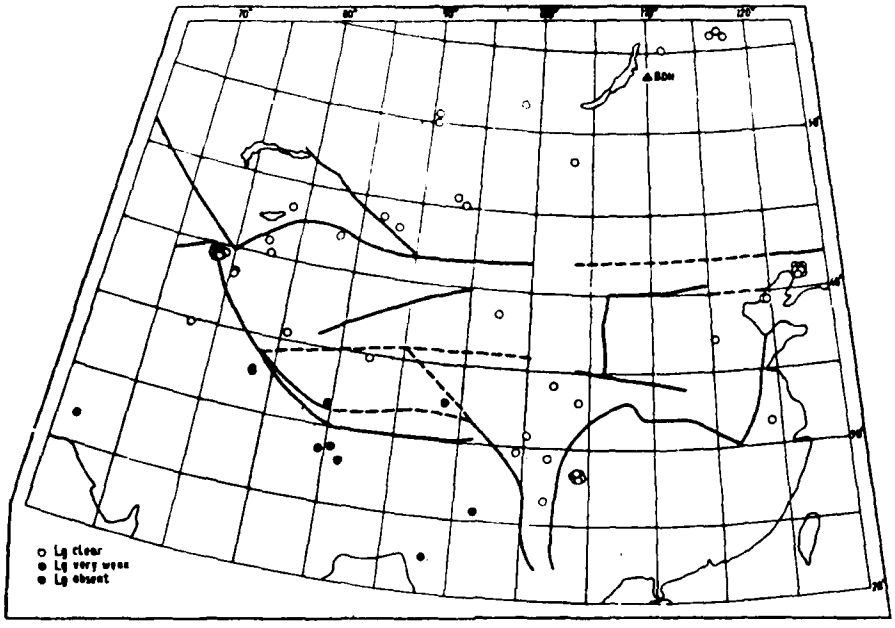

Same as Figure 5a but for Bodon (BDN).

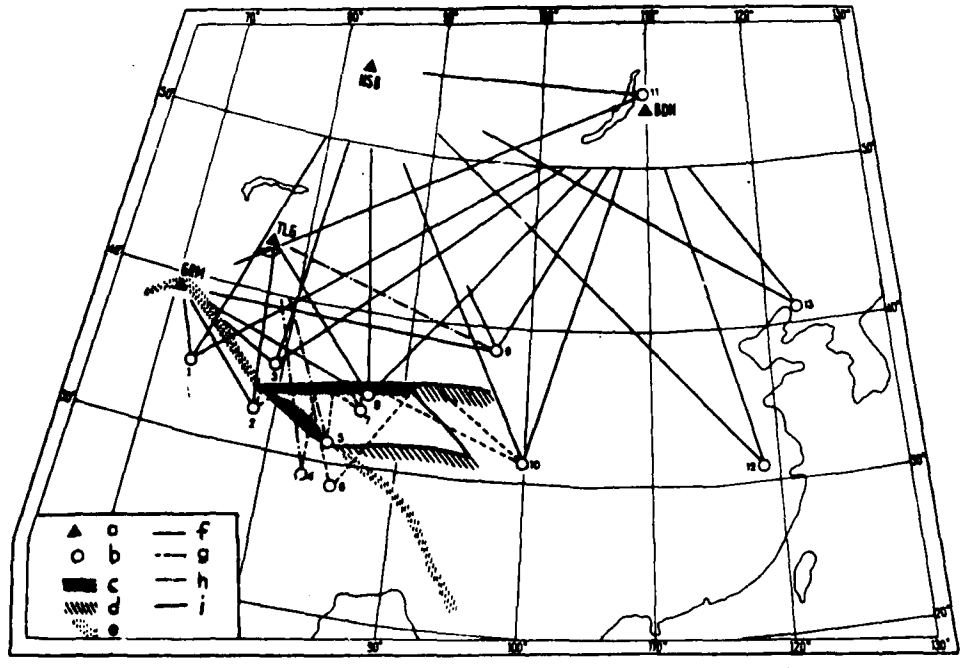

Map showing interpretation of selected paths to Soviet stations: (a) triangles, stations; (b) circles, epicenters; (c) dense hatching, apparent sharp boundaries of Lg propagation; (d) open hatching, less sharp boundaries; (e) dashed hatching, presumed southern boundary; (f) solid line, clear Lg; (g) dashed line, no Lg; (h) dotted-dashed line, weak Lg; and (i) heavy dark line, selected faults on the Soviet tectonic map.

Figure 15d. L_g propagation characteristics in Asia according to Ruzaikin et al (1977).

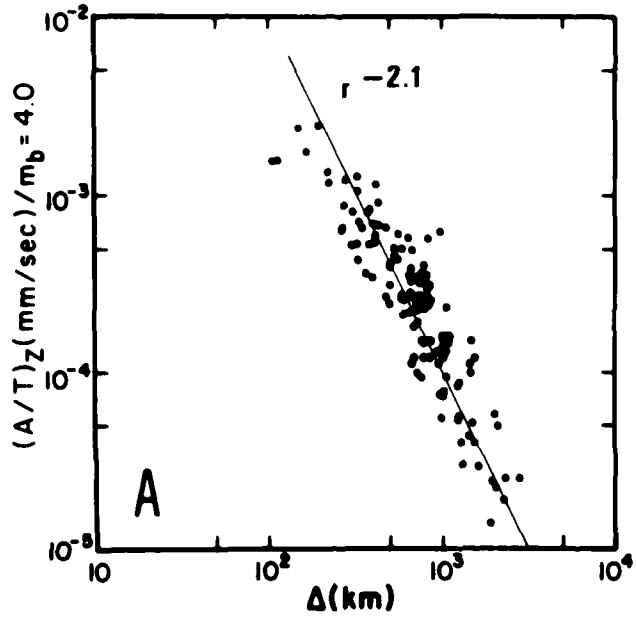

PARAMETERS OF THE SOUTHEASTERN U.S. EARTHQUAKES FOR WHICH *Lg* ATTENUATION DATA WERE OBTAINED IN THIS STUDY

Date	State	Origin Time (UTC)	Epicenter (°N, °W)	m_b*	N†
Feb. 18, 1964	GA	09:32:12	34.8-85.5	4.0 ± 0.2	8
Nov. 25, 1964	WV	02:50:07	37.4-81.7	3.6 ± 0.2	13
Apr. 26, 1965	WV	15:26:20	37.3-81.6	3.5 ± 0.2	7
May 31, 1966	VA	06:19:02	37.6-78.0	3.6 ± 0.2	9
Oct. 23, 1967	SC	09:04:10	33.4-80.7	3.4 ± 0.2	9
Jul. 13, 1969	TN	21:51:09	36.1-83.7	4.2 ± 0.2	8
Nov. 20, 1969	WV	01:00:10	37.4-81.0	4.6 ± 0.3	13
Dec. 13, 1969	NC	10:19:34	35.1-83.0	3.4 ± 0.1	8
Sep. 10, 1970	NC	01:41:10	36.1-81.4	3.1	4
Mar. 14, 1971	AL	17:27:52	33.1-87.9	3.6 ± 0.2	7
May 19, 1971	SC	12:54:03	33.3-80.6	3.7 ± 0.2	7
Jul. 13, 1971	SC	11:42:26	34.8-83.0	3.8 ± 0.3	7
Oct. 9, 1971	TN	16:43:34	35.9-83.5	3.7 ± 0.2	7
Feb. 3, 1972	SC	23:11:08	33.5-80.4	4.5 ± 0.1	8
Nov. 30, 1973	TN	07:48:41	35.8-84.0	4.6	4
Aug. 2, 1974	GA	08:52:10	33.9-82.5	4.1	3
Nov. 22, 1974	SC	05:25:56	32.9-80.1	4.3 ± 0.2	5

* Nuttli (1973) *Lg* formula used to determine the individual stations's m_b.
† Number of stations averaged to obtain the listed m_b's.

Figure 16. L_g amplitude-distance relations from Bollinger (1977).

TABLE I

Decay Rate for P_n

Author	Range (km)	x in r^{-x}	Comments
Romney (1959)	200-800	3.0	Low values at 1000 km, if these points neglected -2.0 works to 2000 km. Profile to Texas and on to Maine. Blanca and Logan (WUS)
Romney et al (1962)	200-1000	3.0	EUS and WUS from GNOME (WUS)
Ryall and Stuart (1963)	200-800	3.3	WUS, NTS to Colorado
Nersesov (1964)		1.6	Southern border USSR, very erratic from Nersesov Figure 6
Evernden (1967)		2.0	EUS 8.5 km/sec refractor
Evernden (1967)	200-1000	3.04	WUS 7.9 km/sec refractor
	1000-1800	2.0	WUS 8.5 km/sec refractor
This study	200-2000	2.5	EUS
	200-1000	3-4 ?	WUS

TABLE II

Decay Rate for P_{max}

Author	Range (km)	x in r^{-x}	Comments
Romney et al (1962)	500-1500	4	GNOME $\overline{P}$
Ryall and Stuart (1963)	200-1000	3.5	This study, fit to P data
Press (1964)	?	3.2	This study, fit for derived Q
Nersesov (1964)	~ 200-1500	2.4	This study, fit to P_g curves
Nersesov (1969)	200-2000	2.3	This study, fit to P_{max} curves
Nersesov (1964)	200-2000	3.1	This study, fit to P_{max} (Pribaikal earthquake)
Evernden (1967)	~ 200-1000 ?	3.0	P_g
This study	200-2000	2.5	EUS
	200-1500	3.0	WUS

TABLE III

Decay Rate for $L_g(R_g)_{max}$

Author	Range (km)	x in r^{-x}	Comments
Richter (1958)	200-600	3.0	WUS
Romney (1959)	200-2000	3.0	WUS, all 3 components, Blanca, Logan
Romney et al (1962)	500-3000	2.0	EUS GNOME
Romney et al (1962)	500-1500	4.0	WUS GNOME
Press (1964)	?	2.2	WUS, this study fit for derived Q
Nersesov (1964)	200-2000	2.3	USSR
Baker (1970)	250-500	1.55	WUS
Baker (1970)	250-500	3.46	WUS
Baker (1970)	200-1100	2.71	WUS
Baker (1970)	200-2000	2.30	WUS
Nuttli (1973)	50-400	0.9	EUS
Nuttli (1973)	400-3000	1.66	EUS (slope assumed and not rejected)
Bollinger (1973)	300-3000	2.0	EUS, cannot reject this slope
Street (1976)	400-3000	~ 2.5	EUS, fit by eye, this study. St. Lawrence earthquake
Jones and Long (1977)	400-900	2.0	EUS, cannot reject this slope
Bollinger (1977)	150-3000	2.0	EUS, cannot reject this slope
This study	250-2000	2.0	EUS
This study	200-1500	3.0	WUS

Discrimination

Willis, DeNoyer and Wilson (1963) and Willis (1963) showed that, although there is some overlap, the ratio of the maximum of the "shear-type" waves to the maximum of the first 10 seconds or so of the compressional motion is greater for earthquakes than for explosions. This is as recorded at distances less than 10° and for frequencies from 0.5 to 10 Hz. Distance corrected network averages are not discussed in these studies; only population means or single-station-event measurements as a function of distance or frequency.

Booker and Mitronovas (1964) used stations in the general range of 15° to define average energy ratios of different phases (velocity windows). Fair discrimination was achieved using ratios of shear to compressional phases. This is the only study in the literature to use network-averaged short-period discriminants.

Lambert and Becker (1975) used vertical records of regional events recorded at NORSAR to show that there is some suggestion that the shear to compressional ratio is greater for earthquakes than for explosions.

Bakun and Johnson (1970), using a rather small sample of natural earthquakes, found that at a regional station natural earthquakes have less high frequency in the P_g phase than do NTS explosions. However, aftershocks of the explosions were similar to the earthquakes. Other workers, Peppin and McEvilly (1974), Murphy (1976) found no spectral discrimination. Peppin (1977 personal communication) has said that use of Bakun and Johnson's discriminant failed on the "natural" Massachusetts Mountain earthquakes at NTS south of Yucca Flats.

Pasechnik (1970) showed travel times for P and S phases out to 200 km and asserted that S/P amplitude ratios are less for explosions than for earthquakes. He also plotted P wave periods for earthquakes and explosions as a function of distance in the range 250 to 800 km. The explosion periods are strikingly shorter. This may be due to earthquakes being located in tectonic regions while explosions are located in stable regions.

DISTANCE AMPLITUDE

Tables IV and V are lists of the earthquakes and explosions analyzed in this study for the purpose of determining accurate amplitude-distance relationships and to determine the ability to use regional phases for discrimination. One of the most illustrative events is the Hebgen Lake earthquake of 1964. This event is almost exactly on the border between the Western United States (WUS) and Eastern United States (EUS) "absorption regions" as characterized by Der, Massé and Gurski (1975). See, e.g., their Figures 12 and 13.

Thus waves from this event offer an excellent opportunity to see the difference in attenuation between the EUS and WUS. In fact, in Figure 17 we see that a decay rate of -3 is appropriate for L_g in the WUS and a value of -2 in the EUS. We also see very vividly how the first arrival on the southeast profile, at GVTX, has a low amplitude which may be understood by virtue of the fact that this path is along the EUS-WUS boundary as delineated by Der et al (1975). The large value at NPNT may be partially understood in that the measured period at this station was 2 seconds, leading to a large period correction for the amplitude. Note that the EUS decay seems to be similar to that in the USSR.

In Figure 18 we see a similar plot for P_{max} and see that the difference between EUS and WUS is not as large as for L_g; the data are consistent with -3 for WUS and -2.5 for EUS. Note that the P_{max} decay for the EUS seems to be similar to that in the USSR.

In Figure 19 we see the amplitude as a function of distance for both L_g and P_{max} for the event SALMON and the closely matched 18 February 1964 Alabama earthquake. Signals from SALMON passed almost directly through the epicenter of this earthquake, only 5° to the Northeast on the way to stations BLWV, BRPA, DHNY, LSNH, and HNME. A particularly well-matched set of stations are BRPA, approximately 8° from the earthquake, and BLWV approximately 10° from SALMON. We shall make extensive use of the recordings of SALMON at BLWV and 18 February at BRPA in comparisons of the two events.

As an indication of the discrimination capabilities of the two phases we see in Figure 19 that although the L_g amplitudes are of equal level for the two events the P_{max} amplitude for SALMON is on the average 0.3 magnitude units (mu) above that of 18 February. We see also from this figure that the slopes of 2.0 and 2.5 for L_g and P_{max} seem appropriate.

TABLE IV

List of earthquakes

Earthquakes - West

Date	Identifier	Lat (N)	Long (W)	O.T.	Log P_{max}	L_g	No. (Stns)	m_b	Event No.
20 Jul 62	Fallon	39.6	118.2	09:02:08.8	1.70	2.01(5)		4.4	1
06 Jan 64	W. Idaho	44.3	114.6	19:35:09.8	0.92	1.31(7)		4.7	2
04 Aug 64	Colorado	39.7	106.0	11:13:25.0	0.52	0.62(4)		4.0	3
21 Oct 64	(W) Hebgen Lake	44.8	111.6	07:38:31.0	2.27	2.41(12)		5.8	4
05 Feb 64	Central CA	35.1	118.8	19:45:58.0	0.28	0.51(6)		4.5	5
14 Sep 65	Colorado	39.7	104.8	22:46:24.1	1.59	1.82(4)		4.7	6
09 Aug 67	Denver	39.9	104.7	13:25:06.2	2.05	2.41(6)		5.3	7
05 Aug 71	Mass Mtn (NTS)	36.9	116.0	17:58:17.1	0.90	1.32(4)		4.3	8

Earthquakes - East

02 Feb 62	New Madrid	36.3	89.4	06:43:28.8	1.99	2.53(12)		N/A	1
10 Apr 62	NY - VT	44.1	73.1	14:30:46.4	1.80	2.43(3)		N/A	2
27 Jun 62	S. Illinois	37.7	88.5	01:28:55.7	1.69	2.37(6)		N/A	3
16 Oct 63	Mass Coast	42.5	70.8	15:31:02.0	1.45	2.04(5)		4.5	4
04 Dec 63	NH	43.6	71.5	21:32L35.1	1.05	1.51(3)		4.5	5
18 Feb 64	Alabama	34.8	85.5	09:31:10.5	1.58	2.11(5)		4.4	6
13 Mar 64	Georgia	33.2	83.4	01:20:18.1	1.24	1.85(3)		4.4	7
21 Oct 64	(E) Hebgen Lake	44.8	111.6	07:38:31.0	2.55	2.95(16)		5.8	8
25 Nov 64	W. VA	37.4	81.5	02:50:05.0	1.28	1.99(4)		4.5	9
31 May 66	Virginia	37.6	78.0	06:19:02.1	1.69	2.02(4)		3.1	10

TABLE VII

List of explosions

Date	Identifier	Lat (N)	Long (W)	O.T.	Log P_{max}	L_g	No. (Stns.)	Comments
10 Dec 61	GNOME	32.3	103.9	19:00:00.0	2.50 2.04	2.28(E) 1.95(W)	(8) (7)	Salt
15 Feb 62	HARDHAT	37.2	116.1	18:00:00.0	1.73	1.48	(17)	NTS, Granite
14 Apr 62	PLATTE	37.2	116.2	18:00:00.0	0.86	0.86	(18)	Tunnel, NTS Tuff
05 Jun 63	YUBA	37.2	116.2	17:00:00.0	0.92	0.97	(15)	Tunnel, NTS, Tuff
13 Sep 63	BILBY	37.1	116.0	17:00:00.0	2.66	2.68	(4)	NTS, Tuff
26 Oct 63	SHOAL	39.2	118.4	17:00:00.0	2.00	1.72	(6)	Close to FALLON earthquake, Granite
22 Oct 64	SALMON	31.1	89.6	16:00:00.0	2.04	2.10	(16)	Salt, near Alabama earthquake
12 May 65	BUTEO	37.2	116.4	18:15:00.1	1.22	0.84	(10)	NTS, Tuff, small & deep
10 Dec 67	GASBUGGY	36.7	107.2	19:30:00.1	2.00	1.69	(7)	Shale, deep
10 Sep 69	RULISON	39.4	107.9	21:00:00.1	2.54	2.13	(2)	Sandstone, deep
19 May 72	MONERO	37.06	116.0	17:00:00.1	1.41	1.47	(5)	Tuff, closest NTS explosion to Mass. Mountain earthquake

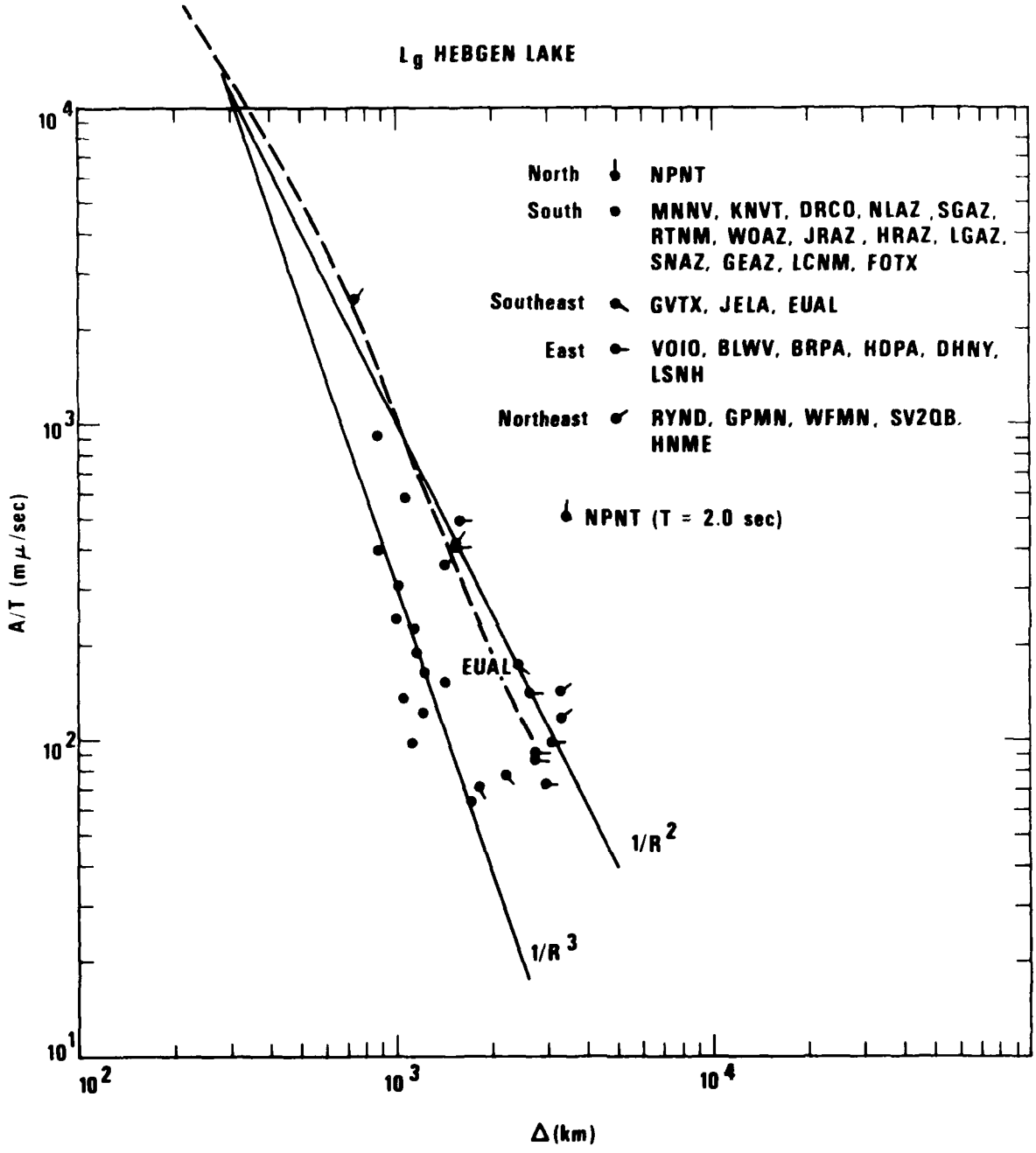

Figure 17. Attenuation of L_g from the Hebgen Lake earthquake of 21 October 1964, located on the EUS-WUS boundary according to Der et al (1975). Different decay rates are seen along the profiles within the EUS and WUS. Dashed line is from Nersesov and Rautian (1964); for S_g and (L_g) average see our Figure 6d.

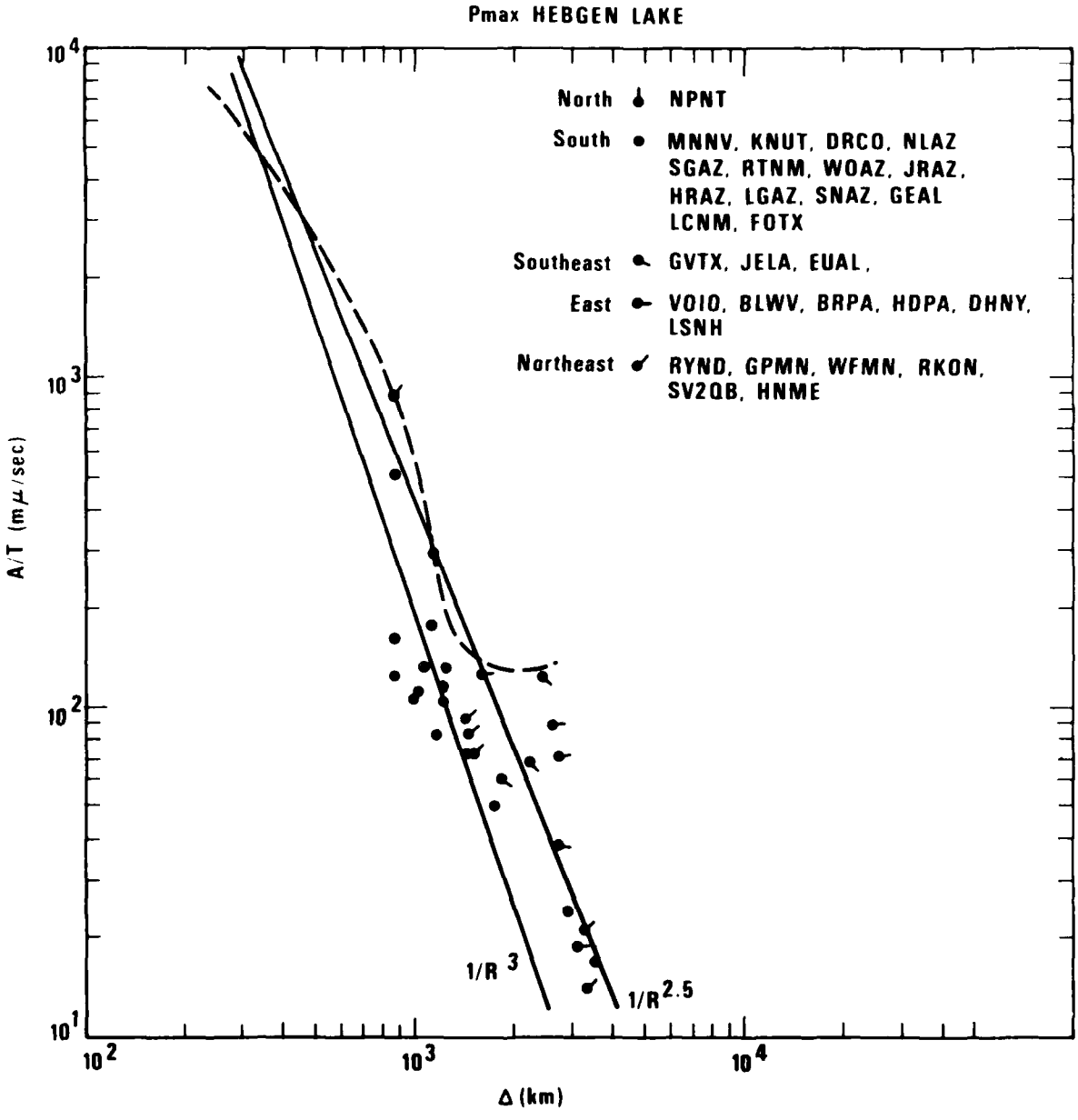

Figure 18. Attenuation of P_{max} from the Hebgen Lake earthquake of 21 October 1964, located on the EUS-WUS boundary according to Der et al (1975). Different decay rates are seen along the profiles within the EUS and WUS. The dashed line is from Nersesov and Rautian (1964) for P_{max} except for Pribaikal. See our Figure 6d.

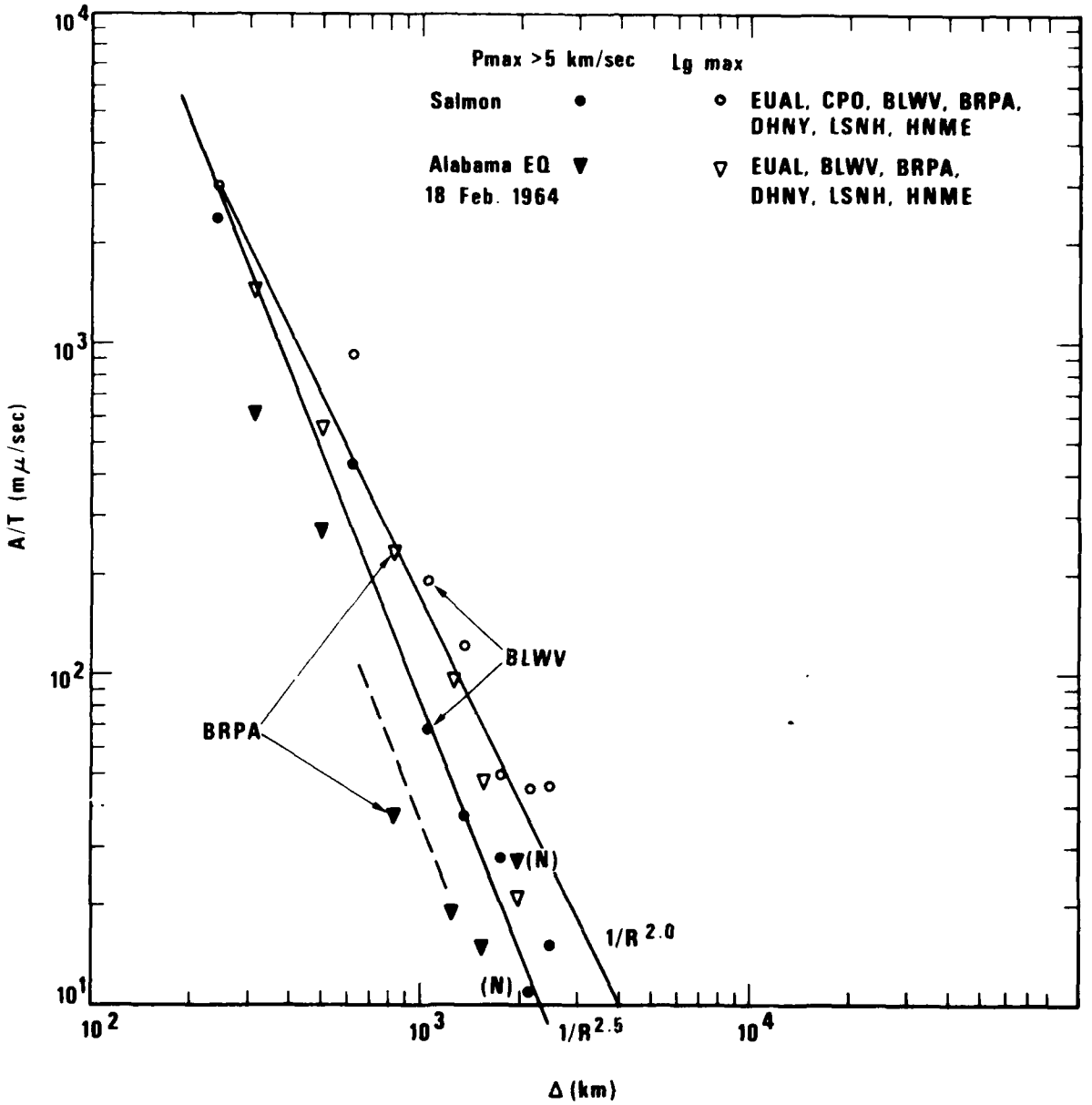

Figure 19. Amplitude-distance relations for P_{max} and L_g along the Northeast profile for SALMON and the 18 February 1964 Alabama earthquake. The two events are seen to have approximately equal L_g amplitude but the P_{max} is less for the earthquake than for the explosion. Also, the two phases are seen to fall off with distance at rates consistent with -2.0 for L_g and -2.5 for P_{max}.

Since the event SALMON is of special interest as the only EUS explosion, we shall include in the body of this report, the P and L_g plots of amplitude data for all profiles out of the epicenter. The P data, separated into first arrival P and P_{max} readings, is found in Figure 20. A least-squares slope of -2.54 has been fitted through the P_{max} data from the Northeast and North profiles. We see that, in general, data at greater than 9° distance along the Western profile falls well below this line. In Figure 21 we have the SALMON L_g data. Analysis of this phase for this event must keep in mind that in many cases a Mexican event is mixed in, thus raising the amplitude. A least-squares fit to the uncontaminated Northeast and North profile data yields a slope of -2.03. Note the large reduction of amplitude between WUS and EUS stations. This difference is greater than that seen for the P phases and suggests that complications in structure affect L_g more than P. This would then suggest that complications in structure are apt to result in earthquakes being identified as explosions unless a careful regionalization is undertaken.

The distance-amplitude relations of the last event to be examined in the main body of the report is that of HARDHAT. This shot was in granite in the WUS and was comprehensively recorded. We see in Figure 22 that the P data is extremely erratic. However, the P_{max} data is more stable and a regression line slope of -3.37 has been fitted. This would be appropriate for the WUS. In Figure 23 we see the data for the HARDHAT L_g phase. Here a slope of -3.13 has been determined by least squares. Stations HBOK and WMO in the EUS have unusually high amplitudes, as might be expected if the decay rate changed to a reduced value when the waves emerged from the WUS.

In Appendix I we have reproduced distance-amplitude figures similar to those just discussed for events of special interest, GNOME, four EUS earthquakes, SHOAL, the earthquake FALLON, and BILBY. Consideration of the least squares slopes determined as discussed above together with the historical results determined by other researchers as tabulated in Tables I, II and III suggests the hypothesized slopes of 2.5, 2.5 and 2.0 in the EUS for P_n, P_{max}, and L_g respectively. For the WUS the hypothesized slopes are 3.5, 3.0 and 3.0. In Table VI we see that in general these slopes cannot be rejected for the data which have been plotted; and so, we adopt these values for our discrimination analysis.

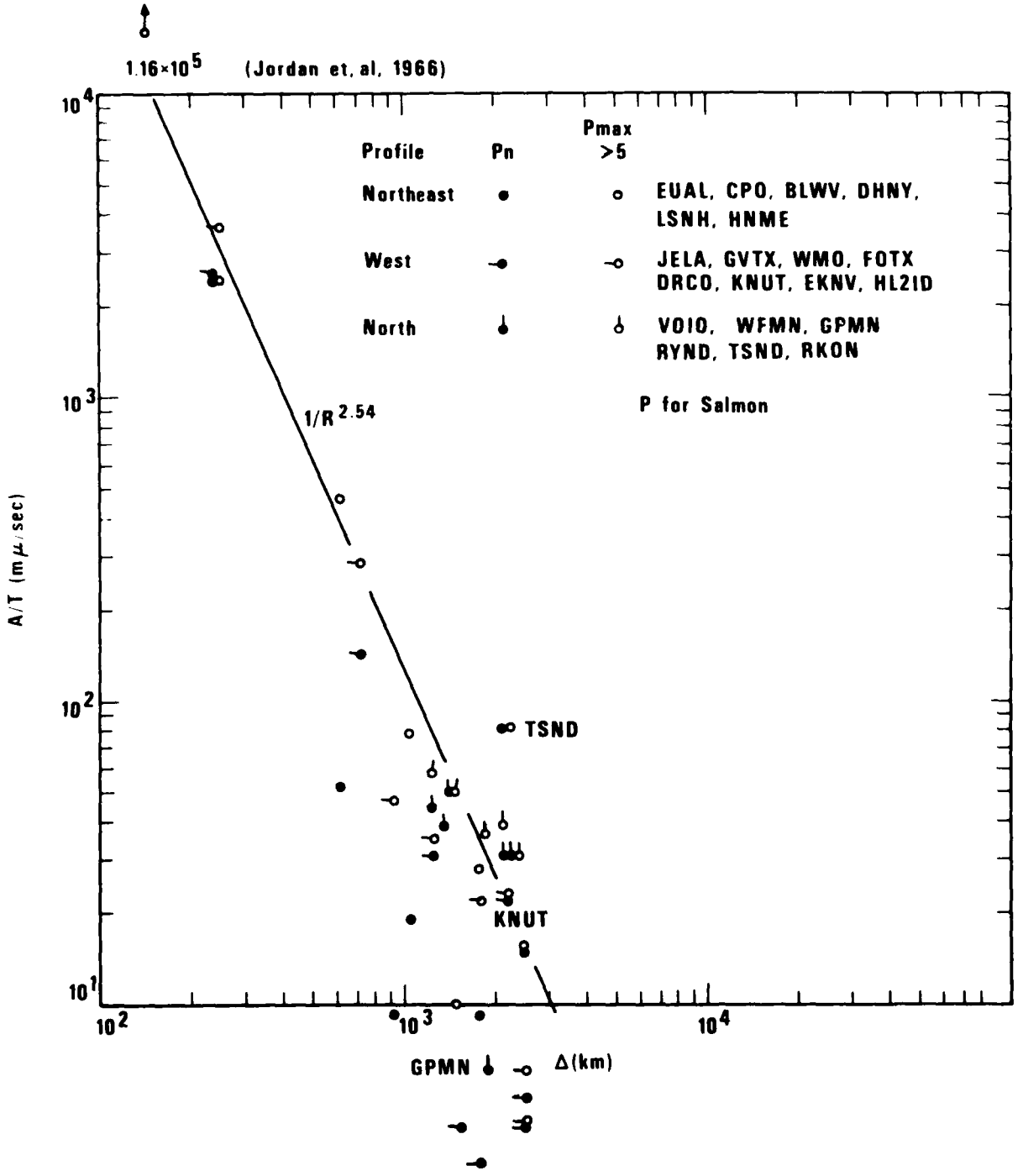

Figure 20. Amplitude-distance relations for the P and P_{max} (phase velocity greater than 5 km/sec) phase from SALMON. A least-squares slope of -2.54 has been fitted to the P_{max} data of the Northeast and North profiles. Note that most of the data along the Western profile fall well below the line.

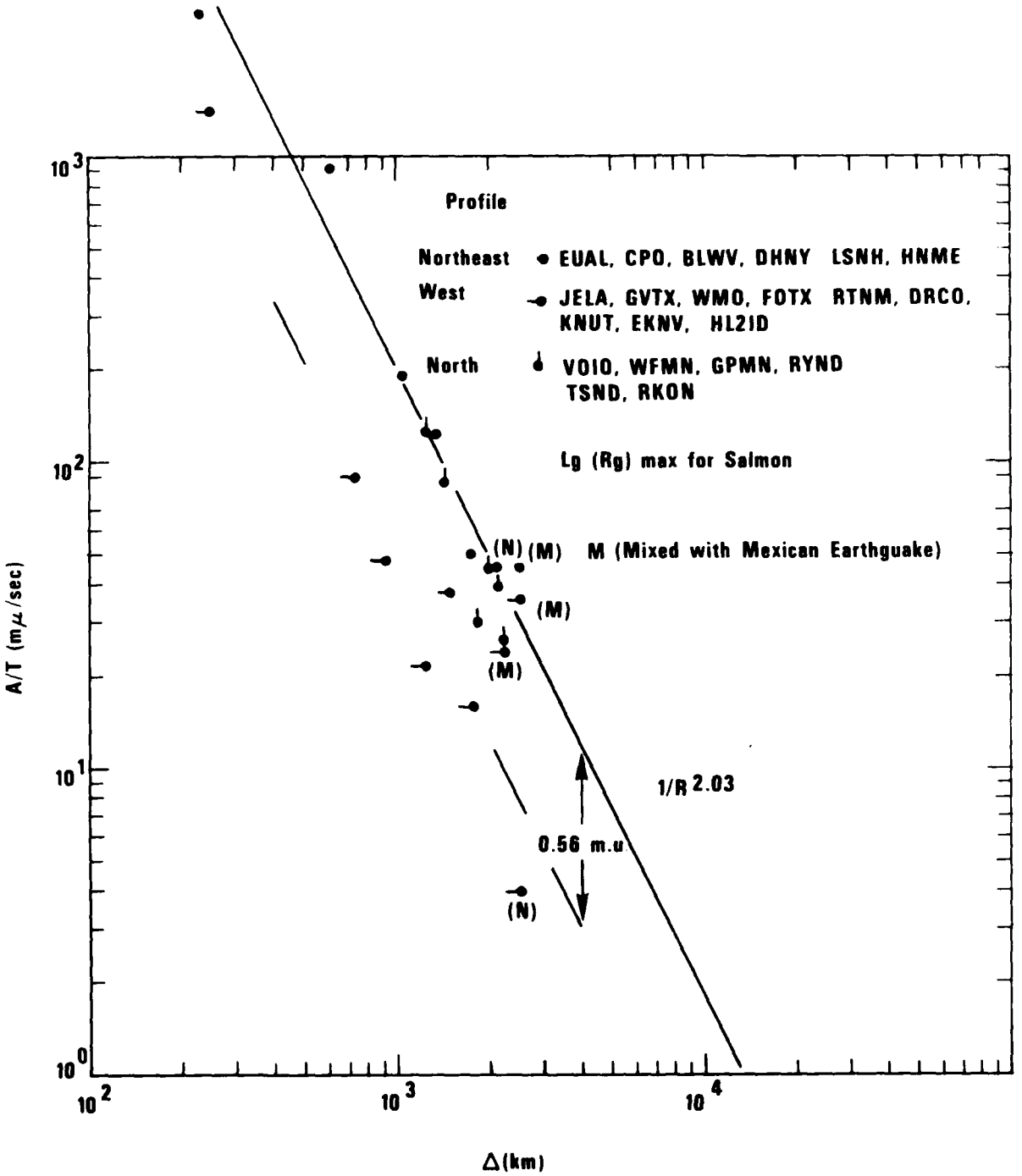

Figure 21. Amplitude-distance relation for $L_g(R_g)_{max}$ for SALMON. A least-squares slope of -2.03 has been fitted to the data along the Northeast and North profiles. Note that most of the data along the Western profile fall well below the line. Some of the data has been contaminated by signals from an earthquake in Mexico which occurred this day. These measurements are marked by (M).

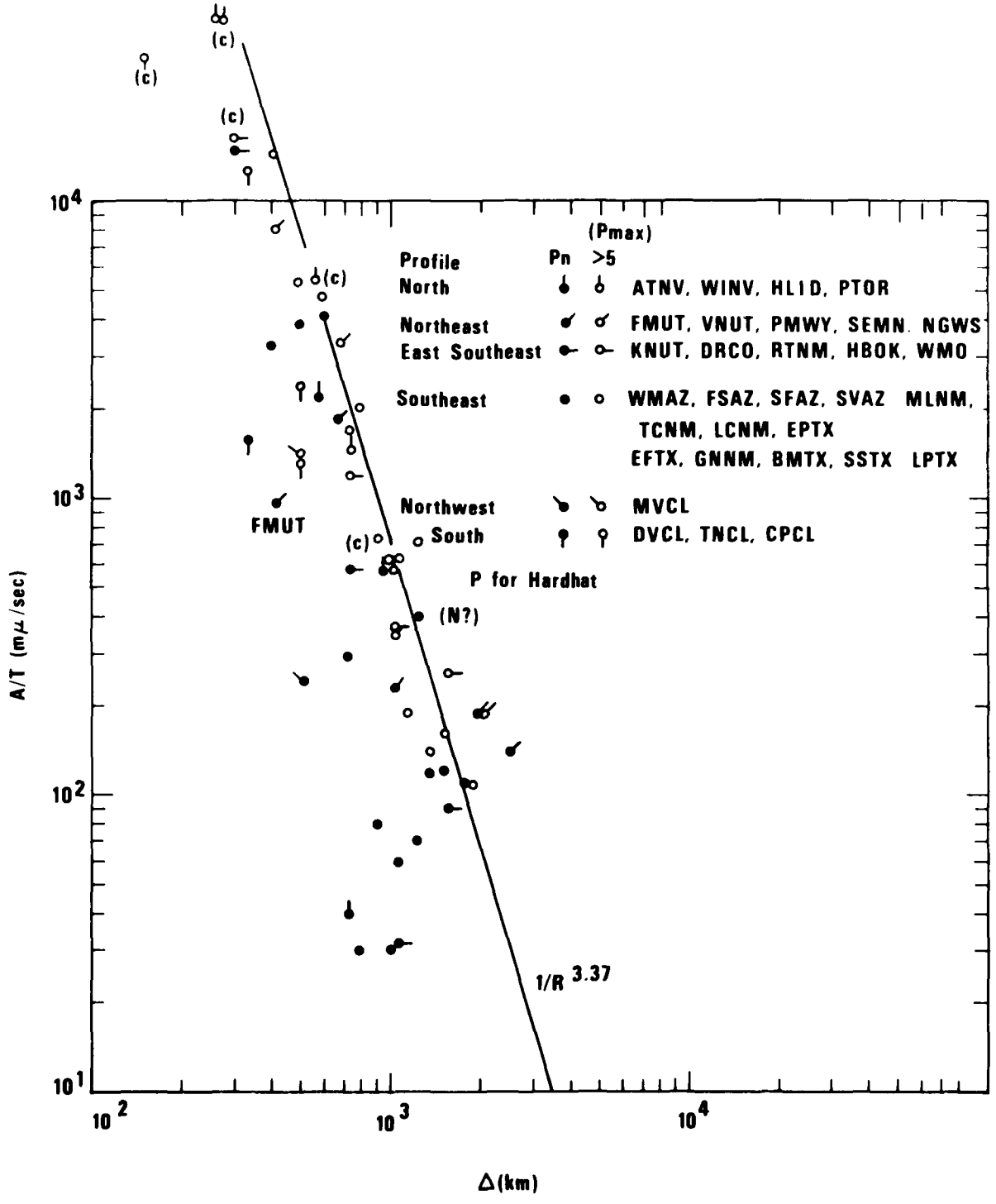

Figure 22. Amplitude-distance relations for the P_n and P_{max} (phase velocity greater than 5 km/sec) phase from HARDHAT. A least-squares slope of -3.37 has been fitted to the P_{max} data. Note that the P_n data is much more erratic. The notation (c) indicates that the data were clipped and that the true value, therefore, lies above the plotted point. (N?) indicates that the measurement may be noise.

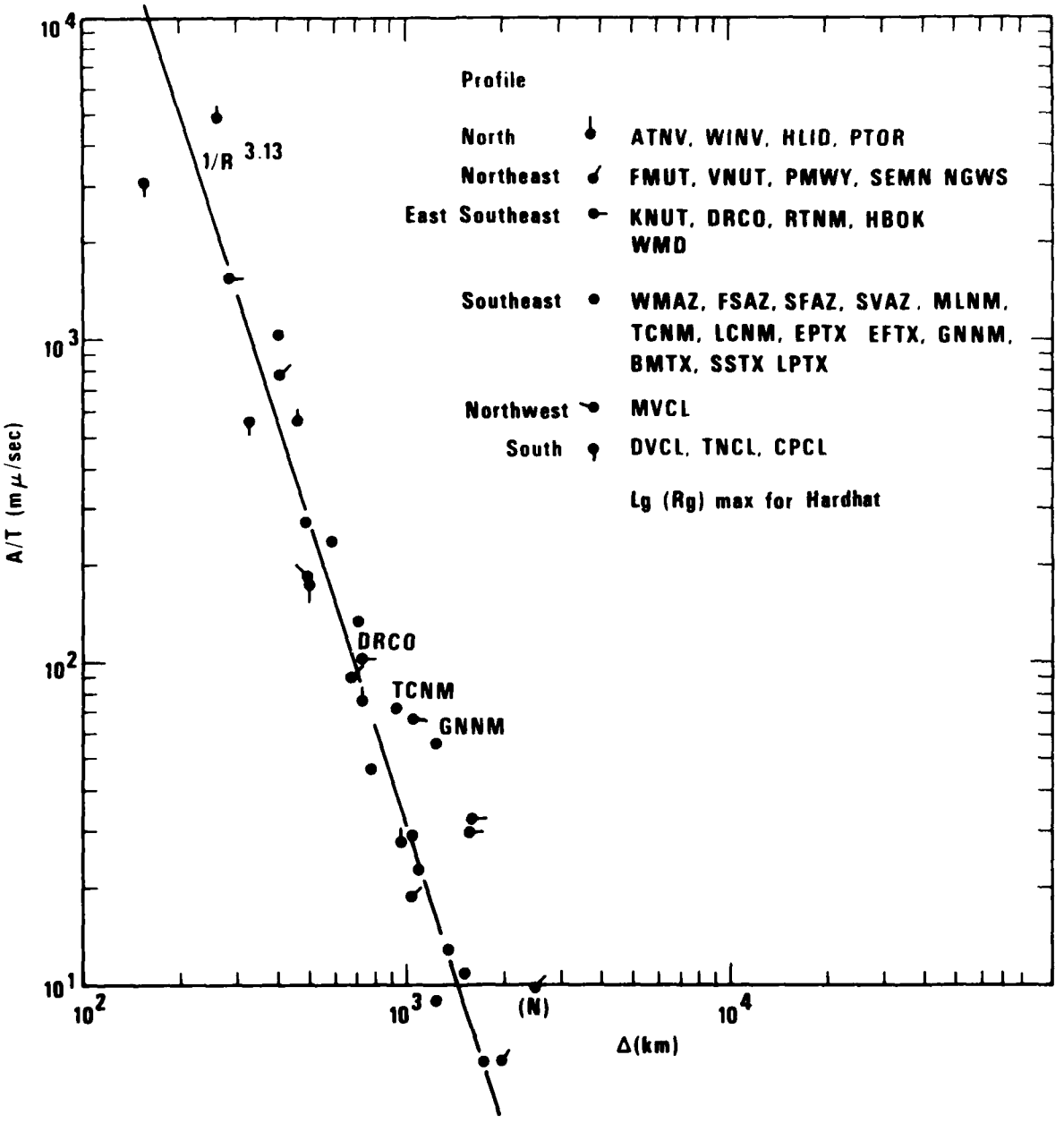

Figure 23. Amplitude-distance relation of $L_g(R_{g\,max})$ for HARDHAT. A least-squares slope of -3.13 has been fitted to the data.

TABLE VI

Summary of amplitude-distance slopes

EUS

	P_n	P_{max}	L_g
SALMON	> 2.5	2.54 → 2.5	2.03 → 2.0
New Madrid	2.5 OK	2.5 OK	2.0 OK
Massachusetts Coast	2.5 OK	2.5 OK	2.0 OK
Southern Illinois	2.5 OK	2.5 OK	2.0 OK
New Hampshire	2.5 OK	2.5 OK	2.0 OK
GNOME	2.5 or > 2.5 OK	2.5 OK	2.0 OK

WUS

	P_n	P_{max}	L_g
HARDHAT	3.5 ?	3.37 → 3.0	3.13 → 3.0
SHOAL	4.0	2.77, 3.0 OK	3.0 OK
FALLON	emergent, erratic	2.0, 3.0 poor fit	3.0 OK
BILBY	3.5 OK	2.0, 3.0 OK	3.0 OK
GNOME	3.0 OK	3.0 OK or >> 3.0 since CPCL very small	3.0 OK

DISCRIMINATION - P_{max}:L_g

In the discrimination analysis we measured periods and amplitudes for P_{max} and L_g for each of the events in Tables IV and V. Measurements were made at the number of stations indicated in the tables. Care was taken that the stations were as well distributed as possible and that the magnitudes of the TFO extended array in Arizona were averaged together to give an array magnitude which was then averaged in with the other stations. Magnitudes were computed only from paths for which at least the first 2/3 of the path was in the same province (EUS or WUS) as the event. The events Hebgen Lake and GNOME were considered to be on the EUS-WUS boundary so that all paths were in one province or the other.

Magnitudes were calculated to be the measured amplitude corrected to 1000 km by the appropriate formula and averaged over the network. The results are seen in Figure 24 where the numbers are keyed to Table IV. First, we see that the EUS earthquakes are well separated from SALMON, the only EUS explosion; and from the GNOME event when its magnitude is computed only on the EUS paths. The separation between the population lines of slope 1.0 is 0.6 magnitude units.

For WUS events the situation is more complicated. The discrimination is not, on the face of it, as good as in the EUS. If we simply take the difference between the population means, then we see a difference of approximately 0.45 magnitude units, slightly less than the 0.6 in the EUS. However, while the earthquake population shows only slightly greater scatter than in the EUS, the scatter in the explosion population is quite large. However, the principal events which contribute to this scatter are BILBY, MONERO, YUBA and PLATTE. BILBY is so large that its low corner frequency may have caused the P_{max} signal to lose amplitude relative to L_g because the L_g always is of low frequency due to modal cut-off.

YUBA and PLATTE were selected because they were extremely small events and MONERO because it was the closest NTS event to the Massachusetts Mountain Earthquake. YUBA and PLATTE are at a depth of only about 200 meters and were detonated in a tunnel at Rainier Mesa. These unusual conditions may be responsible for a low corner frequency for P_{max}, leading to a low amplitude. Evidence for this is that P_n at KNUT has a period of 0.2, 0.6 and 0.4 seconds for BUTEO, YUBA, and PLATTE respectively. BILBY has a period of 0.6 seconds; KNUT was not up for MONERO. BUTEO is probably more characteristic of a true test ban monitoring situation in that it was overburied, a procedure necessary to avoid

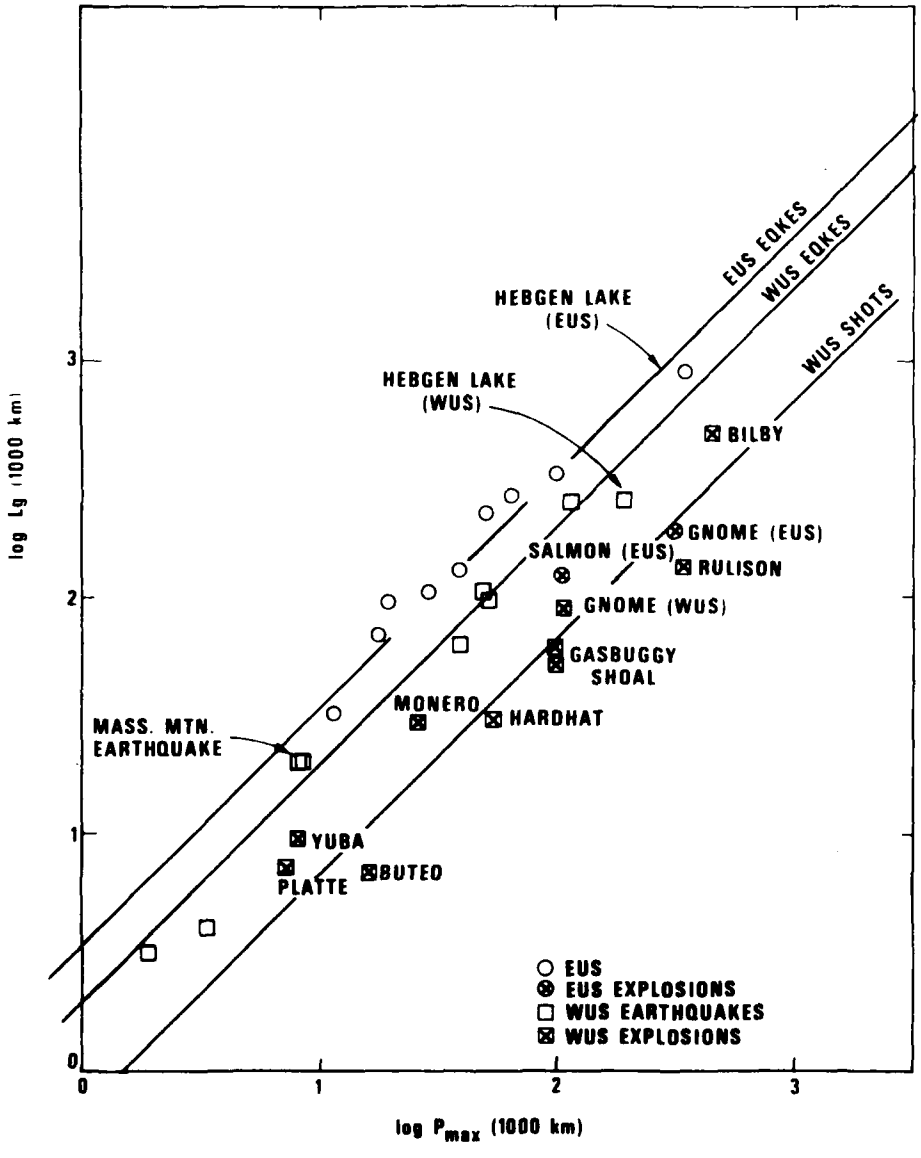

Figure 24. Network L_g plotted as a function of network P_{max} for the events in Tables IV and V. Numbers are keyed to those in Table IV. L_g amplitudes have been corrected to 1000 km before averaging by use of EUS or WUS formulas as appropriate. Separation between explosions and earthquakes is seen in both EUS and WUS. See text for discussion of poor discrimination of YUBA, PLATTE, MONERO, and BILBY. Note reduced amplitude of Hebgen Lake and GNOME in WUS as compared to EUS. Note distinct separation of the Massachusetts Mountain earthquake, located at NTS.

detection of cratering phenomenon. If we do take the remaining WUS explosions to be the population of interest the explosion population is almost as tight as the earthquake population and the separation is about 0.55 magnitude units, almost identical to the 0.6 in the WUS.

Examining the events Hebgen Lake and GNOME in the EUS and WUS shows that for L_g the WUS amplitude is about 0.3 to 0.55 magnitude units less at 1000 km than is the EUS amplitude. Let us take 0.42 magnitude units as the mean difference. Then, assuming r^{-2} in the EUS and r^{-3} in the WUS the waves would be of equal amplitude at 380 km. This can be seen to be a reasonable conclusion by examining Figures 17 and A1-1b. This then further suggests that somewhere around 380 km the amplitude-distance curves of EUS and WUS should begin to merge and this may offer a start toward a unified magnitude scale for the entire United States. In this connection we should note that Nuttli (1973) showed that $\gamma = 0.6$ adequately fitted Richter's (1958) magnitude relation between 40 km and 700 km. It is also true that a slope of r^{-3} closely fits Richter's curve between 200 and 600 km.

Discrimination-Spectra and Transverse/Radial

Figures 25 and 26 show respectively the Alabama earthquake of 18 February as recorded at BRPA, a distance of 823 kilometers, and SALMON as recorded at station BLWV at a distance of 1058 km. These two stations are indicated by Der, McElfresh and Mrazek (1979) to have the same crustal structure so that any differences between the recordings are probably not due to differences in the crustal structure.

We see that the transverse to radial maximum amplitude ratios before and after 5 km/sec are the same for the earthquake and explosion, and that in the time domain there is no noticeable difference in the frequency content between components, or between events for common phases. One distinctive difference which can be seen, however, is that, especially as seen on the transverse component, the earthquake L_g begins abruptly and grows quickly to a maximum amplitude. In contrast, the SALMON L_g shows no clear arrival and increases slowly to its maximum. These differences might be explained by means of decreased SALMON amplitude of shear waves which are needed for a dramatic emergence of the L_g from the P_g and S_n coda, or by the (presumably) deeper focus of the earthquake which excites a higher proportion of higher modes which have faster

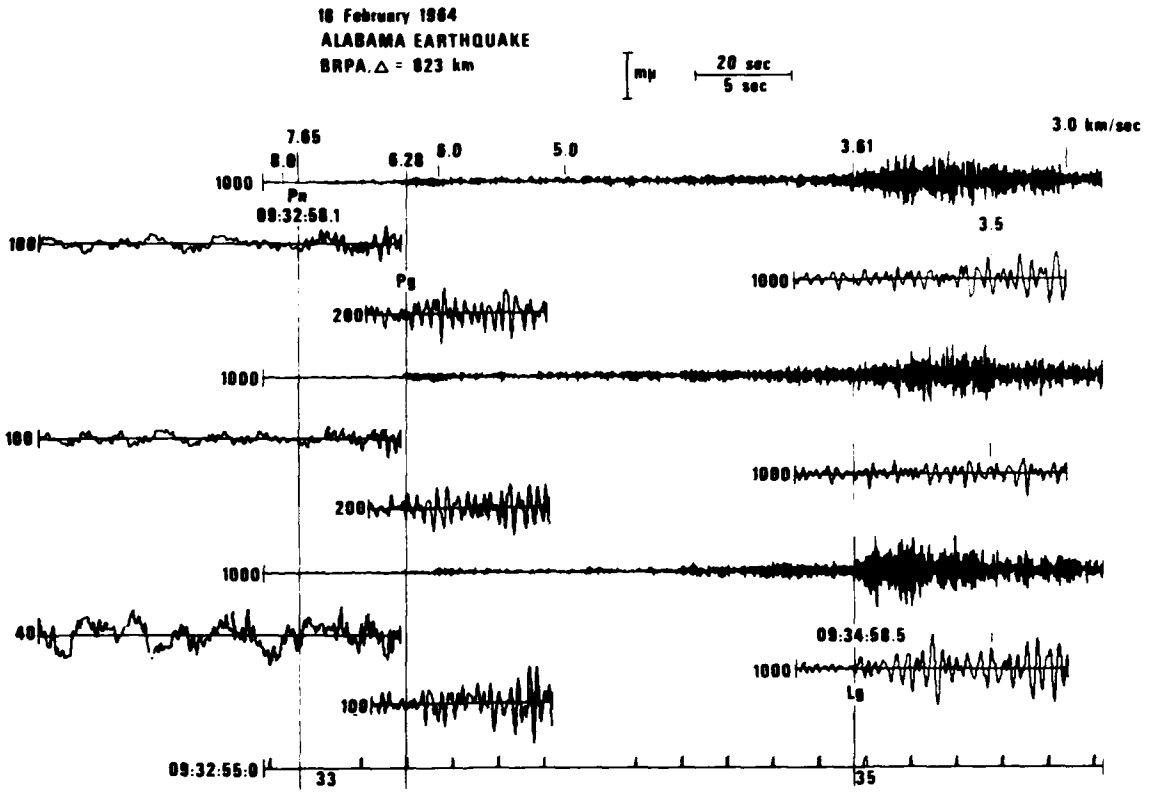

Figure 25. Waveforms of the 18 February 1964 earthquake as recorded at station BRPA. See text for discussion of comparison with SALMON as recorded at BLWV.

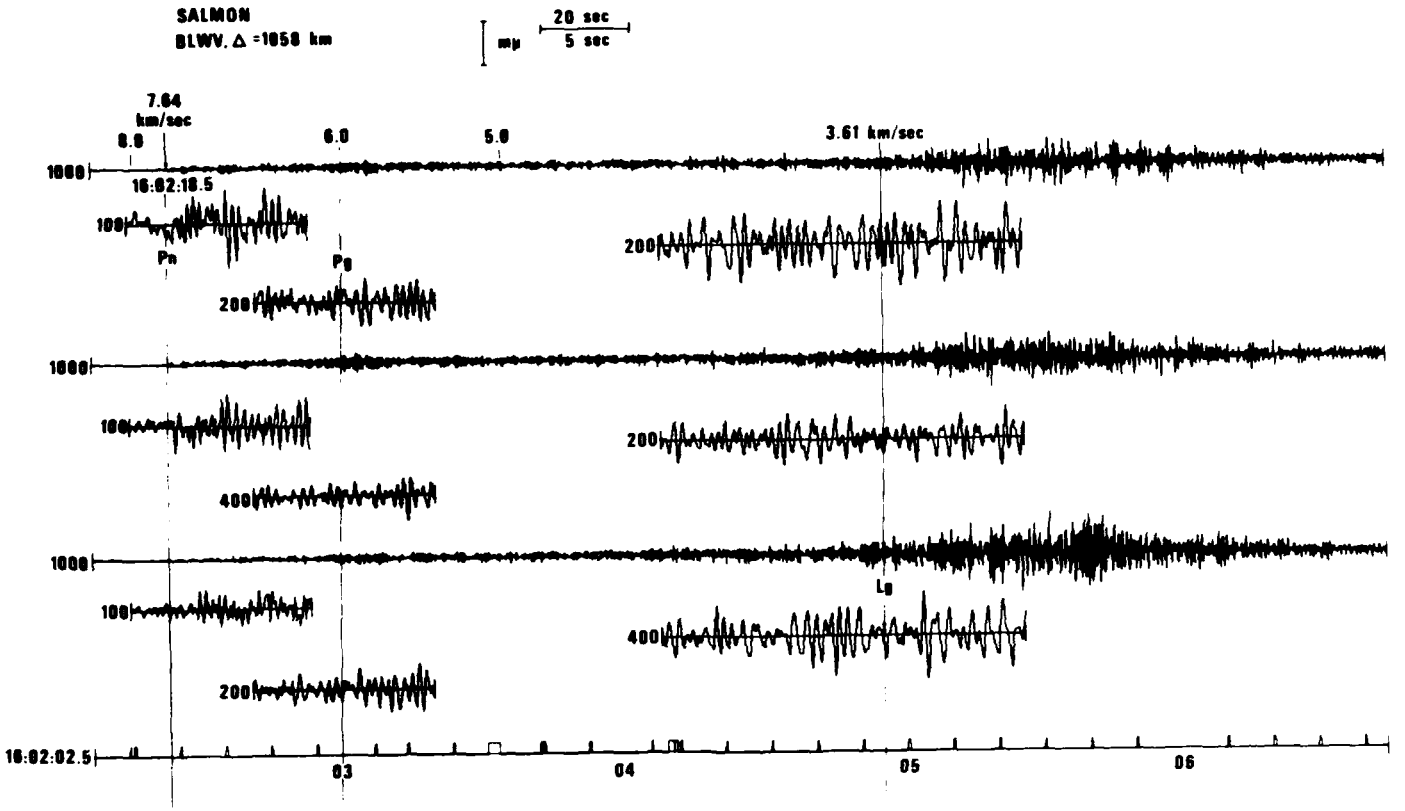

Figure 26. Waveforms of SALMON as recorded at station BLWV. See text for discussion of comparison with 18 February 1964 earthquake as recorded at BRPA.

group velocities. Other possible influences are the difference in the crust at the source and the fact that the earthquake signal does not propagate through the thickly layered sediments which lie between the SALMON and earthquake epicenters. The above observations, are, therefore, mainly of use as guidelines for further research.

Another point which is easily seen in Figure 25 on the transverse component is that there is a sharp decrease in frequency with the arrival of the L_g phase. This figure also shows, however, that it will be difficult to obtain a "true" L_g spectrum at high frequencies because immediately preceding its arrival there is coda signal, and this, presumably, continues "under" the L_g signal. Thus, even if there is a modal cutoff for L_g at high frequencies, there will be high frequency energy in the L_g window which is greater than the ambient noise before the arrival of P_n. Great care must therefore be taken in interpreting this energy in terms of the source spectrum via an L_g normal mode theory which does not take account of scattering from earlier phases. We shall return to this question by using spectral analysis.

The major point to make with respect to discrimination is, of course, that the L_g/P_{max} ratio is greater for the earthquake than for SALMON. This is easily seen on all three components, and reference can be made to Figure 19 to see that the L_g/P_{max} ratio is about a factor of 2 greater for the earthquake than for SALMON. This is less than the average separation of ~ 0.6 magnitude units seen in Figure 24.

Finally, P_n is much more emergent for the earthquake than for the explosion. The P_n/P_{max} ratio is about 1:1 for SALMON and 1:4 for the earthquake. This point, however, has not been studied in detail and may be closely related to crustal structure so we cannot assert that the L_g/P_n ratio would be a reliable discriminant.

Proceeding to the spectral details, we see in Figure 27a,b,c the Z, R, and T SALMON P-wave signal spectra and noise at BLWV, and in Figure 28 the corresponding signal for the 18 February 1964 earthquake at BRPA. The spectra have not been corrected for the LRSM short-period instrument response. In the time domain, as remarked before, the signals seem to have similar frequency content and by overlaying the two log spectral plots for vertical components one can see that they are identical to within experimental error as indicated by the dashed line in Figure 28. Der and McElfresh (1976) have shown that the P spectrum of SALMON at BLWV and BRPA is almost perfectly matched by the SALMON reduced displacement potential without absorption. Thus the spectrum in Figure 27a is the

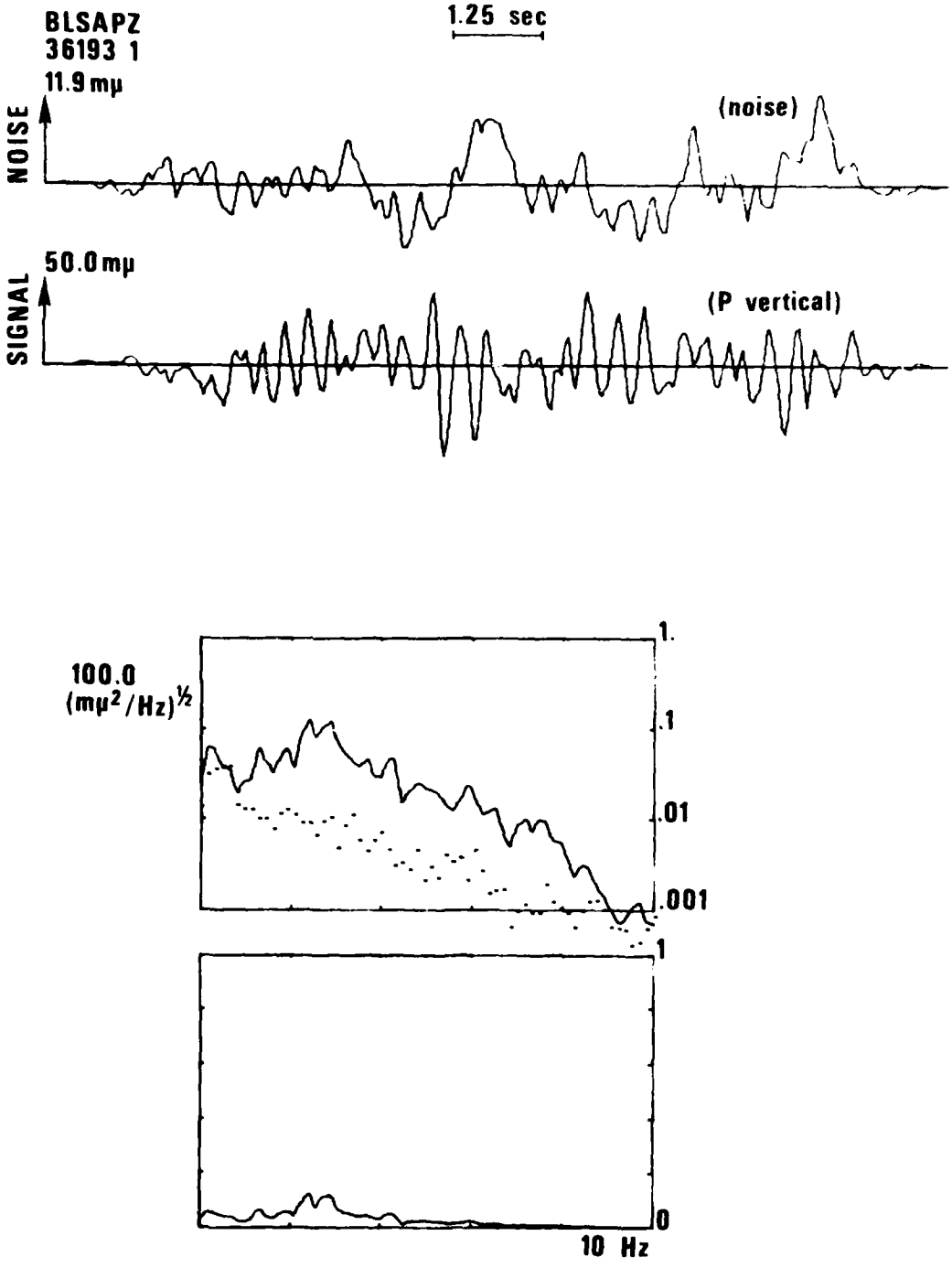

Figure 27a. SALMON P waves and noise, signal and spectra at BLWV, vertical component.

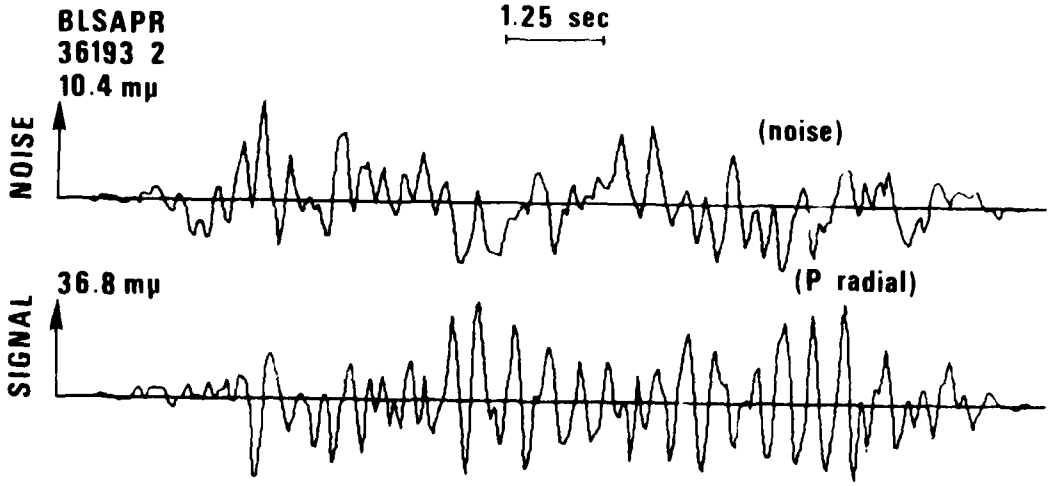

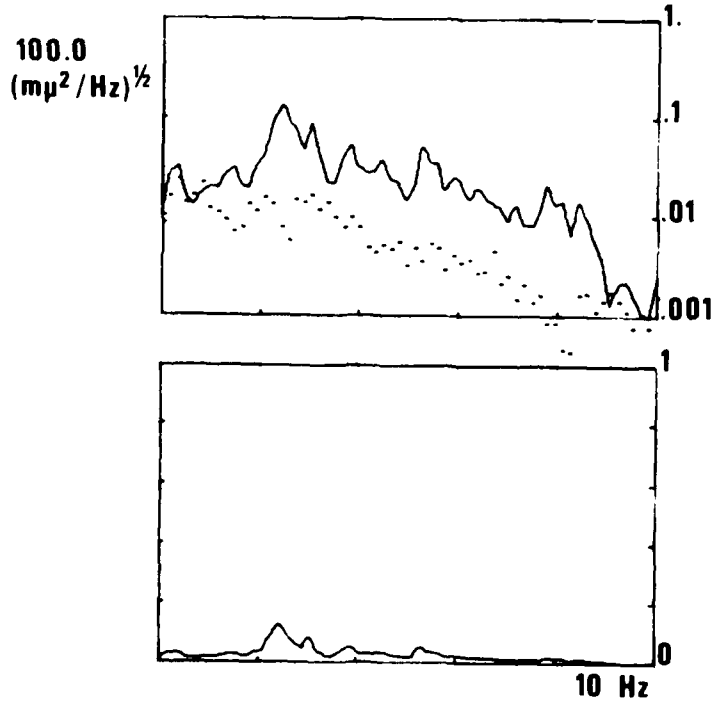

Fig. 27b. SALMON P waves and noise, signal and spectra at BLWV, radial component.

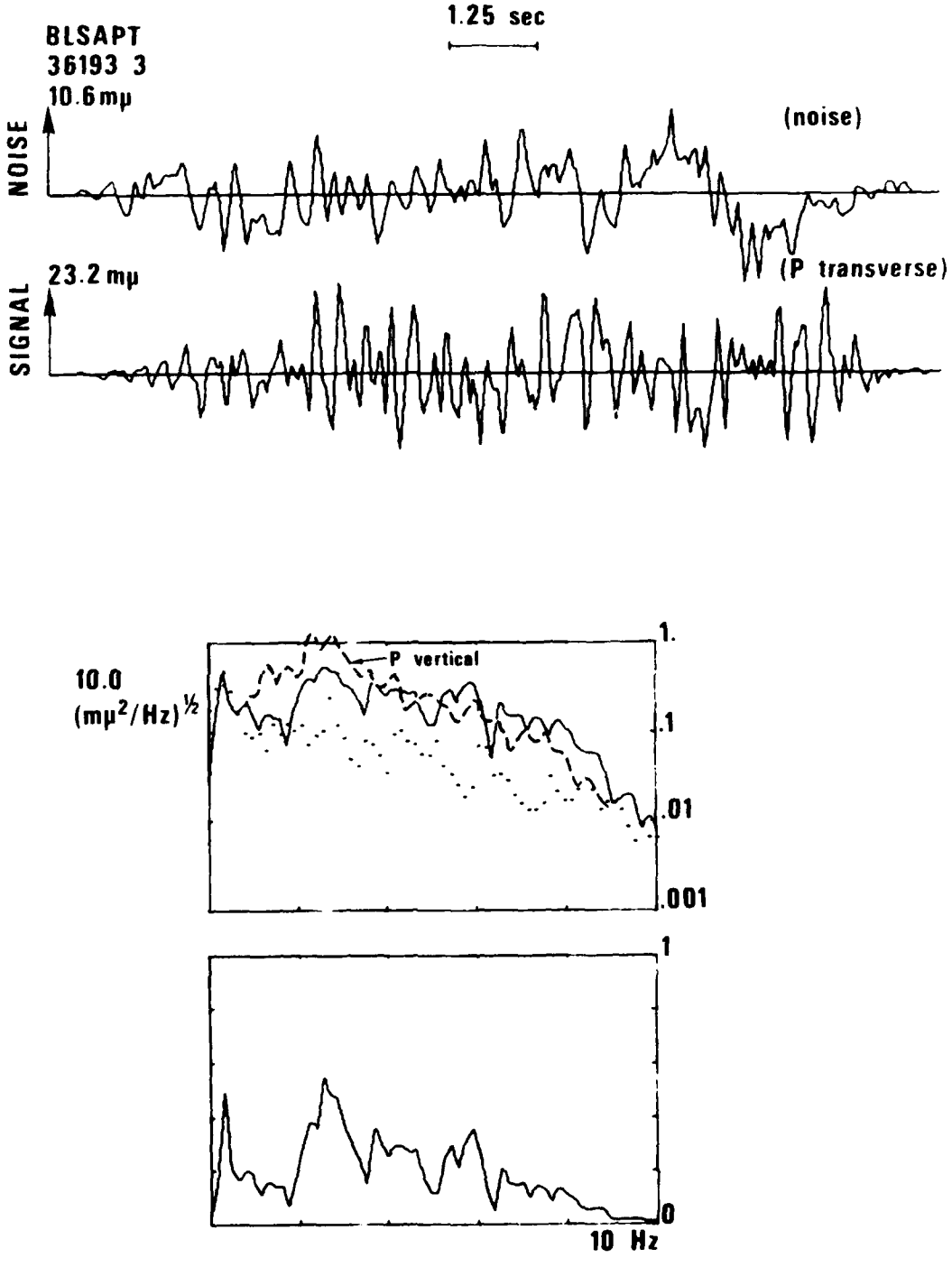

Figure 27c. SALMON P waves and noise, signal and spectra at BLWV, transverse component. Note lower frequency signal on vertical.

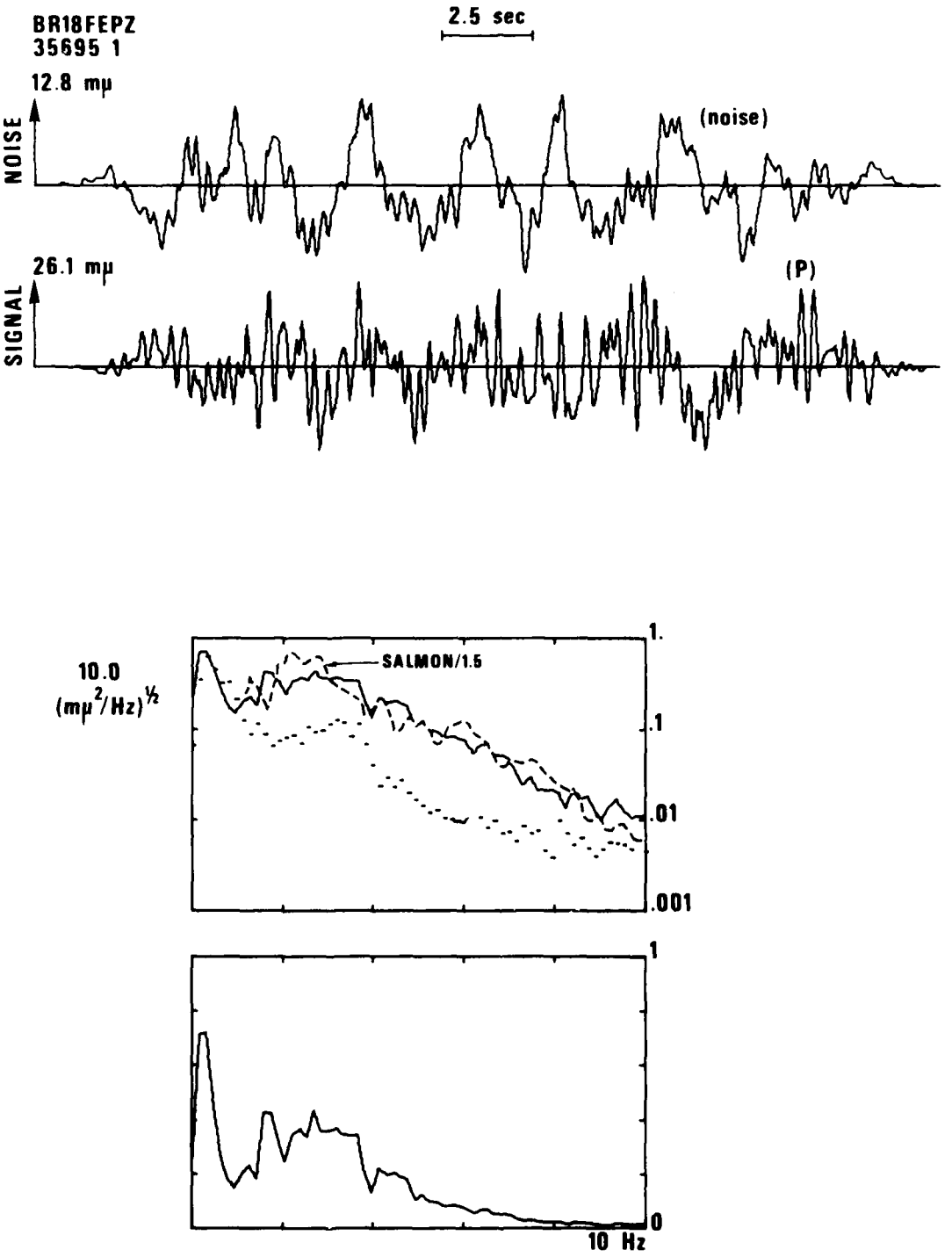

Figure 28. 18 February P waves and noise, signal and spectra at BRPA: note near identity in shape of the superimposed SALMON P spectrum from BLWV.

SALMON source spectrum as seen through the LRSM instrument response, and thus the 18 February earthquake has a source spectrum identical to that of SALMON between 1 and 10 Hz. The same conclusion is reached when the signals are compared at other stations. Comparison of the vertical and transverse components spectra in Figure 27c shows that the transverse P is of slightly higher frequency than the vertical.

The similarity of the earthquake and explosion spectra suggests that spectral discrimination between earthquakes and explosions may be very difficult, if not impossible. It may be objected that this is only one pair of events; however, most studies of spectral differences between earthquakes and explosions use explosions not in tectonic regions so that differences in propagation may explain any differences seen. Also, those spectral differences which do exist may be due to the cancellation of explosion energy at frequencies well below 1 Hz by interference between pP and P. Since for Figure 28 S/N < 1 for f < 1 Hz, this frequency range may possibly still be exploited for discrimination; however, it is clear that in practice it will be necessary to develop methods for decreasing the low-frequency noise.

If the P-wave and other source spectra of the earthquake and explosion are similar, then one might expect that the L_g spectral shapes would be similar to each other since the propagation effects and modal cutoffs are the same. Comparing Figures 29a and 30 (see overlay on Figure 30) we see that this is, in fact, the case. By comparing Figure 29a to Figure 27a or 30 to 28 we see that the L_g spectrum is shifted to lower frequencies as compared to the P wave spectrum. Since the P-wave spectrum is, as we have seen, equal to the source spectrum, it follows that the L_g spectrum is <u>not</u> the source spectrum. This might be expected because of the existence of modal cutoffs. It follows that determinations of corner frequencies and related source parameters from L_g, see e.g. Street (1976) are liable to lead to errors.

Figure 29d as compared to Figure 27a shows that the P_g spectrum is almost the same as P_n. P_g has somewhat more energy around 2 Hz and is therefore somewhat lower in overall frequency content.

The true L_g spectrum is probably even more low-frequency than is immediately apparent by comparison of Figure 27a and 29a. In Figure 29a we have also plotted the P_g spectrum seen in Figure 29d. We see that it merges into the L_g spectrum near 2.4 Hz. Thus the energy in the L_g spectrum above 2.4 Hz is probably scattered coda energy and the true L_g spectrum may be plunging very

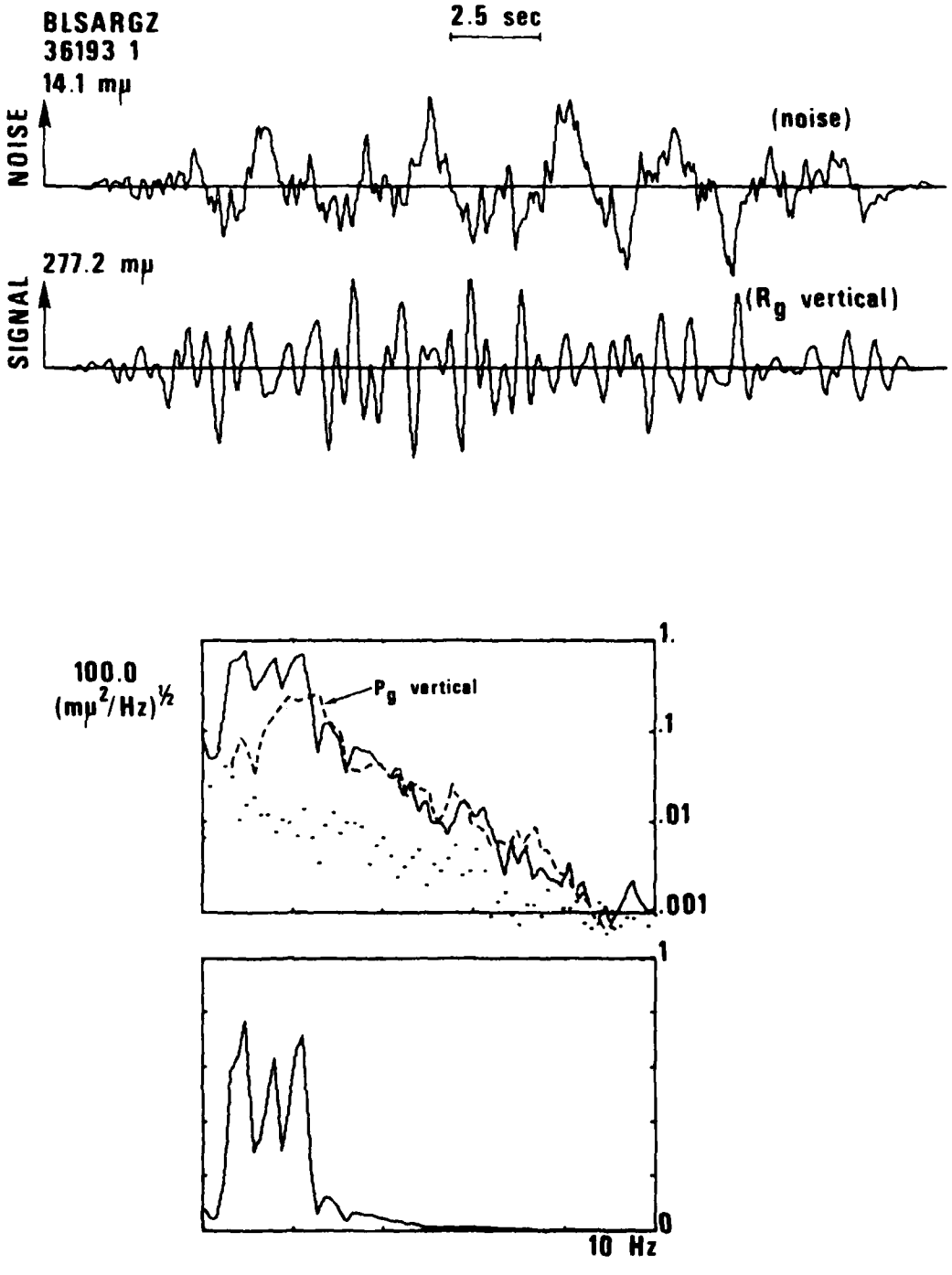

Figure 29a. SALMON L_g waves and noise, signal and spectra at BLWV, vertical component.

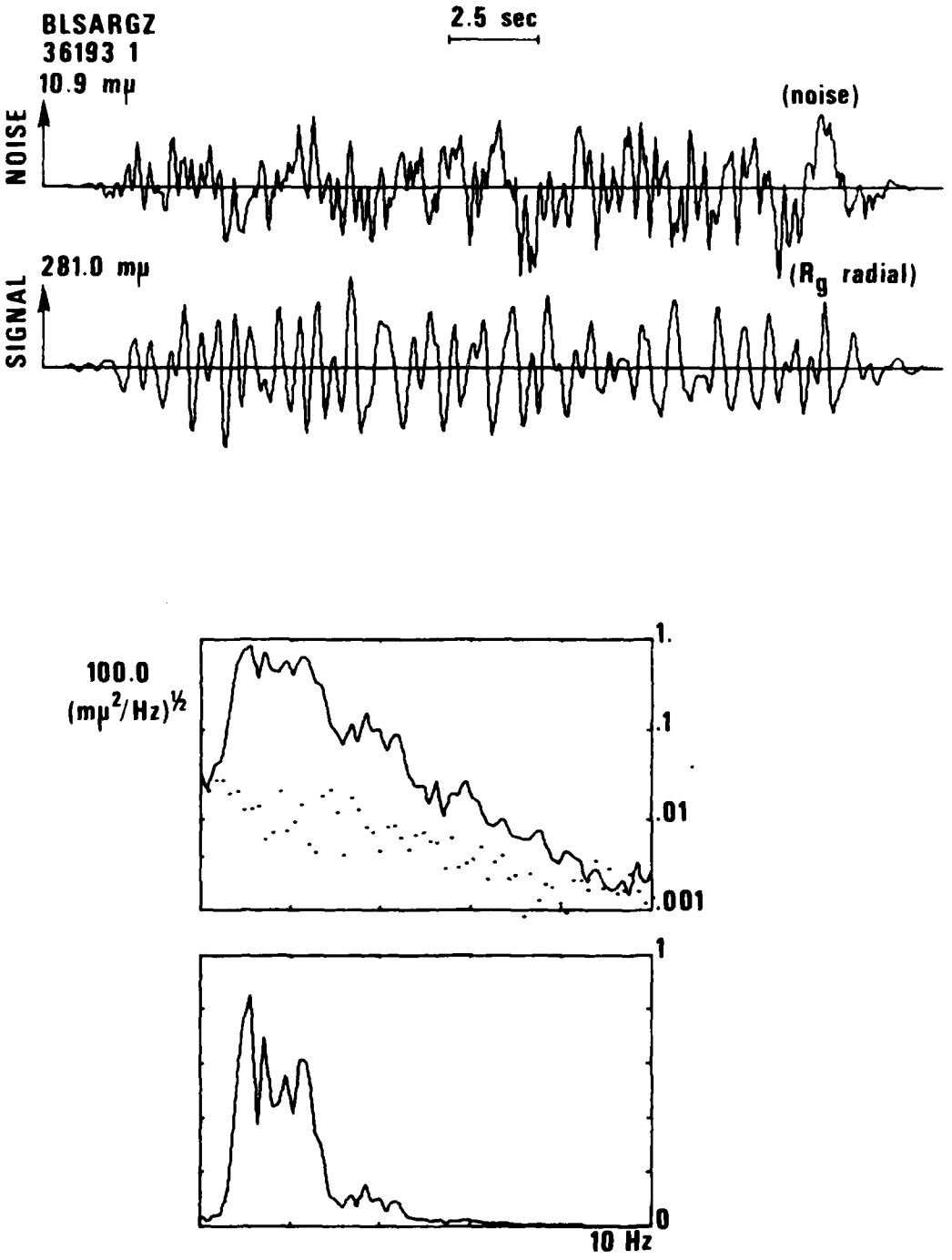

Figure 29b. SALMON L_g waves and noise, signal and spectra at BLWV, radial component.

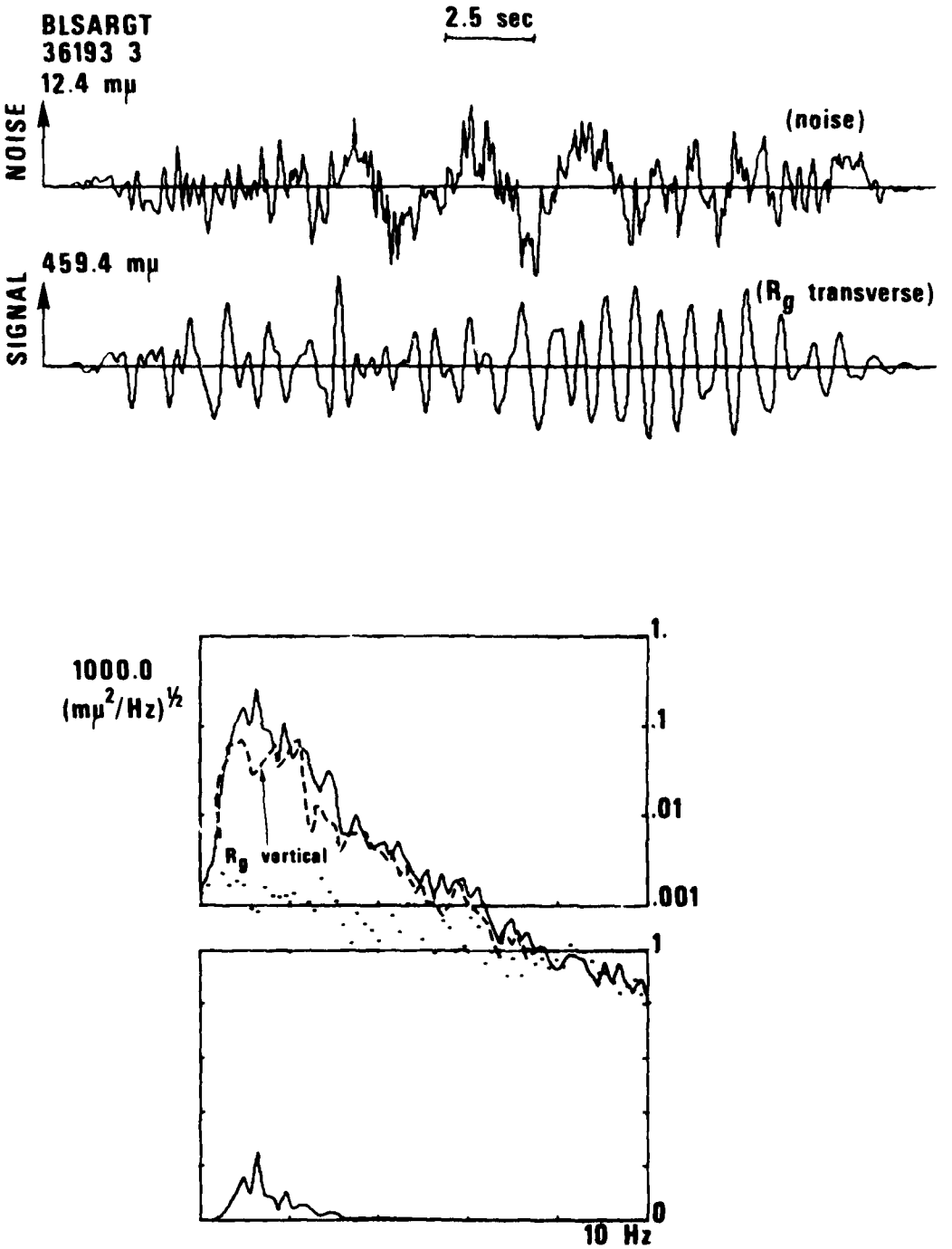

Figure 29c. SALMON P_g waves and noise, signal and spectra at BLWV, transverse component.

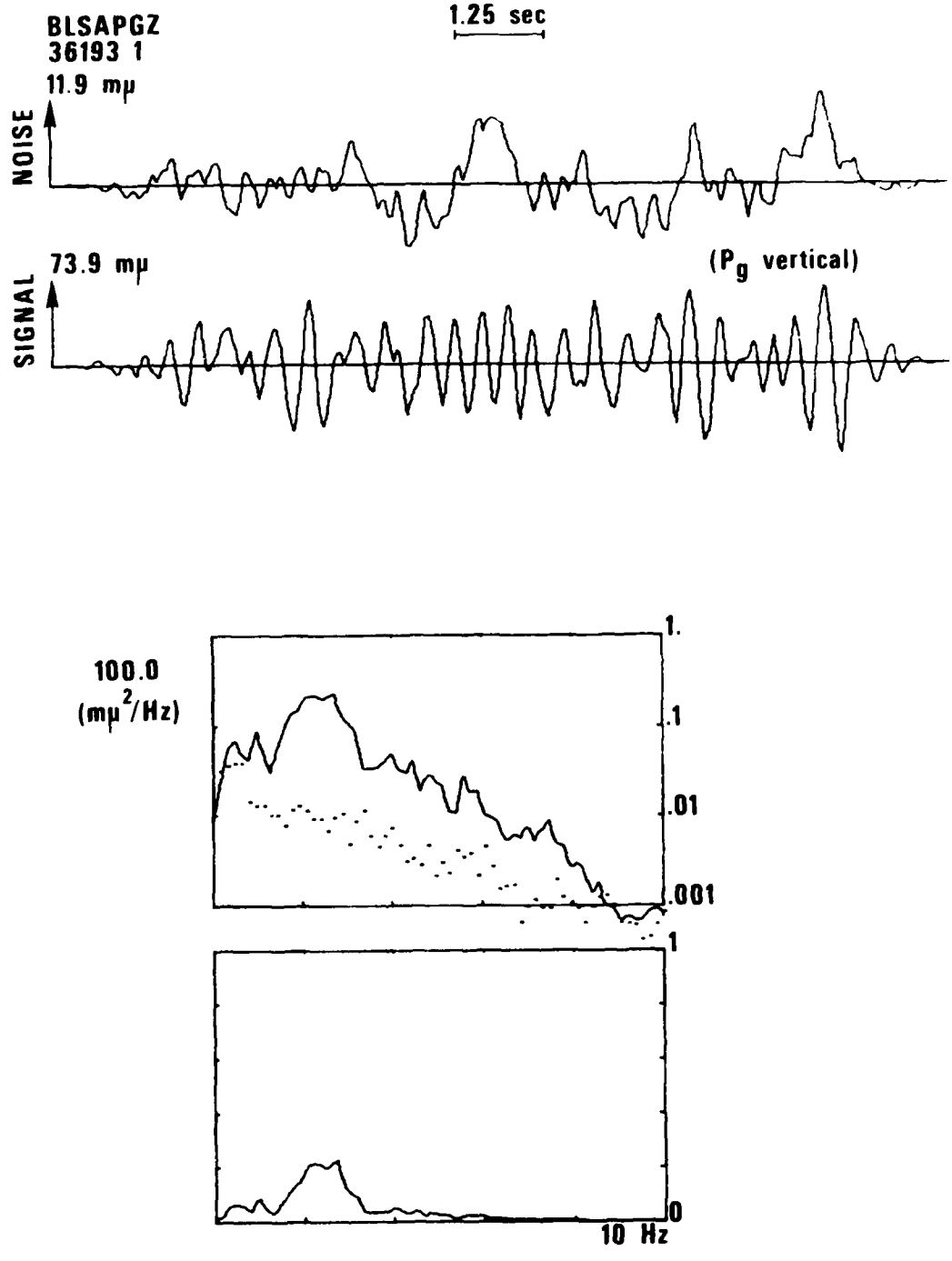

Figure 29d. SALMON P_g waves and noise, signal and spectra at BLWV, vertical component.

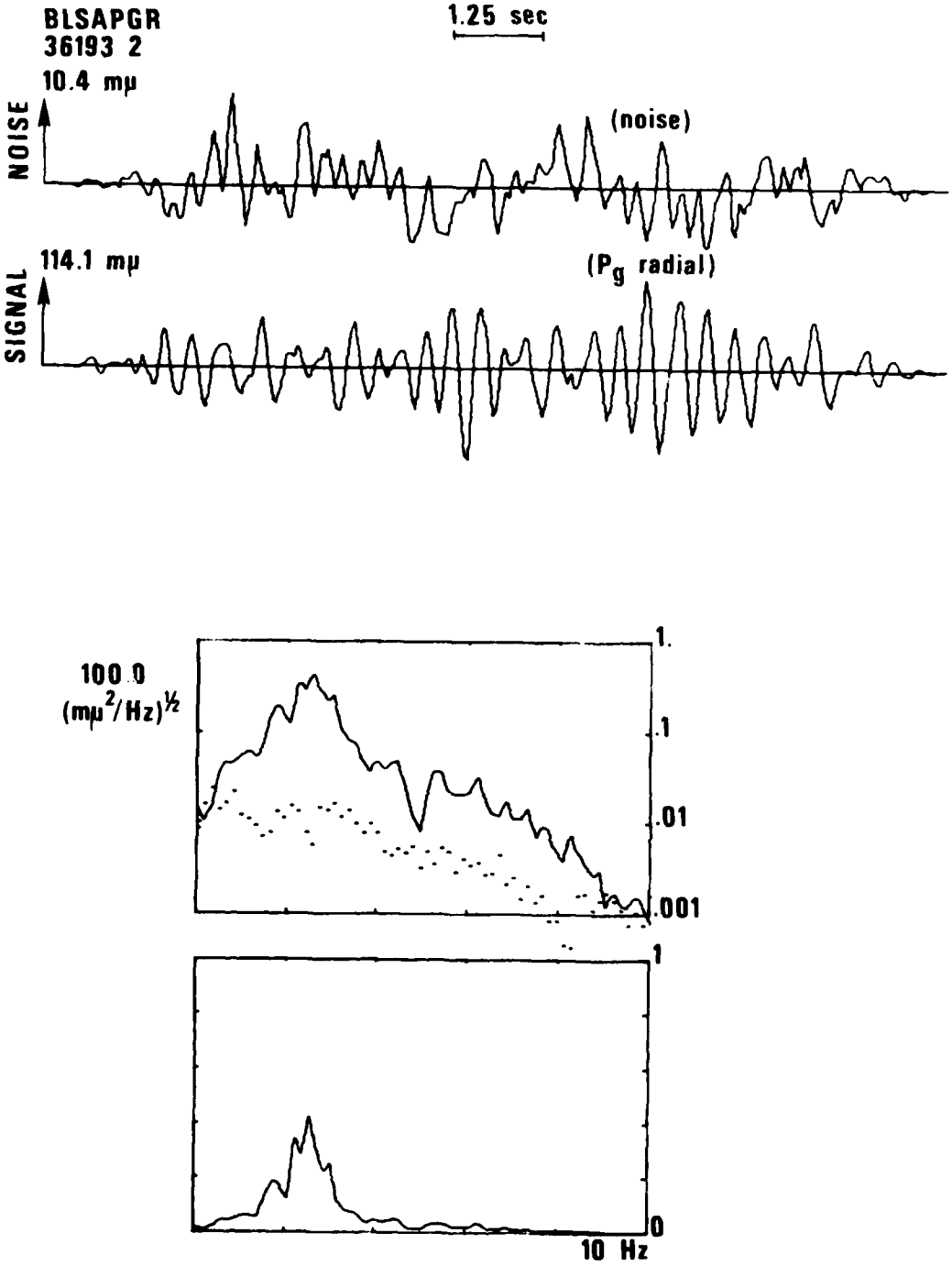

Figure 29e. SALMON P_g waves and noise, signal and spectra at BLWV, radial component.

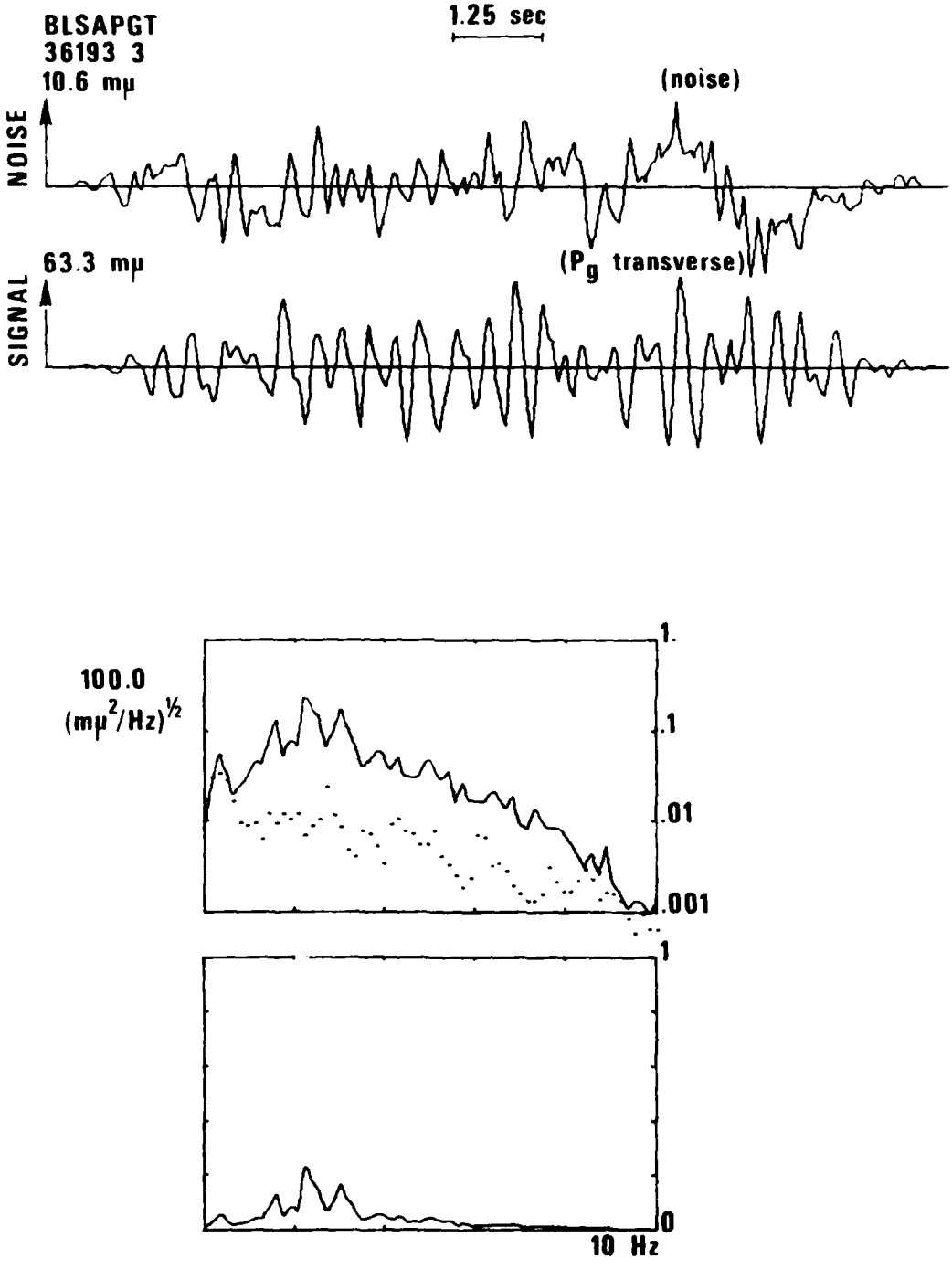

Figure 29f. SALMON L_g waves and noise, signal and spectra at BLWV, transverse component.

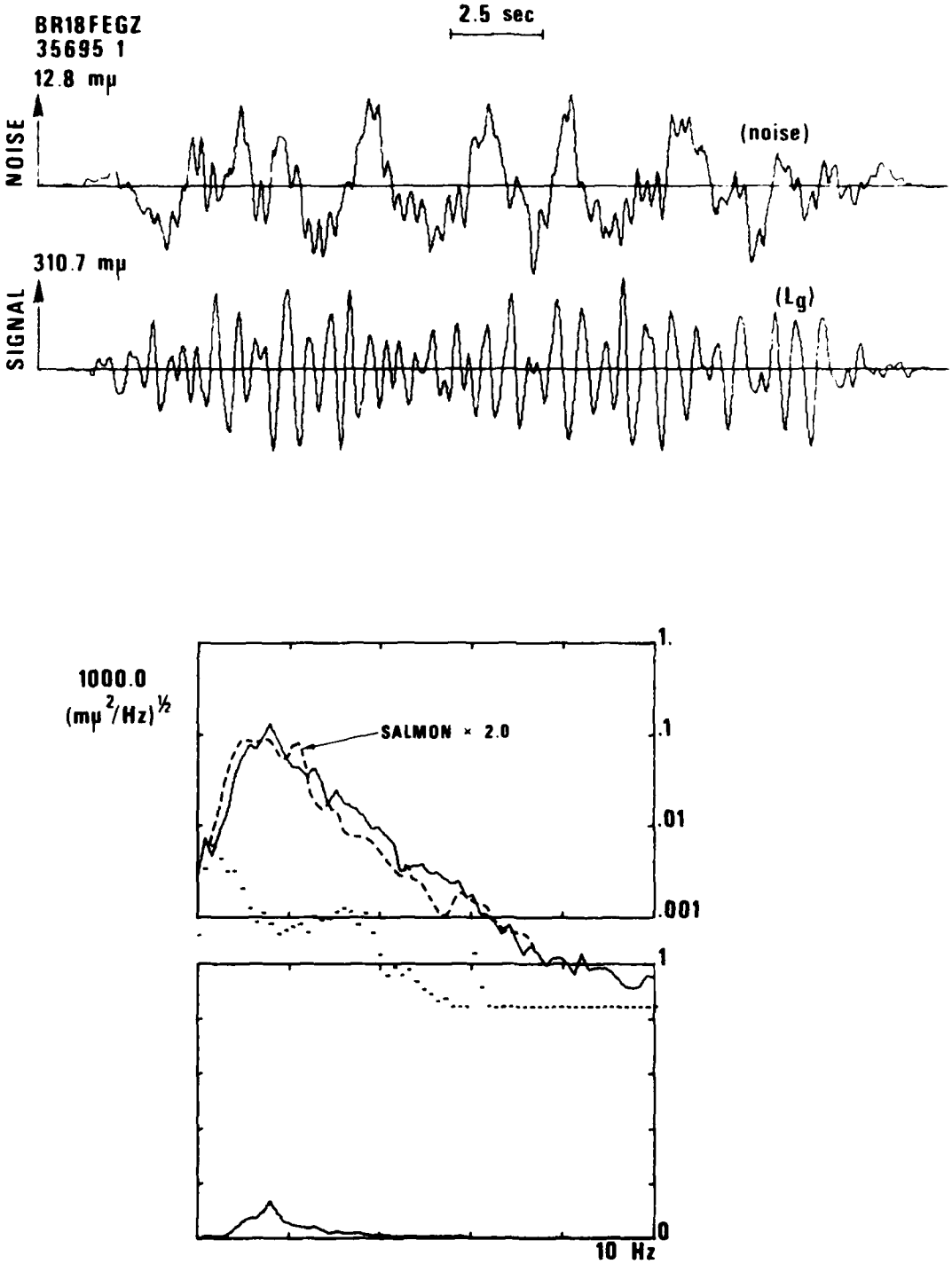

Figure 30. 18 February L_g waves and noise, signal and spectra at BRPA; note superposition of SALMON L_g spectrum from BLWV.

deeply above 2.5 Hz. It will be necessary to keep this fact in mind when comparing observed and theoretical spectra.

The superposition of the vertical spectrum on the transverse in Figure 29c shows that the transverse is slightly lower in frequency in contrast to P_n and P_g in which the transverse is of higher frequency. Comparison of Figures 29d,e,f shows that above 5 Hz the transverse and to some degree the radial components of P_g have somewhat more energy than the vertical .

The contamination of the L_g spectra by coda energy may have made it possible for Street (1976) and other workers to determine fairly accurate corner frequency and high-frequency asymptotes from L_g spectra even though the procedure would not be justifiable from a strict theoretical point of view.

Figures 31 to 34 enable us to reach conclusions identical to those above by using station EUAL which was 242 km from SALMON, and 311 km from the 18 February earthquake.

Figures 35 to 38 are included for completeness. They give SALMON as seen at BRPA, and the 18 February earthquake as seen at BLWV. Thus the events may be compared at common stations but different distances, instead of at more equal distances and different stations, as we did in the analysis of Figures 27 to 30; the same conclusions are reached.

Finally, SALMON signals of special importance are also included: the P and L_g waves as seen at station JELA, a distance of 243 km, (39, 40); and at stations HNME (41) and RKON (41, 42). These stations are constantly used as a basis of comparison.

In particular, note in Figure 41 that the spectrum at HNME has less high frequency than at RKON, even though they are at comparable distances of 22.46° and 19.9°, respectively. The frequency content of the signals seems to be stationary in the time plots, suggesting that triplications are not altering the general trends of the spectra. Thus, there is apparently more absorption under HNME than under RKON. The spectral ratio between 1 and 2 Hz in Figure 41 suggests a Δt^* value of 0.4 sec.

Results at NORSAR

The relative frequency content of P and L_g at regional distances which we have just noted for SALMON and for the February 18 earthquake may also be observed for Soviet explosions as observed at NORSAR. In Table VII is a list of

events which we shall analyze. The first two events in that list are the closest shots to NORSAR and their signals and spectra are given in Figures 44 to 48. Comparing Figures 44 and 45 for the event at 11.92° we see that the L_g spectrum is shifted to lower frequencies as compared to the P spectrum, in agreement with what we saw in comparing Figures (27a, 29a), (32, 33), (37, 38) and (42, 43) for SALMON. The same shift is evident for a Soviet explosion at the distance of 15.69° as seen in Figures 46 and 47. (Figure 45 is from the LP system at NORSAR, and by comparison with Figure 44 we see that it is far easier to detect L_g at 2 Hz than LR at 0.05 Hz, approximately 26 dB or 1.3 magnitude units easier.)

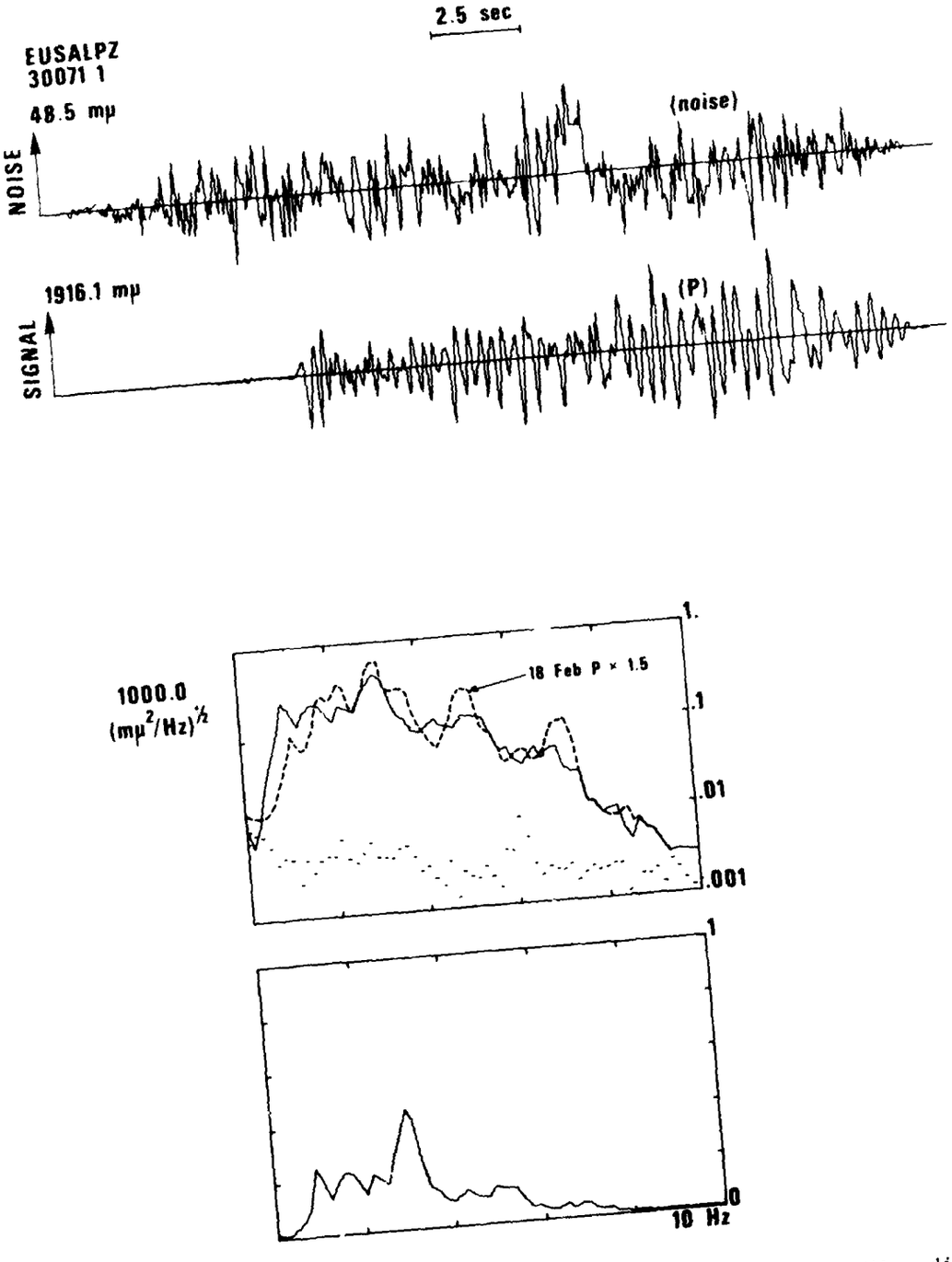

Figure 31. SALMON P waves and noise, signal and spectral at EUAL a distance of 242 km. Note overlay of 18 February 1964 earthquake at EUAL.

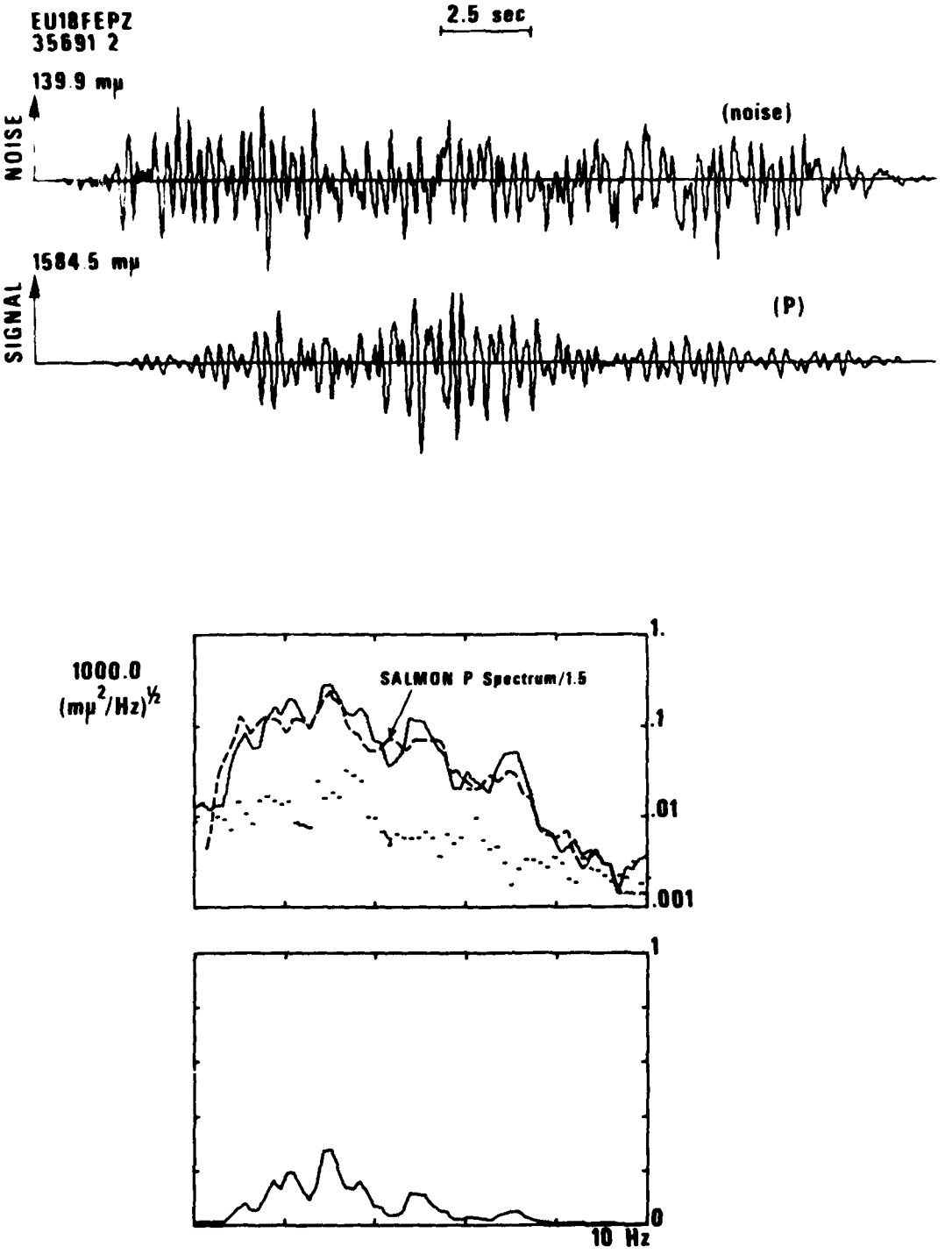

Figure 32. 18 February P waves and noise, signal and spectra at EUAL a distance of 311 km. Note overlay of SALMON P spectrum.

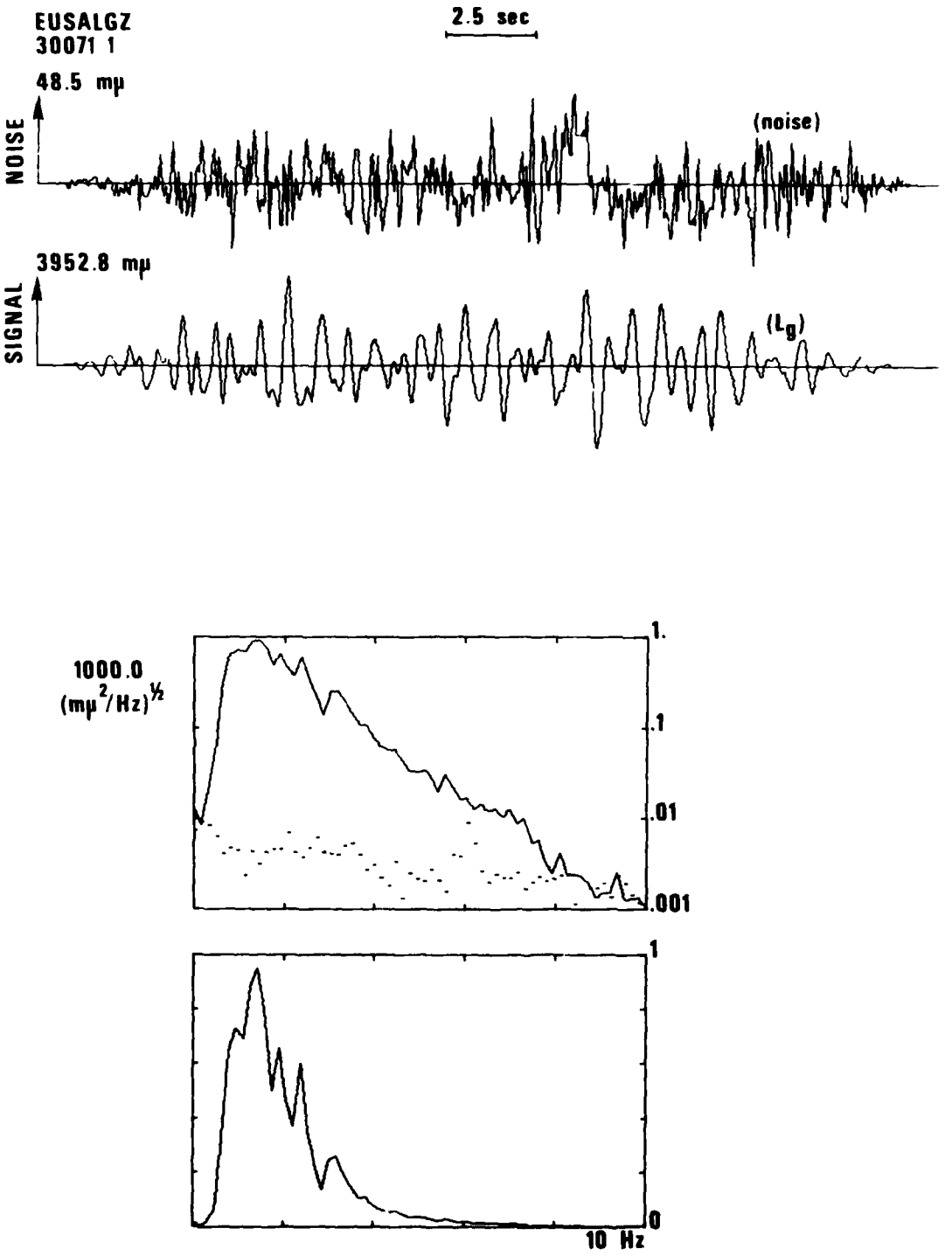

Figure 33. SALMON L_g waves and noise, signals and spectra at EUAL a distance of 242 km.

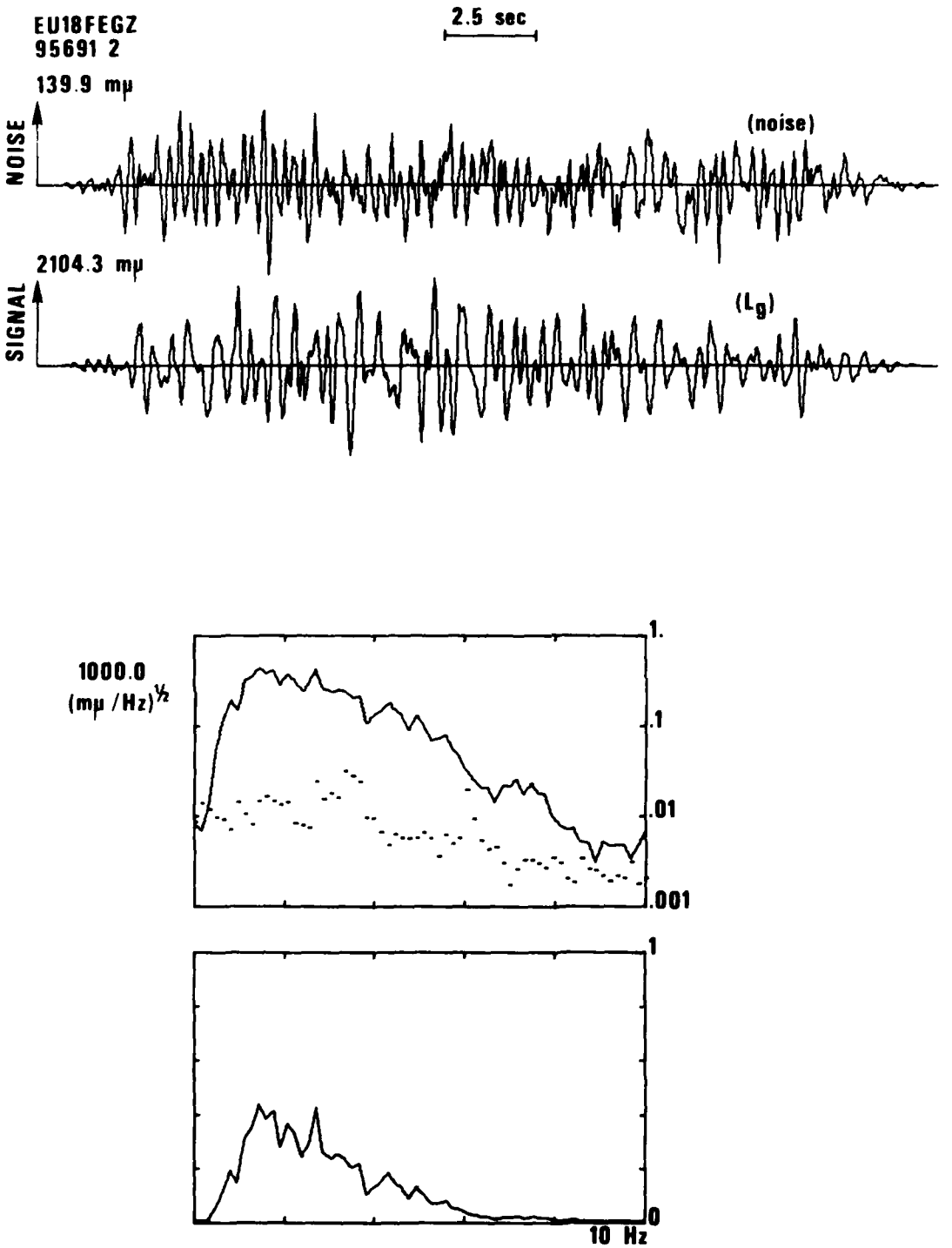

Figure 34. 18 February L_g waves and noise, signals and spectra at EUAL a distance of 311 km.

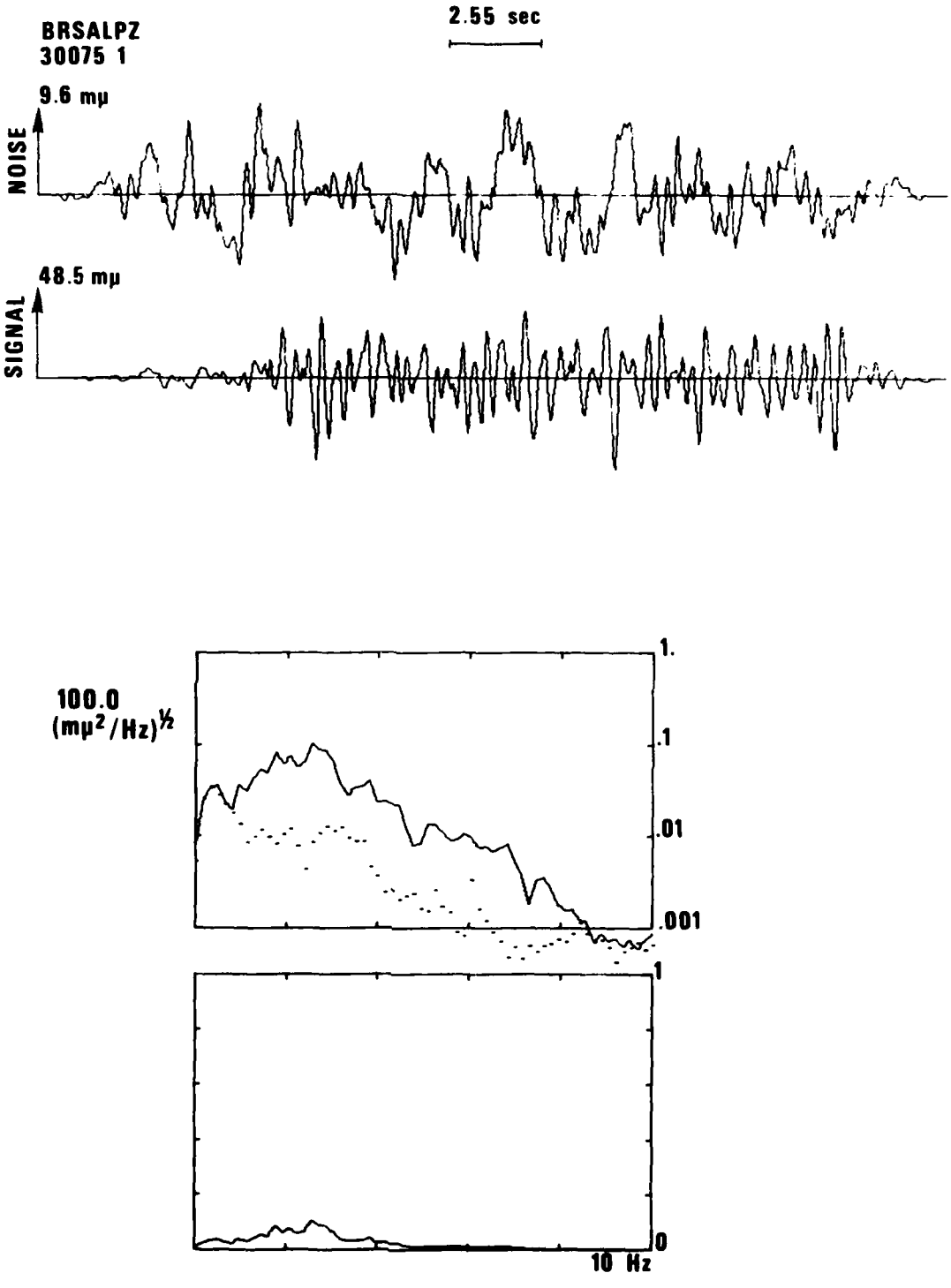

Figure 35. SALMON P wave signals and noise, waveforms and spectra at BRPA.

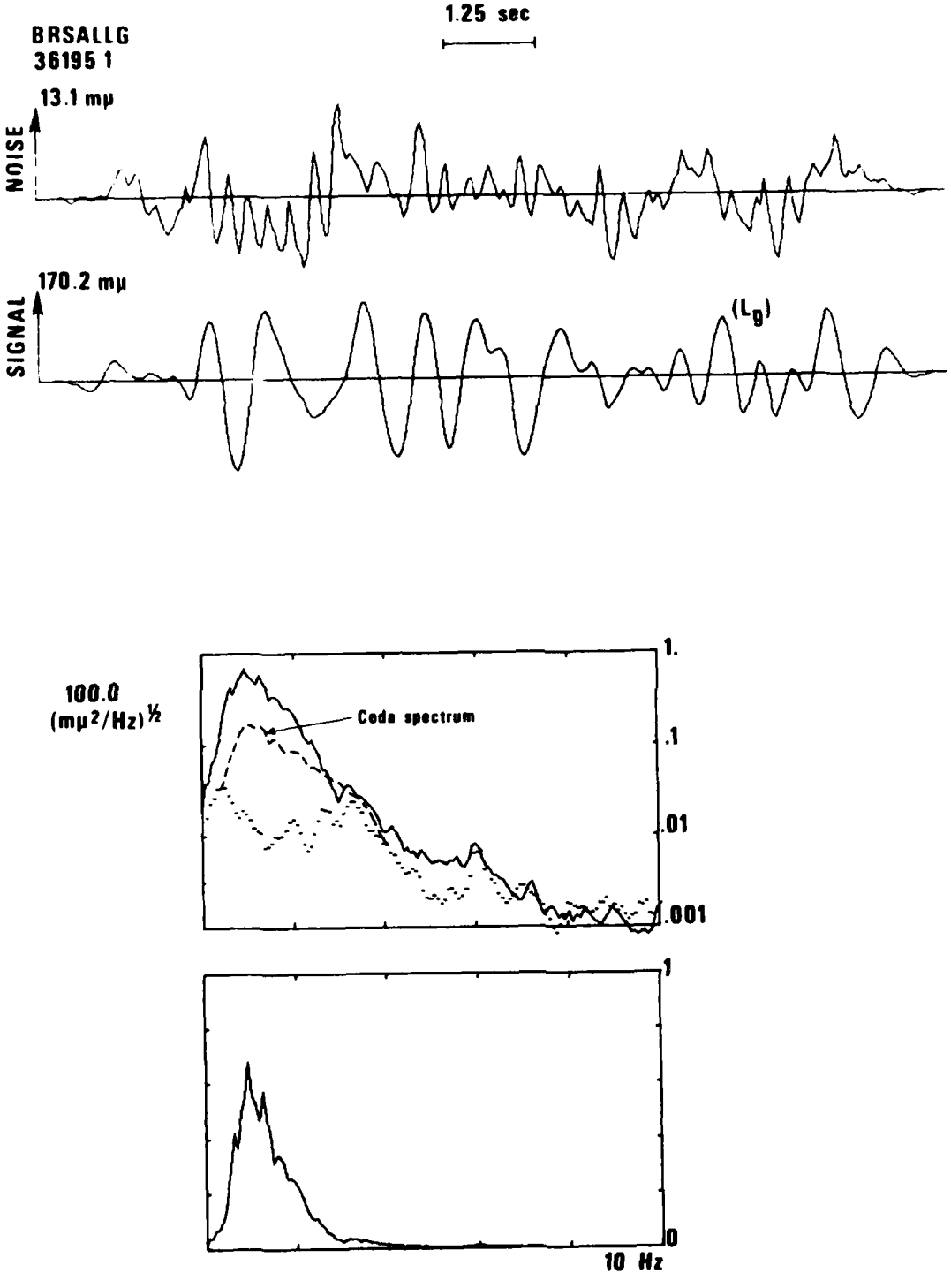

Figure 36. SALMON L_g wave signals and noise, waveforms and spectra at BRPA. Note overlay of spectrum of coda from time just before L_g arrival.

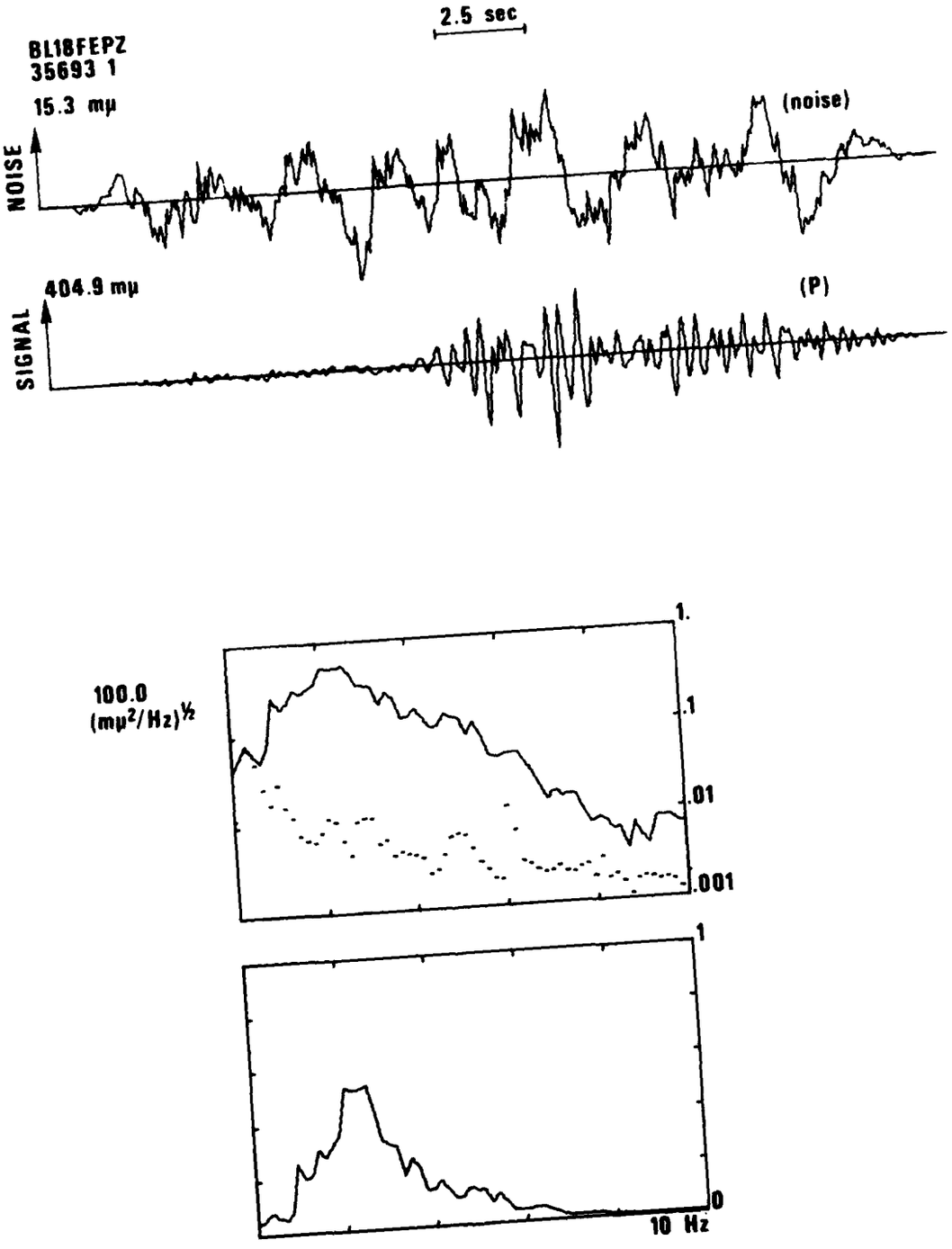

Figure 37. 18 February P wave signals and noise, waveforms and spectra at BLWV.

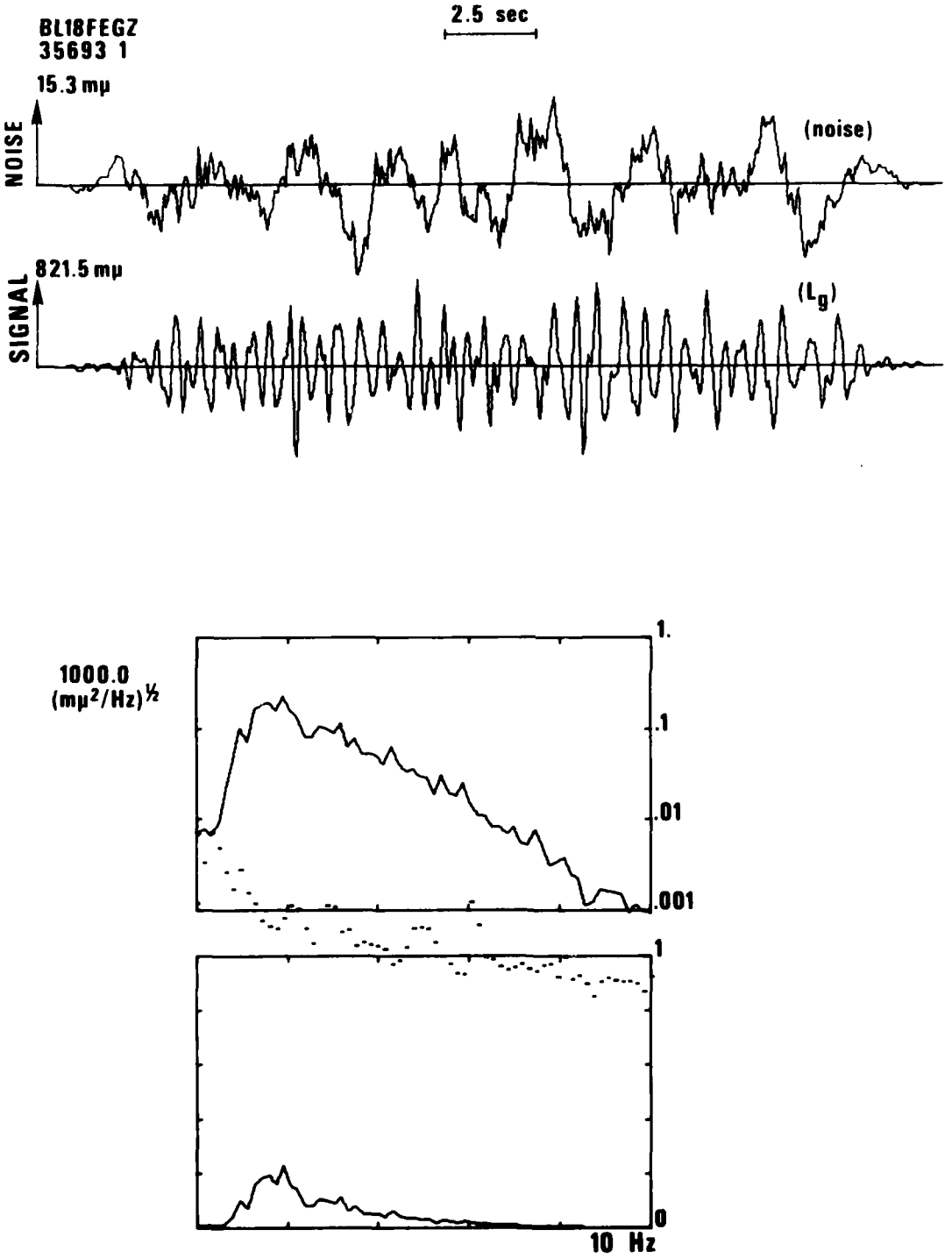

Figure 38. 18 February L_g wave signals and noise, waveforms and spectra at BLWV.

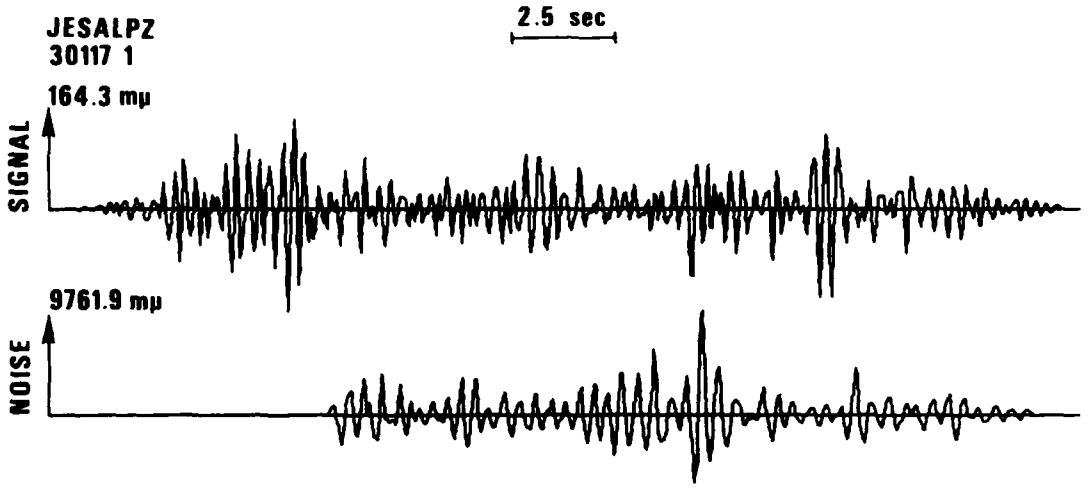

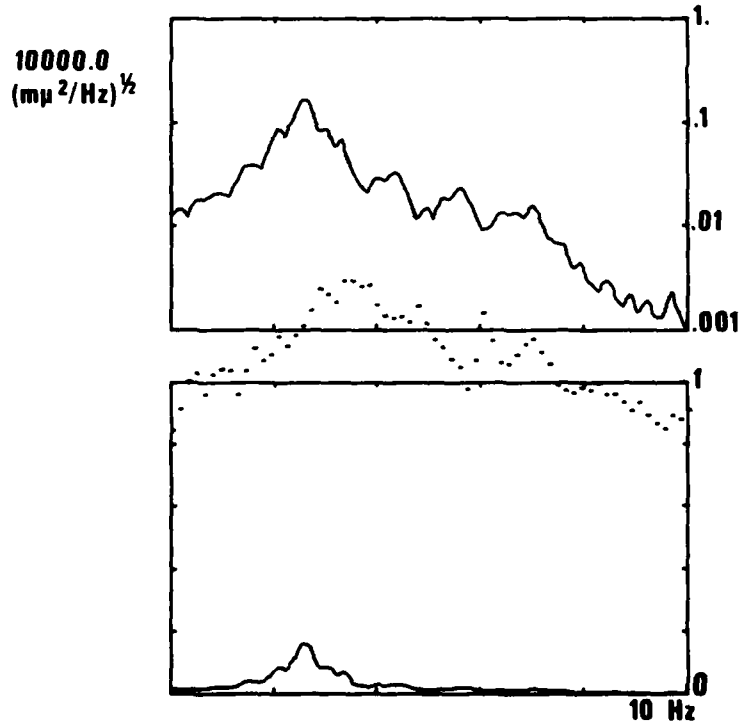

Figure 39. SALMON P wave signals and noise, waveforms and spectra at JELA, a distance of 243 km.

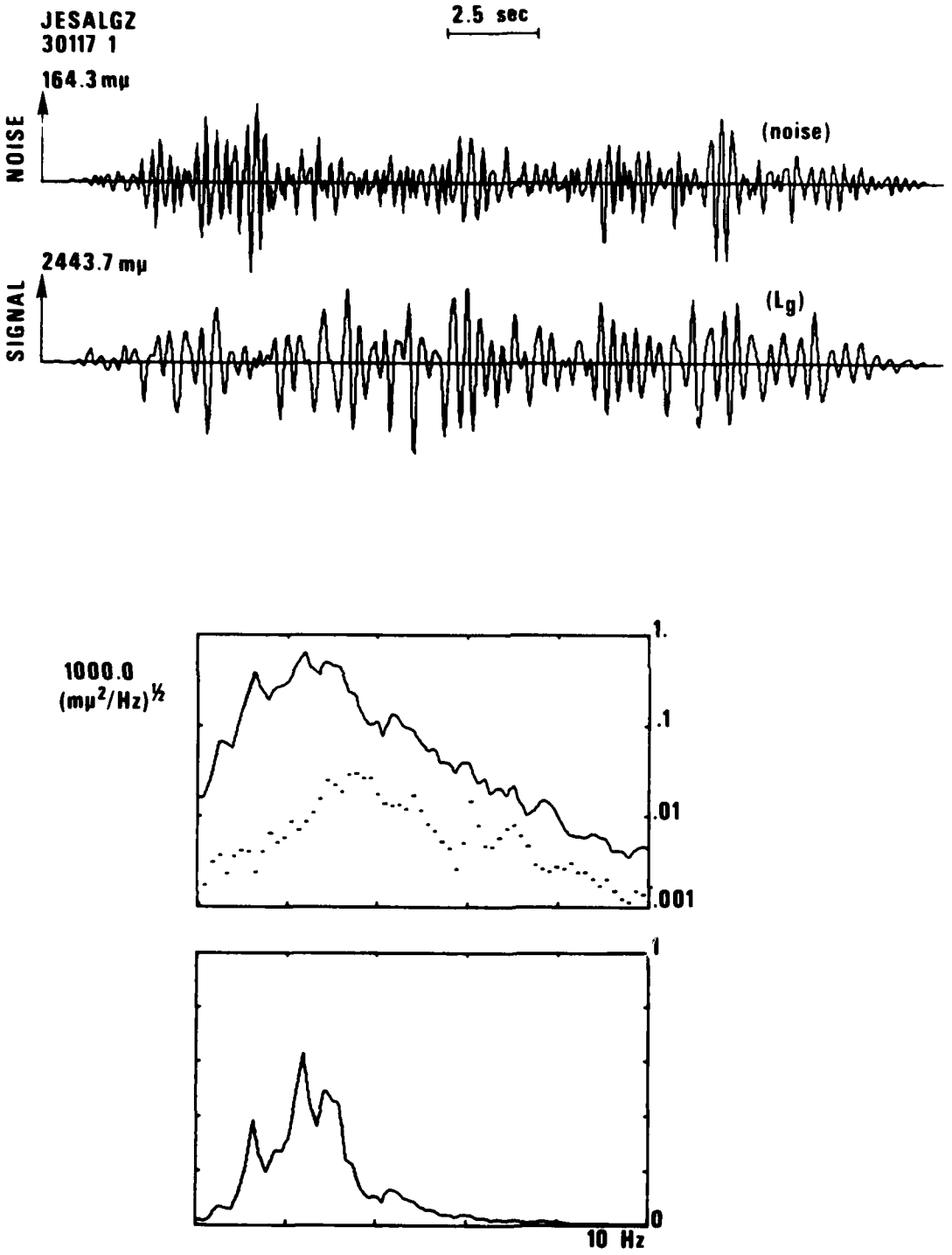

Figure 40. SALMON L_g wave signals and noise, waveforms and spectra at JELA, a distance of 243 km.

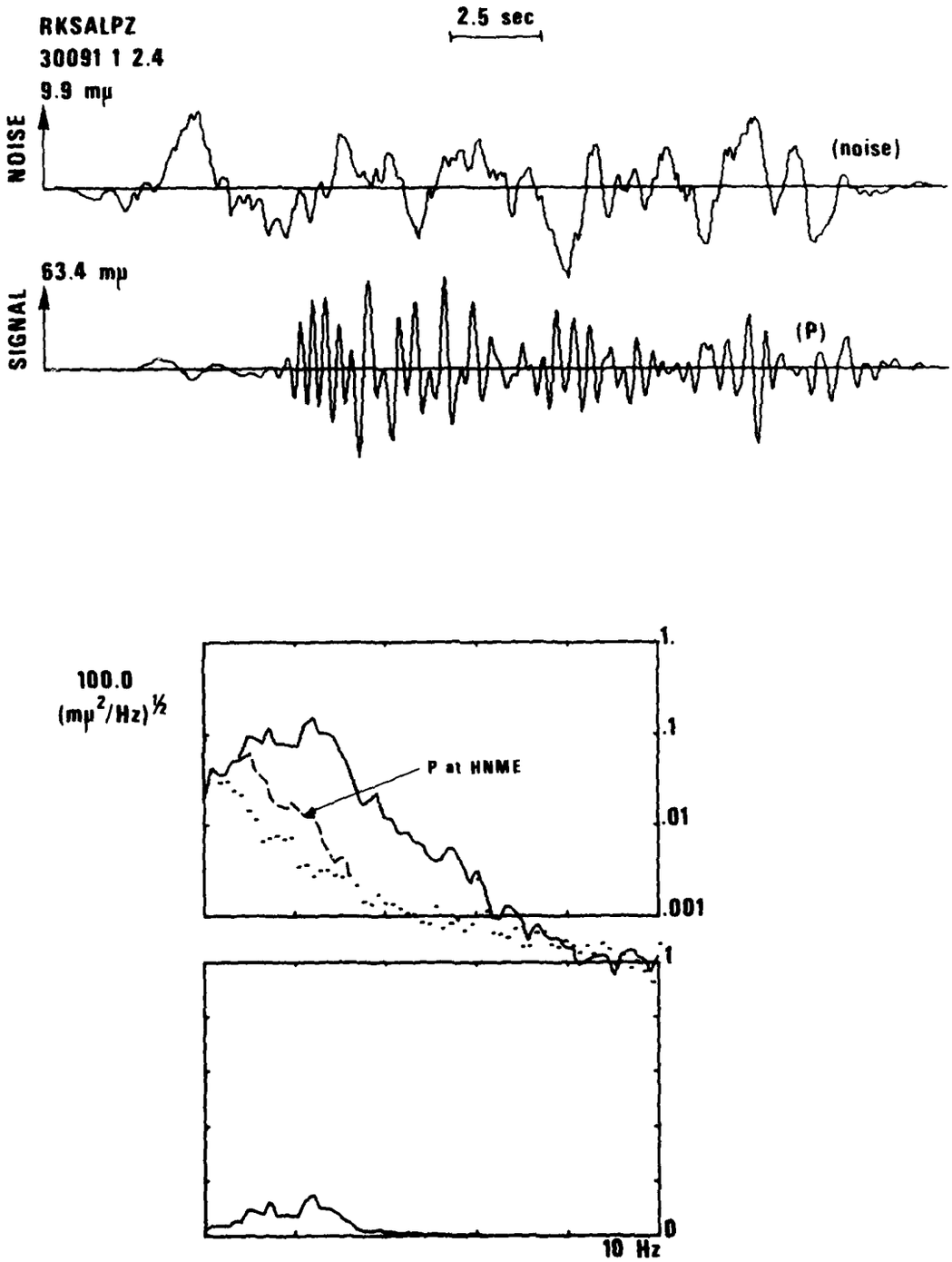

Figure 41. SALMON P wave signals and noise, waveforms and spectra at RKON, a distance of 2214 km. Note overlay of P spectrum at HNME a distance of 2499 km.

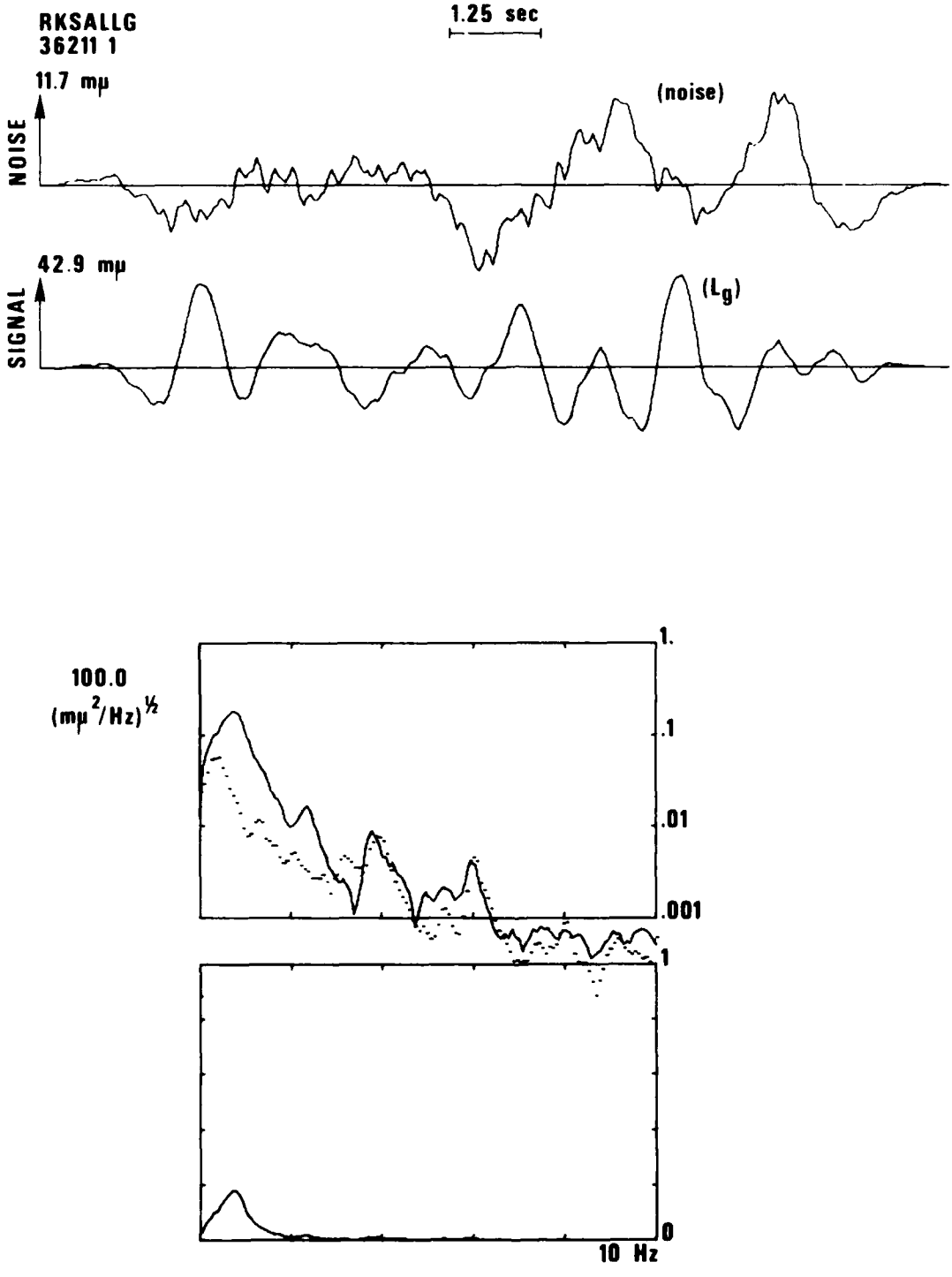

Figure 42. SALMON L_g signals and noise, waveforms and spectra at RKON, a distance of 2214 km.

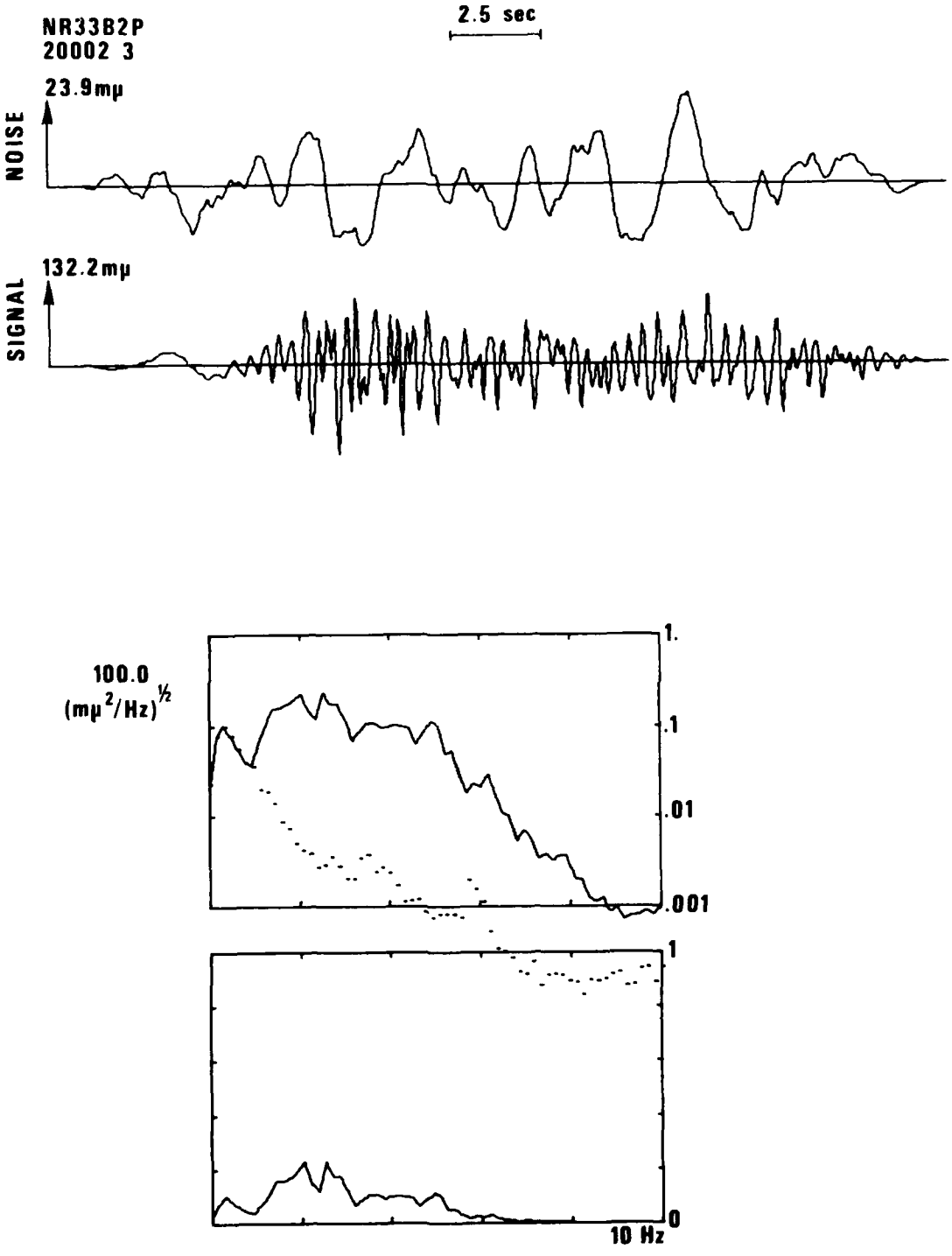

Figure 43. P wave signal and noise, waveform and spectra from Soviet explosion on 72/09/04 at a distance of 11.92° as recorded at C3 element of NORSAR. See Table VI for details.

TABLE VII

List of explosions recorded at NORSAR and analyzed in this report

Date	Origin Time	Lat (N)	Long (E)	Dist. to NORSAR (deg)	m_b (ISC)	In Figures
72/09/04	07:00:04	67.69	33.44	11.92	4.6	43, 44, 45, II-1
71/09/19	11:00:07	57.78	41.10	15.69	4.5	46, 47, II-2
71/10/04	10:00:02	61.61	47.12	17.35	4.6	II-3
72/07/09	06:59:58	49.78	35.40	18.15	4.8	II-4
71/07/10	16:59:59	64.17	55.18	20.43	5.2	II-5
74/08/29	15:00:00	67.23	62.12	22.74	5.0	II-6
71/10/22	05:00:00	51.57	54.54	25.54	5.2	II-7
74/08/14	14:59:58	68.91	75.90	27.45	5.4	II-8
71/07/02	17:00:02	67.66	62.00	33.60	4.7	II-9

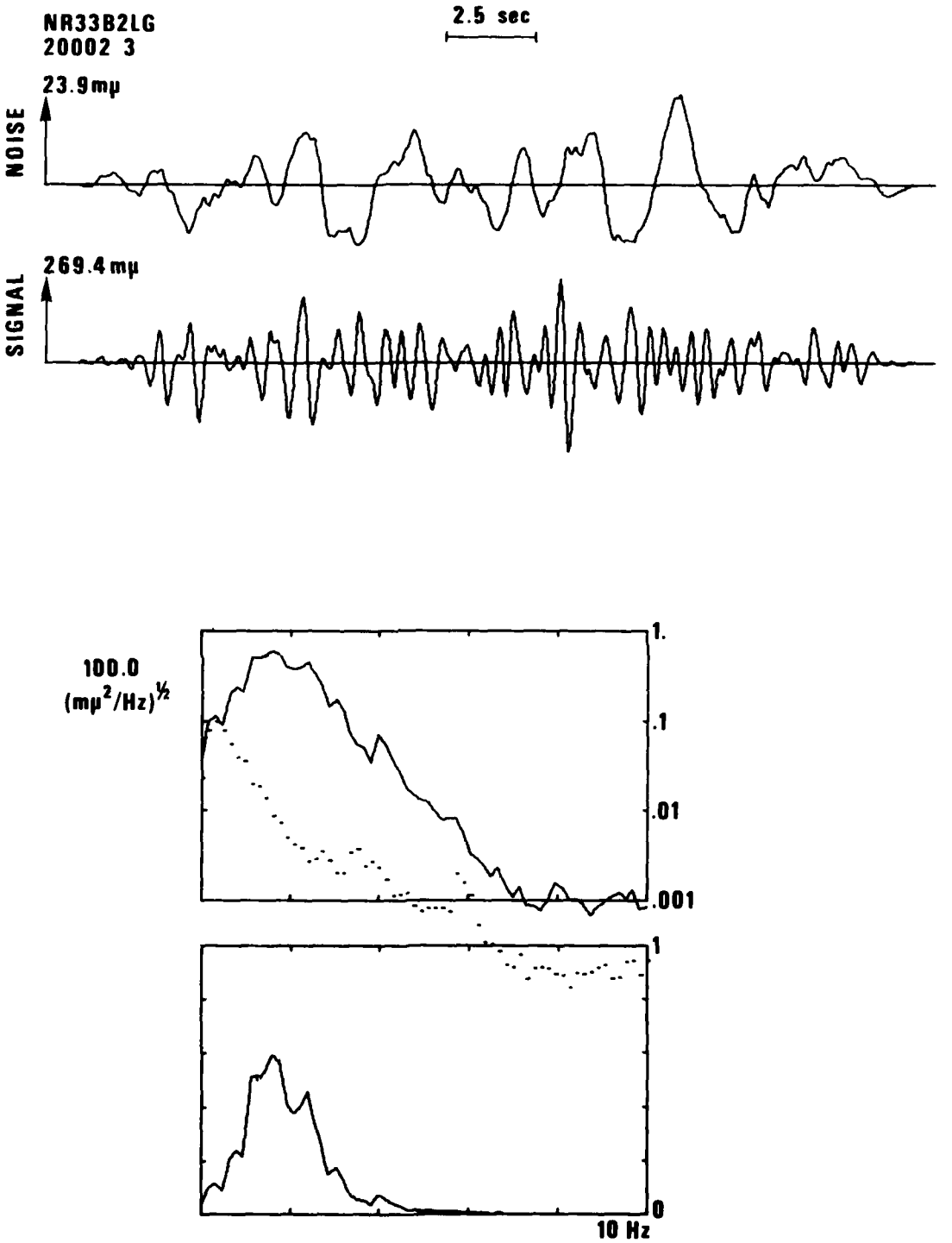

Figure 44. L_g wave signal and noise, waveform and spectra from Soviet explosion 72/09/04 at a distance of 11.92° as recorded at C3 element of NORSAR. See Table VI for details.

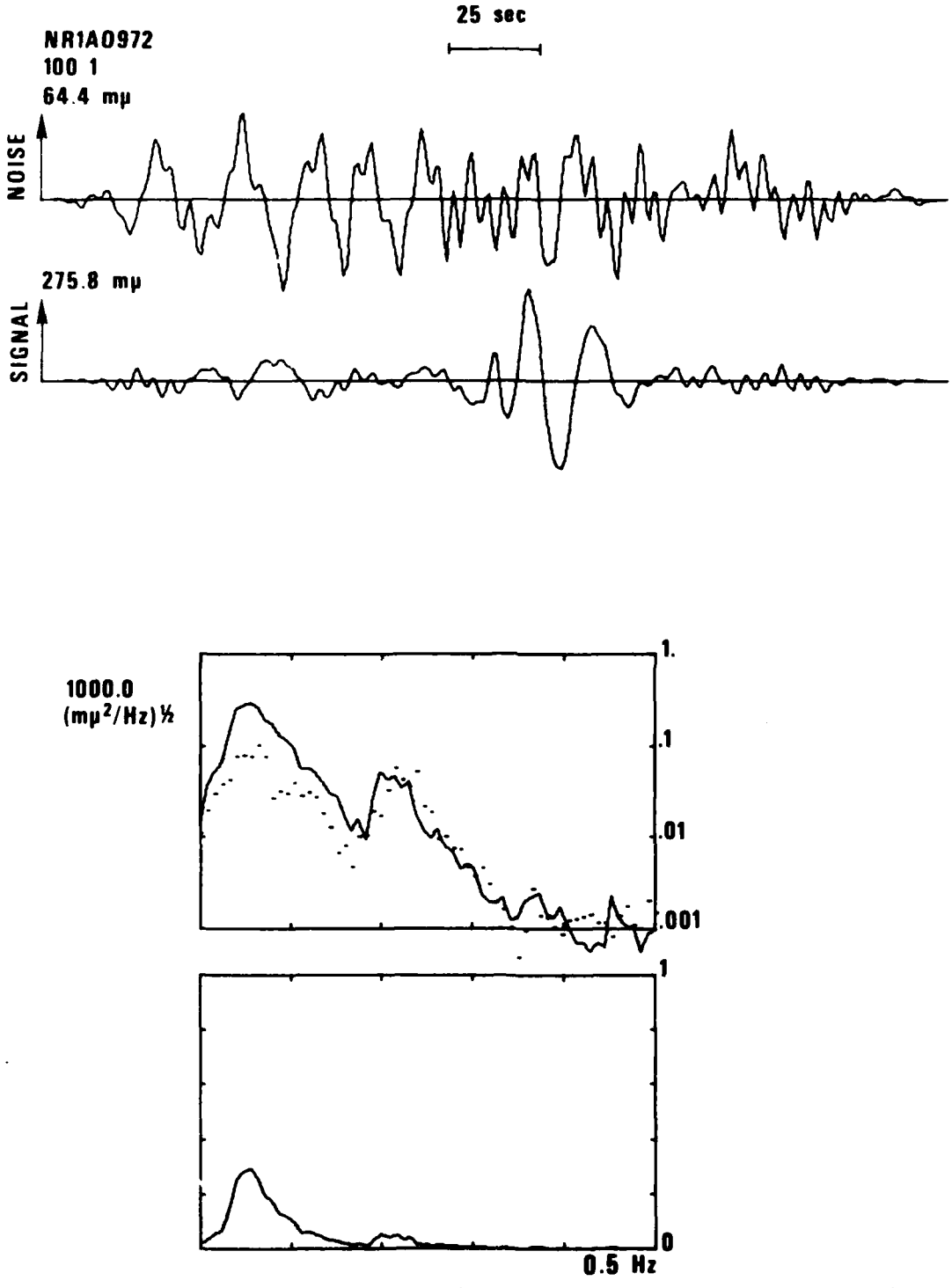

Figure 45. Long period LR wave signal and noise, waveform and spectra from Soviet explosion 72/09/04 at a distance of 11.92° as recorded at C3 element of NORSAR. See Table VI for details.

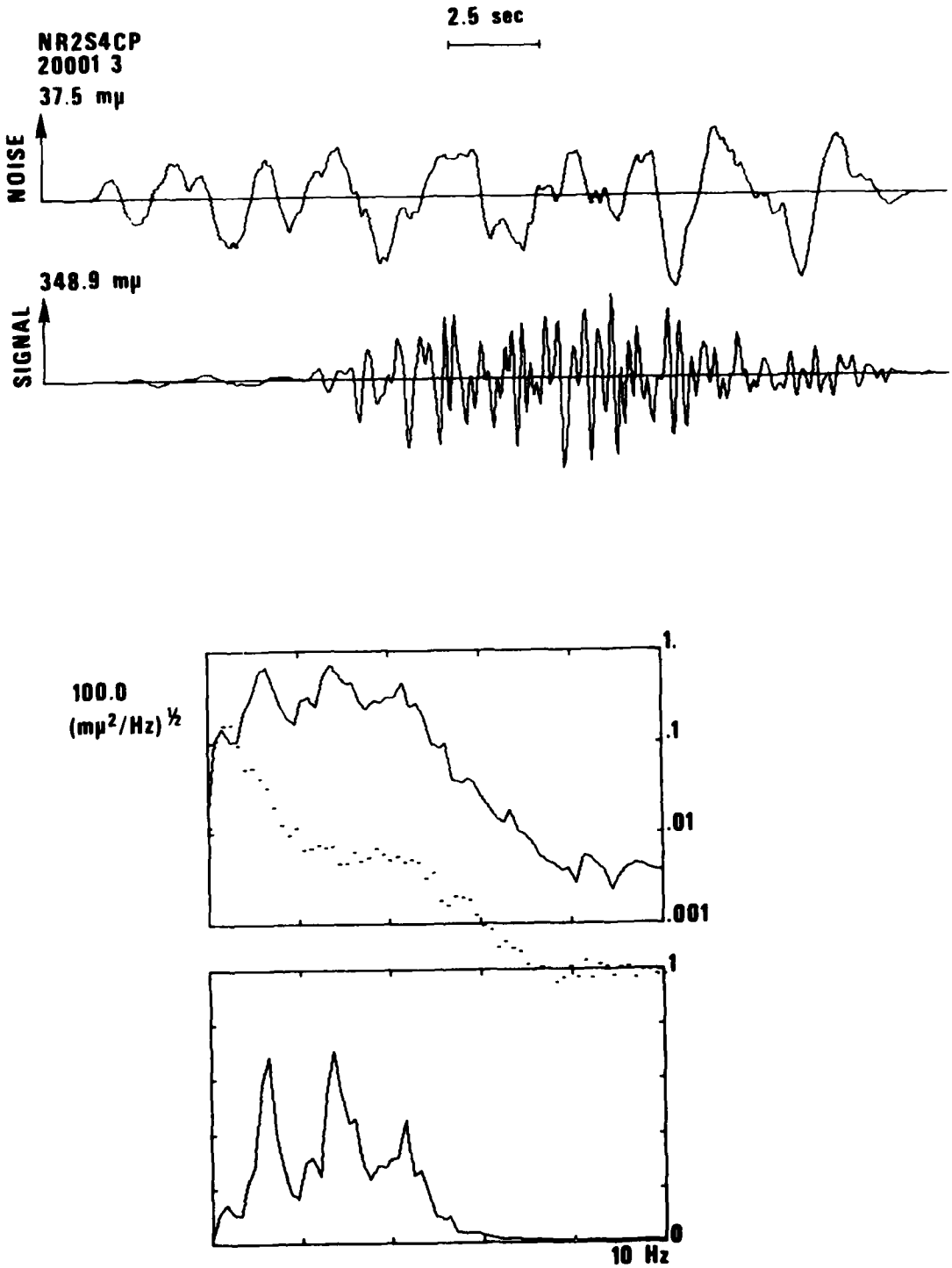

Figure 46. P wave signal and noise, waveform and spectra from Soviet explosion on 71/09/19 at a distance of 15.69° as recorded at C3 element of NORSAR. See Table VI for details.

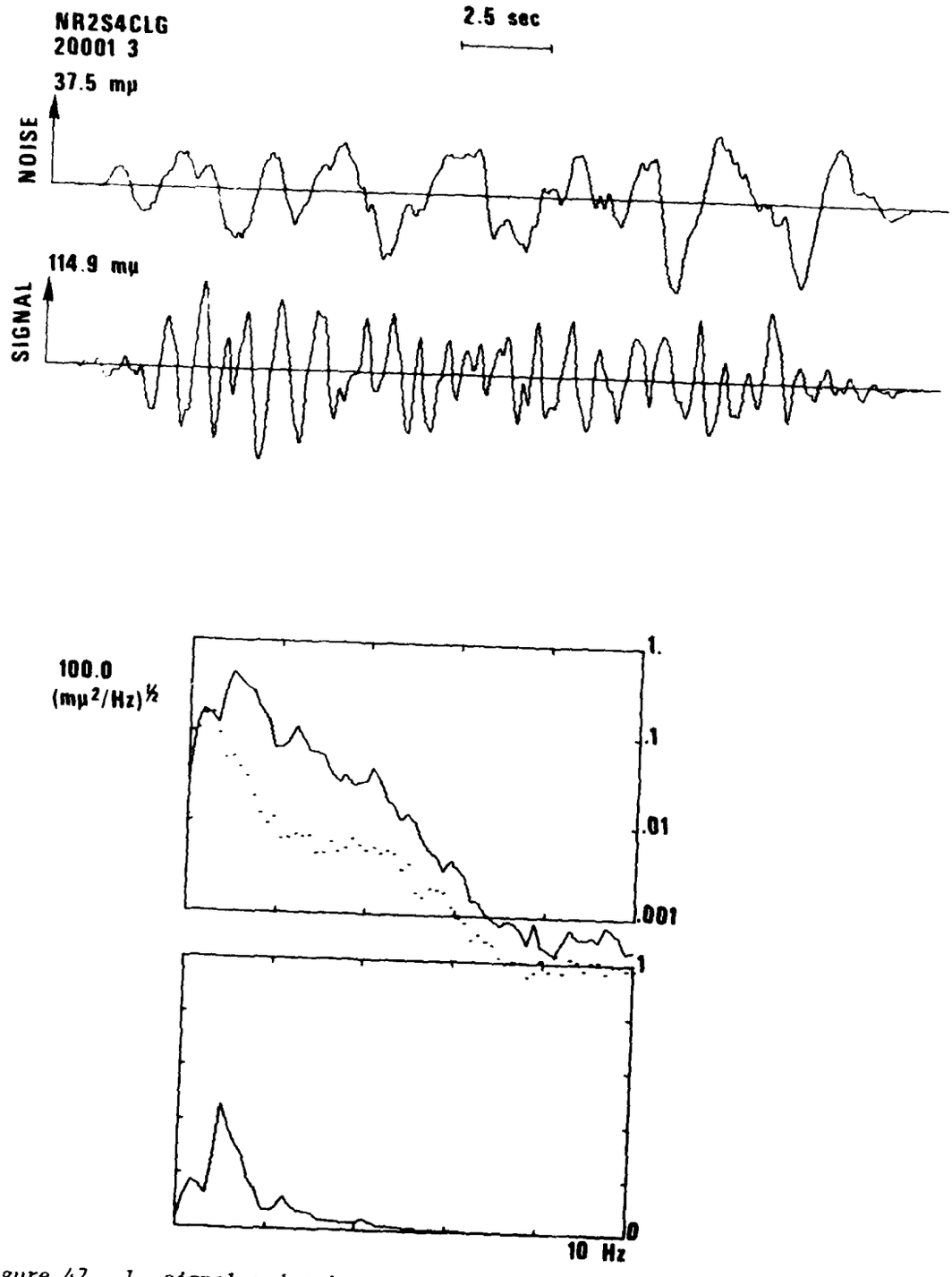

Figure 47. L_g signal and noise, waveform and spectra from Soviet explosion on 71/09/19 at a distance of 15.69° as recorded at C3 element of NORSAR. See Table VI for details.

COMMENTS ON DETECTION

Inspection of Figures (43, 44) and (46, 47) reveals, as mentioned before, that the P waves have more high frequency than the L_g waves. Considering that the P wave amplitude for explosions for the 15.69° event is larger than the L_g, it would seem that detection of explosions (not necessarily earthquakes) will, in general, hinge on the P waves. It is possible with the spectra of the signals in Table VII, as presented in Appendix II, to give a rough estimate of the detection threshold of a single instrument at the site of the C3 subarray. Let us assume that an analyst will detect the P wave when the signal spectrum is equal to the noise spectrum at some frequency. This is reasonable for two reasons. First, the signal to noise ratio is typically flat over a bandwidth of nearly 2 Hz. This is wider than is typically the case for teleseisms and makes the "frequency change" more dramatic. Secondly, these regional signals are more extended in duration than the teleseismic signals, thus giving the analyst a larger window in time over which to establish that the character of the trace has permanently changed from that before the arrival of the signal. (In theoretical signal detection terms, these remarks are equivalent to the statement that regional P signals have a larger BT or bandwidth-time product than teleseismic signals, so that they may be detected at a lower threshold.)

The required calculations are outlined in Table VIII. There we note the S/N in dB at the frequency, f_{max}, at which the S/N is a maximum. Assuming that the S/N is proportional to magnitude, we have then used the ISC m_b values to correct these dB values to those appropriate for a magnitude 4.5 event. These are then further corrected to what they would be at a distance of 10° assuming amplitude proportional to $r^{-2.5}$ as we found in the EUS and by consideration of Nersesov and Rautian's (1964) results. These dB values are then averaged to give a value of 43 dB S/N at 10° for an $m_b = 4.5$ explosion. Then, using $r^{-2.5}$ for extrapolation, we find m_b detection thresholds of 0.9, 2.4, 3.3, and 3.9 m_b at 5°, 10°, 15° and 20° respectively. These are probably low estimates to some degree, because such small events would have more high-frequency energy than the events considered as data. We have not considered whether this is the 50% or 90% threshold so there is, perhaps, a residual 0.3 m_b unit uncertainty. However, since we think analysts would almost certainly detect a properly filtered signal under these conditions, our best estimate is that it is a

TABLE VIII

Calculation of NORSAR single element P-wave magnitude detection threshold for Eurasian shield explosions

Date	f_{max}	dB	m_b	dB (4.5)	Δ°	dB (10°)	
72/09/04	5	45	4.6	43	11.92	49	
							T(5°) = 0.9
71/09/19	4.5	40	4.5	40	15.69	50	
							T(10°) = 2.4
71/10/04	4	23	4.6	21	17.35	33	
							T(15°) = 3.3
72/07/09	4	40	4.8	34	18.15	47	
							T(20°) = 3.9
71/07/10	2	40	5.2	26	20.43	42	
74/08/29	2	30	5.0	20	22.74	38	

average: 43 dB (S/N) @ 10° for m_b = 4.5

Distance-amplitude assumed proportional to $r^{-2.5}$

90% threshold. It must also be stated that this is a shield to shield result. Events in tectonic regions would certainly have less high-frequency and be harder to detect.

It is worth noting that although in Table VIII the peak in S/N changes from 5 Hz at 12° to 2 Hz at 23° (and continues at 2 Hz out to 33° as seen from the remaining spectra in Appendix II), the spectra in Appendix II also show that at NORSAR 10 Hz energy is above the noise all the way out to 33°. The relative usefulness of the 10 Hz energy for detection can only increase for smaller events which have higher corner frequencies. Assuming an asymptotic spectrum proportional to ω^{-2} and a typical corner frequency near 5 Hz for the events studied (SALMON's corner frequency was ~ 3 Hz), then one could regain about 12 dB S/N at 10 Hz. This would still not be a better S/N than we observe in the range 2 to 5 Hz; however, the noise at 10 Hz in the spectra presented may well be system or quantization noise, so that the true S/N at 10 Hz may be greater than is apparent. If so, then it is possible that for a better designed system the S/N might be higher at 10 Hz than at 2 to 5 Hz for small events.

SUMMARY

Amplitude-distance curves are different in the EUS and WUS; P_{max} decays as $r^{-2.5}$ and $r^{-3.0}$ in EUS and WUS, while for the maximum after 3.6 km/sec on the vertical component (termed L_g) the decay rates are r^{-2} and r^{-3}. The EUS results are in general agreement with the literature and with the data presented by Nersesov and Rautian (1964) for events on the northern margin of tectonic regions in the Soviet Union suggesting that discrimination results in the EUS are relevant to NSS stations within the Soviet Union.

Using these distance amplitude relations, network mean amplitudes at 1000 km were computed for L_g and P_{max} for earthquakes and explosions in the EUS and WUS and a separation of 0.6 magnitude units was observed thus forming a regional discriminant. The L_g is larger for earthquakes than for explosions. This conclusion is somewhat uncertain in the WUS because of the large scatter in the explosion population. However, a reasonable explanation for this large scatter is that the small events at NTS are at such shallow depths in dry alluvium that the medium is weak, resulting in a low corner frequency. This decreases the ratio P_g/L_g since P_g contains comparatively more high frequency than L_g. The scatter probably would not be a problem in a true test ban situation since shots will be well buried to avoid surface collapse.

The WUS earthquake P_{max} versus L_g is displaced about 0.2 magnitude units from the EUS curve, reflecting the large P_g phase relative to L_g in the WUS.

The GNOME explosion and the Hebgen Lake earthquake, which are on the border between the EUS and WUS defined by Der, Massé and Gurski (1975), show differences in amplitude distance relations for the same event in different provinces. The greater WUS attenuation results in amplitudes at 10° of about 0.4 magnitude units below that in EUS.

Analysis of the SALMON and 18 February 1964 Alabama earthquake shows that there is no earthquake/explosion discrimination capability using maximum transverse to maximum radial amplitude ratios. We also find that the source spectra of the two events are identical between 1 and 10 Hz, that the L_g spectrum is different from the P spectrum and is therefore not the source spectrum, and that the L_g spectrum is contaminated by scattered coda from earlier phases so that high-frequencies observed in the L_g phase may not be

predictable by any deterministic theory of L_g. Identical conclusions with respect to the P and L_g spectra were obtained by analysis of spectra of Soviet explosions as observed at NORSAR.

In the EUS, 10 Hz energy is observed out to 10°, and for Soviet shots observed at NORSAR, out to 33°. The peak in the S/N varies from 5 Hz at 11° to 2 Hz at 33°; however, for small events which have not yet been studied, the peak may well be at higher frequencies because of higher corner frequencies and because much of the noise on LRSM and NORSAR systems at 10 Hz may be system or quantization noise which can be reduced by more carefully designed systems.

Detection thresholds for a single element at the C3 subarray of NORSAR were determined to be m_b 0.9, 2.4, 3.3, and 3.9 at 5°, 10°, 15° and 20°, respectively. It should be noted that the lower frequency noise levels are high at NORSAR, which is near the sea, and thus that stations on continents might have lower thresholds at large distances where the lower frequencies are the most useful for detection.

ACKNOWLEDGEMENT

We would like to thank I. Gupta for performing some of the network average magnitude calculations.

REFERENCES

Baker, R. G. (1967). Preliminary study for determining magnitude from L_g, Earthquake Notes, 38, 23-28.

Baker, R. G. (1970). Determining magnitude from L_g, Bull. Seism. Soc. Am., 60, 1907-1919.

Bakun, W. H. and L. R. Johnson (1970). Short period spectral discriminants for explosions, Geophys. J. R., Astr. Soc., 22, 139-152.

Båth, M. (1969). Handbook on earthquake magnitude determinations, Seis. Inst., Uppsala, Sweden, 131.

Bollinger, G. (1970). Travel time study of central Appalachian earthquakes, Bull. Seism. Soc. Am., 60, 629-637.

Bollinger, G. A. (1973). Seismicity of the southeastern United States, Bull. Seism. Soc. Am., 63, 1785-1808.

Bollinger, G. A. (1977). unpublished manuscript.

Booker, A. and W. Mitronovas (1964). An application of statistical discrimination to classify seismic events, Bull. Seism. Soc. Am., 54, 961-971.

Brune, J. N. and J. Dorman (1963). Seismic waves and earth structure in the Canadian Shield, Bull. Seism. Soc. Am., 53, 167-210.

Brune, J. N., A. Espinosa and J. Oliver (1963). Relative excitation of surface waves by earthquakes and underground explosions in the California-Nevada region, J. Geophys. Res., 68, 3501-3513.

Chun, K. and T. Yoshii (1977). Crustal structure of the Tibetan plateau: a surface-wave study by a moving window analysis, Bull. Seism. Soc. Am., 67, 735-750.

Der, Z. A. and T. W. McElfresh (1976). Short-period P-wave attenuation along various paths in North America as determined from P-wave spectra of the SALMON nuclear explosion, Bull. Seism. Soc. Am., 66, 1609-1622.

Evernden, J. F. (1967). Magnitude determination at regional and near-regional distances in the United States, Bull. Seism. Soc. Am., 57, 591-639.

Ewing, M., Jardetsky, W., and F. Press (1952). Elastic Waves in Layered Media, McGraw Hill, 300.

Gibowicz, S. J. (1972). The relationship between teleseismic body-wave magnitude M and local magnitude M_L from New Zealand earthquakes, Bull. Seism. Soc. Am., 62, 01-11.

Gumper, F. and P. W. Pomeroy (1970). Seismic wave velocities and earth structure on the African continent, Bull. Seism. Soc. Am., 60, 651-668.

Haskell, N. A. (1964). Total energy and energy spectral density fr[illegible] propagating faults, Bull. Seism. Soc. Am., 54, 1811-1841.

REFERENCES (Continued)

Haskell, N. A. (1966). The leakage attenuation of continental crustal P waves, J. Geophys. Res., 71, 3955-3967.

Isacks, B. L. and C. Stephens (1975). Conversion of S_n and L_g at a continental margin, Bull. Seism. Soc. Am., 65, 235-244.

Jones, F. B., L. T. Long, and J. H. McKee (1977). Study of the attenuation and azimuthal dependence of seismic-wave propagation in the Southeastern United States, Bull. Seism. Soc. Am., 67, 1503-1513.

Jordan, J. N., W. V. Mickey, W. Helterbran, and D. M. Clark (1966). Travel times and amplitudes from the SALMON explosion, J. Geophys. Res., 71, 3469-3482.

Kaila, K. L and D. Sarkar (1975). P-wave amplitude variation with epicentral distance and the magnitude relations, Bull. Seism. Soc. Am., 65, 915-926.

Knopoff, L., F. Schwab, K. Nakanishi, and F. Chang (1974). Evaluation of L_g as a discriminant among different continental crustal structures, Geophys. J. R. Astr. Soc., 39, 41-70.

Lambert, D. G. and S. S. Alexander, unpublished manuscript (1971). Relationship of body and surface wave magnitude for small earthquakes and explosions, Seismic Data Laboratory Report 245, Teledyne Geotech, Alexandria, Virginia.

Lambert, D. G. and E. S. Becker (1975). Basic seismic analysis of regional events observed at NORSAR, Technical Report Number 4, Texas Instruments, Alexandria, Virginia.

Lehmann, I. (1957). On L_g as read in North American records, Anneli di Geofisica, 10, 1-21.

Massé, R. P. and S. S. Alexander (1964). Compressional velocity distribution beneath Scandinavia and Western Russia, Geophys. J. R. Astr. Soc., 39, 587-602.

McEvilly, T. V. (1964). Central U. S. crust-upper mantle structure from Love and Rayleigh wave phase velocity inversion, Bull. Seism. Soc. Am., 54, 1997-2015.

Mitchell, B. J. (1975). Regional Rayleigh wave attenuation in North America, J. Geophys. Res., 80, 4904-4916.

Molnar, P. and J. Oliver (1969). Lateral variations of attenuation in the upper mantle and discontinuities in the lithosphere, J. Geophys. Res., 74, 2648-2682.

Murphy, J. R. (1976). Applications of near-field seismic data in the investigations of source characteristics of explosions and earthquakes (U), Final Technical Report, Computer Sciences Corporation, Falls Church, Virginia.

Nersesov, I. L. and T. G. Rautian (1964). Kinematics and dynamics of seismic waves to distance of 3500 km from the epicenter, Akad. Nauk SSSR, Trudy Inst. Fiziki Zemli, 32, 63-87. (Translated by A. Ryall, DARPA, 12/8/77).

Nuttli, O. W. (1972). The amplitudes of teleseismic P waves, Bull. Seism. Soc. Am., 62, 343-356.

Nuttli, O. W. (1973). Seismic wave attenuation and magnitude relations for Eastern North America, J. Geophys. Res., 78, 876-885.

Oliver, J. and M. Ewing (1957). Higher modes of continental Rayleigh waves, Bull. Seism. Soc. Am., 47, 187-204.

Oliver, J. and M. Ewing (1958). Normal modes of continental surface waves, Bull. Seism. Soc. Am.. 48, 33-49.

Oliver, J. and M. Ewing (1958). The effect of surficial sedimentary layers on continental surface waves, Bull. Seism. Soc. Am., 48, 339-354.

Pasechnik, I. P. (1970). Characteristics of seismic waves from nuclear explosions and earthquakes, Nauka, Moscow. Translated by C. Shishkevish, Geosciences Bulletin, Series A, Volume 1, Rand Corporation, Washington, D.C.

Peppin, W. A. and T. V. McEvilly (1974). Discrimination among small magnitude events on the Nevada Test Sites, Geophys. J. R. Astr. Soc., 37, 227-243.

Press, F. (1964). Seismic wave attenuation in the crust, J. Geophys. Res., 69, 4417-4418.

Press, F. and M. Ewing (1952). Two slow surface waves across North America, Bull. Seism. Soc. Am., 42, 219-228.

Press, F. and B. Gutenberg (1956). Channel P waves in the earth's crust, Trans. Am. Geophys. Union, 37, 754-756.

Richter, C. F. (1958). Elementary Seismology, W. H. Freeman, San Francisco, 345-346.

Romney, C. (1959). Amplitudes of seismic body waves from underground nuclear explosions, J. Geophys. Res., 64, 1489-1498.

Romney, C., B. G. Brooks, R. H. Mansfield, D. S. Carder, J. N. Jordan and D. W. Gordon (1962). Travel times and amplitudes of principal body phases recorded from GNOME, Bull. Seism. Soc. Am., 52, 1057-1074.

Ruzaikin, A. I., I. L Nersesov, V. I. Khalturin, and P. Molnar (1977). Propagation of L_g and lateral variations in crustal structure in Asia, J. Geophys. Res., 82, 307-316.

Ryaboy, V. Z. and Y. K Shchukin (1975). Upper-mantle velocity inhomogeneities and seismicity, Izv. Earth Physics, 7, 419-424, in translation.

Ryall, A. and D. J. Stuart (1963). Travel times and amplitudes from nuclear explosions, Nevada Test Site to Ordway, Colorado, J. Geophys. Res. 68, 5821-5835.

Saha, B. P. (1961). The seismic L_g waves and their propagation along the granitic layer of the crust of the Indian subcontinent, J. Geophys. Res., 12, 609-618.

Shurbet, D. H. (1960). The P phase transmitted by crustal rock to intermediate distances, J. Geophys. Res., 65, 1809-1814.

Street, R. L. (1976). Scaling Northeastern United States/Canadian earthquakes by their L_g waves, Bull. Seism. Soc. Am., 66, 1525-1538.

Veith, K. F. (1975). Refined hypocenters and accurate reliability estimates, Bull. Seism. Soc. Am., 75, 1199-1222.

Vinnik, L. P. and A. A. Godzikovskaya (1972). Sounding of the earth's mantle by method of seismically conjugate points, Izv. Earth Physics, No. 10, 656-663, in translation.

Vinnik, L. P. and A. A. Godzikovskaya (1973) Lateral variations of the absorption by the upper mantle beneath Asia, Izv. Earth Physics, No. 1, 1-8, in translation.

Willis, D. E. (1963). Comparison of seismic waves generated by different types of source, Bull. Seism. Soc. Am., 53, 965-986.

Willis, D. E., J. DeNoyer and J. T. Wilson (1963). Differentiation of earthquakes and underground nuclear explosions on the basis of amplitude characteristics, Bull. Seism. Soc. Am., 53, 979-987.

Yacoub, N. K and B. J. Mitchell (1977). Attenuation of Rayleigh-wave amplitudes across Eurasia, Bull. Seism. Soc. Am., 67, 751-769.

Zhadin, V. V. (1976). Measurements of the Q factor of the upper mantle in the active Kamchatka zone, Izv. Earth Physics, 91-95, in translation.

APPENDIX I

Distance-Amplitude Plots for P_n, P_{max}, L_g

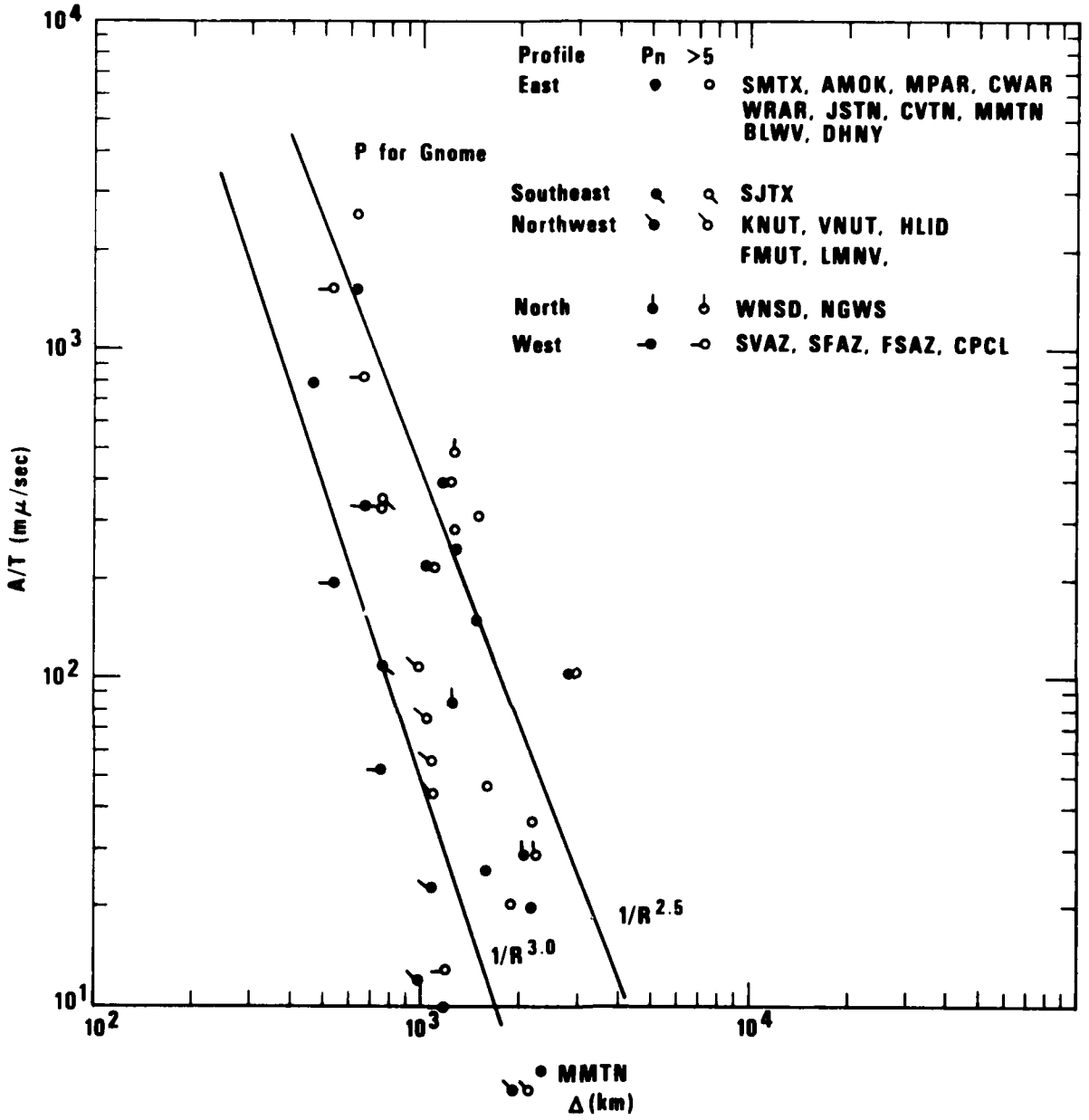
Profile Pn >5
East
SMTX, AMOK, MPAR, CWAR
WRAR, JSTN, CVTN, MMTN
BLWV, DHNY
P for Gnome
Southeast
SJTX
Northwest
KNUT, VNUT, HLID
FMUT, LMNV,
North
WNSD, NGWS
West
SVAZ, SFAZ, FSAZ, CPCL
10^4
10^3
10^2
10^1
A/T (mμ/sec)
$1/R^{2.5}$
$1/R^{3.0}$
10^2
10^3
10^4
MMTN
Δ (km)

Figure I-1a

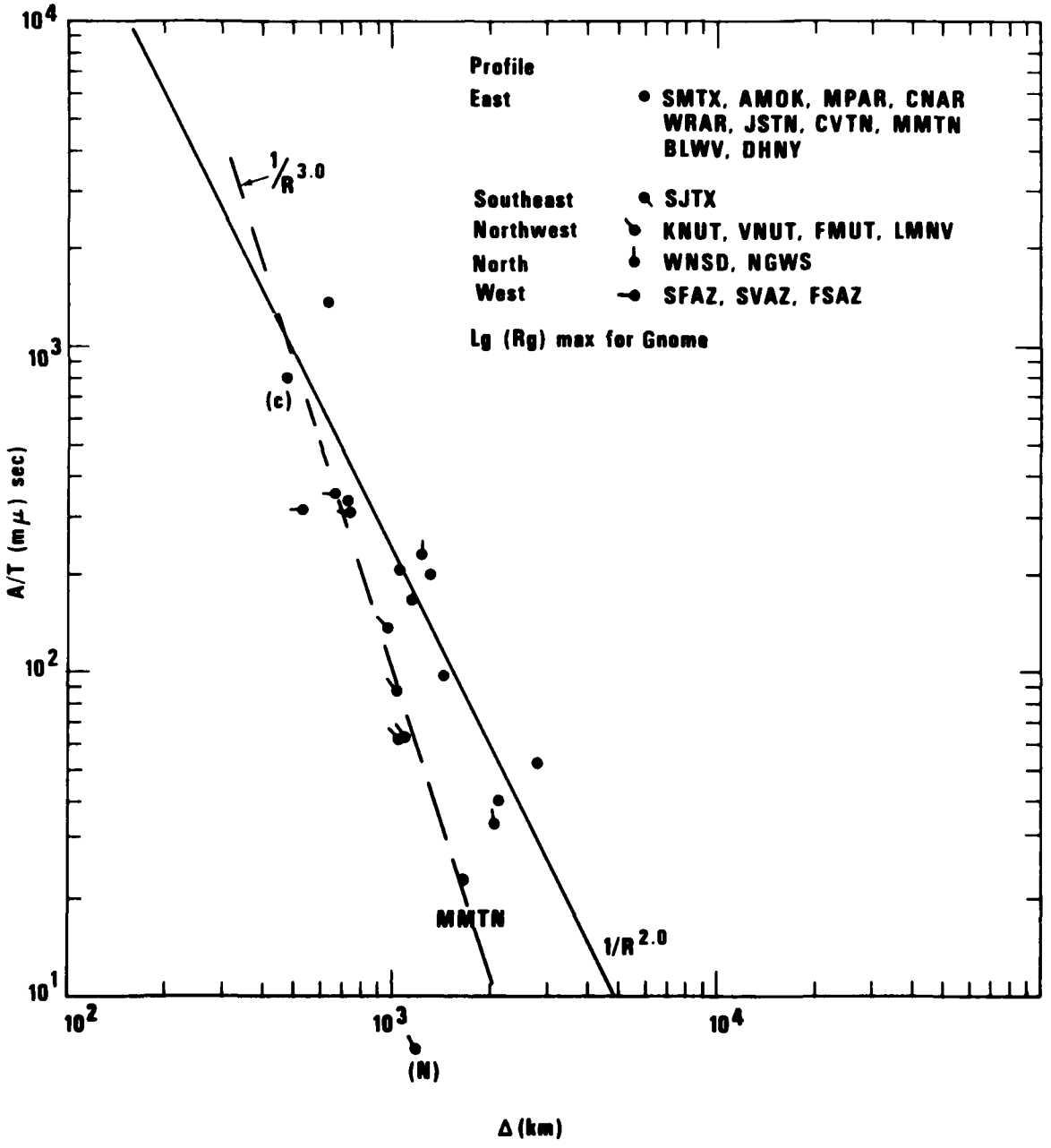
Profile
East
SMTX, AMOK, MPAR, CNAR
WRAR, JSTN, CVTN, MMTN
BLWV, DHNY
Southeast
SJTX
Northwest
KNUT, VNUT, FMUT, LMNV
North
WNSD, NGWS
West
SFAZ, SVAZ, FSAZ
Lg (Rg) max for Gnome
1/R 3.0
1/R 2.0
(c)
MMTN
(N)
A/T (mμ) sec
Δ (km)
10^4
10^3
10^2
10^1
10^2
10^3
10^4

Figure I-1b

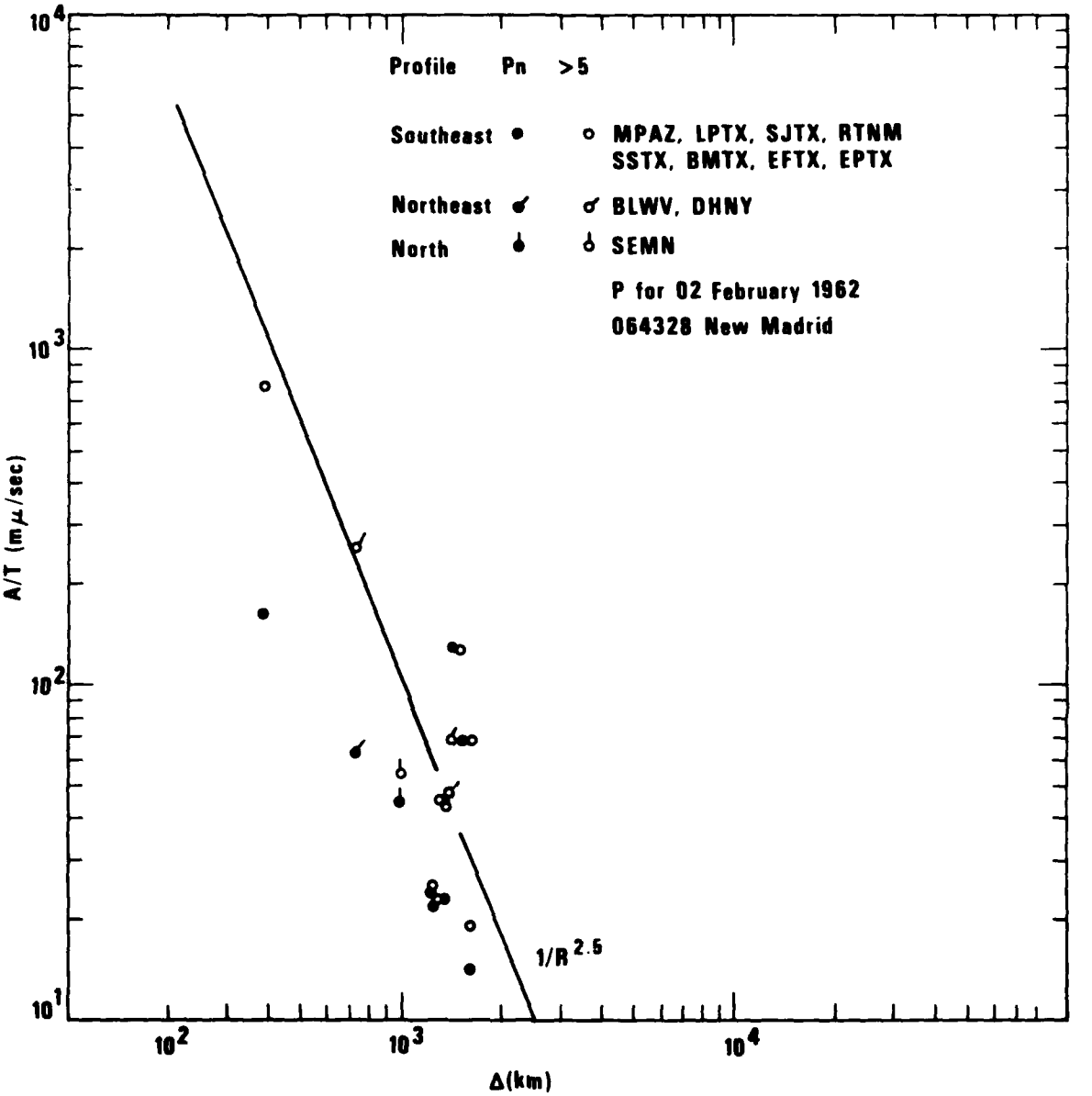
Profile Pn >5
Southeast
MPAZ, LPTX, SJTX, RTNM
SSTX, BMTX, EFTX, EPTX
Northeast
BLWV, DHNY
North
SEMN
P for 02 February 1962
064328 New Madrid
1/R 2.5
A/T (mμ/sec)
Δ(km)
10^4
10^3
10^2
10^1
10^2
10^3
10^4

Figure I-2a

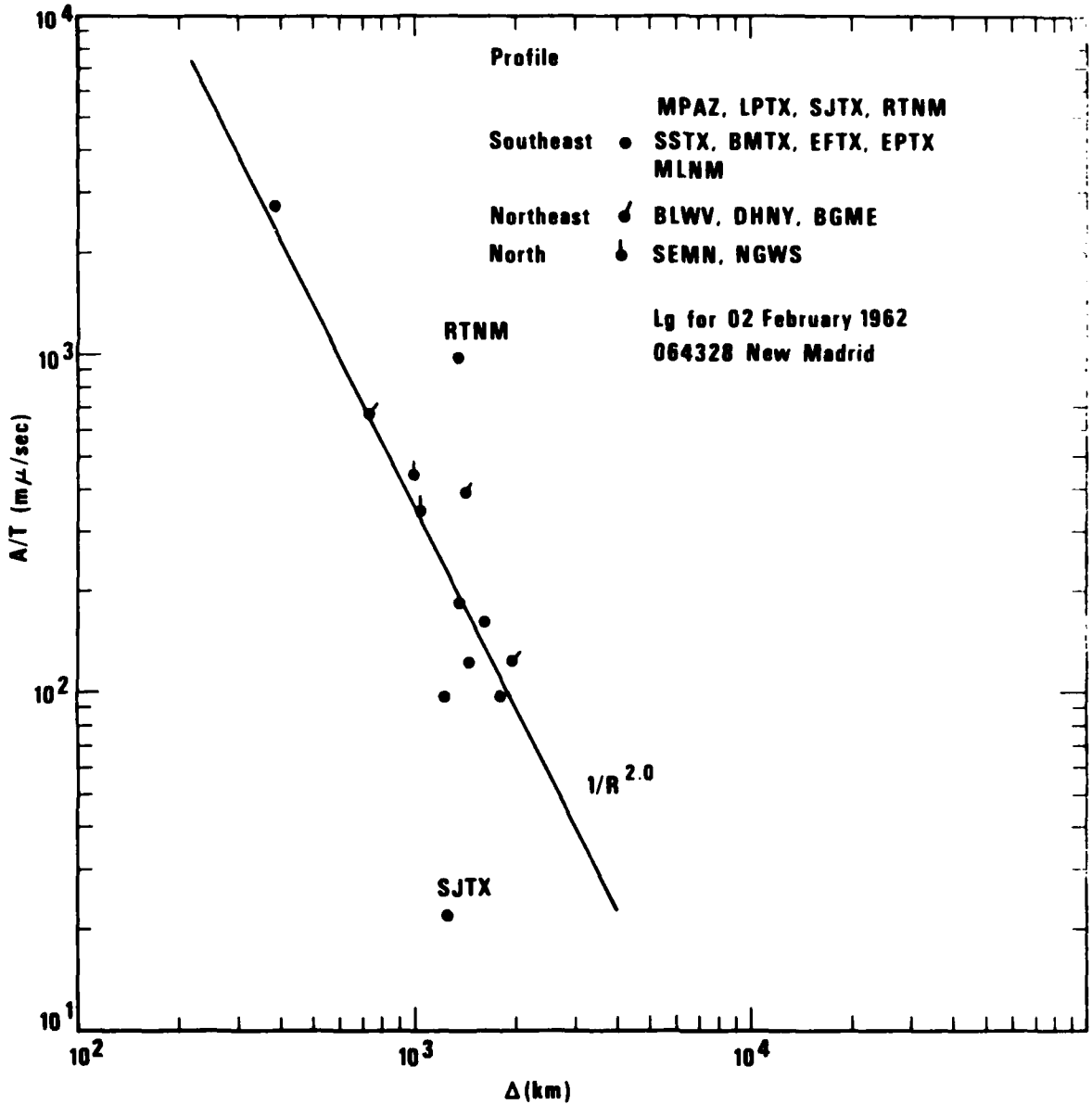
Profile
MPAZ, LPTX, SJTX, RTNM
Southeast
SSTX, BMTX, EFTX, EPTX
MLNM
Northeast
BLWV, DHNY, BGME
North
SEMN, NGWS
Lg for 02 February 1962
064328 New Madrid
RTNM
SJTX
1/R 2.0
A/T (mμ/sec)
Δ(km)
10 4
10 3
10 2
10 1
10 2
10 3
10 4

Figure I-2b

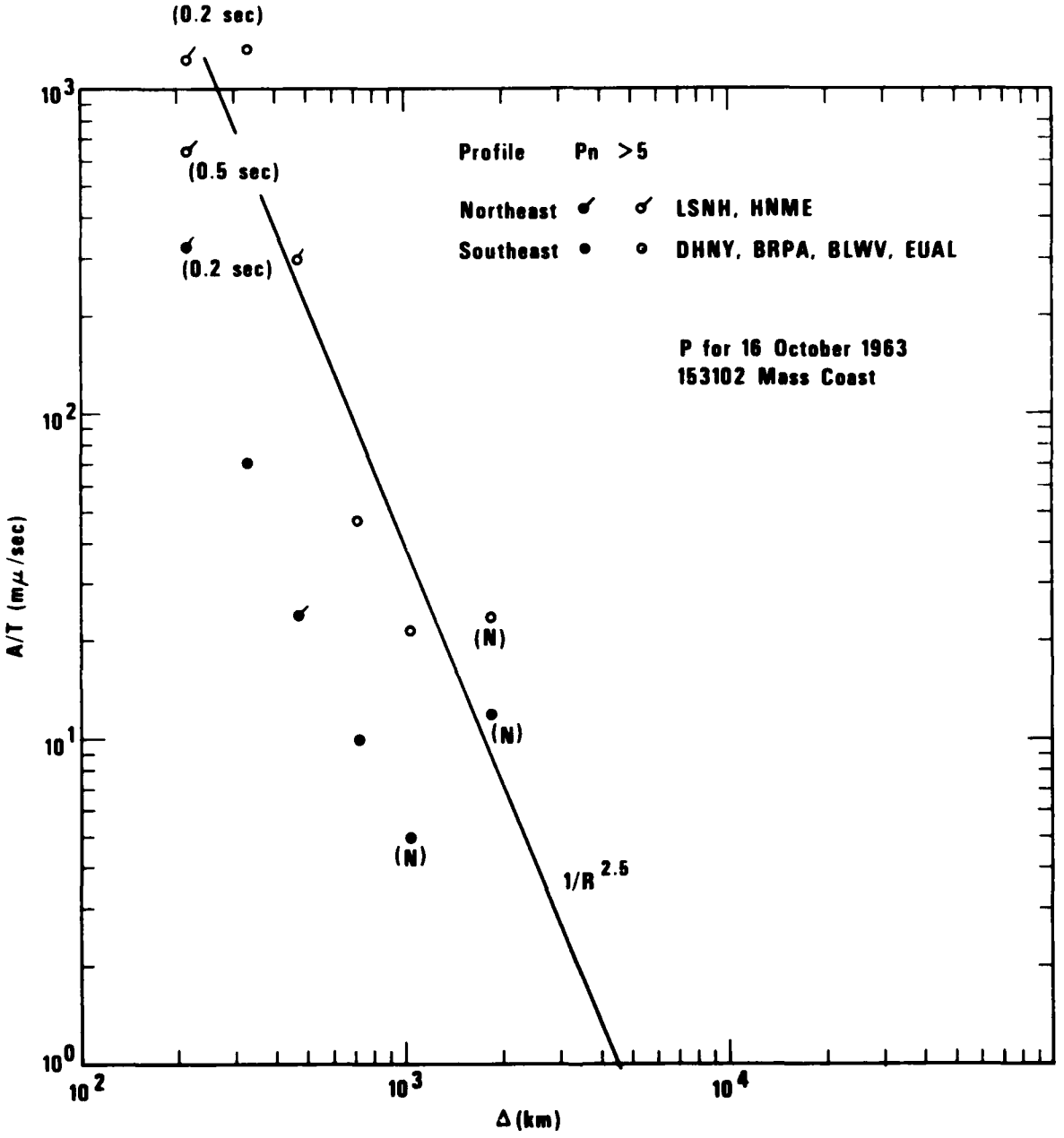
(0.2 sec)
(0.5 sec)
(0.2 sec)
Profile Pn >5
Northeast LSNH, HNME
Southeast DHNY, BRPA, BLWV, EUAL
P for 16 October 1963
153102 Mass Coast
(N)
(N)
(N)
1/R 2.5
A/T (mμ/sec)
Δ (km)
10^3
10^2
10^1
10^0
10^2
10^3
10^4

Figure I-3a

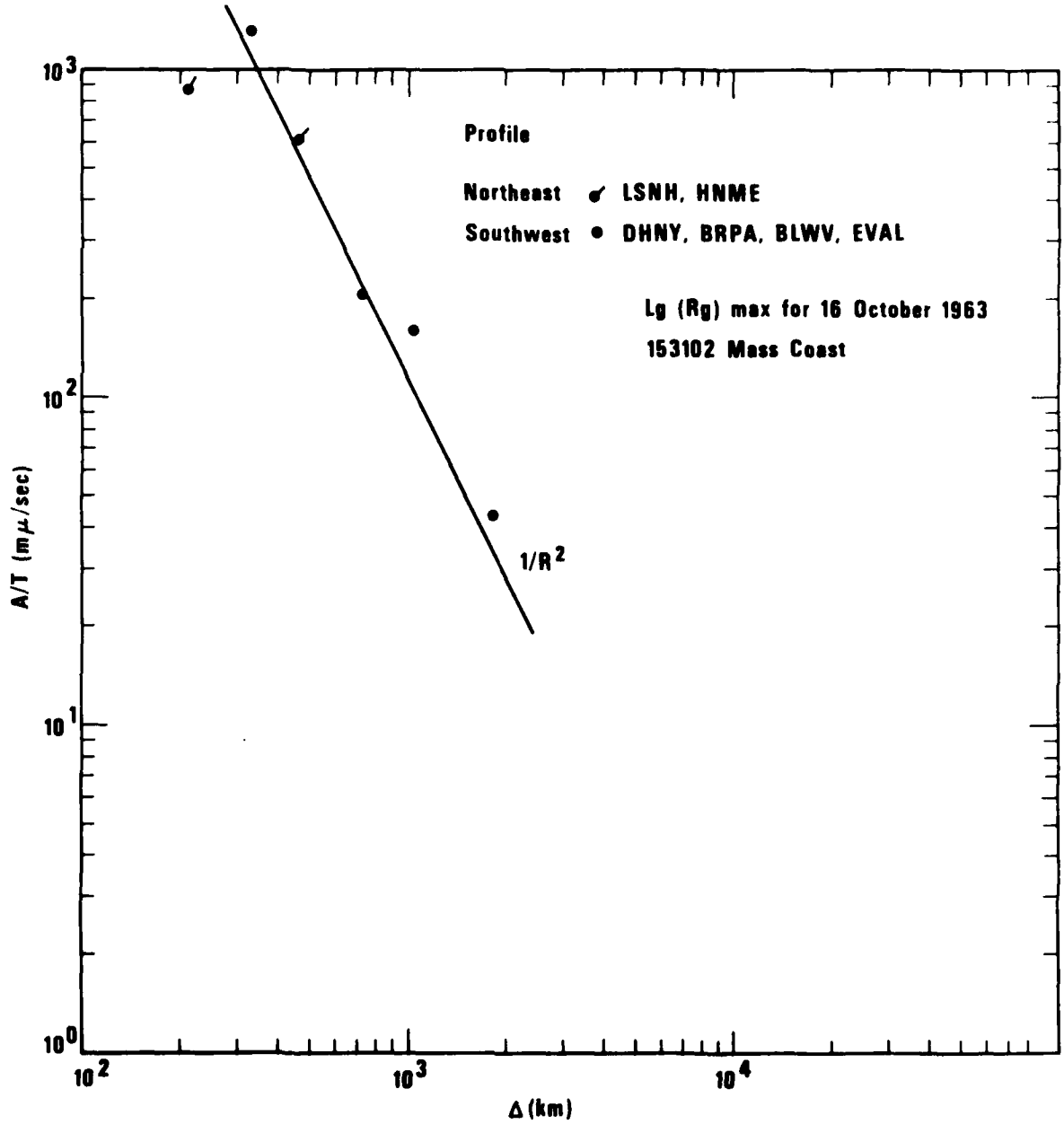
Profile
Northeast LSNH, HNME
Southwest DHNY, BRPA, BLWV, EVAL
Lg (Rg) max for 16 October 1963
153102 Mass Coast
1/R²
A/T (mμ/sec)
Δ (km)
10³
10²
10¹
10⁰
10²
10³
10⁴

Figure I-3b

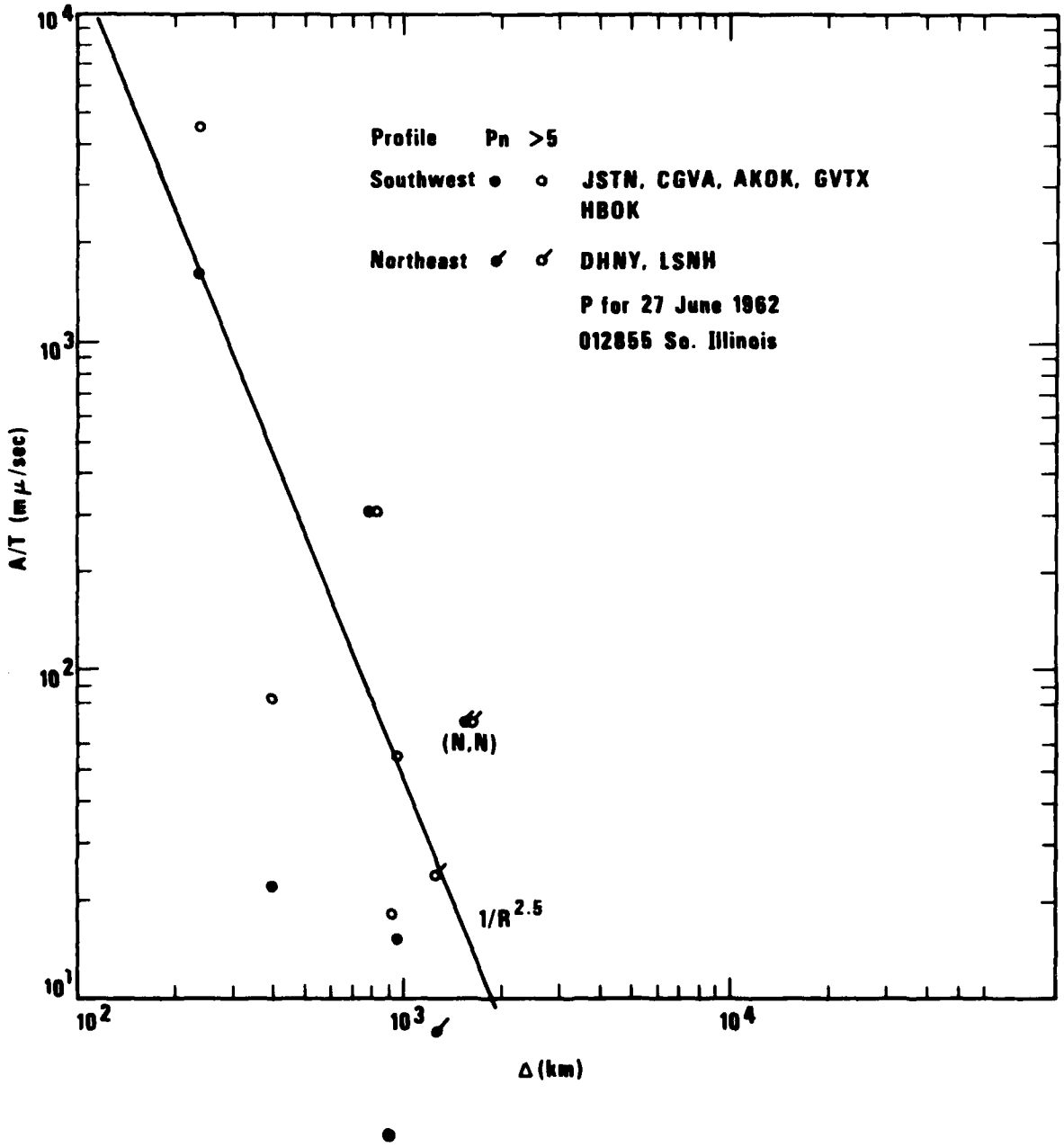
Profile Pn >5
Southwest ● ○ JSTN, CGVA, AKOK, GVTX
HBOK
Northeast ♂ ♂ DHNY, LSNH
P for 27 June 1962
012855 So. Illinois
(N,N)
1/R^2.5
A/T (mμ/sec)
Δ (km)
10^4
10^3
10^2
10^1
10^2
10^3
10^4

Figure I-4a

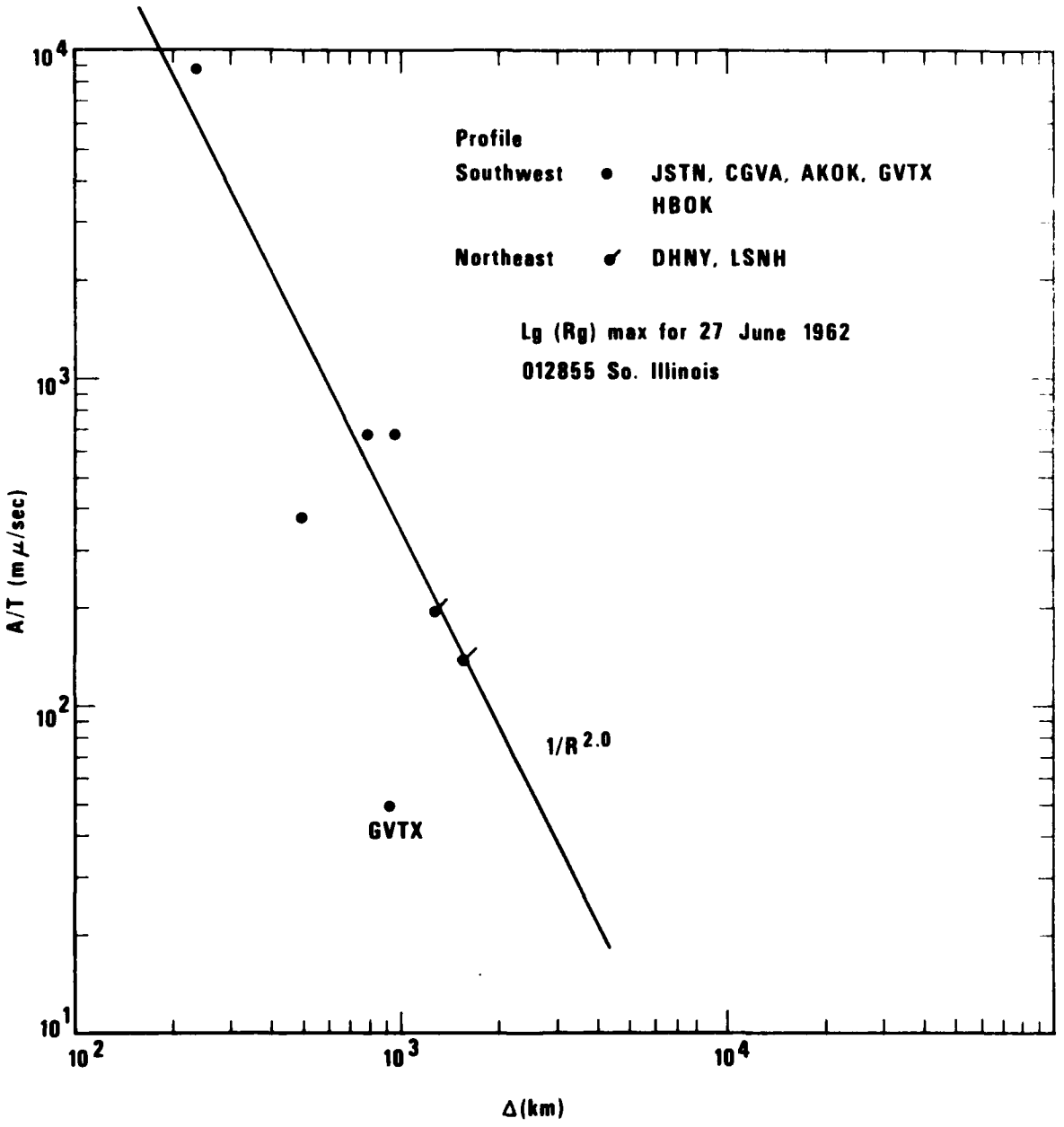
Profile
Southwest • JSTN, CGVA, AKOK, GVTX
HBOK
Northeast ✓ DHNY, LSNH
Lg (Rg) max for 27 June 1962
012855 So. Illinois
1/R 2.0
GVTX
A/T (mμ/sec)
Δ(km)
10^4
10^3
10^2
10^1
10^2
10^3
10^4

Figure I-4b

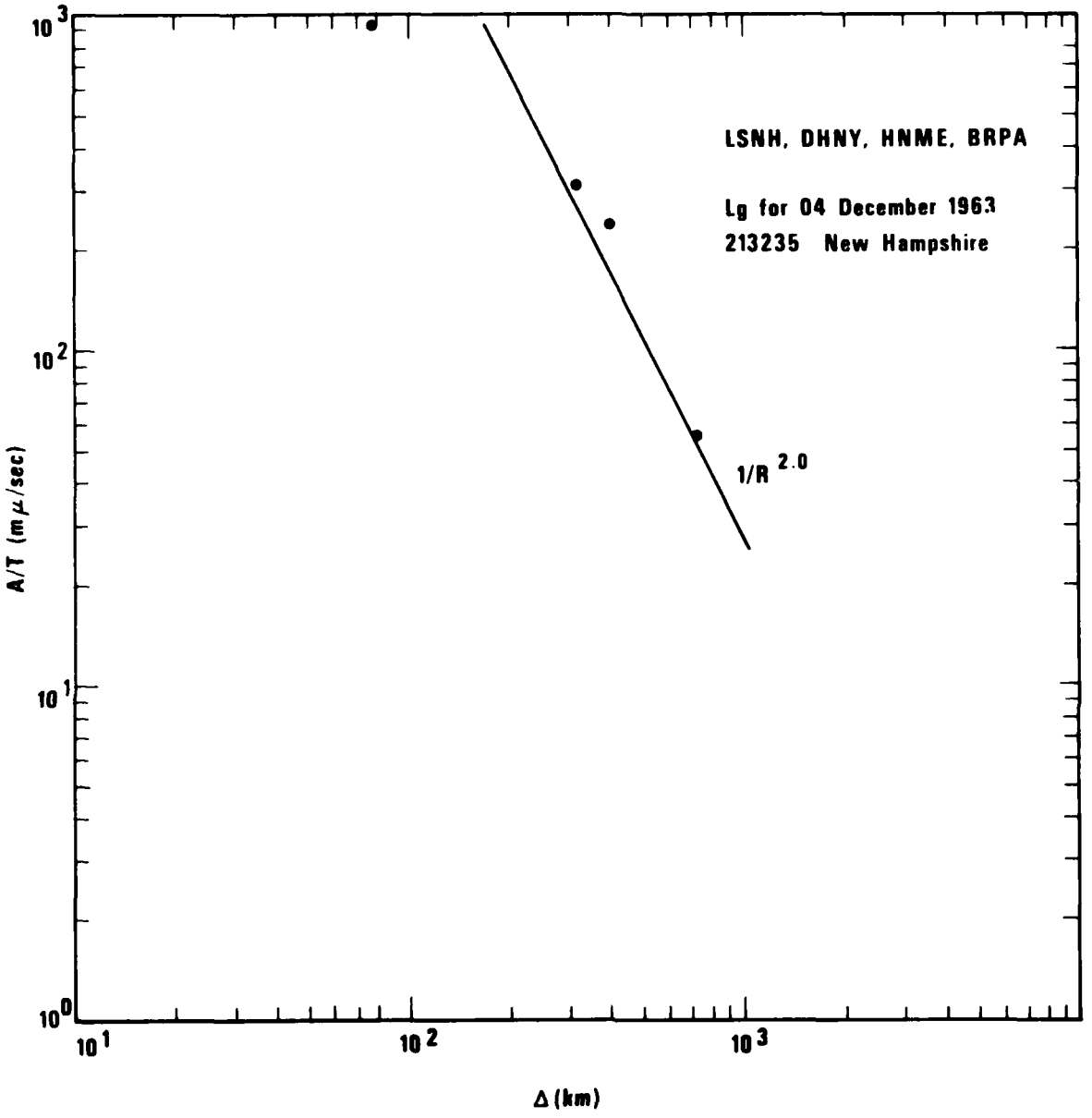
LSNH, DHNY, HNME, BRPA
Lg for 04 December 1963
213235 New Hampshire
1/R 2.0
A/T (mμ/sec)
Δ (km)
10^3
10^2
10^1
10^0
10^1
10^2
10^3

Figure I-5

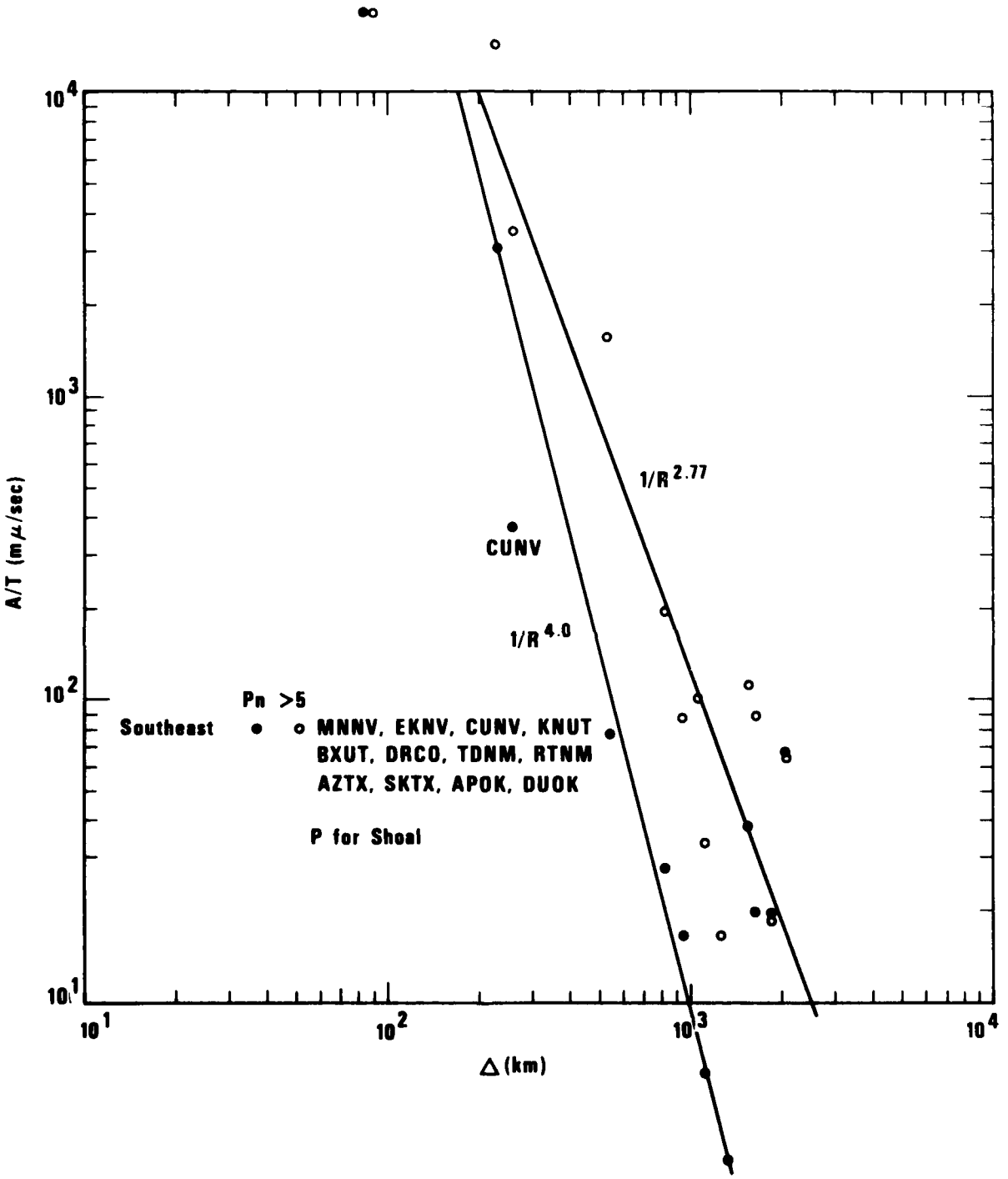
10^4
10^3
10^2
10^1
A/T (mμ/sec)
10^1
10^2
10^3
10^4
Δ (km)
1/R 2.77
1/R 4.0
CUNV
Pn >5
Southeast
MNNV, EKNV, CUNV, KNUT
BXUT, DRCO, TDNM, RTNM
AZTX, SKTX, APOK, DUOK
P for Shoal

Figure I-6a

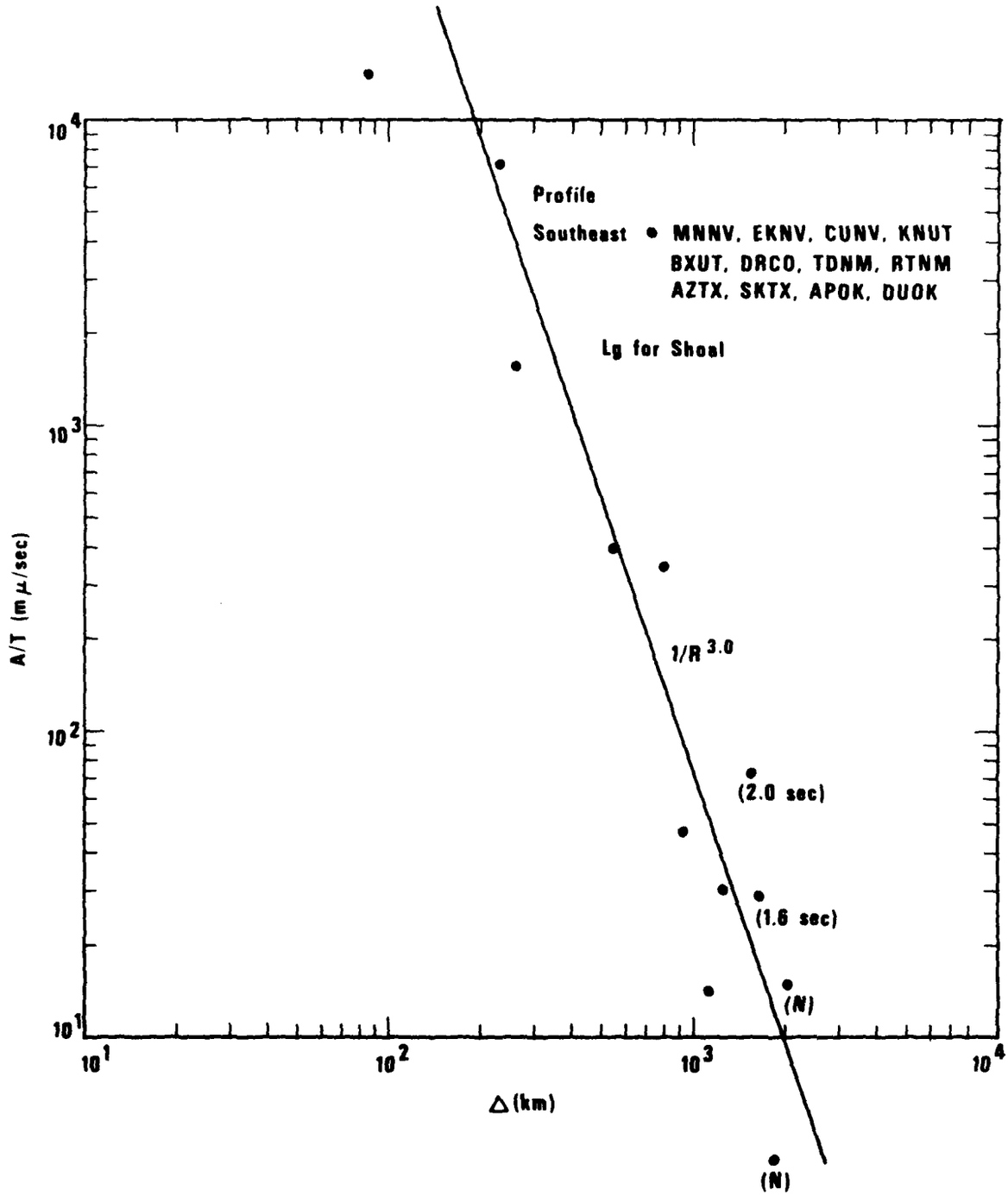
Profile
Southeast • MNNV, EKNV, CUNV, KNUT
BXUT, DRCO, TDNM, RTNM
AZTX, SKTX, APOK, DUOK
Lg for Shoal
1/R 3.0
(2.0 sec)
(1.6 sec)
(N)
(N)
A/T (mμ/sec)
Δ(km)
10^4
10^3
10^2
10^1
10^1
10^2
10^3
10^4

Figure I-6b

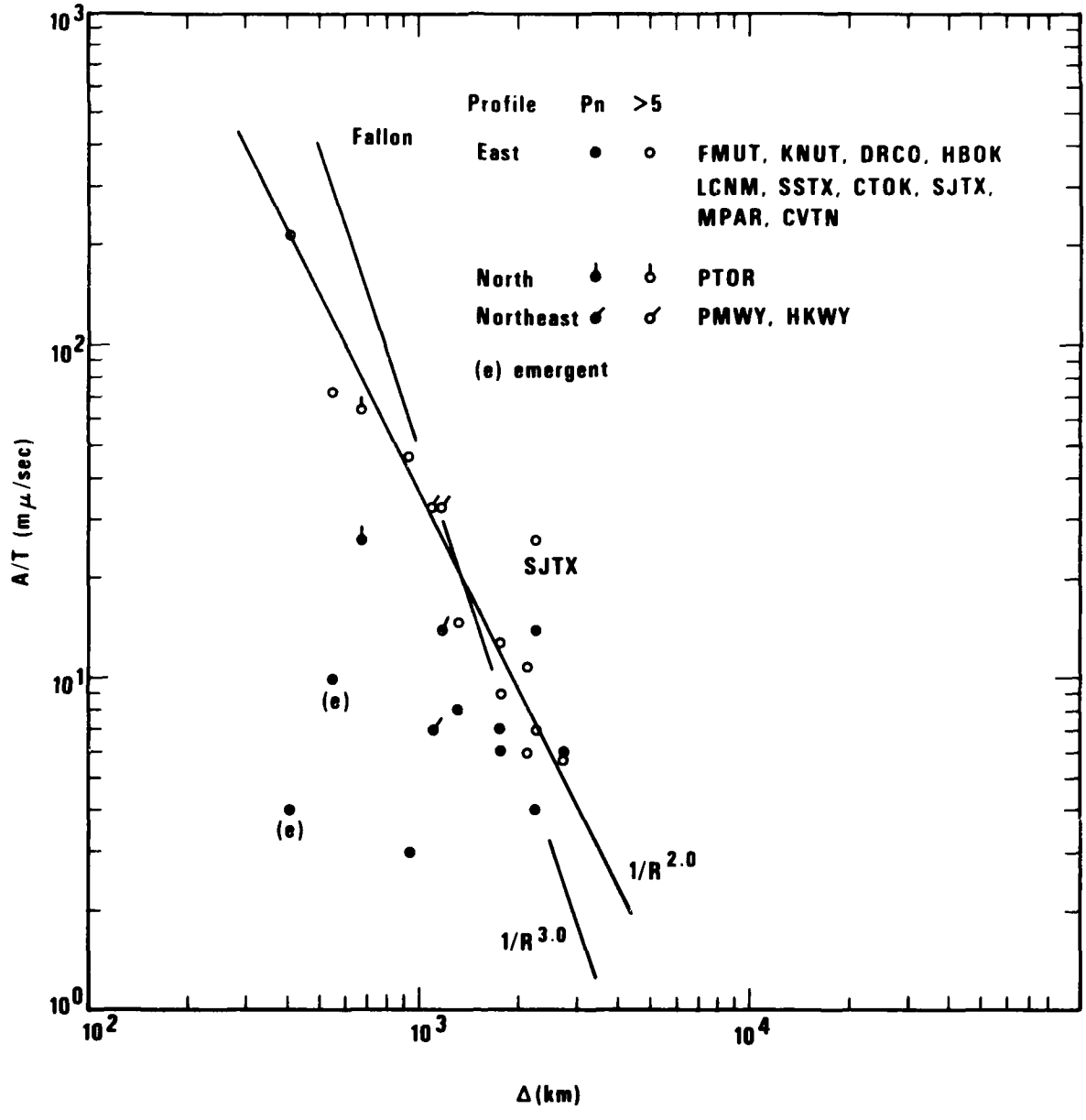
Profile Pn >5
East
FMUT, KNUT, DRCO, HBOK
LCNM, SSTX, CTOK, SJTX,
MPAR, CVTN
North
PTOR
Northeast
PMWY, HKWY
(e) emergent
Fallon
SJTX
(e)
(e)
1/R 2.0
1/R 3.0
A/T (mμ/sec)
Δ(km)
10^3
10^2
10^1
10^0
10^2
10^3
10^4

Figure I-7a

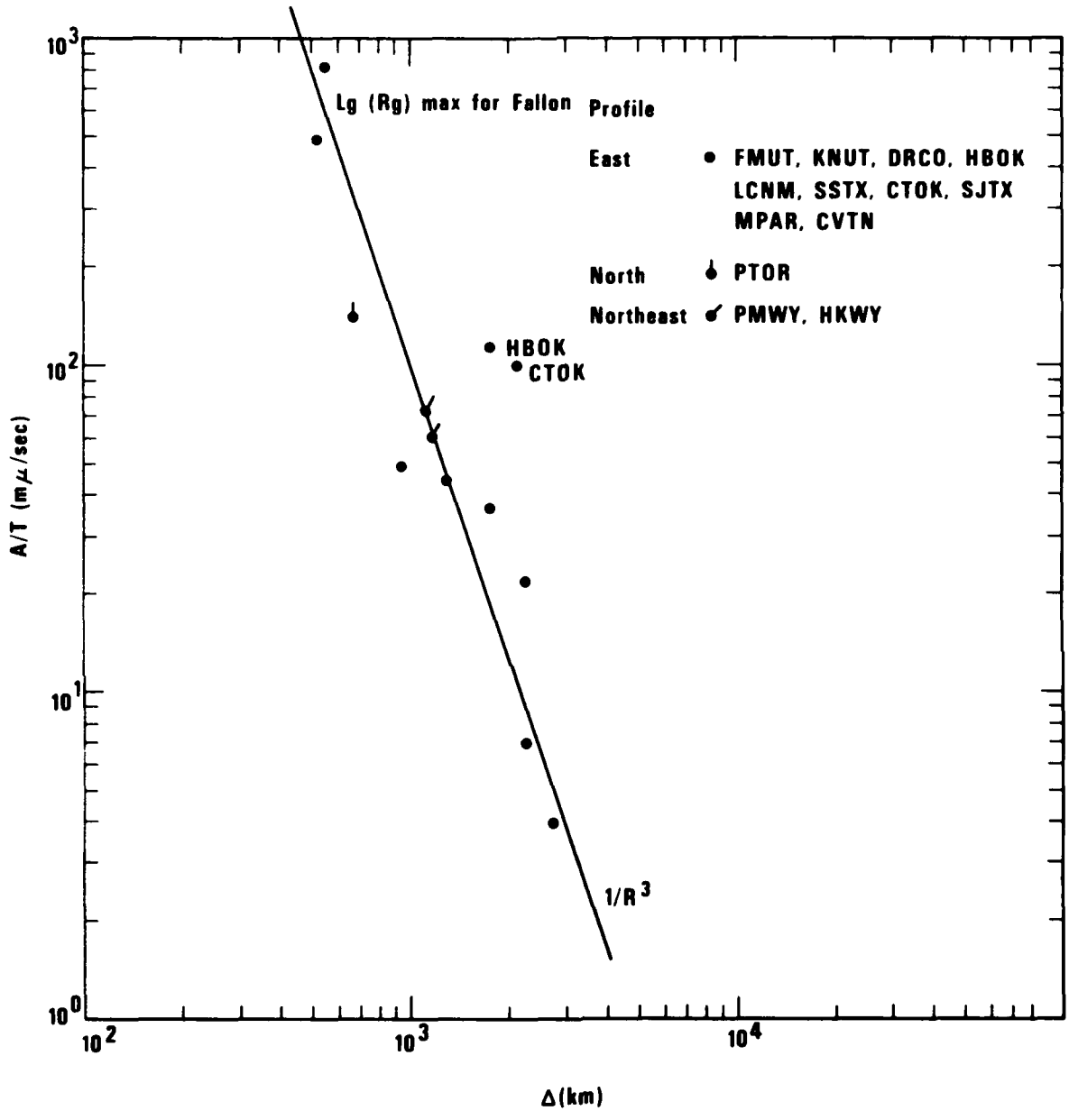
Lg (Rg) max for Fallon
Profile
East
FMUT, KNUT, DRCO, HBOK
LCNM, SSTX, CTOK, SJTX
MPAR, CVTN
North
PTOR
Northeast
PMWY, HKWY
HBOK
CTOK
1/R 3
A/T (mμ/sec)
Δ(km)
10 3
10 2
10 1
10 0
10 2
10 3
10 4

Figure I-7b

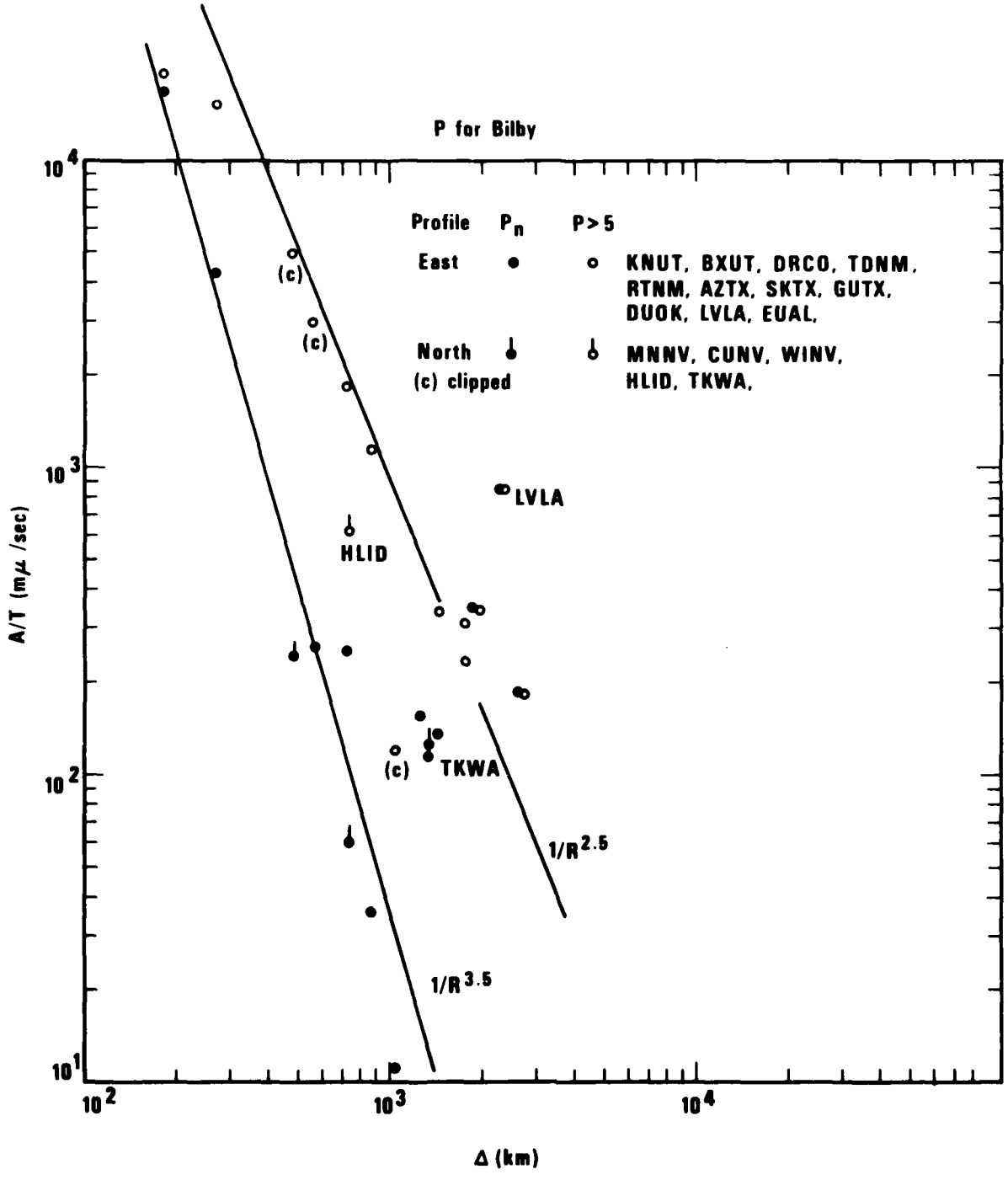
P for Bilby
Profile
P_n
P>5
East
North
(c) clipped
KNUT, BXUT, DRCO, TDNM, RTNM, AZTX, SKTX, GUTX, DUOK, LVLA, EUAL,
MNNV, CUNV, WINV, HLID, TKWA,
(c)
(c)
LVLA
HLID
(c)
TKWA
$1/R^{2.5}$
$1/R^{3.5}$
A/T (mμ /sec)
Δ (km)
10^4
10^3
10^2
10^1
10^2
10^3
10^4

Figure I-8a

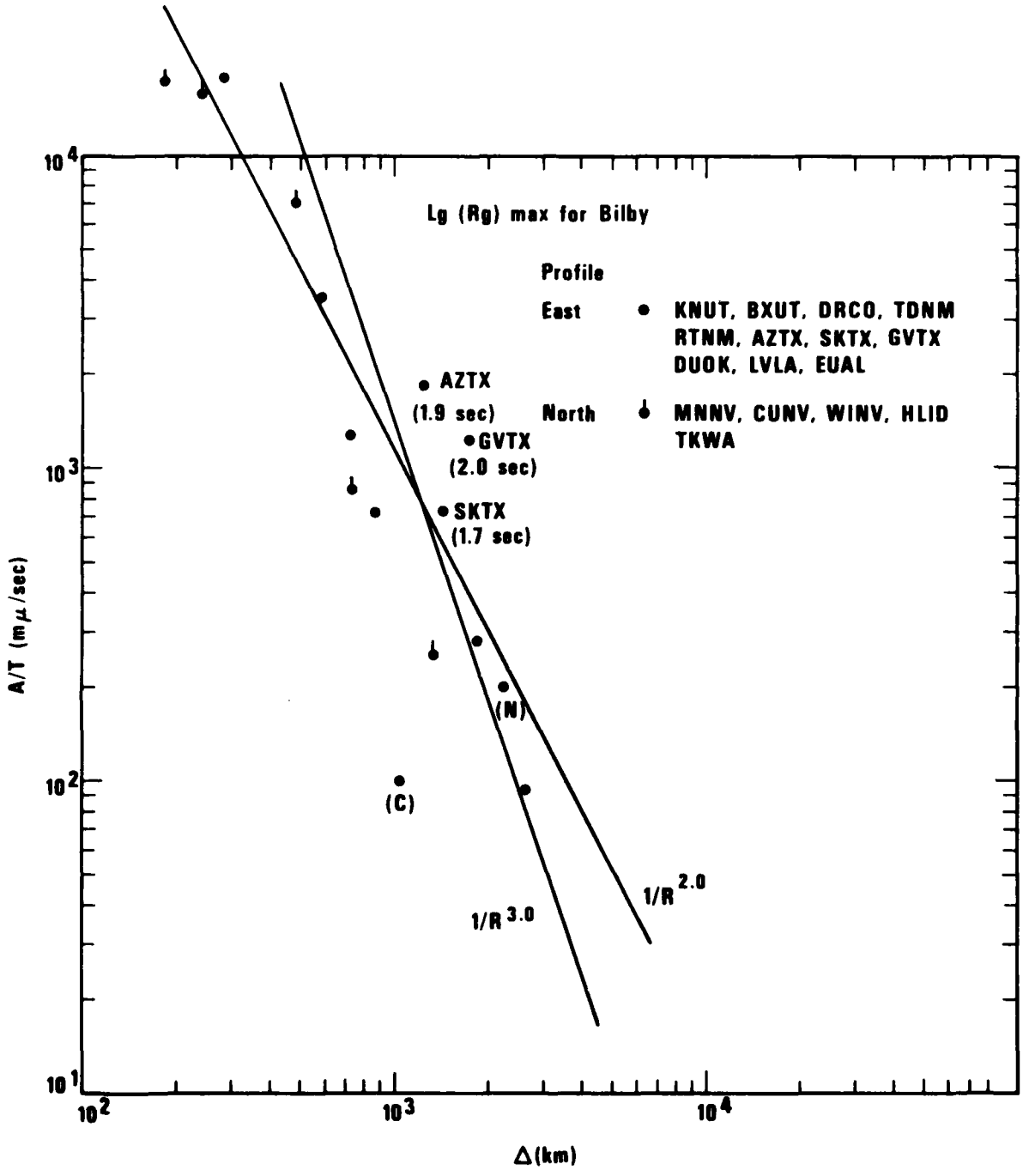
Lg (Rg) max for Bilby
Profile
East
KNUT, BXUT, DRCO, TDNM
RTNM, AZTX, SKTX, GVTX
DUOK, LVLA, EUAL
North
MNNV, CUNV, WINV, HLID
TKWA
AZTX
(1.9 sec)
GVTX
(2.0 sec)
SKTX
(1.7 sec)
(N)
(C)
1/R 2.0
1/R 3.0
A/T (mμ/sec)
Δ(km)
10^4
10^3
10^2
10^1
10^2
10^3
10^4

Figure I-8b

APPENDIX II

P-Wave Spectra For Soviet Explosions Of Table VI.
Data From The Center Element Of The C3 Subarray.

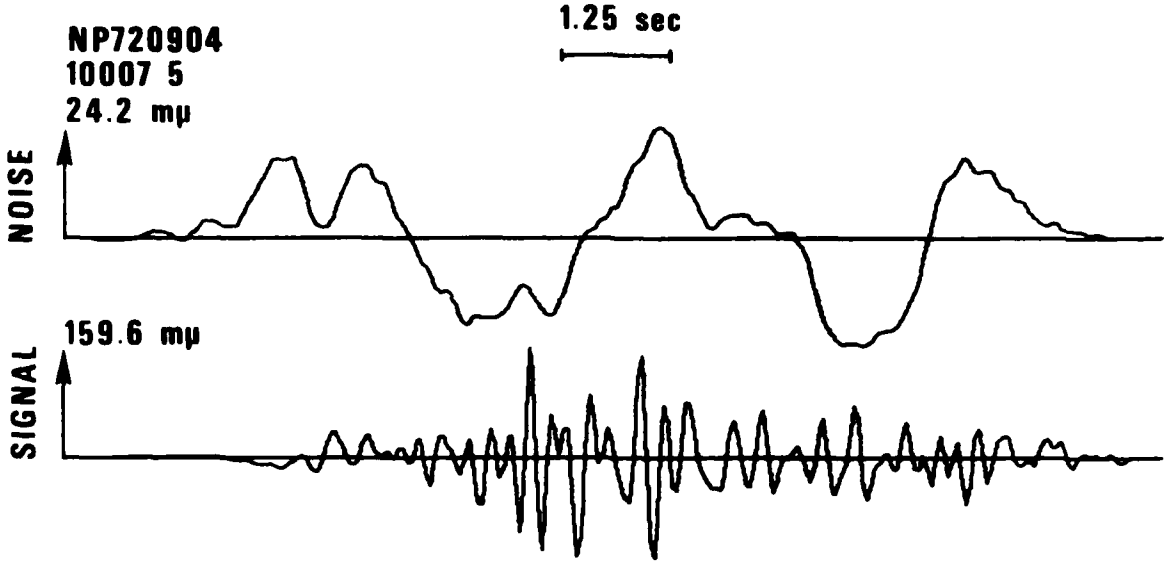
NP720904
10007 5
24.2 mμ
1.25 sec
NOISE
159.6 mμ
SIGNAL

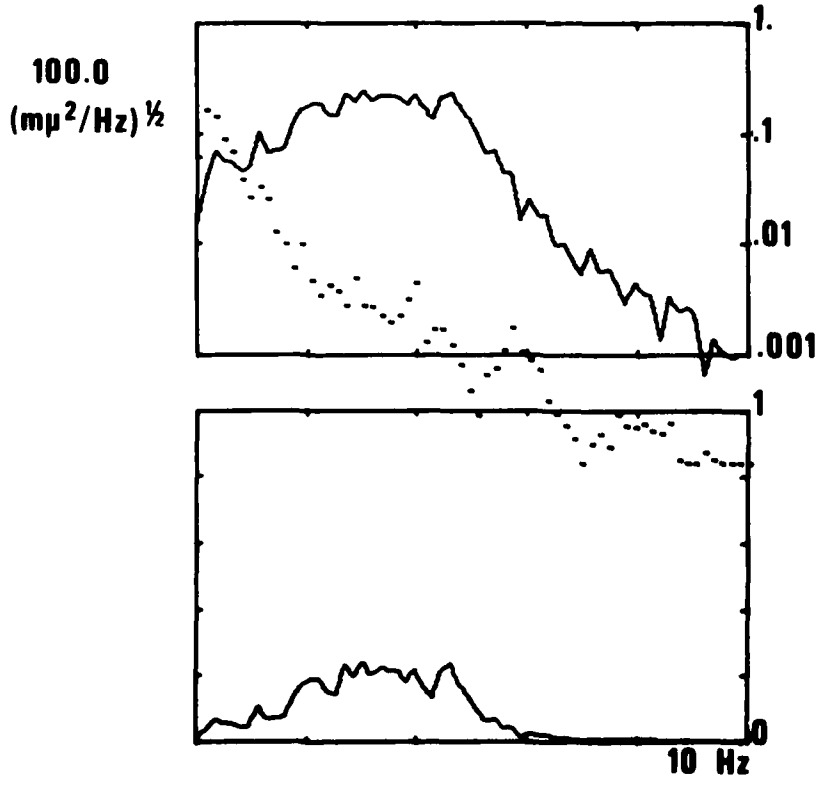
100.0
(mμ²/Hz)½
1.
.1
.01
.001
1
0
10 Hz

Figure II-1

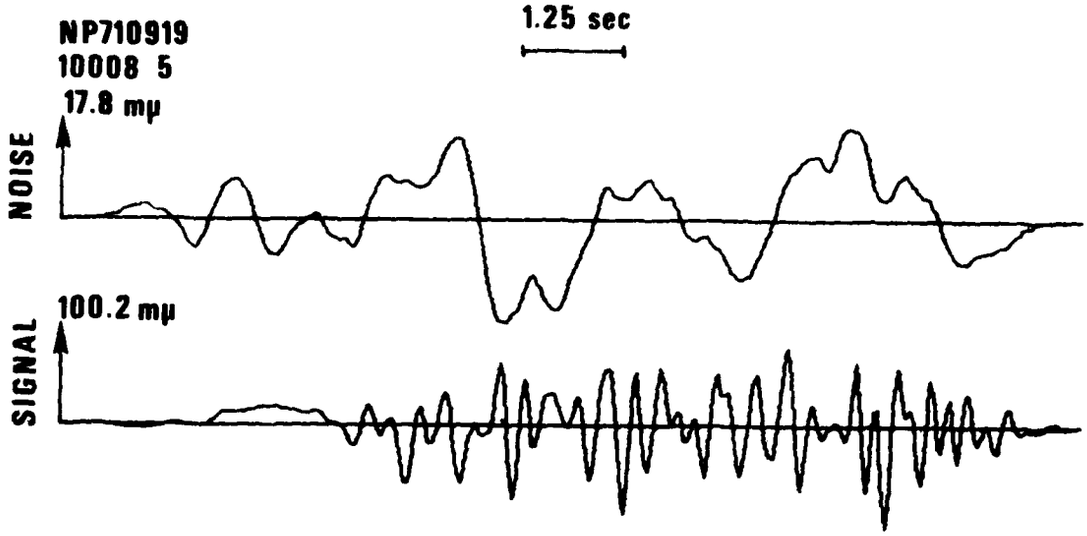
NP710919
10008 5
17.8 mμ
1.25 sec
NOISE
100.2 mμ
SIGNAL

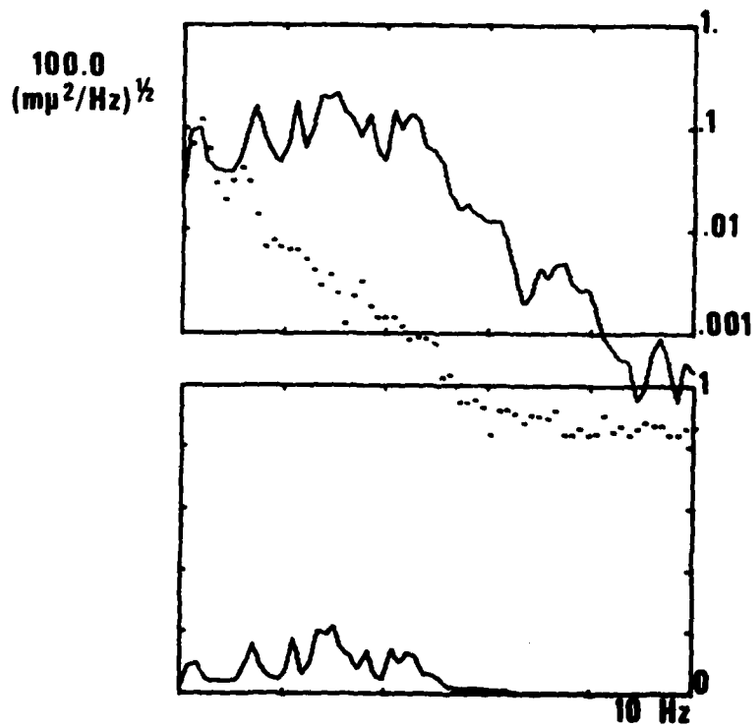
100.0
(mμ²/Hz)½
1.
.1
.01
.001
1
0
10 Hz

Figure II-2

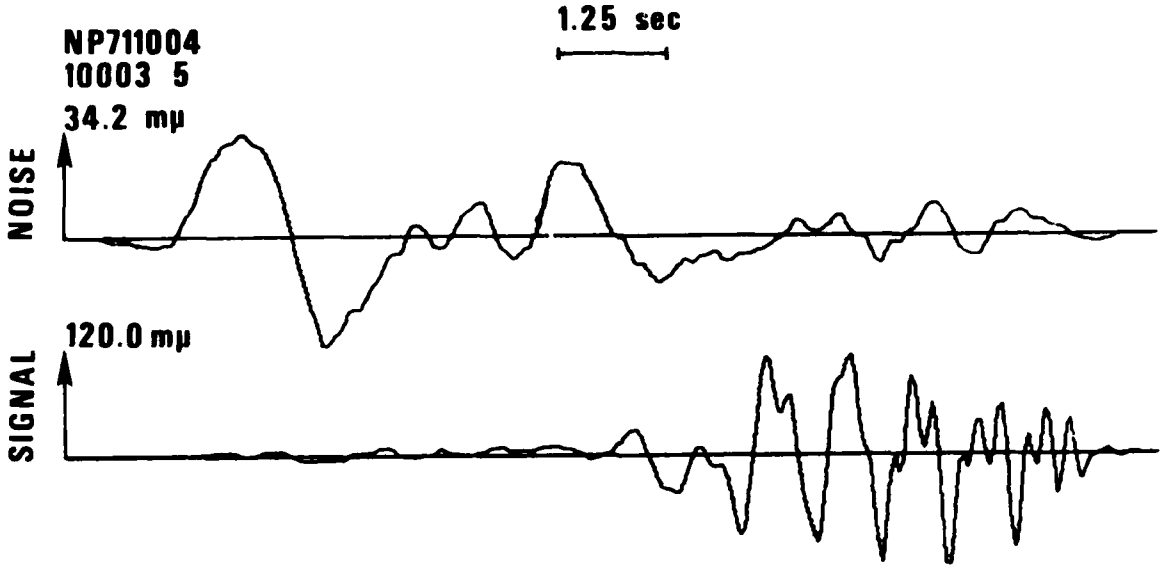
1.25 sec
NP711004
10003 5
34.2 mμ
NOISE
120.0 mμ
SIGNAL

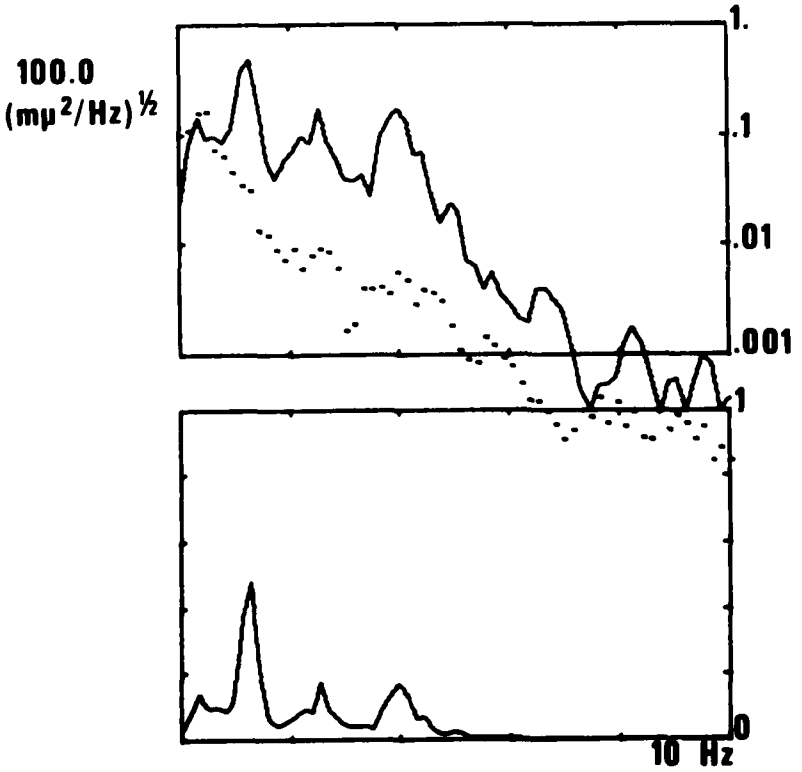
100.0
(mμ²/Hz)½
1.
.1
.01
.001
1
0
10 Hz

Figure II-3

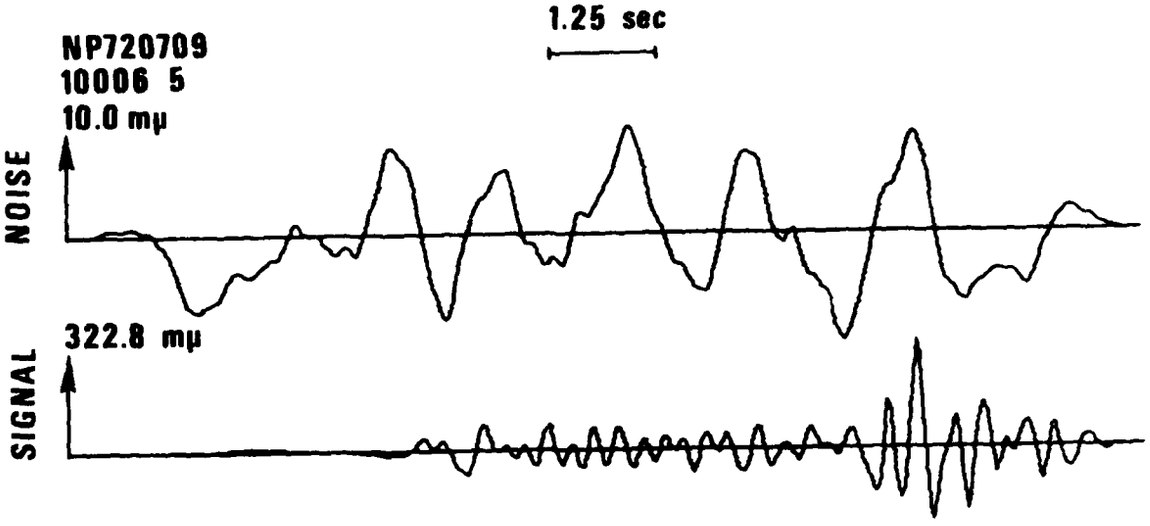
1.25 sec
NP720709
10006 5
10.0 mμ
NOISE
322.8 mμ
SIGNAL

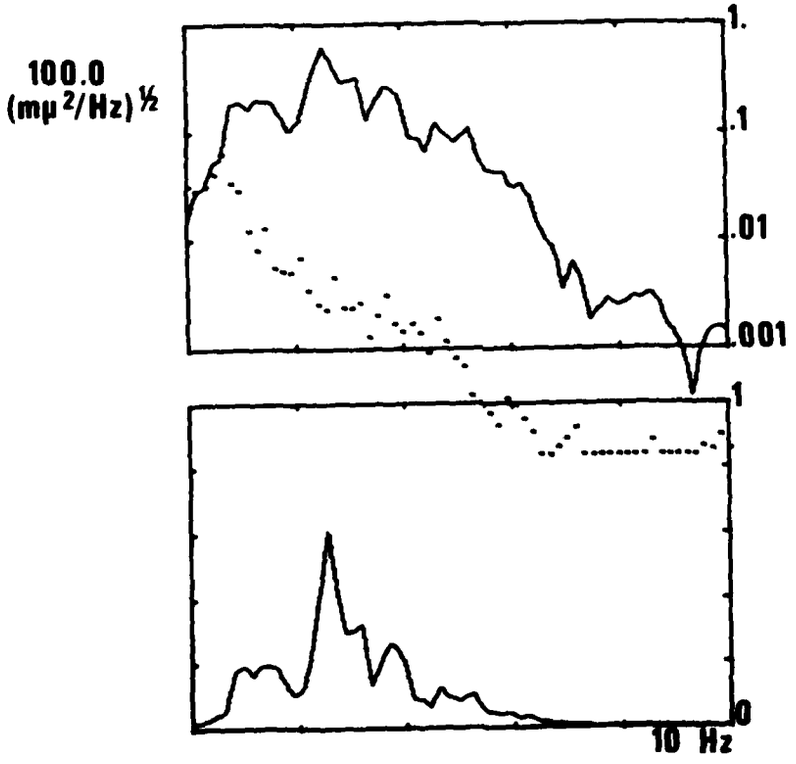
100.0
(mμ²/Hz)½
1.
.1
.01
.001
1
0
10 Hz

Figure II-4

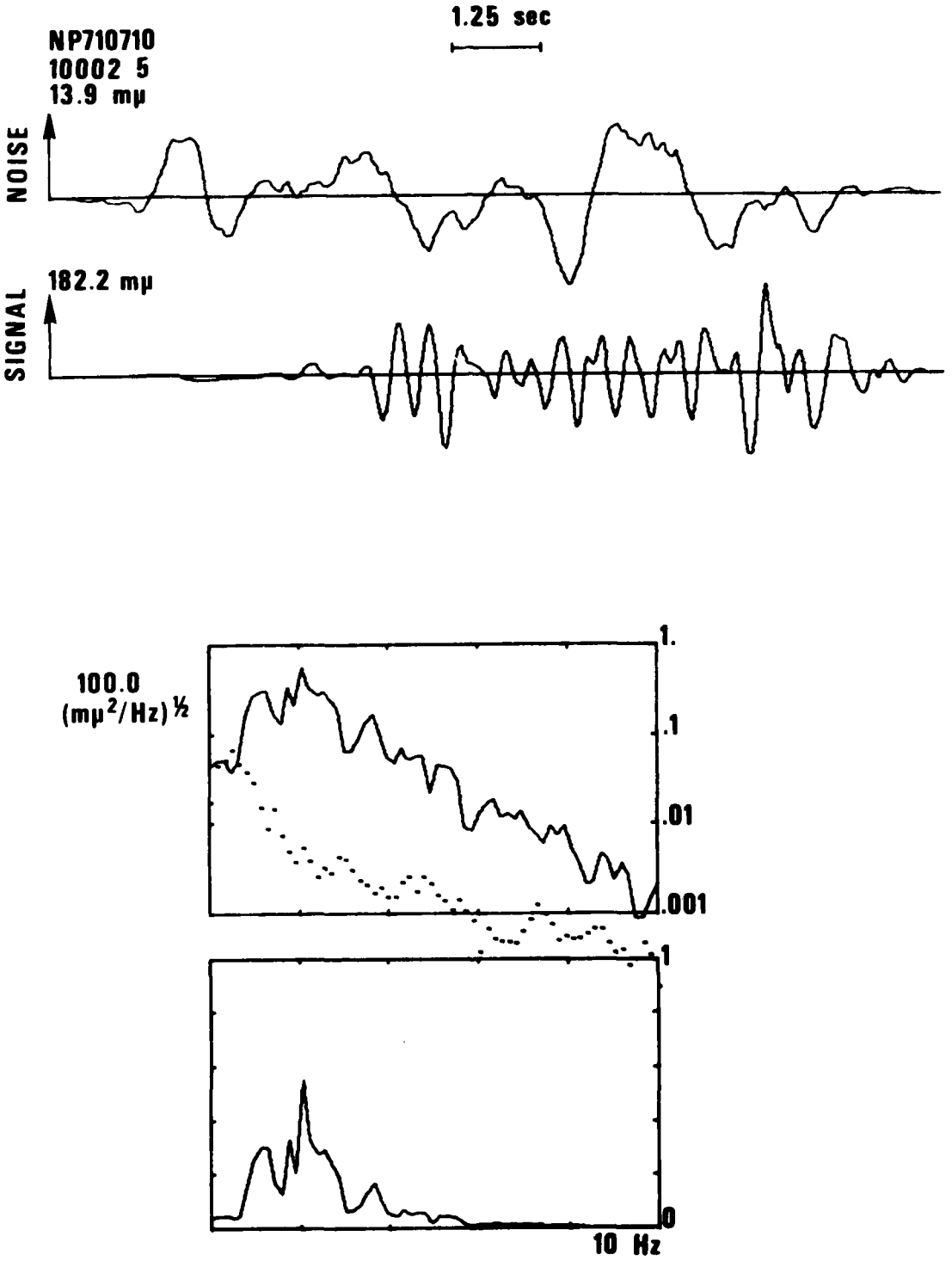
1.25 sec
NP710710
10002 5
13.9 mμ
NOISE
182.2 mμ
SIGNAL
100.0
(mμ²/Hz)½
1.
.1
.01
.001
1
0
10 Hz

Figure II-5

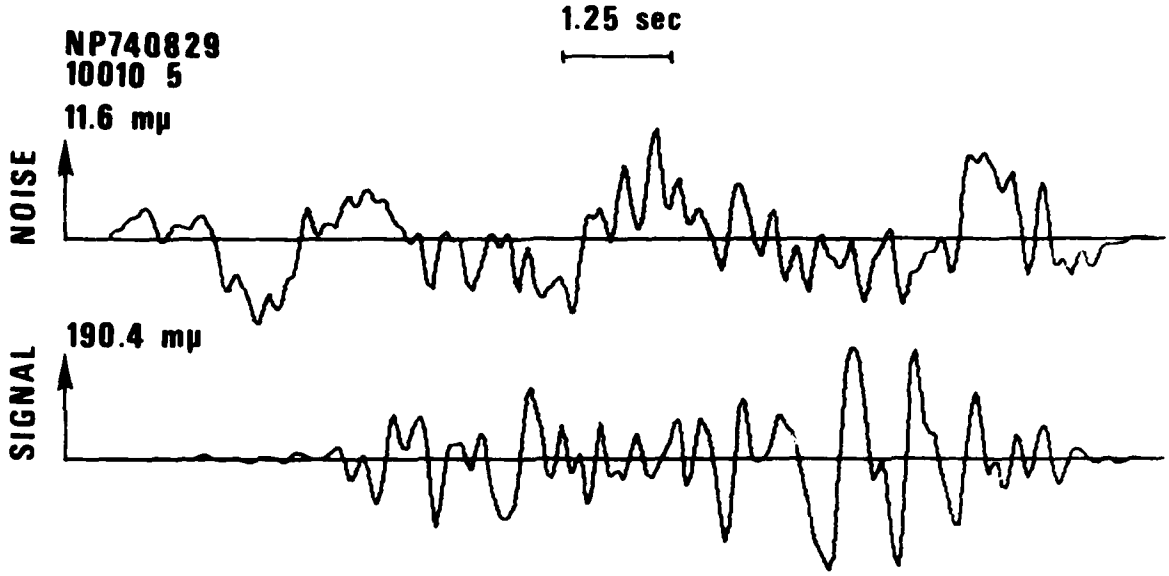
1.25 sec
NP740829
10010 5
11.6 mμ
NOISE
190.4 mμ
SIGNAL

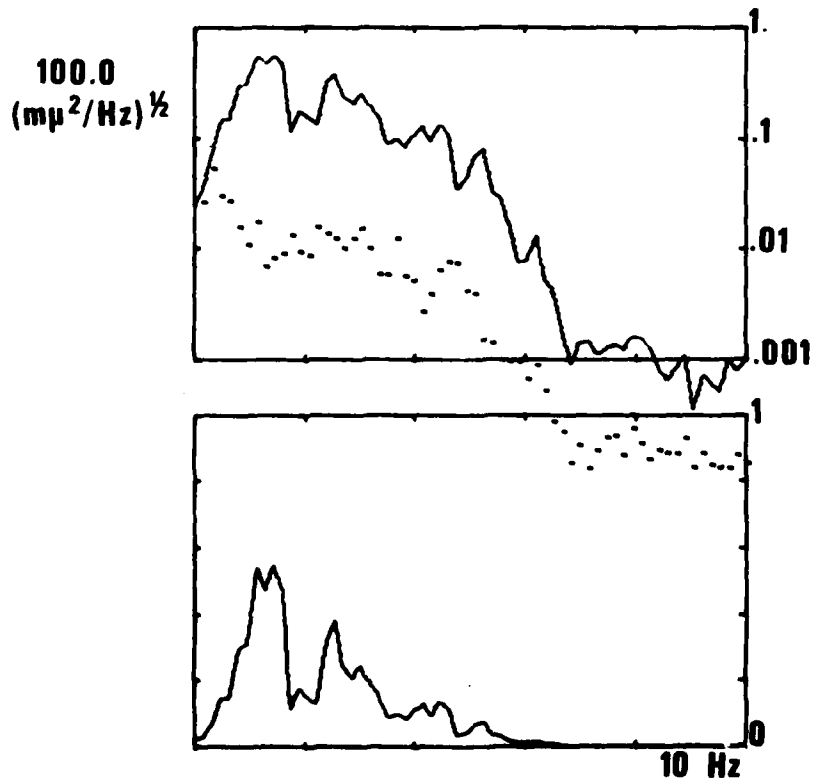
100.0
(mμ²/Hz)½
1
.1
.01
.001
1
0
10 Hz

Figure II-6

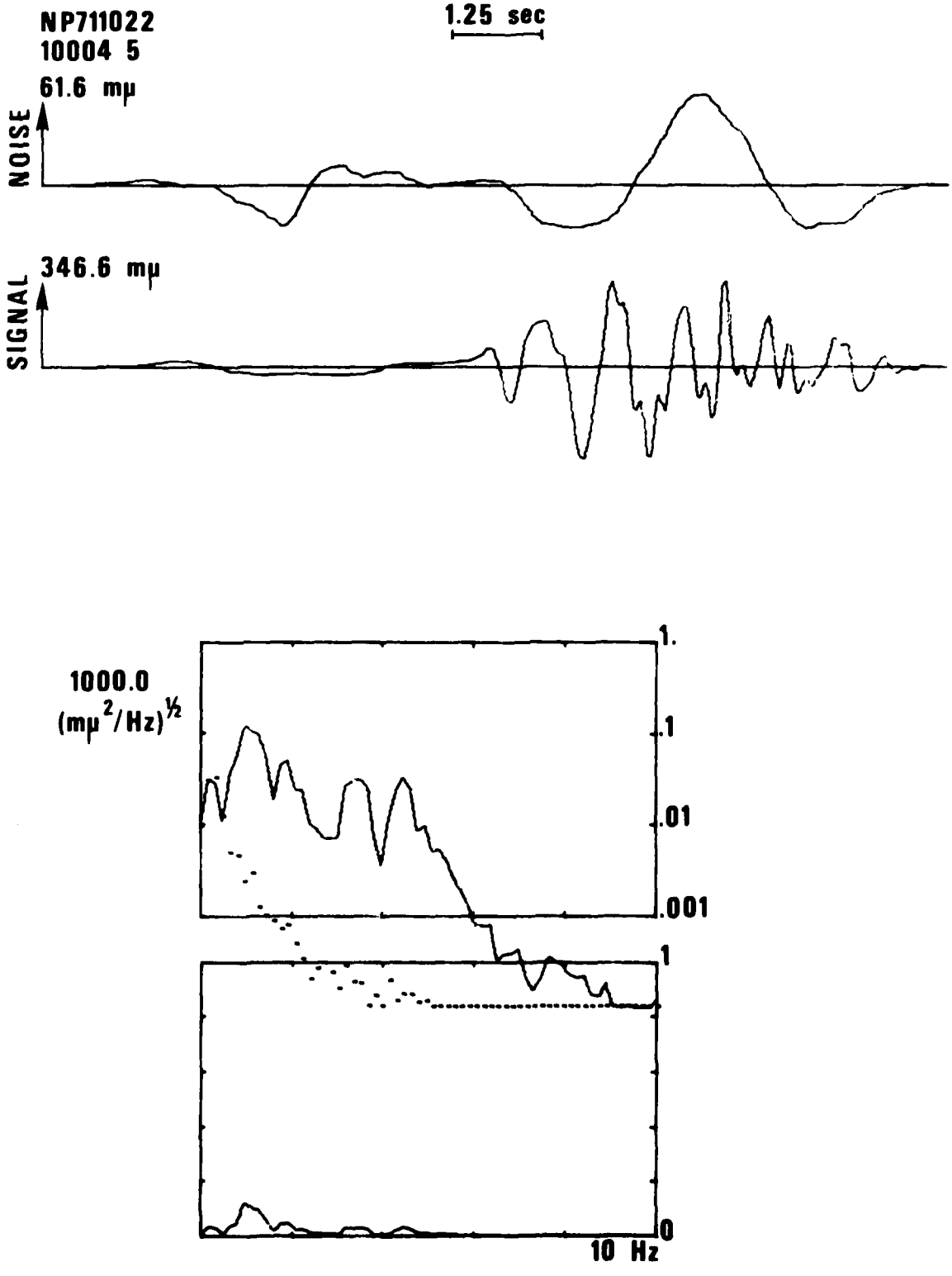
NP711022
10004 5
1.25 sec
61.6 mμ
NOISE
346.6 mμ
SIGNAL
1000.0
(mμ²/Hz)½
1.
.1
.01
.001
1
0
10 Hz

Figure II-7

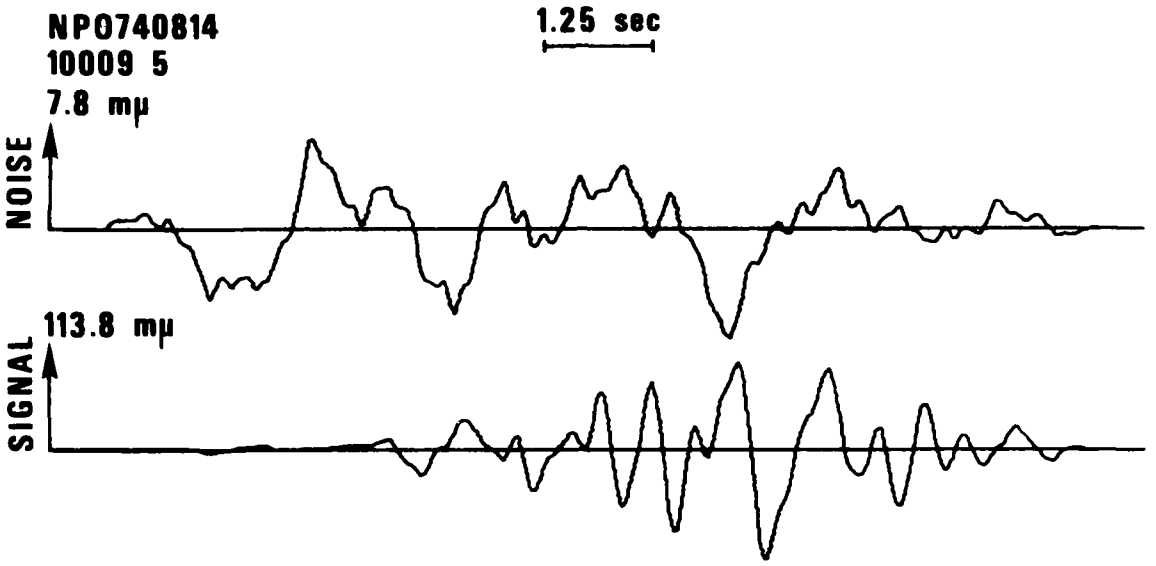
NP0740814
10009 5
7.8 mμ
1.25 sec
NOISE
113.8 mμ
SIGNAL

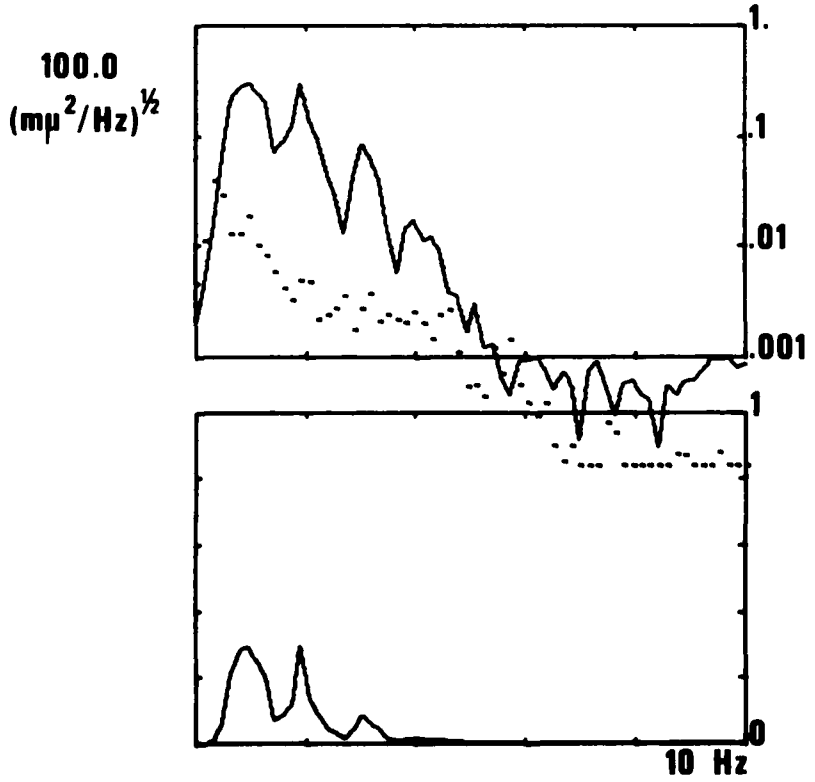
100.0
(mμ²/Hz)½
1.
.1
.01
.001
1
0
10 Hz

Figure II-8

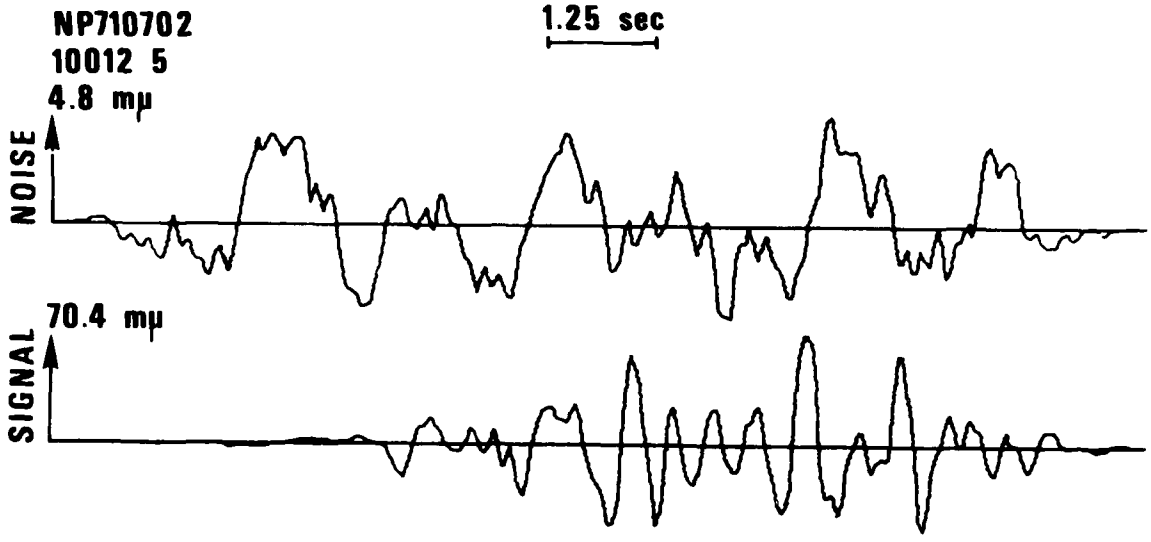
NP710702
10012 5
4.8 mμ
1.25 sec
NOISE
70.4 mμ
SIGNAL

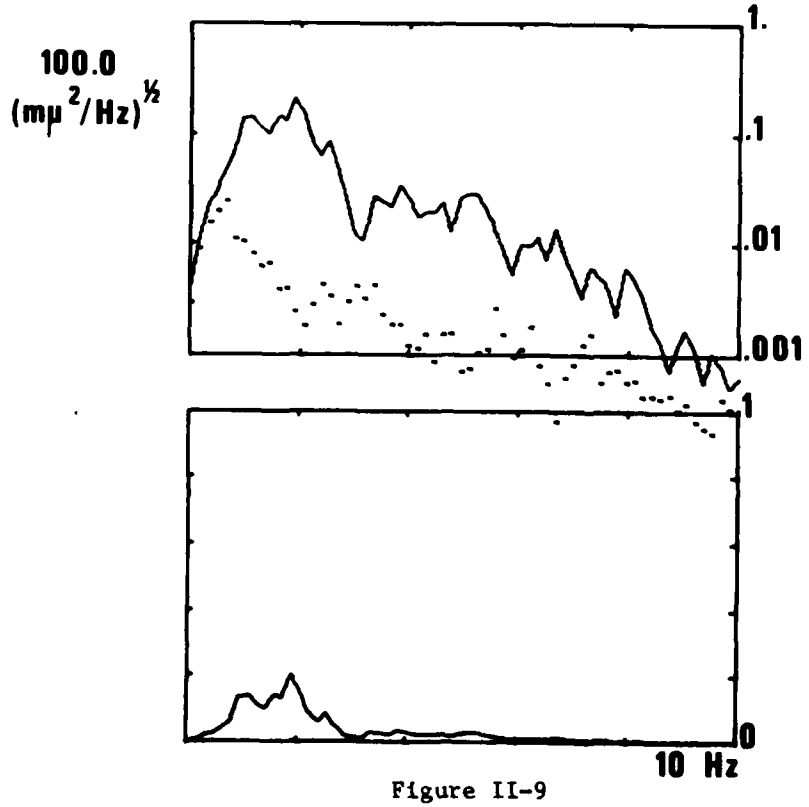
100.0
(mμ²/Hz)½
1.
.1
.01
.001
1
0
10 Hz

Figure II-9